

---

## Global Aromaticity in a Partially Fused 8-Porphyrin Nanoring

Sebastian M. Kopp, Henrik Gotfredsen, Jie-Ren Deng, Tim D. W. Claridge, and Harry L. Anderson\*

Department of Chemistry, University of Oxford, Chemistry Research Laboratory, Oxford OX1 3TA,  
UK

Correspondence to: [harry.anderson@chem.ox.ac.uk](mailto:harry.anderson@chem.ox.ac.uk).

---

### Table of Contents

1. General methods .....	S2
2. Overview of Porphyrin Nanoring Complexes .....	S4
3. Synthetic Procedures .....	S5
4. <sup>1</sup> H NMR Assignment of Rings and Complexes .....	S19
5. Analysis of Global Ring Currents.....	S24
6. Overview of NMR Spectra of Nanoring Complexes.....	S27
7. Observed NMR Shifts in Oxidation Titrations.....	S31
8. Counting of $\pi$ -Electrons in a Global <i>c</i> -P8[b <sub>6</sub> f <sub>2</sub> ] Circuit.....	S33
9. Summary of Experimental Results and NICS Calculations .....	S34
10. Full NMR Oxidation Titrations .....	S36
11. Computational Chemistry Methods .....	S41
12. Time-Dependent Density Functional Theory .....	S42
13. Natural Transition Orbital Pair Calculations .....	S46
14. NICS and ACID calculations .....	S49
15. NMR and Mass Spectra of Novel Compounds .....	S55
16. NMR Spectra of Oxidation States .....	S125
17. DOSY Analysis of the Self-assembly Complexes.....	S135
18. References.....	S142

## 1. General methods

Diisopropylamine (*i*-Pr<sub>2</sub>NH) and dichloromethane for reactions were obtained from an MBraun MBSPS-5-BenchTop solvent purification system kept under nitrogen. Copper(I) chloride was prepared before use according to a known procedure.<sup>1</sup> Chloroform-*d* for NMR was stored over K<sub>2</sub>CO<sub>3</sub> prior to use. All other reagents and solvents were obtained from commercial suppliers and used as received unless otherwise stated. Thin-layer chromatography (TLC) was carried out using commercially available aluminum sheets precoated with silica gel with fluorescence indicator and visualized under UV light at 254 or 360 nm. Purification by column chromatography was carried out on silica gel (SiO<sub>2</sub>, 60 Å, 40–63 µm). Petroleum ether (PE) of boiling range: 40–60 °C was used for chromatography. Size exclusion chromatography (SEC) was carried out using Bio-Rad Bio-Beads S-X1 (40–80 µm bead size). Analytical GPC was carried out using JAIGEL-3H-A (8 × 500 mm) and JAIGEL-4H-A (8 × 500 mm) columns in THF + 1% pyridine as eluent with a flow rate of 1.0 mL/min. Semi-preparative GPC was carried out on a Shimadzu recycling GPC system equipped with a LC-20 AD pump, SPD-20A UV detector and a set of JAIGEL 3H (20 × 600 mm) and JAIGEL 4H (20 × 600 mm) columns in toluene + 1% pyridine as the eluent at a flow rate of 3.5 mL/min.

<sup>1</sup>H and <sup>13</sup>C NMR spectra were recorded on either a Bruker AVIII HD 400, a Bruker AVIII HD 500, a Bruker AVII 500 with a <sup>13</sup>C(<sup>1</sup>H) dual cryo-probe, or a Bruker AVIII 600 with a broadband cryo-probe. <sup>19</sup>F NMR spectra were recorded on a Bruker AVIIIHD 500 instrument. Chemical shift values are quoted in ppm and coupling constants (*J*) in Hertz to the nearest 0.1 Hz. <sup>1</sup>H and <sup>13</sup>C NMR spectra are referenced against the residual solvent peak (CHCl<sub>3</sub> δ<sub>H</sub> = 7.26 ppm, CDCl<sub>3</sub> δ<sub>C</sub> = 77.16 ppm; CH<sub>2</sub>Cl<sub>2</sub> δ<sub>H</sub> = 5.32 ppm, CD<sub>2</sub>Cl<sub>2</sub> δ<sub>C</sub> = 53.84 ppm). <sup>19</sup>F NMR spectra are referenced against hexafluorobenzene (δ<sub>F</sub> = –164.8 ppm) which was added to the samples. Unless stated otherwise, NMR spectra were recorded at 298 K. <sup>1</sup>H-<sup>1</sup>H NOESY spectra were recorded with a mixing time of 0.4 s for **c-P8[b<sub>6</sub>f<sub>2</sub>]**, 0.5 s for **c-P8[b<sub>6</sub>f<sub>2</sub>](T<sub>4</sub>)<sub>2</sub>**, **c-P8[b<sub>6</sub>f<sub>2</sub>](T<sub>4</sub><sub>1,4F</sub>)<sub>2</sub>**, **c-P8[b<sub>6</sub>f<sub>2</sub>](T<sub>4</sub><sub>2,3F</sub>)<sub>2</sub>**, **c-P8[b<sub>8</sub>](T<sub>4</sub>)<sub>2</sub>**, **c-P8[b<sub>8</sub>](T<sub>4</sub><sub>1,4F</sub>)<sub>2</sub>**, and **c-P8[b<sub>8</sub>](T<sub>4</sub><sub>2,3F</sub>)<sub>2</sub>**, and 0.8 sec for **Si-/P2[f<sub>1</sub>]-Si**, **H-/P8[b<sub>5</sub>f<sub>2</sub>]-H**, **T<sub>4</sub>**, **T<sub>4</sub><sub>1,4F</sub>**, **T<sub>4</sub><sub>2,3F</sub>**, **c-P8[b<sub>6</sub>f<sub>2</sub>](T<sub>4</sub>)<sub>2</sub><sup>4+</sup>**, **c-P8[b<sub>6</sub>f<sub>2</sub>](T<sub>4</sub>)<sub>2</sub><sup>6+</sup>**, **c-P8[b<sub>6</sub>f<sub>2</sub>](T<sub>4</sub>)<sub>2</sub><sup>8+</sup>**, **c-P8[b<sub>6</sub>f<sub>2</sub>](T<sub>4</sub><sub>1,4F</sub>)<sub>2</sub><sup>8+</sup>**, and **c-P8[b<sub>6</sub>f<sub>2</sub>](T<sub>4</sub><sub>2,3F</sub>)<sub>2</sub><sup>8+</sup>**. 1D <sup>1</sup>H-<sup>19</sup>F HOESY spectra were recorded with 0.4 s mixing time.

UV-Vis-NIR measurements were carried out in a 1 cm path length quartz cuvette at 298 K using either a Perkin-Lambda 20 or a Jasco V770 spectrophotometer. Chloroform (stored over K<sub>2</sub>CO<sub>3</sub>) was used as solvent.

MALDI-ToF mass spectra were measured at the EPSRC UK National Mass Spectrometry Facility (NMSF, Swansea) on a Bruker ultrafleXtreme MALDI-TOF/TOF instrument or at the University of Oxford using a Bruker MALDI Autoflex Speed instrument. Either dithranol or *trans*-2-[3-(4-tert-butylphenyl)-2-methyl-2-propenylidene]malononitrile (DCTB) was used as matrix. ESI spectra were measured at the University of Oxford on a Thermo Orbitrap Exactive mass spectrometer.

Nanoring complexes containing fluorinated templates: **c-P8[b<sub>6</sub>f<sub>2</sub>](T<sub>4</sub><sub>1,4F</sub>)<sub>2</sub>**, **c-P8[b<sub>6</sub>f<sub>2</sub>](T<sub>4</sub><sub>2,3F</sub>)<sub>2</sub>**, **c-P8[b<sub>8</sub>](T<sub>4</sub><sub>1,4F</sub>)<sub>2</sub>**, and **c-P8[b<sub>8</sub>](T<sub>4</sub><sub>1,4F</sub>)<sub>2</sub>** were formed from the corresponding T<sub>4</sub>-complexes: **c-P8[b<sub>6</sub>f<sub>2</sub>](T<sub>4</sub>)<sub>2</sub>** and **c-P8[b<sub>8</sub>](T<sub>4</sub>)<sub>2</sub>** isolated from synthesis. Template removal was done in accordance with a previously published procedure<sup>2</sup> by passing the nanoring complexes through either a 2.5 M DABCO or a 30% pyridine/toluene solution on a SEC column (toluene). Formation of the fluorinated complexes was achieved by titrating an excess amount of template into a CDCl<sub>3</sub> solution of free nanoring. The <sup>1</sup>H-NMR signals of free template marked the endpoint of the titration, and the solution was passed through a SEC column (CHCl<sub>3</sub>) followed (in some instances) by filtration through a short pad of silica (CHCl<sub>3</sub>/*n*-hexane 1:5) for removing minor aliphatic impurities.

Oxidative NMR titrations on porphyrin nanoring complexes were carried out similarly to previous descriptions.<sup>3,4</sup> The nanoring complexes were transferred to J. Young NMR tubes, dissolved in CD<sub>2</sub>Cl<sub>2</sub>, and handled under argon using standard Schlenk techniques. A well-stirred suspension of the oxidant, thianthrenium hexafluoroantimonate (Thn<sup>+</sup>, *E*<sub>red</sub> = 0.86 V versus Fc/Fc<sup>+</sup>) in CD<sub>2</sub>Cl<sub>2</sub> (ca. 20–30 mM), kept under argon was used for the titrations. The titrations were carried out using a Schlenk adaptor for the J. Young NMR tubes, enabling

the addition of oxidant under a counterflow of argon. While having the NMR tube positioned in the Schlenk adaptor, the lower part of the tube was simultaneously immersed in a dry ice/acetone mixture ( $-78\text{ }^{\circ}\text{C}$ ) in a Dewar to preserve the integrity of oxidized nanoring complexes. After the first addition of oxidant, the samples were kept at low-temperatures throughout the titration experiments using either a dry ice/acetone Dewar or the  $\text{N}_2$  cooling ( $-50\text{ }^{\circ}\text{C}$ ) as used for the NMR probe. Only during transfers ( $\leq 30$  seconds) from the NMR instrument to the Dewar or from the NMR tube adaptor to the Dewar were the samples momentarily subjected to room temperature conditions. Prior to each titration, a  $^1\text{H}$  spectrum was recorded at 298 K to confirm integrity and purity of the porphyrin nanoring complex. At the end of a titration, the oxidized porphyrin nanoring complex was reduced (using decamethylferrocene) back to recover the neutral state, as confirmed by  $^1\text{H}$  NMR at 298 K. The titration endpoint (at which each porphyrin unit is oxidized to the 1+ state) is evident from the disappearance of the neutral oxidant (thianthrene)  $^1\text{H}$  signals, resulting from signal broadening caused by exchange between neutral thianthrene and excess thianthrenium.

## 2. Overview of Porphyrin Nanoring Complexes

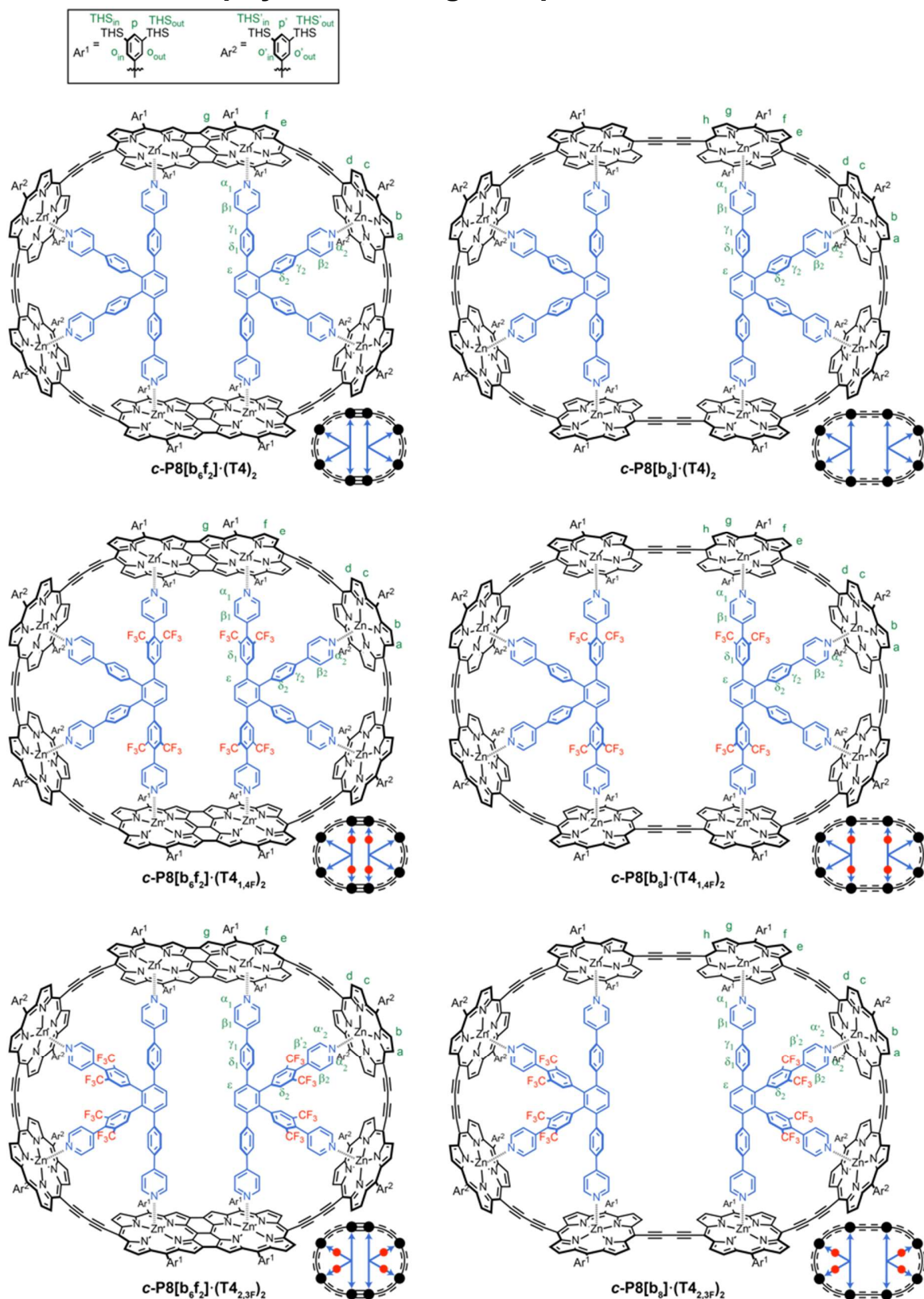
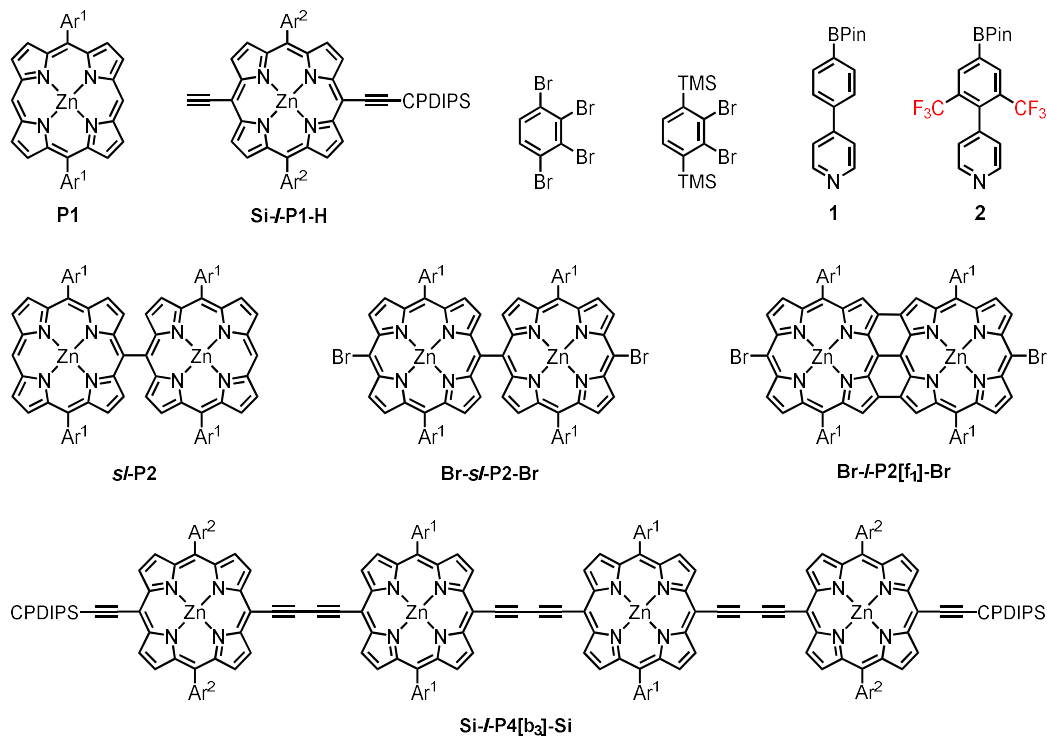


**Figure S1.** Overview of all nanoring-template complexes included in this study. Ar<sup>1</sup> = Ar<sup>2</sup> = 3,5-bis(trihexylsilyl)phenyl.



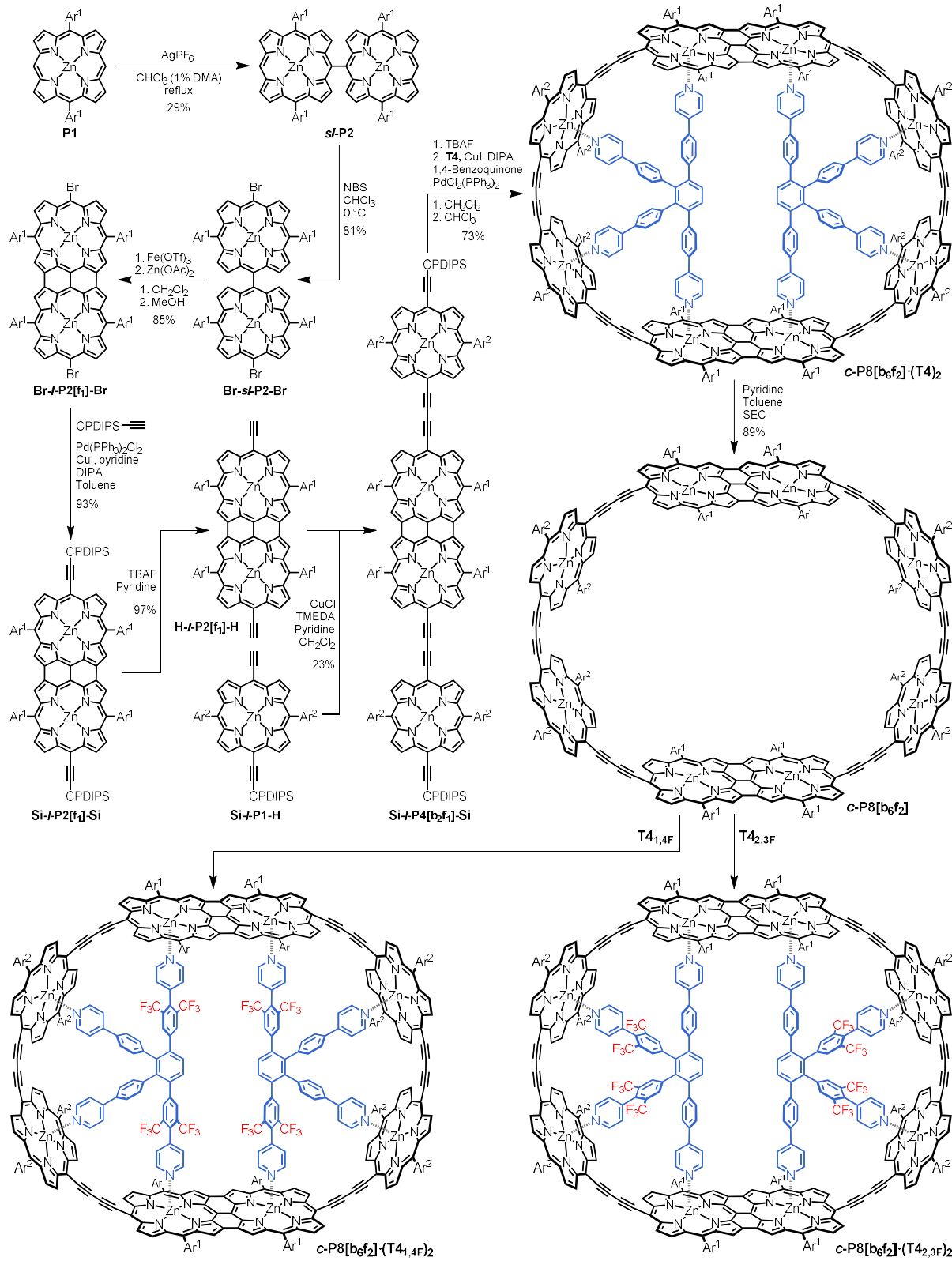
### 3. Synthetic Procedures

Porphyrin derivatives: **P1**,<sup>5</sup> **Si-*l*-P1-H**,<sup>6</sup> ***si*-P2**,<sup>7</sup> **Br-*si*-P2-Br**,<sup>7</sup> **Br-*l*-P2[f<sub>1</sub>]-Br**,<sup>7</sup> and **Si-*l*-P4[b<sub>3</sub>]-Si**<sup>6</sup> as well as template precursors: 1,2,3,4-tetrabromobenzene,<sup>8</sup> 1,4-bis(trimethylsilyl)-2,3-dibromobenzene,<sup>9</sup> and arylboronic acid pinacol esters **1**<sup>10</sup> and **2**<sup>4</sup> were synthesized as reported previously (**Scheme S1**).



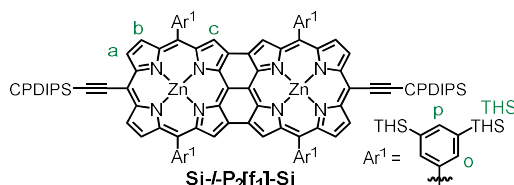
**Scheme S1.** Compounds prepared according to reported procedures.

### Synthesis of *c*-P8[b<sub>6</sub>f<sub>2</sub>]•(T4)<sub>2</sub>, *c*-P8[b<sub>6</sub>f<sub>2</sub>]•(T4<sub>1,4F</sub>)<sub>2</sub>, and *c*-P8[b<sub>6</sub>f<sub>2</sub>]•(T4<sub>2,3F</sub>)<sub>2</sub>



**Scheme S2.** Synthesis of **c-P8[b<sub>6</sub>f<sub>2</sub>]•(T4)<sub>2</sub>** and free **c-P8[b<sub>6</sub>f<sub>2</sub>]**, and preparation of fluorinated complexes **c-P8[b<sub>6</sub>f<sub>2</sub>]•(T4<sub>1,4</sub>F)<sub>2</sub>** and **c-P8[b<sub>6</sub>f<sub>2</sub>]•(T4<sub>2,3</sub>F)<sub>2</sub>**. Ar<sup>1</sup> = Ar<sup>2</sup> = 3,5-bis(trihexylsilyl)phenyl. CPDIPS = cyanopropylidisopropylsilyl.

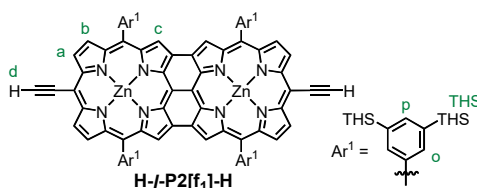
### Si-*I*-P2[f<sub>1</sub>]-Si:



In a Schlenk flask, bromo-porphyrin dimer **Br-*I*-P2[f<sub>1</sub>]-Br** (380 mg, 0.110 mmol, 1 equiv.), Pd(PPh<sub>3</sub>)<sub>2</sub>Cl<sub>2</sub> (16 mg, 0.023 mmol), and CuI (5 mg, 0.026 mmol) were dissolved in toluene (11 mL), *i*-Pr<sub>2</sub>NH (2 mL), and pyridine (0.3 mL) and subjected to three freeze-pump-thaw cycles. Cyanopropyldiisopropylsilylacetylene (104 μL, 0.456 mmol, 4 equiv.) was added and the reaction mixture heated to 50 °C. After stirring for 2 hours, the mixture was cooled to room temperature, and the volatiles were removed *in vacuo*. The crude mixture was purified by flash column chromatography (SiO<sub>2</sub>; eluent: 40% CH<sub>2</sub>Cl<sub>2</sub>/PE<sub>40-60</sub>) to afford the desired product **Si-*I*-P2[f<sub>1</sub>]-Si** (380 mg, 93%) as a dark green solid.

<sup>1</sup>H NMR (500 MHz, CDCl<sub>3</sub>, 298 K) δ<sub>H</sub> = 8.41 (d, *J* = 4.6 Hz, 4H, a), 7.81 (s, 4H, p), 7.78 (s, 8H, o), 7.47 (d, *J* = 4.6 Hz, 4H, b), 7.06 (s, 4H, c), 2.44 (t, *J* = 6.8 Hz, 4H, CPDIPS-CH<sub>2</sub>), 2.04–1.95 (m, 4H, CPDIPS-CH<sub>2</sub>), 1.01–0.97 (m, 4H, CPDIPS-CH<sub>2</sub>), 1.45–0.75 (m, 340H, THS + CPDIPS-CH + CPDIPS-CH<sub>3</sub>) ppm. **MALDI-ToF** *m/z* 3714.257 (calculated for [C<sub>232</sub>H<sub>376</sub>N<sub>10</sub>Si<sub>10</sub>Zn<sub>2</sub>]<sup>+</sup>: 3714.604). **UV-vis-NIR** (CDCl<sub>3</sub>) λ<sub>max</sub> (log ε): 1133 (4.60), 994 (4.42), 580 (5.28), 487 (4.76), 438 (5.20).

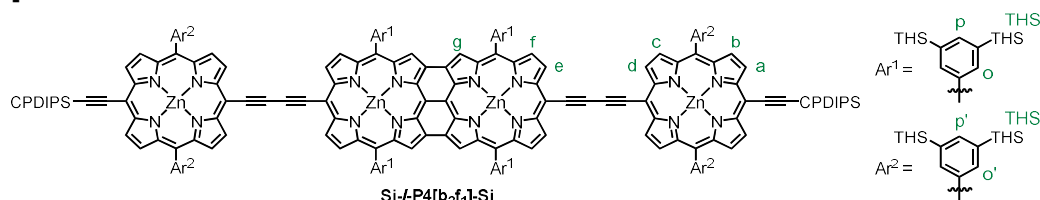
### H-*I*-P2[f<sub>1</sub>]-H:



**Si-*I*-P2[f<sub>1</sub>]-Si** (80 mg, 21.5 μmol) was dissolved in CH<sub>2</sub>Cl<sub>2</sub> (10 mL) and pyridine (0.1 mL). TBAF (1.0 M in THF, 0.25 mL, 0.25 mmol) was added and the reaction mixture was stirred for 25 minutes at room temperature before being passed through a pad of silica (eluent: 60% CHCl<sub>3</sub>/PE<sub>40-60</sub> + 1% pyridine). The volatiles were removed *in vacuo* to afford **H-*I*-P2[f<sub>1</sub>]-H** (70 mg, 97%) as a green solid.

<sup>1</sup>H NMR (400 MHz, CDCl<sub>3</sub>, 298 K) δ<sub>H</sub> = 8.45 (d, *J* = 4.7 Hz, 4H, a), 7.81 (d, *J* = 1.2 Hz, 4H, p), 7.80 (d, *J* = 1.2 Hz, 8H, o), 7.48 (d, *J* = 4.7 Hz, 4H, b), 7.08 (s, 4H, c), 3.77 (s, 2H, d), 1.43–0.79 (m, 312H, THS) ppm.

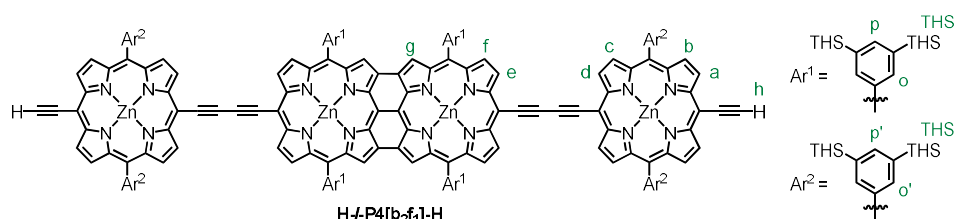
### Si-*I*-P4[b<sub>2</sub>f<sub>1</sub>]-Si:



In a 500 mL round bottom flask, **H-*I*-P2[f<sub>1</sub>]-H** (70 mg, 20.9 μmol) and **Si-*I*-P1-H** (240 mg, 0.127 mmol) were dissolved in CH<sub>2</sub>Cl<sub>2</sub> (10 mL) and pyridine (0.1 mL). CuCl (167 mg, 1.69 mmol) and TMEDA (0.25 mL) were added, and the mixture was stirred vigorously under an oxygen rich atmosphere. After 35 minutes, the reaction was filtered through a pad of silica (eluent: CHCl<sub>3</sub> + 1% pyridine) and concentrated *in vacuo*. The crude residue was purified by SEC (toluene + 1% pyridine) and further purified by recycling GPC (toluene + 1% pyridine) to afford **Si-*I*-P4[b<sub>2</sub>f<sub>1</sub>]-Si** (35 mg, 23%) as a green solid.

**$^1\text{H}$  NMR** (500 MHz,  $\text{CDCl}_3$ , 298 K)  $\delta_{\text{H}}$  = 9.73 (d,  $J$  = 4.6 Hz, 4H, d), 9.63 (d,  $J$  = 4.6 Hz, 4H, a), 8.88 (d,  $J$  = 4.6 Hz, 4H, c), 8.86 (d,  $J$  = 4.6 Hz, 4H, b), 8.59 (d,  $J$  = 4.5 Hz, 4H, e), 8.23 (s, o'), 7.99 (s, 4H, p'), 7.81 (s, 4H, p), 7.80 (s, 8H, o), 7.48 (d,  $J$  = 4.5 Hz, 4H, f), 6.96 (s, 4H, g), 2.54 (t,  $J$  = 6.8 Hz, 4H, CPDIPS-CH<sub>2</sub>), 2.23–2.16 (m, 4H, CPDIPS-CH<sub>2</sub>), 1.19–1.14 (m, 4H, CPDIPS-CH<sub>2</sub>), 1.55–0.64 (m, 652H, THS + THS' + CPDIPS-CH + CPDIPS-CH<sub>3</sub>) ppm.  **$^{13}\text{C}$  NMR** (126 MHz,  $\text{CDCl}_3$ , 298 K)  $\delta_{\text{C}}$  = 155.9, 154.8, 154.2, 153.3, 153.1, 152.3, 150.8, 150.5, 144.9, 140.5, 139.3, 139.0, 138.8, 136.5, 135.3, 135.0, 133.3, 133.1, 132.3, 130.9, 129.4, 127.7, 124.6, 123.2, 119.9, 101.3, 33.7, 33.6, 31.8, 31.7, 31.1, 29.9, 24.2, 24.1, 22.82, 22.79, 21.8, 21.2, 18.8, 18.5, 14.3, 12.79, 12.77, 12.6, 12.5, 10.3, 1.2 ppm. **MALDI-ToF**  $m/z$  7123.020 (calculated for  $[\text{C}_{448}\text{H}_{716}\text{N}_{18}\text{Si}_{18}\text{Zn}_4]^+$ : 7121.974). **UV-vis-NIR** ( $\text{CDCl}_3$ )  $\lambda_{\text{max}}$  (log  $\epsilon$ ): 1137 (5.08), 992 (4.78), 687 (5.16), 583 (5.27), 443 (5.73).

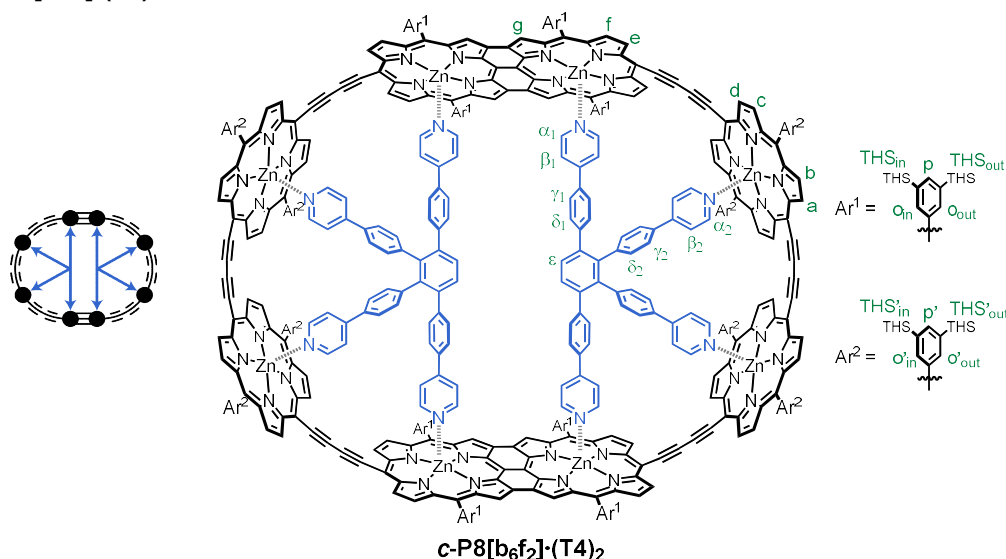
#### H-*I*-P4[b<sub>2</sub>f<sub>1</sub>]-H:



**Si-*I*-P4[b<sub>2</sub>f<sub>1</sub>]-Si** (5.60 mg, 0.789  $\mu\text{mol}$ ) was dissolved in  $\text{CH}_2\text{Cl}_2$  (2 mL) and pyridine (0.02 mL). TBAF (1.0 M in THF, 0.08 mL, 0.08 mmol) was added and the reaction mixture was stirred for 25 minutes at room temperature before being passed through a pad of silica (eluent: 20%  $\text{CH}_2\text{Cl}_2/\text{PE}_{40-60}$  + 1% pyridine). The volatiles were removed *in vacuo* to afford **H-*I*-P4[b<sub>2</sub>f<sub>1</sub>]-H** (5.05 mg, 95%) as a green solid.

**$^1\text{H}$  NMR** (400 MHz,  $\text{CDCl}_3$ )  $\delta_{\text{H}}$  = 9.80 (d,  $J$  = 4.6 Hz, 4H, d), 9.72 (d,  $J$  = 4.6 Hz, 4H, a), 8.96 (d,  $J$  = 4.6 Hz, 4H, c), 8.92 (d,  $J$  = 4.6 Hz, 4H, b), 8.67 (d,  $J$  = 4.6 Hz, 4H, e), 8.27 (d,  $J$  = 1.1 Hz, 8H, o'), 8.01 (t,  $J$  = 1.1 Hz, 4H, p'), 7.85 (d,  $J$  = 1.2 Hz, 8H, o), 7.84 (d,  $J$  = 1.2 Hz, 4H, p), 7.57 (d,  $J$  = 4.6 Hz, 4H, f), 7.08 (s, 4H, h), 4.19 (s, 2H, h), 1.49–0.80 (m, 624H, THS + THS') ppm.

#### Complex c-P8[b<sub>6</sub>f<sub>2</sub>](T4)<sub>2</sub>:



**Procedure A:** **H-*I*-P4[b<sub>2</sub>f<sub>1</sub>]-H** (5.05 mg, 0.747  $\mu\text{mol}$ ) and **T4** (0.52 mg, 0.753  $\mu\text{mol}$ ) were dissolved in  $\text{CHCl}_3$  (2 mL) and sonicated for 2 hours to allow for the complex formation. A catalyst mixture of  $\text{PdCl}_2(\text{PPh}_3)_2$  (0.33 mg, 0.470  $\mu\text{mol}$ ), CuI (0.47 mg, 2.47  $\mu\text{mol}$ ), 1,4-benzoquinone (1.08 mg, 10.0  $\mu\text{mol}$ ), and *i*-Pr<sub>2</sub>NH (15  $\mu\text{L}$ ) in  $\text{CHCl}_3$  (0.5 mL) was added, and the reaction progress was monitored by analytical GPC (THF + 1% pyridine). After 4 hours, the mixture was passed through a pad of silica (eluent:  $\text{CHCl}_3$  + 1% pyridine) and concentrated *in vacuo*.

The resulting residue was purified by SEC (toluene + 1% pyridine) before further purification by recycling GPC (toluene + 1% pyridine) to afford **c-P8[b<sub>6</sub>f<sub>2</sub>](T4)<sub>2</sub>** (4.00 mg, 72%) as a brown solid and analytical amounts of **H-/P8[b<sub>5</sub>f<sub>2</sub>]-H** as a green solid. Additional **c-P8[b<sub>6</sub>f<sub>2</sub>](T4)<sub>2</sub>** was synthesized in two larger batches following procedure A: 1) **H-/P4[b<sub>2</sub>f<sub>1</sub>]-H** (14.3 mg, 2.12 μmol), **T4** (1.47 mg, 2.13 μmol). Yield: 10.4 mg, 66%; 2) **H-/P4[b<sub>2</sub>f<sub>1</sub>]-H** (17.4 mg, 2.57 μmol), **T4** (1.79 mg, 2.59 μmol). Yield: 12.1 mg, 63%.

Procedure B (reduced equivalents of CuI): Following the general approach of procedure A, **H-/P4[b<sub>2</sub>f<sub>1</sub>]-H** (16.3 mg, 2.41 μmol) and **T4** (2.34 mg, 3.39 μmol) were reacted using an adapted catalyst mixture of PdCl<sub>2</sub>(PPh<sub>3</sub>)<sub>2</sub> (1.06 mg, 1.51 μmol), CuI (0.54 mg, 2.84 μmol), 1,4-benzoquinone (3.49 mg, 32.3 μmol), and *i*-Pr<sub>2</sub>NH (48 μL). The reaction was monitored by analytical GPC (THF + 1% pyridine) and stopped after 14 hours when a 1:2 ratio of **H-/P8[b<sub>5</sub>f<sub>2</sub>]-H** and **c-P8[b<sub>6</sub>f<sub>2</sub>](T4)<sub>2</sub>** was reached. Workup and purification as described in procedure A gave **H-/P8[b<sub>5</sub>f<sub>2</sub>]-H** (1.36 mg, 8%) for full characterization.

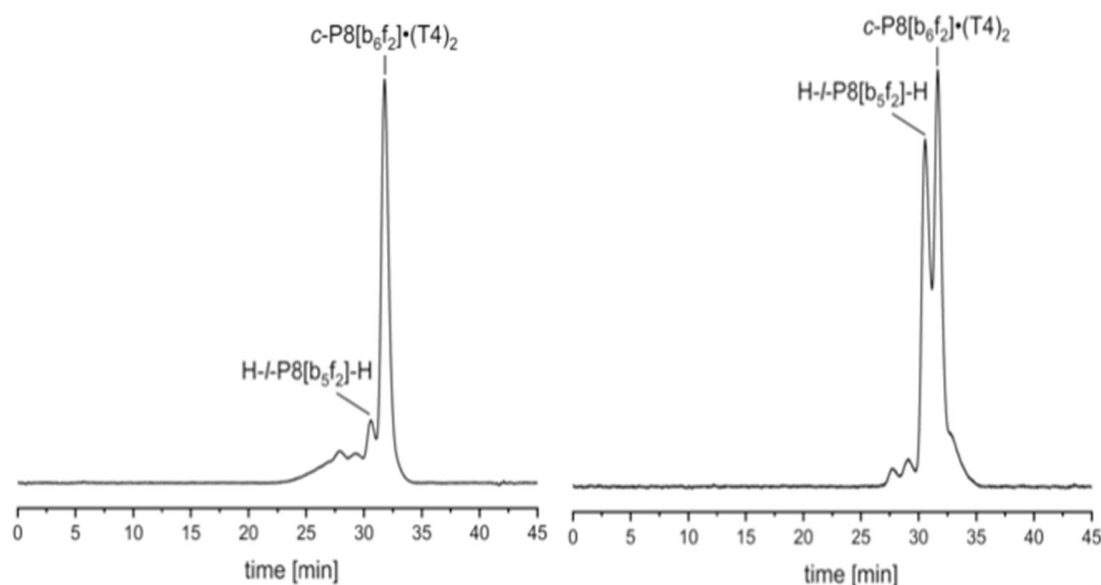
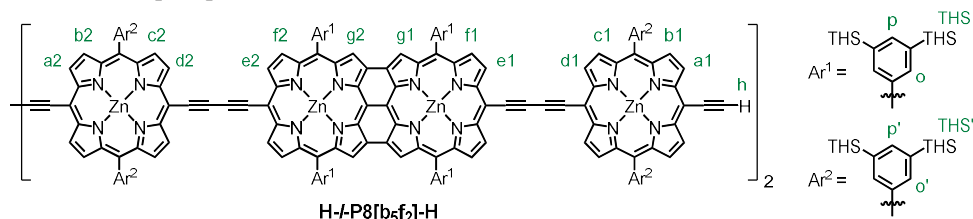


**Figure S2.** Analytical GPC traces (THF + 1% pyridine,  $\lambda = 440$  nm) for the synthesis of **c-P8[b<sub>6</sub>f<sub>2</sub>](T4)<sub>2</sub>** following procedure A after 4 hours (left) and the adapted synthesis of **H-/P8[b<sub>5</sub>f<sub>2</sub>]-H** following procedure B after 14 hours (right).

Characterization of **c-P8[b<sub>6</sub>f<sub>2</sub>](T4)<sub>2</sub>**:

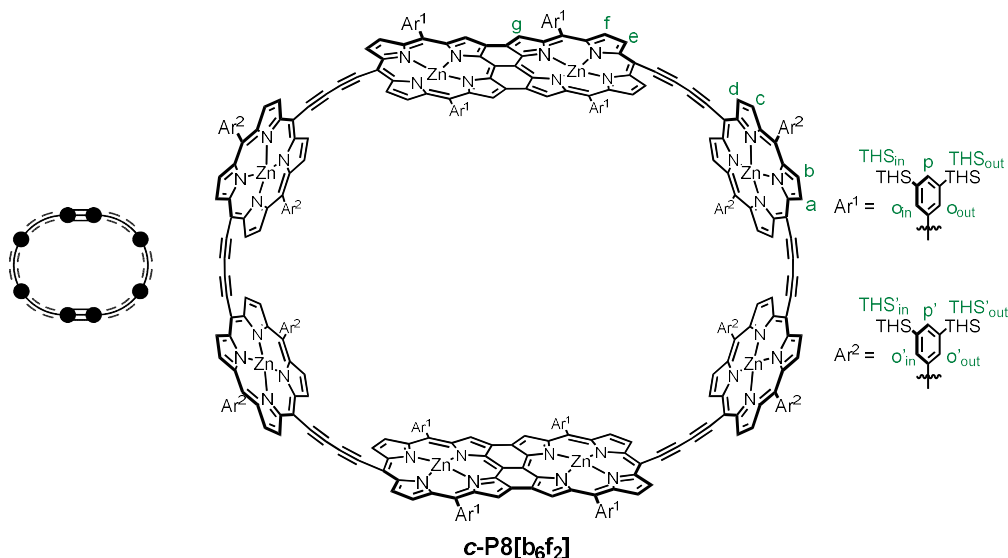
**<sup>1</sup>H NMR** (600 MHz, CD<sub>2</sub>Cl<sub>2</sub>, 298 K)  $\delta_{\text{H}}$  = 9.58 (d,  $J$  = 4.3 Hz, 8H, a), 9.45 (d,  $J$  = 4.3 Hz, 8H, d), 8.78 (d,  $J$  = 4.3 Hz, 8H, b), 8.72 (d,  $J$  = 4.3 Hz, 8H, c), 8.40 (s, 8H, o'<sub>in</sub>), 8.27 (d,  $J$  = 4.3 Hz, 8H, e), 8.02 (s, 8H, o'<sub>out</sub>), 7.99 (s, 8H, p'), 7.75 (s, 8H, p), 7.73 (s, 8H, o<sub>out</sub>), 7.65 (s, 8H, o<sub>in</sub>), 7.36 (d,  $J$  = 4.3 Hz, 8H, f), 6.97 (s, 4H,  $\epsilon$ ), 6.74 (s, 8H, g), 6.50 (d,  $J$  = 8.7 Hz, 8H,  $\gamma_1$ ), 6.40 (d,  $J$  = 8.7 Hz, 8H,  $\delta_1$ ), 6.34 (d,  $J$  = 6.4 Hz, 8H,  $\beta_1$ ), 5.87 (d,  $J$  = 8.8 Hz, 8H,  $\delta_2$ ), 5.75 (d,  $J$  = 8.8 Hz, 8H,  $\gamma_2$ ), 5.59 (d,  $J$  = 6.4 Hz, 8H,  $\alpha_1$ ), 5.23 (d,  $J$  = 6.2 Hz, 8H,  $\beta_2$ ), 2.41 (d,  $J$  = 6.2 Hz, 8H,  $\alpha_2$ ), 1.53–0.61 (m, 1248H, THS<sub>in</sub> + THS<sub>out</sub> + THS'<sub>in</sub> + THS'<sub>out</sub>) ppm. **MALDI-ToF**  $m/z$  13516 (calculated for [C<sub>856</sub>H<sub>1352</sub>N<sub>32</sub>Si<sub>32</sub>Zn<sub>8</sub>]<sup>+</sup> = **c-P8[b<sub>6</sub>f<sub>2</sub>]<sup>+</sup>**: 13513). **UV-vis-NIR** (CDCl<sub>3</sub>)  $\lambda_{\text{max}}$  (log  $\epsilon$ ): 1304 (5.49), 1254 (5.31), 1122 (5.17), 872 (5.39), 735 (5.31), 592 (5.58), 502 (5.64), 439 (5.71).

### Characterization for **H-*P*8[b<sub>5</sub>f<sub>2</sub>]-H**:



**<sup>1</sup>H NMR** (500 MHz, CDCl<sub>3</sub>, 298 K)  $\delta_{\text{H}}$  = 9.94 (d,  $J$  = 4.6 Hz, 4H, a1/a2), 9.85–9.82 (m, 4H, d1/d2), 9.81 (d,  $J$  = 4.5 Hz, 4H, d1/d2), 9.54 (d,  $J$  = 4.6 Hz, 4H, a1/a2), 9.01 (d,  $J$  = 4.6 Hz, 4H, b1/b2), 8.99 (d,  $J$  = 4.5 Hz, 4H, c1/c2), 8.97 (d,  $J$  = 4.5 Hz, 4H, c1/c2), 8.95 (d,  $J$  = 4.6 Hz, b1/b2), 8.70–8.66 (m, 8H, e1+e2), 8.32 (s, 8H, Ar<sup>2</sup> o'), 8.28 (s, 8H, Ar<sup>2</sup> o'), 8.04 (s, 4H, Ar<sup>2</sup> p'), 8.01 (s, 4H, Ar<sup>2</sup> p'), 7.88–7.83 (m, 24H, Ar<sup>1</sup>), 7.60–7.56 (m, 8H, f1+f2), 7.09 (s, 8H, g1+g2), 3.73–3.63 (m, 2H, h), 1.56–0.69 (m, 1248H, THS + THS') ppm. **MALDI-ToF**  $m/z$  13591 (calculated for [C<sub>861</sub>H<sub>1359</sub>N<sub>33</sub>Si<sub>32</sub>Zn<sub>8</sub>]<sup>+</sup> = **[H-*P*8[b<sub>5</sub>f<sub>2</sub>]-H+pyridine]<sup>+</sup>**: 13595). **UV-vis-NIR** (CDCl<sub>3</sub>)  $\lambda_{\text{max}}$  (log  $\epsilon$ ): 1140 (5.51), 993 (5.20), 719 (5.33), 673 (5.41), 582 (5.62), 440 (5.96).

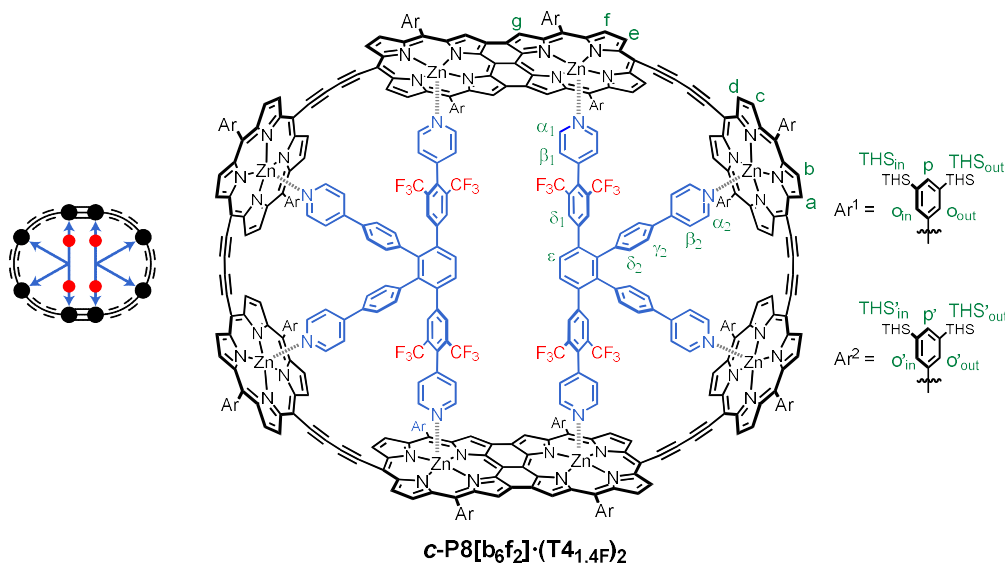
### Free ring **c-P8[b<sub>6</sub>f<sub>2</sub>]**:



A 3.7 M (30%) solution of pyridine (15 mL) in toluene (35 mL) was eluted into a SEC column (toluene; diameter = 3.5 cm; height = 25 cm). A solution of the complex **c-P8[b<sub>6</sub>f<sub>2</sub>](T4)<sub>2</sub>** (10.4 mg, 0.698  $\mu\text{mol}$ ) in toluene (5 mL) was loaded onto the SEC column and eluted through the pyridine solution with additional toluene. The collected fraction was washed with water (5 x 50 mL), dried over MgSO<sub>4</sub>, and concentrated *in vacuo*. The crude residue was further purified by SEC (CHCl<sub>3</sub>) to afford free nanoring **c-P8[b<sub>6</sub>f<sub>2</sub>]** (8.4 mg, 89%) as a brown solid.

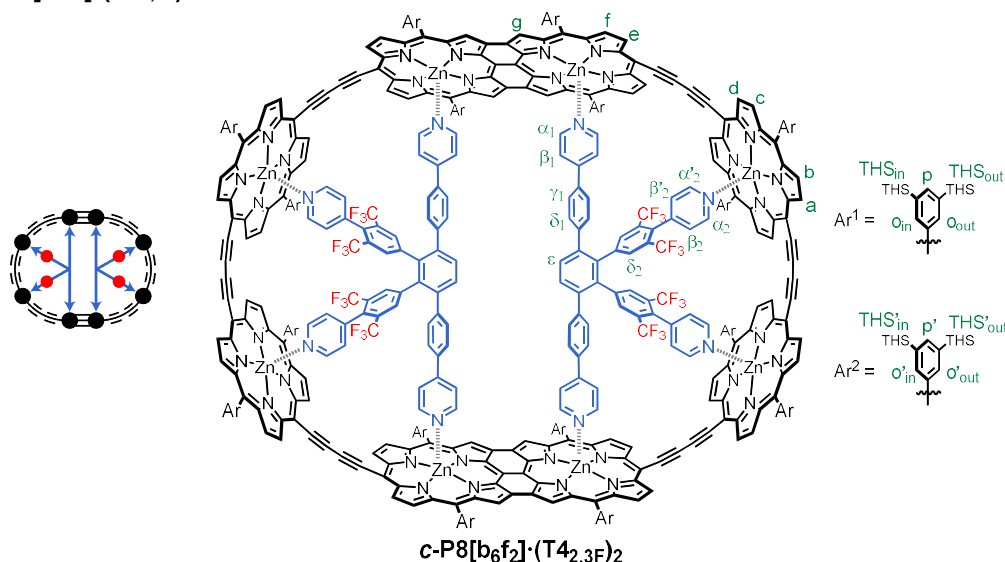
**<sup>1</sup>H NMR** (600 MHz, CD<sub>2</sub>Cl<sub>2</sub>, 298 K)  $\delta_{\text{H}}$  = 9.72 (d,  $J$  = 4.5 Hz, 8H, a), 9.61 (d,  $J$  = 4.5 Hz, 8H, d), 8.85 (d,  $J$  = 4.5 Hz, 8H, b), 8.81 (d,  $J$  = 4.5 Hz, 8H, c), 8.51 (d,  $J$  = 4.5 Hz, 8H, e), 8.19 (s, 16H, o'), 7.97 (s, 8H, p'), 7.77 (s, 8H, p), 7.73 (s, 16H, o), 7.49 (d,  $J$  = 4.5 Hz, 8H, f), 6.92 (s, 8H, g), 1.48–0.72 (m, 1248H, THS + THS') ppm. **MALDI-ToF**  $m/z$  13516 (calculated for [C<sub>856</sub>H<sub>1352</sub>N<sub>32</sub>Si<sub>32</sub>Zn<sub>8</sub>]<sup>+</sup>: 13513). **UV-vis-NIR** (CDCl<sub>3</sub>)  $\lambda_{\text{max}}$  (log  $\epsilon$ ): 1158 (5.32), 1009 (5.05), 782 (5.28), 691 (5.31), 585 (5.54), 491 (5.66), 435 (5.74) nm.

**Complex c-P8[b<sub>6</sub>f<sub>2</sub>](T<sub>4,4F</sub>)<sub>2</sub>:**



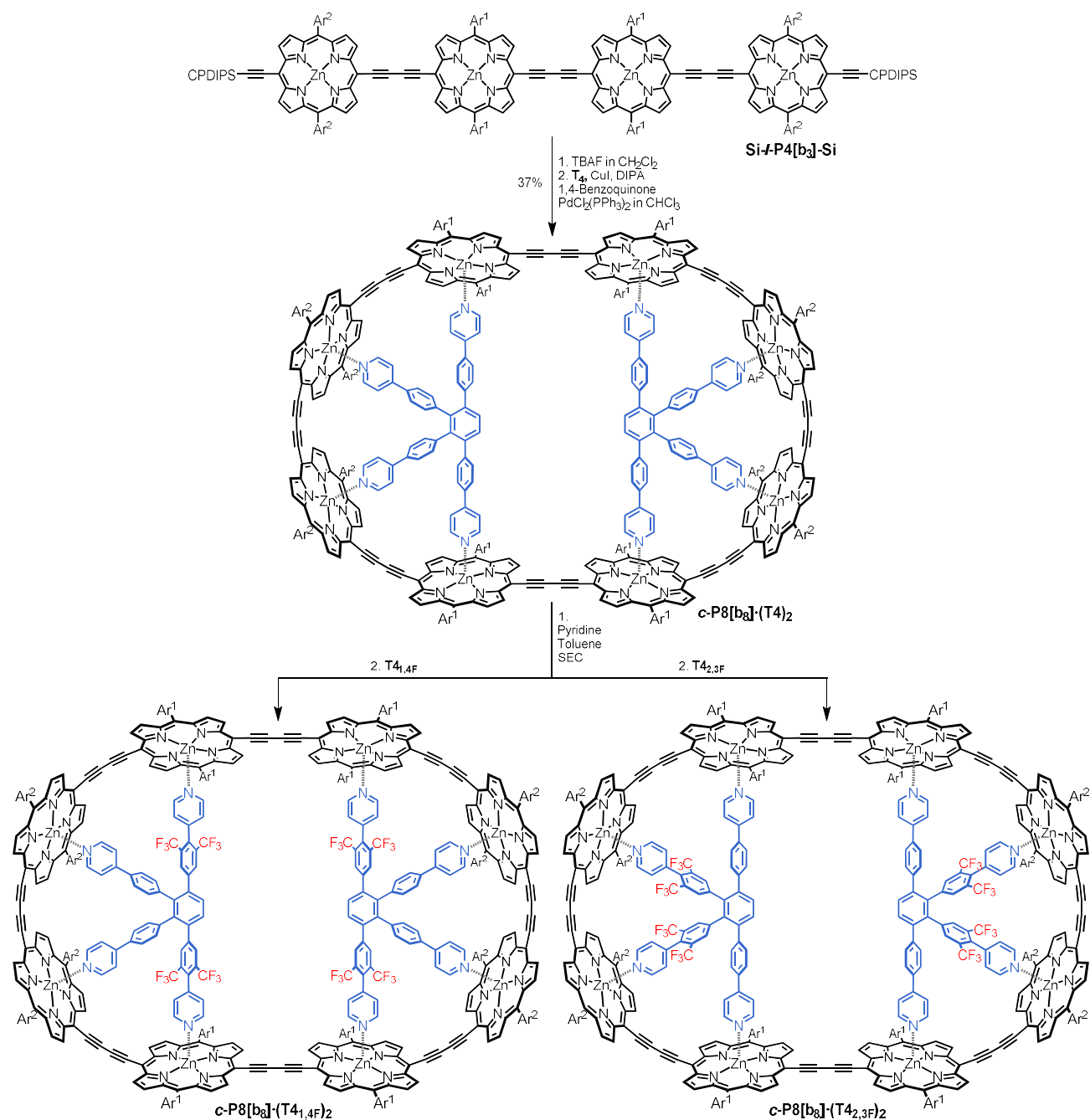
**<sup>1</sup>H NMR** (600 MHz, CD<sub>2</sub>Cl<sub>2</sub>, 298 K)  $\delta_{\text{H}} = 9.57$  (d,  $J = 4.3$  Hz, 8H, a), 9.49 (d,  $J = 4.4$  Hz, 8H, d), 8.79 (d,  $J = 4.3$  Hz, 8H, b), 8.75 (d,  $J = 4.4$  Hz, 8H, c), 8.43 (s, 8H, o'<sub>in</sub>), 8.26 (d,  $J = 4.4$  Hz, 8H, e), 8.05 (s, 8H, o'<sub>out</sub>), 8.03 (s, 8H, p'), 7.74 (s, 16H, p + o<sub>out</sub>), 7.51 (s, 8H, o<sub>in</sub>), 7.26 (d,  $J = 4.4$  Hz, 8H, f), 7.20 (s, 4H,  $\epsilon$ ), 6.95 (s, 8H,  $\delta_1$ ), 6.72 (s, 8H, g), 6.07 (d,  $J = 6.2$  Hz, 8H,  $\beta_1$ ), 5.99 (d,  $J = 8.8$  Hz, 8H,  $\delta_2$ ), 5.90 (d,  $J = 8.8$  Hz, 8H,  $\gamma_2$ ), 5.70 (d,  $J = 6.2$  Hz, 8H,  $\alpha_1$ ), 5.25 (d,  $J = 6.9$  Hz, 8H,  $\beta_2$ ), 2.51–2.46 (m, 8H,  $\alpha_2$ ), 1.64–0.55 (m, 1248H, THS<sub>in</sub> + THS<sub>out</sub> + THS'<sub>in</sub> + THS'<sub>out</sub>) ppm. **<sup>19</sup>F NMR** (470 MHz, CD<sub>2</sub>Cl<sub>2</sub>, 298 K)  $\delta_{\text{F}} = -60.63$  ppm. **MALDI-ToF**  $m/z$  13515 (calculated for [C<sub>856</sub>H<sub>1352</sub>N<sub>32</sub>Si<sub>32</sub>Zn<sub>8</sub>]<sup>+</sup> = **c-P8[b<sub>6</sub>f<sub>2</sub>]<sup>+</sup>**: 13513).

**Complex c-P8[b<sub>6</sub>f<sub>2</sub>](T<sub>4,3F</sub>)<sub>2</sub>:**



**<sup>1</sup>H NMR** (600 MHz, CD<sub>2</sub>Cl<sub>2</sub>, 298 K)  $\delta_{\text{H}} = 9.67$  (d,  $J = 4.4$  Hz, 8H, a), 9.46 (d,  $J = 4.3$  Hz, 8H, d), 8.76 (d,  $J = 4.4$  Hz, 8H, b), 8.67 (d,  $J = 4.3$  Hz, 8H, c), 8.33 (d,  $J = 4.4$  Hz, 8H, e), 8.21 (s, 8H, o'<sub>in</sub>), 8.03 (s, 8H, o'<sub>out</sub>), 7.98 (s, 8H, p'), 7.79 (s, 8H, p), 7.77 (s, 8H, o<sub>out</sub>), 7.71 (s, 8H, o<sub>in</sub>), 7.38 (d,  $J = 4.4$  Hz, f), 7.11 (s, 4H,  $\epsilon$ ), 6.78 (s, 8H, g), 6.65 (d,  $J = 8.4$  Hz, 8H,  $\gamma_1$ ), 6.47 (d,  $J = 8.4$  Hz, 8H,  $\delta_1$ ), 6.39 (d,  $J = 6.7$  Hz, 8H,  $\beta_1$ ), 6.36 (s, 8H,  $\delta_2$ ), 5.70–5.66 (m, 8H,  $\alpha_1$ ), 5.00 (d,  $J = 6.6$  Hz, 4H,  $\beta'_2$ ), 4.81 (d,  $J = 6.5$  Hz, 4H,  $\beta_2$ ), 2.56–2.52 (m, 4H,  $\alpha_2$ ), 2.46–2.42 (m, 4H,  $\alpha'_2$ ), 1.50–0.67 (m, 1248H, THS<sub>in</sub> + THS<sub>out</sub> + THS'<sub>in</sub> + THS'<sub>out</sub>) ppm. **<sup>19</sup>F NMR** (470 MHz, CD<sub>2</sub>Cl<sub>2</sub>, 298 K)  $\delta_{\text{F}} = -61.23$  ppm. **MALDI-ToF**  $m/z$  13515 (calculated for [C<sub>856</sub>H<sub>1352</sub>N<sub>32</sub>Si<sub>32</sub>Zn<sub>8</sub>]<sup>+</sup> = **c-P8[b<sub>6</sub>f<sub>2</sub>]<sup>+</sup>**: 13513).

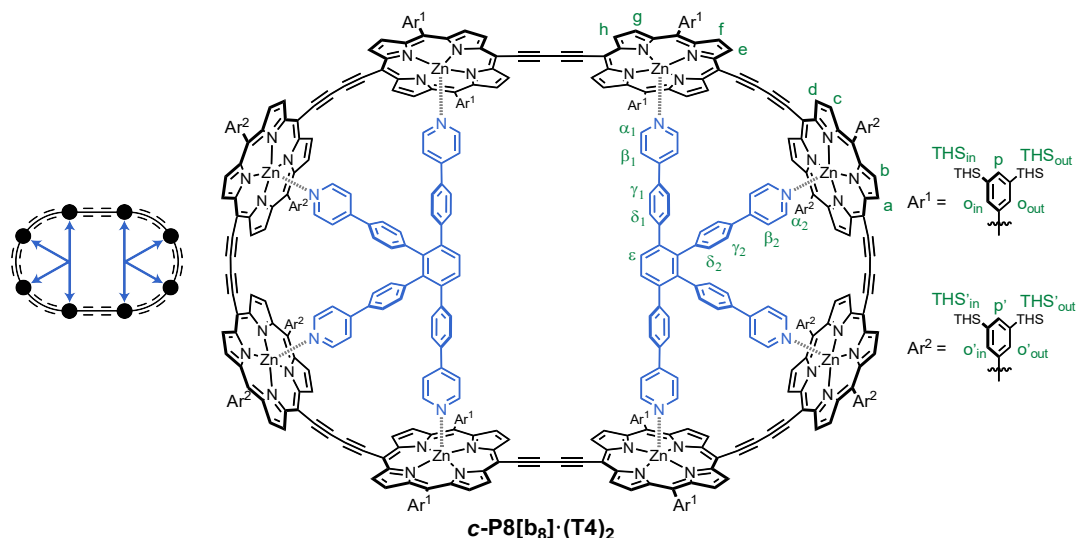
# Synthesis of **c-P8[b<sub>8</sub>](T<sub>4</sub>)<sub>2</sub>**, **c-P8[b<sub>8</sub>](T<sub>4</sub><sub>1,4F</sub>)<sub>2</sub>**, **c-P8[b<sub>8</sub>](T<sub>4</sub><sub>2,3F</sub>)<sub>2</sub>**



**Scheme S3.** Synthesis of **c-P8[b<sub>8</sub>](T<sub>4</sub>)<sub>2</sub>** and formation of fluorinated complexes **c-P8[b<sub>6f2</sub>](T<sub>4</sub><sub>1,4F</sub>)<sub>2</sub>** and **c-P8[b<sub>6f2</sub>](T<sub>4</sub><sub>2,3F</sub>)<sub>2</sub>**. Ar<sup>1</sup> = Ar<sup>2</sup> = 3,5-bis(trihexylsilyl)phenyl. CPDIPS = cyanopropyl-diisopropylsilyl.



**Complex  $c\text{-P8}[\text{b}_8]\cdot(\text{T4})_2$ :**



**H-/-P4[b<sub>3</sub>]-H** (143 mg, 21.0 μmol) and **T4** (15.9 mg, 23.0 μmol) were dissolved in  $\text{CHCl}_3$  (40 mL) and sonicated for 2 hours to allow for the complex formation. A catalyst mixture of  $\text{PdCl}_2(\text{PPh}_3)_2$  (9.3 mg, 13.3 μmol),  $\text{CuI}$  (13.2 mg, 69.3 μmol), 1,4-benzoquinone (30.4 mg, 281 μmol), and *i*-Pr<sub>2</sub>NH (0.42 mL) in  $\text{CHCl}_3$  (10 mL) was added, and the reaction progress was monitored by analytical GPC (THF + 1% pyridine). After 4 hours, the mixture was passed through a pad of silica (eluent:  $\text{CHCl}_3$  + 1% pyridine) and concentrated *in vacuo*. The crude residue was purified by SEC (toluene + 1% pyridine) before further purification by recycling GPC (toluene + 1% pyridine) to afford  **$c\text{-P8}[\text{b}_8]\cdot(\text{T4})_2$**  (53.2 mg, 37%) as a brown solid.

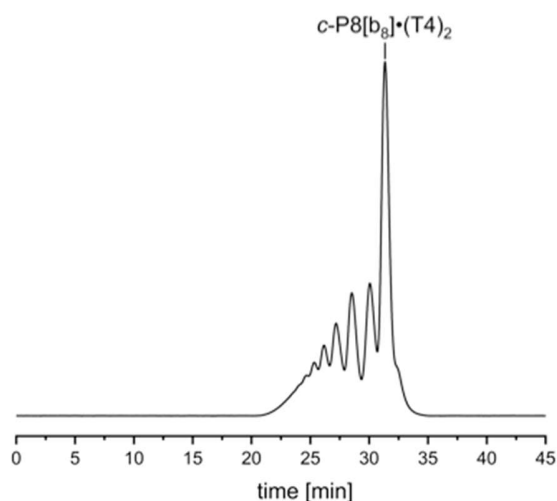
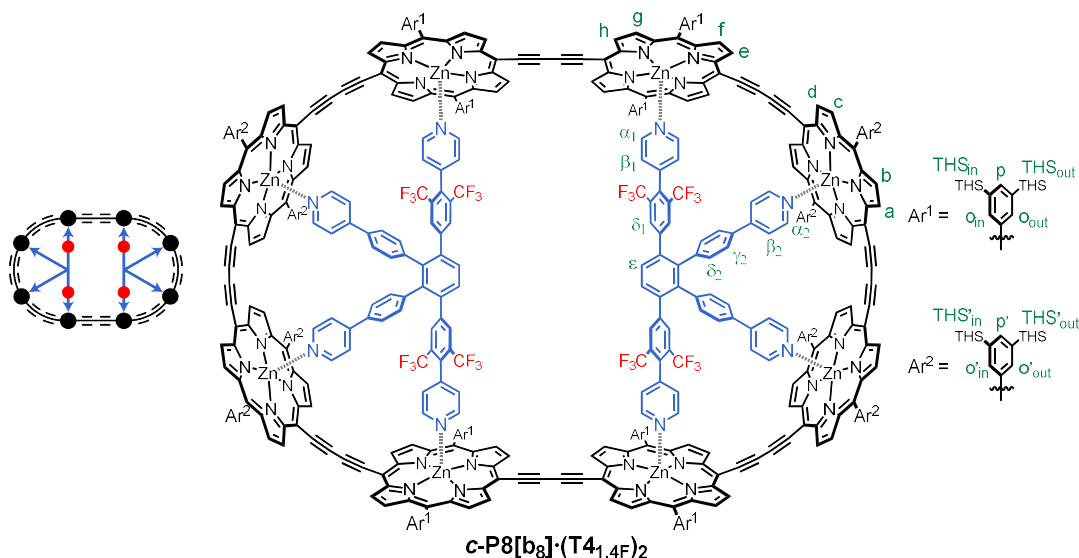


**Figure S3.** Analytical GPC trace (THF + 1% pyridine,  $\lambda = 440$  nm) for the synthesis of  **$c\text{-P8}[\text{b}_8]\cdot(\text{T4})_2$**  after 4 hours.

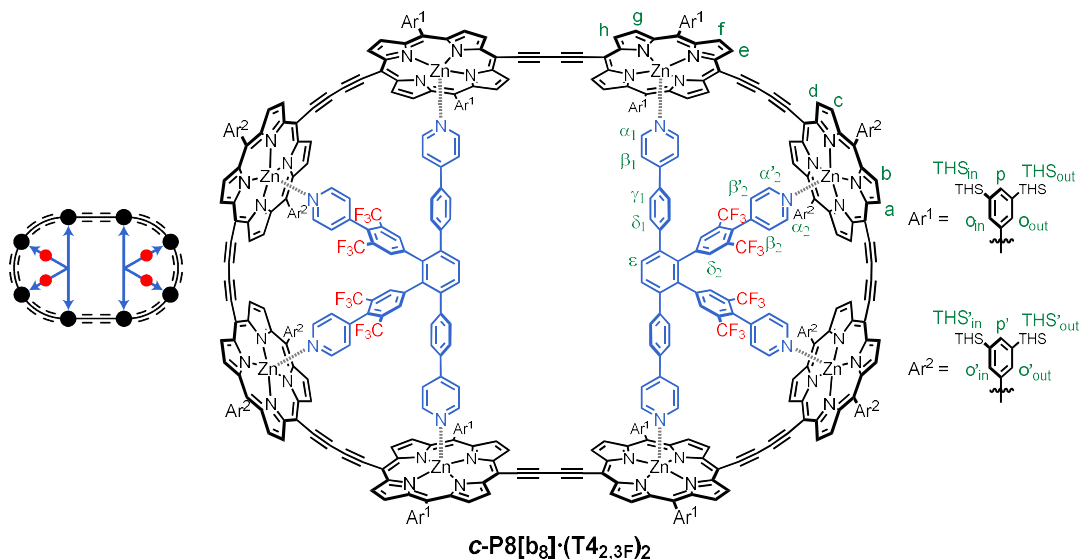
**$^1\text{H}$  NMR** (600 MHz,  $\text{CD}_2\text{Cl}_2$ , 298 K)  $\delta_{\text{H}} = 9.76$  (d,  $J = 4.0$  Hz, 8H, e/h), 9.64 (d,  $J = 4.1$  Hz, 8H, a/d), 9.63–9.60 (m, 16H, a/d + e/h), 8.87 (d,  $J = 4.0$  Hz, 8H, f/g), 8.84–8.77 (m, 24H, b + c + f/g), 8.41 (s, 8H, o'<sub>in</sub>), 8.30 (s, 8H, o<sub>in</sub>), 8.20 (s, 8H, o<sub>out</sub>), 8.08 (s, 8H, o'<sub>out</sub>), 8.05 (s, 8H, p), 8.03 (s, 8H, p'), 6.68 (s, 4H,  $\epsilon$ ), 6.14 (d,  $J = 9.5$  Hz, 8H,  $\delta_1$ ), 6.02 (d,  $J = 9.5$  Hz, 8H,  $\gamma_1$ ), 5.70 (d,  $J = 8.7$  Hz, 8H,  $\delta_2$ ), 5.64 (d,  $J = 8.7$  Hz, 8H,  $\gamma_2$ ), 5.39 (d,  $J = 7.3$  Hz, 8H,  $\beta_1$ ), 5.16 (d,  $J = 6.6$  Hz, 8H,  $\beta_2$ ), 2.64–2.55 (m, 8H,  $\alpha_1$ ), 2.46–2.36 (m, 8H,  $\alpha_2$ ), 1.59–0.71 (m, 1248H, THS<sub>in</sub> + THS<sub>out</sub> + THS'<sub>in</sub> + THS'<sub>out</sub>) ppm. **UV-vis-NIR** ( $\text{CDCl}_3$ )  $\lambda_{\text{max}}$  (log  $\epsilon$ ): 860 (5.98), 812 (5.68), 769 (5.51), 729 (5.09), 497 (5.98), 443 (5.74) nm. **MALDI-ToF**  $m/z$  13615 (calculated for  $[\text{C}_{864}\text{H}_{1360}\text{N}_{32}\text{Si}_{32}\text{Zn}_8]^+ = c\text{-P8}[\text{b}_8]^+$ : 13618).

**Complex c-P8[b<sub>8</sub>](T4<sub>1,4F</sub>)<sub>2</sub>:**



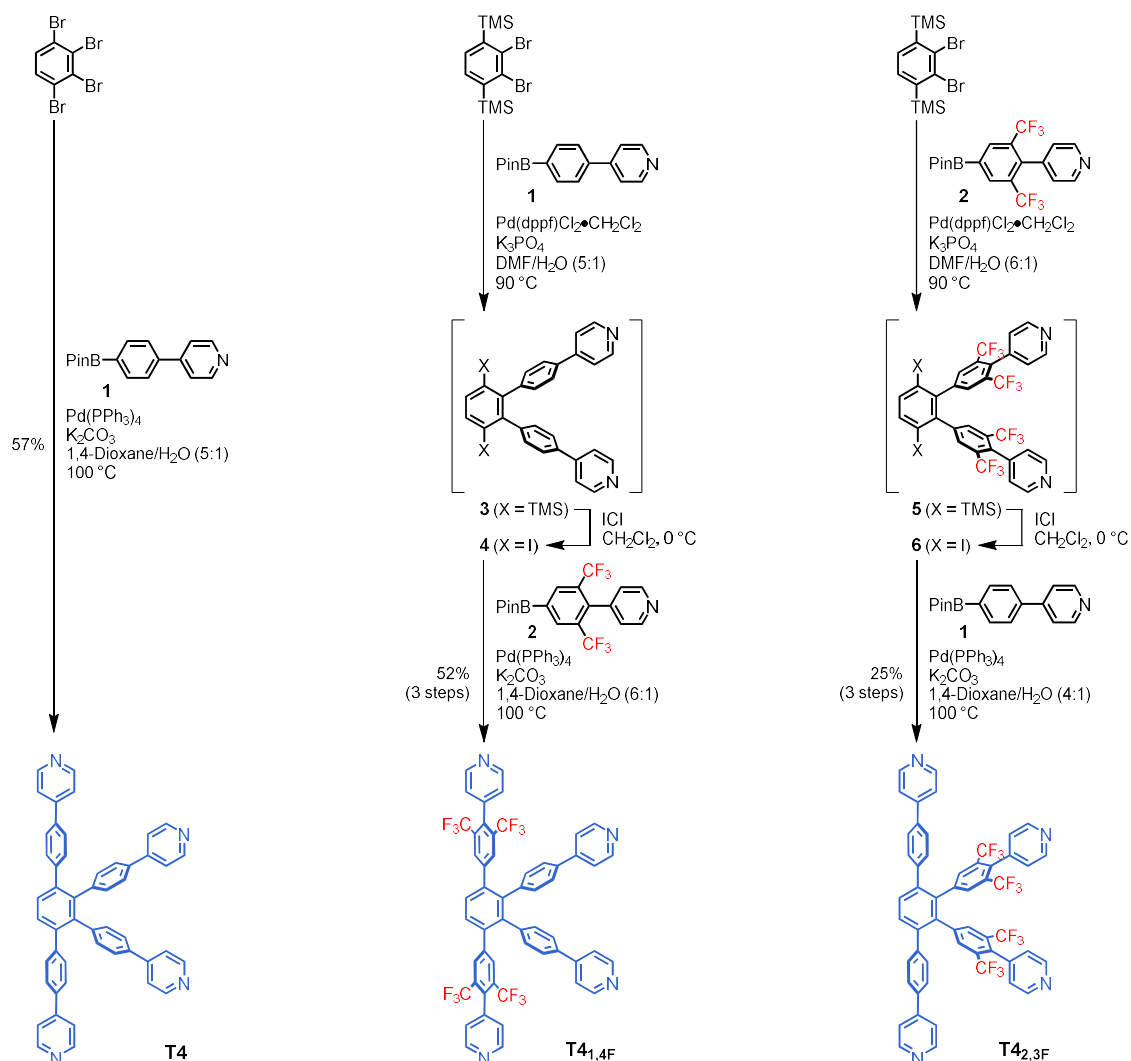
**<sup>1</sup>H NMR** (600 MHz, CD<sub>2</sub>Cl<sub>2</sub>, 298 K)  $\delta_{\text{H}}$  = 9.81 (d,  $J$  = 4.1 Hz, 8H, e/h), 9.68 (d,  $J$  = 4.2 Hz, 8H, a/d), 9.64–9.58 (m, 16H, a/d + e/h), 8.87–8.83 (m, 16H, b/c + f/g), 8.82 (d,  $J$  = 4.2 Hz, 8H, b/c), 8.75 (d,  $J$  = 4.1 Hz, 8H, f/g), 8.44 (s, 8H, o'<sub>in</sub>), 8.22 (s, 8H, o<sub>out</sub>), 8.13 (s, 8H, o<sub>in</sub>), 8.11 (s, 8H, o'<sub>out</sub>), 8.06 (s, 8H, p'), 8.00 (s, 8H, p), 6.83 (s, 4H, ε), 6.67 (s, 8H, δ<sub>1</sub>), 5.82 (d,  $J$  = 8.7 Hz, 8H, δ<sub>2</sub>), 5.77 (d,  $J$  = 8.7 Hz, γ<sub>2</sub>), 5.19 (d,  $J$  = 6.6 Hz, 8H, β<sub>2</sub>), 5.10 (d,  $J$  = 7.6 Hz, 8H, β<sub>1</sub>), 2.57–2.52 (m, 8H, α<sub>1</sub>), 2.50–2.44 (m, 8H, α<sub>2</sub>), 1.66–0.57 (m, 1248H, THS<sub>in</sub> + THS<sub>out</sub> + THS'<sub>in</sub> + THS'<sub>out</sub>) ppm. **<sup>19</sup>F NMR** (470 MHz, CD<sub>2</sub>Cl<sub>2</sub>, 298 K)  $\delta_{\text{F}}$  = –61.05 ppm. **MALDI-ToF**  $m/z$  13615 (calculated for [C<sub>864</sub>H<sub>1360</sub>N<sub>32</sub>Si<sub>32</sub>Zn<sub>8</sub>]<sup>+</sup> = **c-P8[b<sub>8</sub>]<sup>+</sup>**: 13618).

**Complex c-P8[b<sub>8</sub>](T4<sub>2,3F</sub>)<sub>2</sub>:**



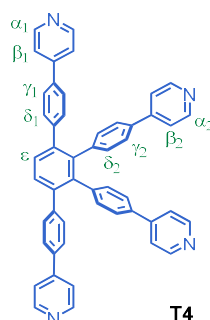
**<sup>1</sup>H NMR** (600 MHz, CD<sub>2</sub>Cl<sub>2</sub>, 298 K)  $\delta_{\text{H}}$  = 9.76 (d,  $J$  = 4.0 Hz, 8H, e/h), 9.69 (d,  $J$  = 4.4 Hz, 8H, a), 9.68 (d,  $J$  = 4.0 Hz, 8H, e/h), 9.64 (d,  $J$  = 4.3 Hz, 8H, d), 8.89 (d,  $J$  = 4.0 Hz, 8H, f/g), 8.85 (d,  $J$  = 4.0 Hz, 8H, f/g), 8.78 (d,  $J$  = 4.4 Hz, 8H, b), 8.75 (d,  $J$  = 4.3 Hz, 8H, c), 8.37 (s, 8H, o<sub>in</sub>), 8.21 (s, 16H, o'<sub>in</sub> + o<sub>out</sub>), 8.09 (s, 8H, o'<sub>out</sub>), 8.05 (s, 8H, p), 8.01 (s, 8H, p'), 6.82 (s, 4H, ε), 6.18 (d,  $J$  = 9.7 Hz, 8H, δ<sub>1</sub>), 6.17–6.13 (m, 16H, γ<sub>1</sub> + δ<sub>2</sub>), 5.44 (d,  $J$  = 7.3 Hz, 8H, β<sub>1</sub>), 4.93 (d,  $J$  = 6.3 Hz, 4H, β'<sub>2</sub>), 4.73 (d,  $J$  = 6.0 Hz, 4H, β<sub>2</sub>), 2.74–2.66 (m, 8H, α<sub>1</sub>), 2.52–2.46 (m, 4H, α<sub>2</sub>), 2.45–2.41 (m, 4H, α'<sub>2</sub>), 1.58–0.71 (m, 1248H, THS<sub>in</sub> + THS<sub>out</sub> + THS'<sub>in</sub> + THS'<sub>out</sub>) ppm. **<sup>19</sup>F NMR** (470 MHz, CD<sub>2</sub>Cl<sub>2</sub>, 298 K)  $\delta_{\text{F}}$  = –61.32 ppm. **MALDI-ToF**  $m/z$  13615 (calculated for [C<sub>864</sub>H<sub>1360</sub>N<sub>32</sub>Si<sub>32</sub>Zn<sub>8</sub>]<sup>+</sup> = **c-P8[b<sub>8</sub>]<sup>+</sup>**: 13618).

## Synthesis of templates T4, T4<sub>1,4F</sub>, and T4<sub>2,3F</sub>



**Scheme S4.** Synthesis of all templates: **T4**, **T4<sub>1,4F</sub>**, and **T4<sub>2,3F</sub>**. TMS = trimethylsilyl. dppf = 1,1'-bis(diphenylphosphino)ferrocene.

### Template T4:

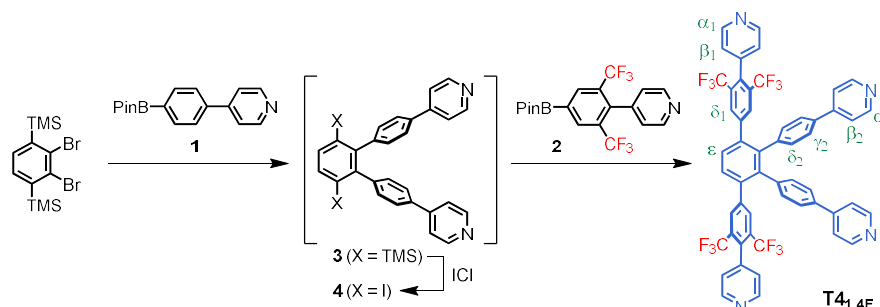


In a Schlenk flask, 1,2,3,4-tetrabromobenzene (356 mg, 0.904 mmol), boronic acid ester **1** (3.56 g, 12.7 mmol), and  $\text{K}_2\text{CO}_3$  (3.90 g, 28.2 mmol) were dissolved in 1,4-dioxane (240 mL) and  $\text{H}_2\text{O}$  (50 mL) and subjected to two freeze-pump-thaw cycles. While the mixture was still frozen,  $\text{Pd(PPh}_3)_4$  (406 mg, 351  $\mu\text{mol}$ ) was added followed by an additional freeze-pump-thaw cycle. The mixture was heated to  $100^\circ\text{C}$  for 4 days, filtered through a short pad of silica (eluent: 20%  $\text{MeOH/CHCl}_3$ ), and concentrated *in vacuo*. Purification by flash column

chromatography (SiO<sub>2</sub>, gradient elution: 0 to 10% MeOH/CHCl<sub>3</sub>) followed by precipitation from CHCl<sub>3</sub>/hexane afforded template **T4** (355 mg, 57%) as an off-white solid.

**<sup>1</sup>H NMR** (500 MHz, CDCl<sub>3</sub>, 298 K)  $\delta_{\text{H}}$  = 8.64–8.60 (m, 4H,  $\alpha_1$ ), 8.58–8.54 (m, 4H,  $\alpha_2$ ), 7.62 (s, 2H,  $\epsilon$ ), 7.50 (d,  $J$  = 8.4 Hz, 4H,  $\gamma_1$ ), 7.48–7.45 (m, 4H,  $\beta_1$ ), 7.39–7.36 (m, 4H,  $\beta_2$ ), 7.31 (d,  $J$  = 8.4 Hz, 4H,  $\gamma_2$ ), 7.27 (d,  $J$  = 8.4 Hz, 4H,  $\delta_1$ ), 7.00 (d,  $J$  = 8.4 Hz, 4H,  $\delta_2$ ) ppm. **<sup>13</sup>C NMR** (126 MHz, CDCl<sub>3</sub>, 298 K)  $\delta_{\text{C}}$  = 150.42, 150.35, 147.7, 147.6, 142.5, 140.8, 140.7, 139.8, 136.3, 135.5, 132.4, 130.7, 130.1, 126.5, 125.9, 121.5, 121.3 ppm. **HRMS** (ESI):  $m/z$  calcd for C<sub>50</sub>H<sub>35</sub>N<sub>4</sub><sup>+</sup> ([M+H]<sup>+</sup>) 691.2856, found 691.2856.

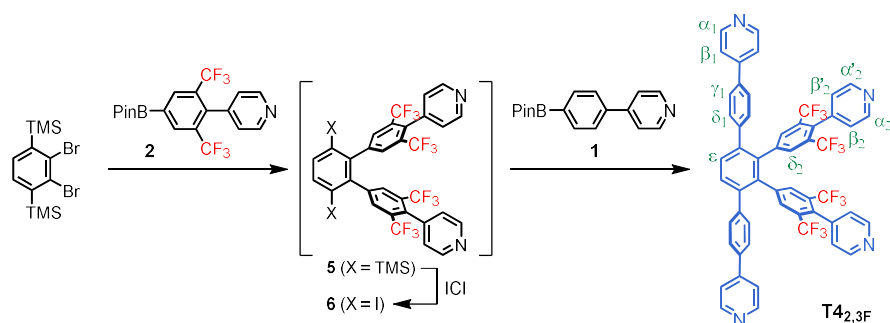
#### Template **T4**<sub>1,4F</sub>:



Step 1: A Schlenk flask charged with 1,4-bis(trimethylsilyl)-2,3-dibromobenzene (100 mg, 0.263 mmol), boronic acid ester **1** (185 mg, 0.657 mmol), K<sub>3</sub>PO<sub>4</sub> (335 mg, 1.58 mmol), and Pd(dppf)Cl<sub>2</sub>•CH<sub>2</sub>Cl<sub>2</sub> (21.5 mg, 0.026 mmol) in DMF (2.5 mL) and H<sub>2</sub>O (0.5 mL) was subjected to three freeze-pump-thaw cycles and heated to 90 °C. After stirring for 17 hours, the mixture was cooled to room temperature and filtered through a short pad of silica (eluent: 20% MeOH/CHCl<sub>3</sub>). The crude mixture was purified by flash column chromatography (SiO<sub>2</sub>, gradient elution: 1. 3/7 EtOAc/CHCl<sub>3</sub>, 2. 3% MeOH/CHCl<sub>3</sub>) to afford the bis-coupled product **3** (137 mg, 99%) as a pale, yellow solid containing minor impurities, presumably from desilylation. Step 2: The Suzuki-coupled product **3** (136 mg, 0.189 mmol) was dissolved in CH<sub>2</sub>Cl<sub>2</sub> (3 mL) and cooled using an ice-water bath. A solution of iodine monochloride (1.13 mL, 1.13 mmol, 1.0 M in CH<sub>2</sub>Cl<sub>2</sub>) was added dropwise and the resulting mixture was stirred for one hour at which point complete conversion was confirmed by TLC. The orange suspension was transferred to a separatory funnel containing a sat. aq. solution of Na<sub>2</sub>S<sub>2</sub>O<sub>7</sub> (100 mL) and CHCl<sub>3</sub> (100 mL). The phases were thoroughly mixed and the organic phase separated. The aqueous phase was extracted once more with CHCl<sub>3</sub> (50 mL) and the combined organic extracts were washed with brine (100 mL) and H<sub>2</sub>O (100 mL), dried over MgSO<sub>4</sub>, filtered, and concentrated *in vacuo*. Purification by flash column chromatography (SiO<sub>2</sub>, gradient elution: 0 to 5% MeOH/CHCl<sub>3</sub>) gave the doubly iodinated product **4** (127 mg, 78%) as a purple-grey solid containing minor impurities. Step 3: A Schlenk flask charged with doubly iodinated product **4** (60 mg, 0.094 mmol), boronic acid ester **2** (98 mg, 0.236 mmol), and K<sub>2</sub>CO<sub>3</sub> (78 mg, 0.566 mmol) in 1,4-dioxane (3 mL) and H<sub>2</sub>O (0.5 mL) was subjected to two freeze-pump-thaw cycles and while the mixture was still frozen, Pd(PPh<sub>3</sub>)<sub>4</sub> (27 mg, 0.024 mmol) was added, and three additional freeze-pump-thaw cycles were performed. The mixture was heated to 100 °C for 1.5 days, filtered through a short pad of silica (eluent: 15% MeOH/CHCl<sub>3</sub>), and concentrated under reduced pressure. Purification by flash column chromatography (SiO<sub>2</sub>, gradient elution: 0 to 7% MeOH/CHCl<sub>3</sub>) gave the title compound **T4**<sub>1,4F</sub> (62 mg, 68%) as a grey, off-white solid. Yield over 3 steps: 52%.

**<sup>1</sup>H NMR** (500 MHz, CDCl<sub>3</sub>)  $\delta_{\text{H}}$  = 8.66–8.62 (m, 4H,  $\alpha_1$ ), 8.62–8.59 (m, 4H,  $\alpha_2$ ), 7.76 (s, 2H,  $\epsilon_1$ ), 7.74 (s, 4H,  $\delta_1$ ), 7.39 (d,  $J$  = 8.2 Hz, 4H,  $\gamma_2$ ), 7.37–7.34 (m, 4H,  $\beta_2$ ), 7.15 (br d,  $J$  = 5.4 Hz, 4H,  $\beta_1$ ), 7.06 (d,  $J$  = 8.2 Hz, 4H,  $\delta_2$ ) ppm. **<sup>19</sup>F NMR** (470 MHz, CDCl<sub>3</sub>)  $\delta_{\text{F}}$  = –60.49 ppm (vs. C<sub>6</sub>F<sub>6</sub>,  $\delta_{\text{F}}$  = –164.80 ppm). **<sup>13</sup>C NMR** (126 MHz, CDCl<sub>3</sub>)  $\delta_{\text{C}}$  = 150.5, 148.9, 147.5, 142.3, 141.9, 140.7, 139.2, 139.1, 137.3, 135.3, 132.1, 130.62 (q,  $J_{\text{C-F}}$  = 5.6 Hz), 130.59 (q,  $J_{\text{C-F}}$  = 30.3 Hz), 130.1, 126.6, 124.9 (br s), 122.9 (q,  $J_{\text{C-F}}$  = 274.8 Hz), 121.5 ppm. **HRMS** (ESI):  $m/z$  calcd for C<sub>54</sub>H<sub>31</sub>N<sub>4</sub>F<sub>12</sub><sup>+</sup> ([M+H]<sup>+</sup>) 963.2352, found 963.2346.

# **Template T4<sub>2,3F</sub>:**



Step 1: A Schlenk flask charged with 1,4-bis(trimethylsilyl)-2,3-dibromobenzene (60 mg, 0.158 mmol), boronic acid ester **2** (165 mg, 0.394 mmol), K<sub>3</sub>PO<sub>4</sub> (201 mg, 0.947 mmol), and Pd(dppf)Cl<sub>2</sub>·CH<sub>2</sub>Cl<sub>2</sub> (12.9 mg, 0.016 mmol) in DMF (3.0 mL) and H<sub>2</sub>O (0.5 mL) was subjected to four freeze-pump-thaw cycles and heated to 90 °C. After stirring for 8.5 hours, the mixture was cooled to room temperature and filtered through a short pad of silica (eluent: 15% MeOH/CHCl<sub>3</sub>). The crude mixture was purified by flash column chromatography (SiO<sub>2</sub>, gradient elution: 10 to 20 to 30% EtOAc/toluene) to afford the bis-coupled product **5** (48 mg, 38%) as an off-white solid containing minor impurities, presumably from desilylation. Step 2: The Suzuki-coupled product **5** (48 mg, 0.060 mmol) was dissolved in CH<sub>2</sub>Cl<sub>2</sub> (2 mL) and cooled using an ice-water bath. A solution of iodine monochloride (1.8 mL, 1.8 mmol, 1.0 M in CH<sub>2</sub>Cl<sub>2</sub>) was added dropwise and the resulting mixture was stirred for three hours at which point complete conversion was confirmed by TLC. The mixture was diluted with CHCl<sub>3</sub> (50 mL) and washed with a sat. aq. solution of Na<sub>2</sub>S<sub>3</sub>O<sub>7</sub> (2 x 50 mL), brine (100 mL), and H<sub>2</sub>O (100 mL), dried over MgSO<sub>4</sub>, filtered, and concentrated under reduced pressure. Purification by flash column chromatography (SiO<sub>2</sub>, 3% MeOH/CHCl<sub>3</sub>) gave the doubly iodinated product **6** (51 mg, 94%) as an off-white solid containing minor impurities. Step 3: A Schlenk flask charged with doubly iodinated product **6** (51 mg, 0.056 mmol), boronic acid ester **1** (63 mg, 0.225 mmol), and K<sub>2</sub>CO<sub>3</sub> (93 mg, 0.674 mmol) in 1,4-dioxane (2 mL) and H<sub>2</sub>O (0.5 mL) was subjected to two freeze-pump-thaw cycles, and while the mixture was still frozen, Pd(PPh<sub>3</sub>)<sub>4</sub> (19.5 mg, 0.017 mmol) was added, and three additional freeze-pump-thaw cycles were performed. The mixture was heated to 100 °C for 1.5 days, filtered through a short pad of silica (eluent: 15% MeOH/CHCl<sub>3</sub>), and concentrated *in vacuo*. Purification by flash column chromatography (SiO<sub>2</sub>, gradient elution: 0 to 7% MeOH/CHCl<sub>3</sub>) followed by precipitation from CHCl<sub>3</sub>/hexane 1:1 gave the title compound T4<sub>2,3F</sub> (38 mg, 70%) as a white solid. Yield over 3 steps: 25%.

**<sup>1</sup>H NMR** (500 MHz, CDCl<sub>3</sub>) δ<sub>H</sub> = 8.71–8.65 (m, 4H, α<sub>1</sub>), 8.62 (br d, *J* = 3.8 Hz, 4H, α<sub>2</sub>/α'<sub>2</sub>), 7.77 (s, 2H, ε<sub>1</sub>), 7.62 (d, *J* = 8.3 Hz, 4H, γ<sub>1</sub>), 7.51–7.46 (m, 4H, β<sub>1</sub>), 7.41 (s, 4H, δ<sub>2</sub>), 7.31 (d, *J* = 8.3 Hz, 4H, δ<sub>1</sub>), 7.10 (br d, *J* = 3.8 Hz, 2H, β<sub>2</sub>/β'<sub>2</sub>), 6.96 (br d, *J* = 3.8 Hz, 2H, β<sub>2</sub>/β'<sub>2</sub>) ppm. **<sup>19</sup>F NMR** (470 MHz, CDCl<sub>3</sub>) δ<sub>F</sub> = –60.70 ppm (vs. C<sub>6</sub>F<sub>6</sub>, δ<sub>F</sub> = –164.80 ppm). **<sup>13</sup>C NMR** (126 MHz, CDCl<sub>3</sub>) δ<sub>C</sub> = 150.6, 149.1, 148.8, 147.5, 141.9, 141.2, 140.7, 140.4, 137.7, 137.3, 135.4, 132.6 (q, *J* = 5.0 Hz), 131.4, 130.7, 130.4 (q, *J* = 30.4 Hz), 127.2, 124.8, 124.6, 122.6 (q, *J* = 275.0 Hz), 121.7 ppm. **HRMS** (ESI): *m/z* calcd for C<sub>54</sub>H<sub>31</sub>N<sub>4</sub>F<sub>12</sub><sup>+</sup> ([M+H]<sup>+</sup>) 963.2352, found 963.2344.

Comparison of the analytical GPC traces for the synthesis of  $c\text{-P8}[\text{b}_6\text{f}_2]\cdot(\text{T4})_2$  and  $c\text{-P8}[\text{b}_8]\cdot(\text{T4})_2$

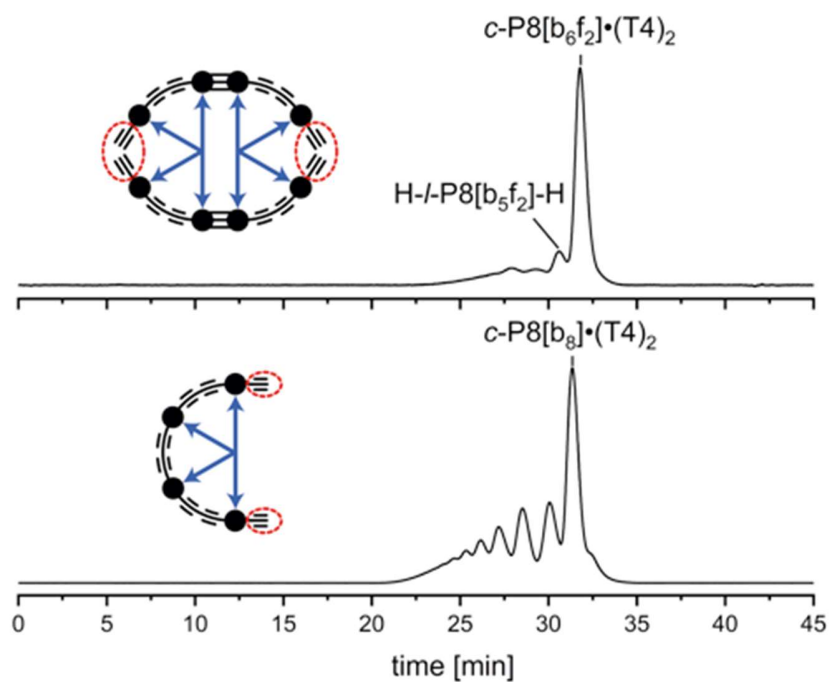


**Figure S4.** Comparison of the analytical GPC traces (THF + 1% pyridine,  $\lambda = 440$  nm) of the crude reaction mixtures for the synthesis of  $c\text{-P8}[\text{b}_6\text{f}_2]\cdot(\text{T4})_2$  (top) and  $c\text{-P8}[\text{b}_8]\cdot(\text{T4})_2$  (bottom). Cartoon inserts show the preorganized complexes ( $\text{H-/-P4}[\text{b}_2\text{f}_1]_2\cdot(\text{T4})_2$  (top) and ( $\text{H-/-P4}[\text{b}_3]\cdot(\text{T4})$  (bottom) directing the synthesis of  $c\text{-P8}[\text{b}_6\text{f}_2]\cdot(\text{T4})_2$  and  $c\text{-P8}[\text{b}_8]\cdot(\text{T4})_2$ , respectively.

## 4. $^1\text{H}$ NMR Assignment of Rings and Complexes

### Fused ring systems

A summary of the most important correlations used to assign fused ring **c-P8[b<sub>6</sub>f<sub>2</sub>]** and its complexes **c-P8[b<sub>6</sub>f<sub>2</sub>](T4)<sub>2</sub>**, **c-P8[b<sub>6</sub>f<sub>2</sub>](T4<sub>1,4F</sub>)<sub>2</sub>**, and **c-P8[b<sub>6</sub>f<sub>2</sub>](T4<sub>2,3F</sub>)<sub>2</sub>** is given in **Figure S5**. Please confer **Tables S17**, **S15**, **S18**, and **S19** for the complete list of NMR correlations.

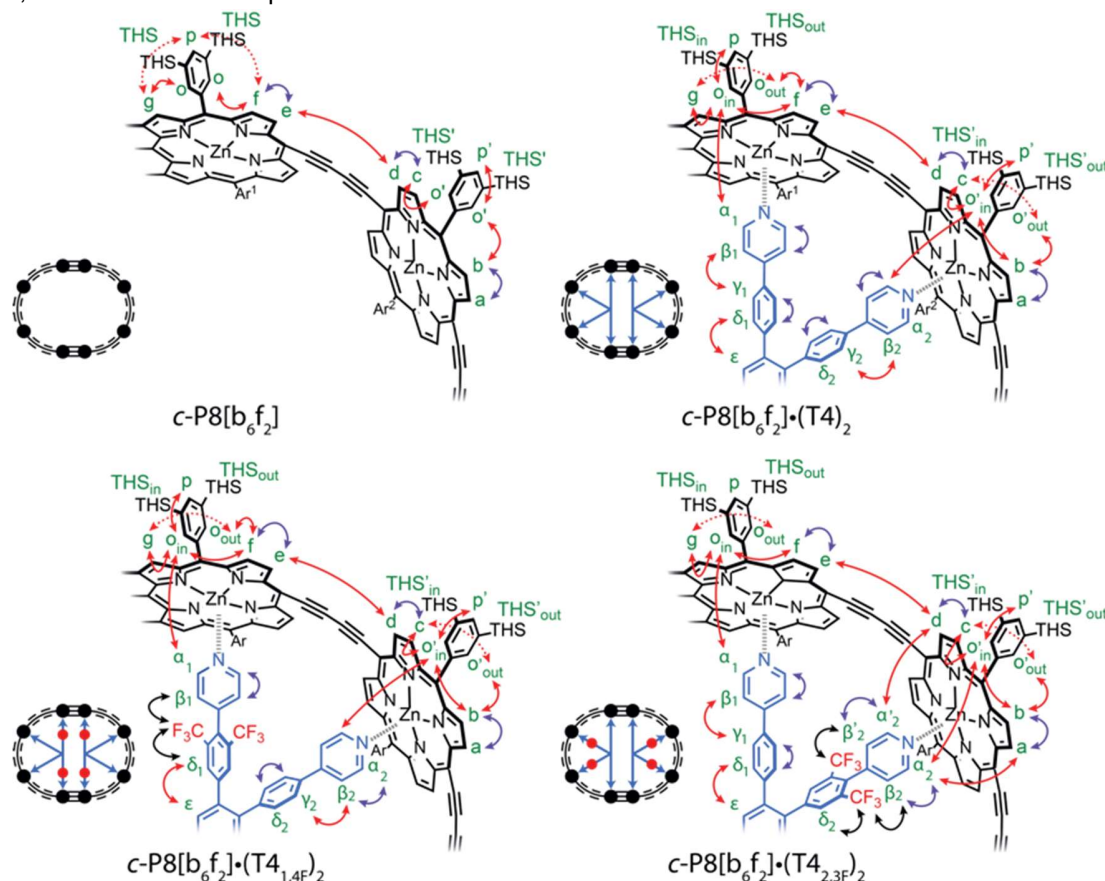


**Figure S5.** A summary of key NOESY (red arrows), COSY (purple arrows), and 1D  $^1\text{H}$ - $^{19}\text{F}$  HOESY (black arrows) correlations used in the assignment of all fused ring systems.

Template resonances in complexes **c-P8[b<sub>6</sub>f<sub>2</sub>](T4)<sub>2</sub>**, **c-P8[b<sub>6</sub>f<sub>2</sub>](T4<sub>1,4F</sub>)<sub>2</sub>**, and **c-P8[b<sub>6</sub>f<sub>2</sub>](T4<sub>2,3F</sub>)<sub>2</sub>** can be assigned based on NOESY, COSY, and 1D  $^1\text{H}$ - $^{19}\text{F}$  HOESY correlations. The  $\epsilon$  resonance is the only signal expected to present as a singlet corresponding to 4H, and thus constitutes a reasonable starting point for the assignment. Correlations between adjacent phenylene/pyridyl rings are mainly established by NOESY (and to a minor extent HOESY), while COSY gives the correlations within each of these rings. In complexes **c-P8[b<sub>6</sub>f<sub>2</sub>](T4<sub>1,4F</sub>)<sub>2</sub>** and **c-P8[b<sub>6</sub>f<sub>2</sub>](T4<sub>2,3F</sub>)<sub>2</sub>**, with fluorinated templates, 1D  $^1\text{H}$ - $^{19}\text{F}$  HOESY provides the  $\delta_1$  and  $\beta_1$  resonances, as these exhibit the most intense and second most intense correlations, respectively, to the  $\text{CF}_3$  groups. In addition, for complex **c-P8[b<sub>6</sub>f<sub>2</sub>](T4<sub>2,3F</sub>)<sub>2</sub>**, the difference in signal intensity between proton signals  $\beta_2$  and  $\beta'_2$  in HOESY, provides a way of distinguishing these resonances. With the rotation being restricted about the fluorinated leg, on average,  $\beta_2$  is closer than  $\beta'_2$  to the  $\text{CF}_3$  groups in the neighboring leg, and consequently, the  $\beta_2$  resonance experiences a greater hOe than  $\beta'_2$  (**Figure S6**).

The inner ortho resonances of the aryl sidechains,  $\text{o}_{\text{in}}$  and  $\text{o}'_{\text{in}}$ , are identified based on their NOESY correlations to the nearest pyridyl protons ( $\alpha$  and  $\beta$ ). From there on, NOESY allows identification of the outer ortho protons,  $\text{o}_{\text{out}}$  and  $\text{o}'_{\text{out}}$ , as these, aside from  $\text{o}_{\text{in}}$  and  $\text{o}'_{\text{in}}$ , are the only aryl side chain resonances, with strong nOe correlations to porphyrin protons. The para resonances can be identified based on their NOESY correlations to



the inner or outer ortho resonances within the respective aryl ring taken together with their weaker correlations to resonances within the nearest porphyrin unit.

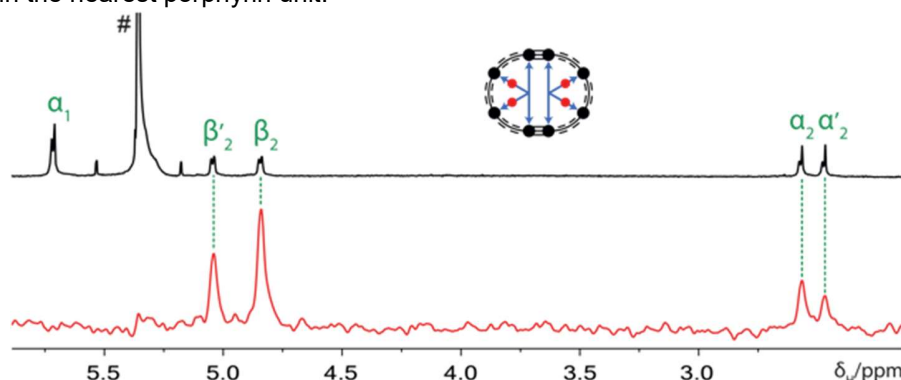


**Figure S6.** Region of  $^1\text{H}$  (top) and 1D  $^1\text{H}$ - $^{19}\text{F}$  HOESY (bottom, red) spectra of complex **c-P8[b<sub>6</sub>f<sub>2</sub>]•(T<sub>42,3F</sub>)<sub>2</sub>** recorded in  $\text{CD}_2\text{Cl}_2$ . The differences in hOe intensities are used to assign alpha and beta resonances in the fluorinated leg of the template. Peak assigned with # arise from  $\text{CHCl}_3$ .

Porphyrin resonances of the tape unit can be distinguished from resonances of the all butadiyne-linked porphyrin unit based on chemical shift differences. In these systems, the tape resonances are in all cases located at lower chemical shift values than those of the all-butadiyne linked porphyrin unit, decreasing from resonance e to f to g in the tape porphyrin (**Figure S7**). In addition, tape resonance g is readily identified, as it is the only porphyrin proton expected to yield a singlet in the  $^1\text{H}$  spectrum. Starting from g, the tape and all-butadiyne linked porphyrin resonances are assigned using NOESY and COSY correlations. The NOESY correlation across the butadiyne link between e and d allows for the distinction between resonances a/d and b/c within the all-butadiyne linked porphyrin unit. Due to splitting of the alpha protons in complex **c-P8[b<sub>6</sub>f<sub>2</sub>]•(T<sub>42,3F</sub>)<sub>2</sub>**, differentiation between a/d and b/c is further supported by nOe correlations between a and  $\alpha_2$  and between d and  $\alpha'_2$ .

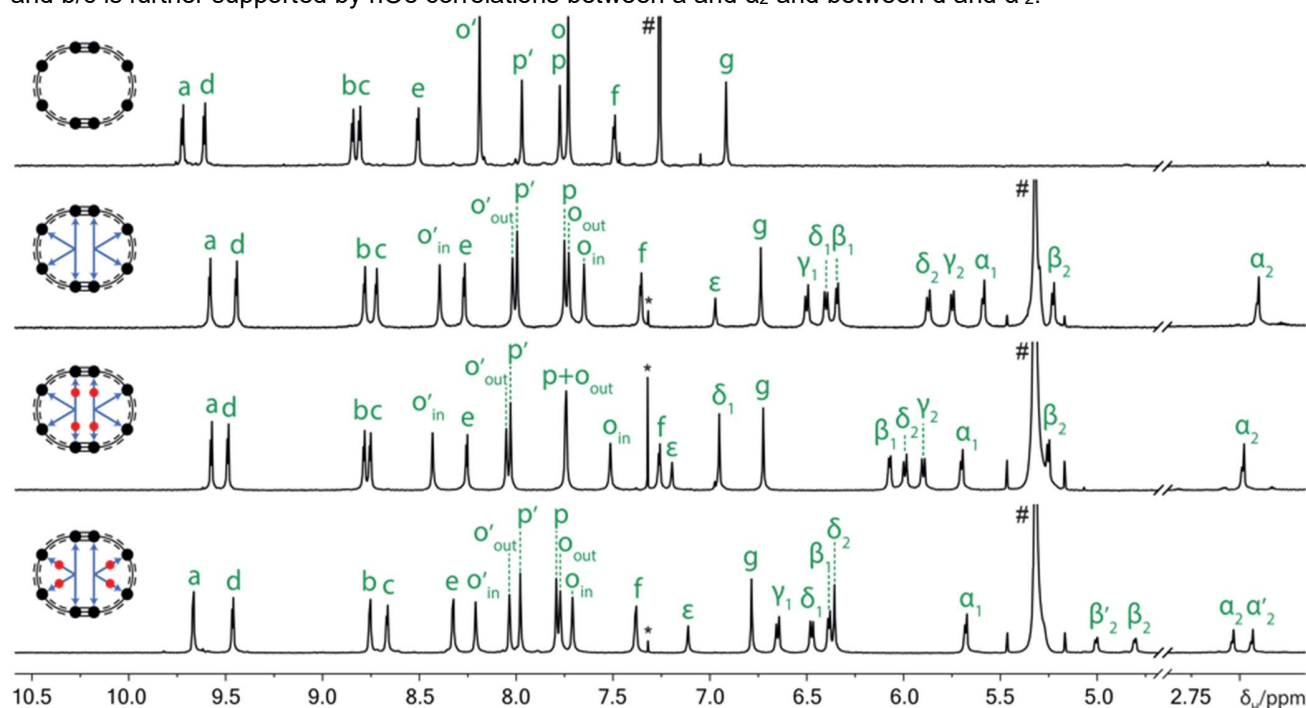


**Figure S7.** Assigned  $^1\text{H}$  spectra of **c-P8[b<sub>6</sub>f<sub>2</sub>]**, **c-P8[b<sub>6</sub>f<sub>2</sub>]•(T<sub>4</sub>)<sub>2</sub>**, **c-P8[b<sub>6</sub>f<sub>2</sub>]•(T<sub>41,4F</sub>)<sub>2</sub>**, and **c-P8[b<sub>6</sub>f<sub>2</sub>]•(T<sub>42,3F</sub>)<sub>2</sub>** from top to bottom recorded in  $\text{CDCl}_3$  for **c-P8[b<sub>6</sub>f<sub>2</sub>]** and  $\text{CD}_2\text{Cl}_2$  for the template complexes. The THS signals at ca.  $\delta_{\text{H}} = 1.7\text{--}0.5$  ppm are omitted for clarity. Peaks assigned with # and \* arise from  $\text{CHCl}_3$  (**c-P8[b<sub>6</sub>f<sub>2</sub>]**) or  $\text{CHDCl}_2$  (**c-P8[b<sub>6</sub>f<sub>2</sub>]** complexes) and neutral thianthrene, respectively.



### All-butadiyne linked ring systems

A summary of the most important correlations used to assign all-butadiyne linked ring complexes **c-P8[b<sub>8</sub>](T4)<sub>2</sub>**, **c-P8[b<sub>8</sub>](T4<sub>1,4F</sub>)<sub>2</sub>**, and **c-P8[b<sub>8</sub>](T4<sub>2,3F</sub>)<sub>2</sub>** is given in **Figure S8**. Please confer **Table S20**, **S21**, and **S22** for the complete list of NMR correlations.

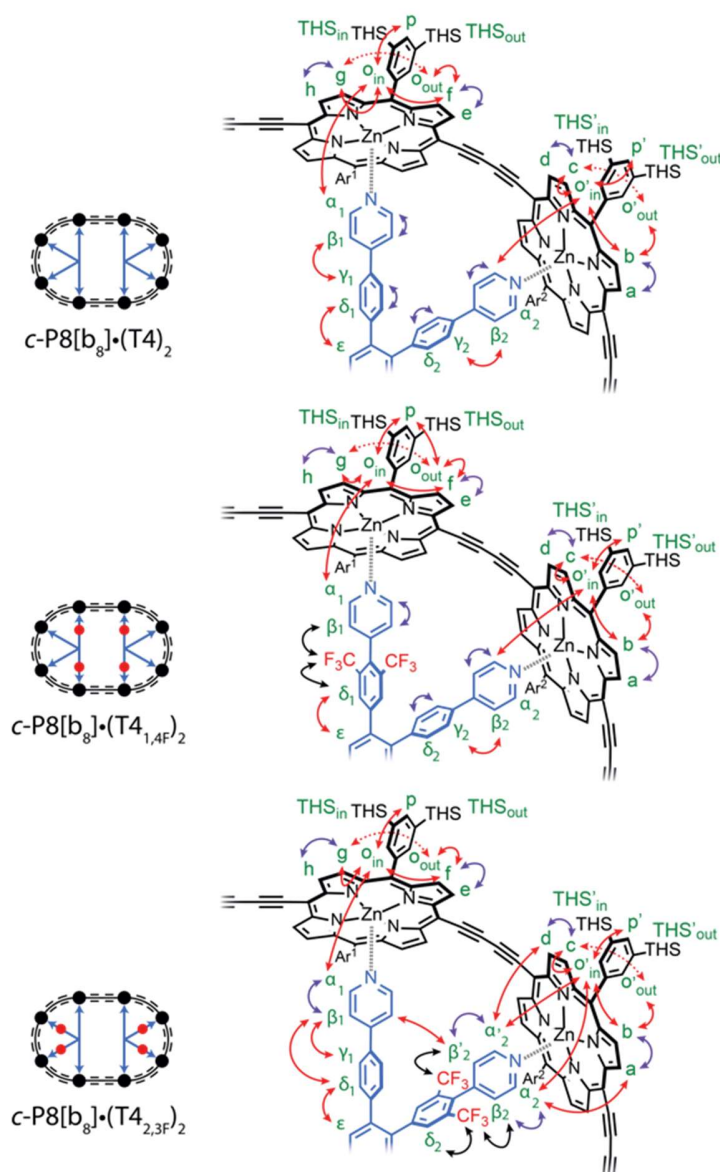


**Figure S8.** A summary of key NOESY (red arrows), COSY (purple arrows), and 1D <sup>1</sup>H-<sup>19</sup>F HOESY (black arrows) correlations used in the assignment of all-butadiyne linked complexes.

The <sup>1</sup>H assignment of the butadiyne linked complexes is analogous to the approach described for the fused ring systems. Similarly, the ε resonance is a good starting point, as it is the only proton expected to result in a singlet corresponding to 4H. From ε, the template resonances are assigned based on NOESY and COSY correlations, as well as 1D <sup>1</sup>H-<sup>19</sup>F HOESY in the case of fluorinated complexes **c-P8[b<sub>8</sub>](T4<sub>1,4F</sub>)<sub>2</sub>**, and **c-P8[b<sub>8</sub>](T4<sub>2,3F</sub>)<sub>2</sub>**. The δ and β resonances within the same leg as the CF<sub>3</sub> groups are readily identified via HOESY, given that these two resonances experience the most and second most intense hOes, respectively. For the fluorinated complex **c-P8[b<sub>8</sub>](T4<sub>2,3F</sub>)<sub>2</sub>**, the split alpha and beta resonances are also assigned using HOESY, once again by consideration of their relative differences in signal intensity (**Figure S9**). In addition, this assignment is supported by a weak NOESY correlation between beta resonances (β'<sub>2</sub> and β<sub>1</sub>) in different template legs (**Figure S10**).

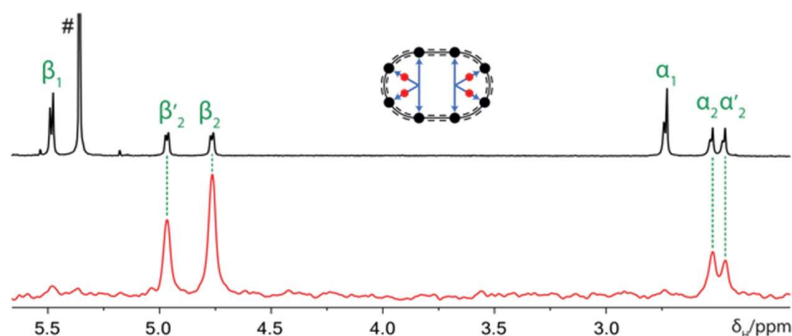


**Figure S9.** Region of  $^1\text{H}$  (top) and 1D  $^1\text{H}$ - $^{19}\text{F}$  HOESY (bottom, red) spectra of complex **c-P8[b<sub>8</sub>](T<sub>42,3F</sub>)<sub>2</sub>** recorded in  $\text{CD}_2\text{Cl}_2$ . The differences in signal intensities in HOESY are used to assign alpha and beta resonances in the fluorinated leg of the template. Peak assigned with # arise from  $\text{CHDCl}_2$ .

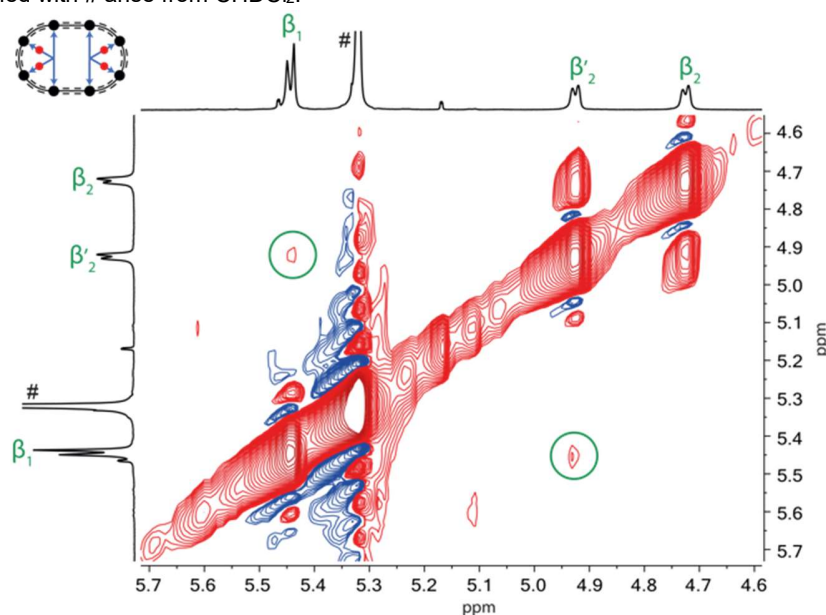


**Figure S10.** Region of the NOESY spectrum of complex **c-P8[b<sub>8</sub>](T<sub>42,3F</sub>)<sub>2</sub>** recorded in  $\text{CD}_2\text{Cl}_2$ . The weak correlation (circled) between resonances  $\beta_1$  and  $\beta'_2$  is used to assign the split beta protons in the fluorinated leg. Peaks assigned with # arise from  $\text{CHDCl}_2$ .

The inner ortho protons,  $\text{o}_{\text{in}}$  and  $\text{o}'_{\text{in}}$ , are identified based on their NOESY correlations to the closest pyridyl protons (alpha and beta). All the aryl side chain resonances correlate by NOESY within the same aryl ring, and both types of ortho resonances exhibit strong NOESY correlations to porphyrin resonances, whereas the para resonances do not. This allows for the assignment of outer ortho and para resonances.

The porphyrin resonances are identified, as to which of the two porphyrin units they belong to, based on their NOESY correlations to both the nearest template pyridyl protons and side chain ortho protons. Also used, the characteristic chemical shift feature of butadiyne-linked porphyrins being that the porphyrin protons closest to the acetylenes are at higher  $\delta_{\text{H}}$  (usually ca. 10–9.5 ppm) compared to the protons sitting next to the aryl side group (usually ca. 9.0–8.5 ppm).

For complexes **c-P8[b<sub>8</sub>](T<sub>4</sub>)<sub>2</sub>** and **c-P8[b<sub>8</sub>](T<sub>41,4F</sub>)<sub>2</sub>**, it is not possible to distinguish resonances of the same porphyrin unit that correspond to protons on directly opposite sides of the aryl side group. Hence, the proton couples: a/d, e/h, b/c, and f/g cannot be distinguished. The NOESY correlation between resonances d and e that would allow this distinction is absent in these complexes; likely due to the close spacing of the porphyrin signals. For complex **c-P8[b<sub>8</sub>](T<sub>42,3F</sub>)<sub>2</sub>**, the split template alpha and beta resonances offers a way of telling the porphyrin sides apart. Thereby, the porphyrin resonances of the unit closest to the fluorinated leg can be resolved via the

NOESY correlations between a and  $\alpha_2$  and between d and  $\alpha'_2$ . The assigned spectra are shown below (**Figure S11**).

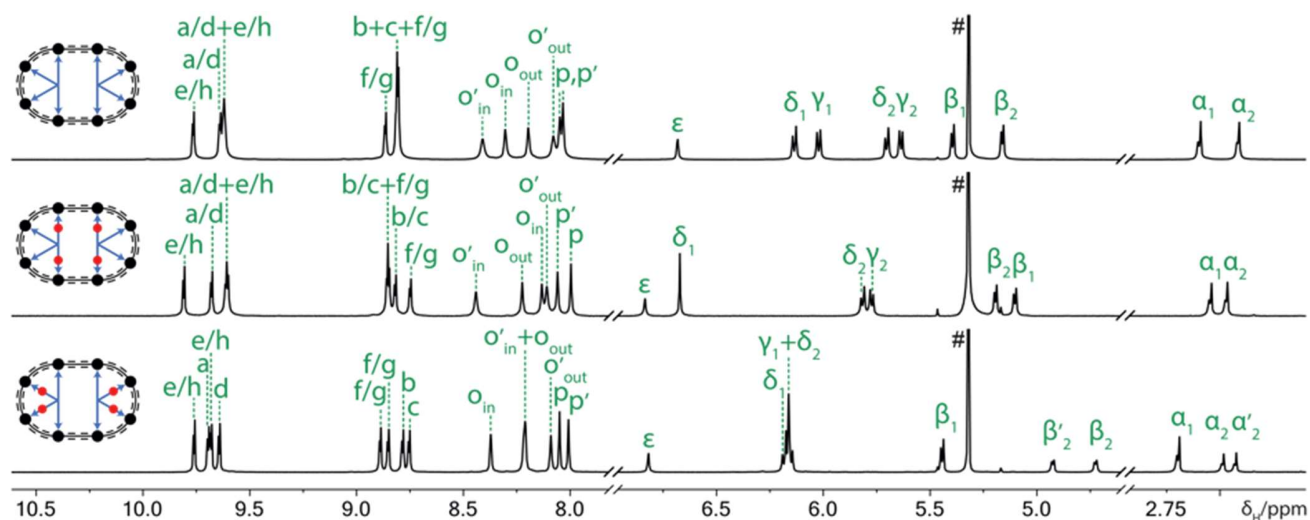
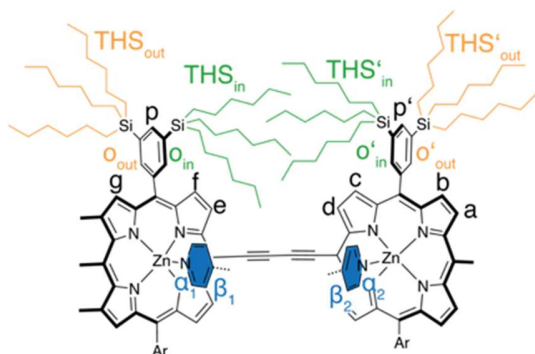


**Figure S11.** Assigned  $^1\text{H}$  spectra of **c-P8[b8]•(T4)<sub>2</sub>**, **c-P8[b8]•(T4<sub>1,4F</sub>)<sub>2</sub>**, and **c-P8[b8]•(T4<sub>2,3F</sub>)<sub>2</sub>** from top to bottom recorded in  $\text{CD}_2\text{Cl}_2$ . The THS signals at ca.  $\delta_{\text{H}} = 1.7\text{--}0.5$  ppm are omitted for clarity. Peaks assigned with # arise from  $\text{CHDCl}_2$ .

## 5. Analysis of Global Ring Currents



The presence and character of a global ring current around the circumference of a porphyrin nanoring complex is established based on the induced chemical shift differences of resonances inside and outside the ring. The induced magnetic field lines are focused towards the center of the ring and consequently, resonances located within the circumference of the ring will be affected to a larger extent by a global current than resonances located on the outside. The porphyrin ring complexes investigated in this work possess three distinct chemical shift environments within the circumference of the ring: 1) being the template resonances, in particular the  $\alpha_{1/2}$  and  $\beta_{1/2}$  protons on

the pyridyl groups facing the porphyrin units and the  $\text{CF}_3$  groups in the fluorinated templates; 2) the inner trihexylsilyl protons,  $\text{THS}^{(\text{i})}_{\text{in}}$  on the aryl residues; and 3) the inner *ortho* protons,  $\text{o}^{(\text{i})}_{\text{in}}$ , in the aryl residues. The second set of trihexylsilyl protons,  $\text{THS}^{(\text{o})}_{\text{out}}$  and *ortho* resonances,  $\text{o}^{(\text{o})}_{\text{out}}$  are pointing towards the outside of the porphyrin ring. The remaining porphyrin *beta* protons a, b, c, d, e, f, g, and – in the case of all butadiyne linked complexes – h, and the *para*-aryl protons  $\text{p}^{(\text{i})}$  are located on the circumference of the ring and will thus only experience small chemical shift differences resulting from an induced global ring current.

A combination of COSY, NOESY, and 1D  $^1\text{H}$ - $^{19}\text{F}$  HOESY experiments were used to partially assign and identify key resonances in the spectra of each oxidation state corresponding to **c-P8[b<sub>6</sub>f<sub>2</sub>](T4)<sub>2</sub>**, **c-P8[b<sub>6</sub>f<sub>2</sub>](T4<sub>1,4F</sub>)<sub>2</sub>**, and **c-P8[b<sub>6</sub>f<sub>2</sub>](T4<sub>2,3F</sub>)<sub>2</sub>** (Figures S13–S15). The key resonances in the spectra of the oxidized complexes of **c-P8[b<sub>8</sub>](T4<sub>1,4F</sub>)<sub>2</sub>** and **c-P8[b<sub>8</sub>](T4<sub>2,3F</sub>)<sub>2</sub>** were assigned based on the reported assignment of an analogous complex, **c-P8[b<sub>8</sub>](T4)<sub>2</sub>** (Figures S16 + S17).<sup>4</sup>

The inner and outer THS resonances in the region between 4 and –3 ppm can be distinguished based on their chemical shift differences in all oxidation states. The inner THS resonances,  $\text{THS}^{(\text{i})}_{\text{in}}$ , are significantly affected by oxidation and an induced ring current, and are thus identified as the multiplet of protons which shifts upon oxidation. On the other hand, the outer THS resonances,  $\text{THS}^{(\text{o})}_{\text{out}}$ , remain almost at identical chemical shift in all oxidation states. This assignment is further supported by NOESY and 1D  $^1\text{H}$ - $^{19}\text{F}$  HOESY correlations of template resonances to the  $\text{THS}^{(\text{i})}_{\text{in}}$  resonances, whereas none are observed to the outer,  $\text{THS}^{(\text{o})}_{\text{out}}$  resonances (Figure S12). No HSQC correlations between the template and inner THS resonances were observed in **c-P8[b<sub>6</sub>f<sub>2</sub>](T4)<sub>2</sub>**, **c-P8[b<sub>6</sub>f<sub>2</sub>](T4<sub>1,4F</sub>)<sub>2</sub>**, and **c-P8[b<sub>6</sub>f<sub>2</sub>](T4<sub>2,3F</sub>)<sub>2</sub>** despite the use of long acquisition times (up to 8 hours). Given a proton line-width dependency of the HSQC experiment, this may be ascribed to signal broadening effects from the presence of open-shell species, existing between the endpoints of the oxidative titration.

Due to the similar chemical structures of complexes **c-P8[b<sub>6</sub>f<sub>2</sub>](T4)<sub>2</sub>**, **c-P8[b<sub>6</sub>f<sub>2</sub>](T4<sub>1,4F</sub>)<sub>2</sub>**, and **c-P8[b<sub>6</sub>f<sub>2</sub>](T4<sub>2,3F</sub>)<sub>2</sub>**, we employed a cross-assignment approach for identifying resonances in each oxidation state: In the first step, resonances of the individual nanoring complex were assigned based on the respective 2D NMR experiments. Then, the assigned spectra of the three different complexes in each oxidation states were correlated, and the findings summarized in an overall assignment of the proton spectra of **c-P8[b<sub>6</sub>f<sub>2</sub>](T4)<sub>2</sub>** (Figures S18–S20). Cross-assignment of the template resonances was directed by the correlation of the  $\alpha_1$  and  $\alpha_2$  resonances as they experience little change in their immediate chemical environment within templates of different fluorination patterns. The individual assignment of the non-fluorinated complex **c-P8[b<sub>6</sub>f<sub>2</sub>](T4)<sub>2</sub>** was based on NOESY spectra of the +4 and +6 oxidation states and a combination of NOESY and COSY experiments in the +8 state. In the assignment of complexes **c-P8[b<sub>6</sub>f<sub>2</sub>](T4<sub>1,4F</sub>)<sub>2</sub>**, and **c-P8[b<sub>6</sub>f<sub>2</sub>](T4<sub>2,3F</sub>)<sub>2</sub>**, we exploited the additional information of the fluorine probes by recording 1D  $^1\text{H}$ - $^{19}\text{F}$  HOESY spectra of the +4 and +6 oxidation states and a combination of NOESY, COSY, and 1D  $^1\text{H}$ - $^{19}\text{F}$  HOESY experiments in the +8 state. Template resonances could be readily identified via HOESY given that the  $\delta$  and  $\beta$  resonances within the same

leg as the CF<sub>3</sub> groups experience the most and second most intense hOes, respectively followed by the β and α resonances. NOESY and COSY experiments highlighted the correlations within the template and beta porphyrin regions, and in the case of NOESY experiments, also correlations between the template and the porphyrin resonances.

In some cases, not all resonances could be unambiguously assigned, even after substantially extending the number of scans. These resonances have not been labeled in the different spectra.

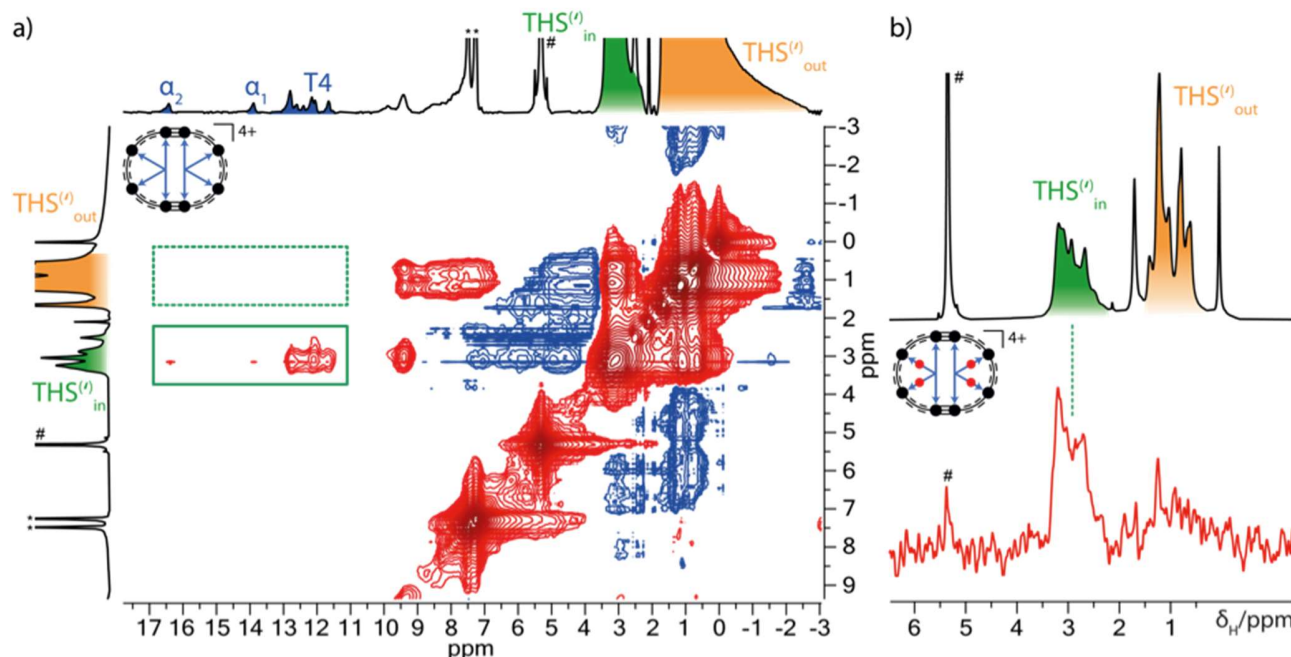


**Figure S12.** Representative regions of the <sup>1</sup>H-<sup>1</sup>H NOESY spectrum of **c-P8[b<sub>6</sub>f<sub>2</sub>]•(T<sub>4</sub>)<sub>2</sub><sup>4+</sup>** in CD<sub>2</sub>Cl<sub>2</sub> at 223 K (a) and the 1D <sup>1</sup>H-<sup>19</sup>F HOESY spectrum of **c-P8[b<sub>6</sub>f<sub>2</sub>]•(T<sub>4,3F</sub>)<sub>2</sub><sup>4+</sup>** in CD<sub>2</sub>Cl<sub>2</sub> at 223 K (b), highlighting the correlations between the inner THS (THS<sup>(i)</sup><sub>in</sub>) and template resonances. Peaks assigned with # and \* arise from CHDCl<sub>2</sub> and neutral thianthrene, respectively.

### Use of chemical shift differences as a measure for relative ring current strengths

i) Following the Biot-Savart law<sup>11</sup> and the NMR Larmor frequency definition, a direct relation between the chemical shift difference ( $\Delta\delta$ ) and the (anti)aromatic ring current ( $I$ ) can be established. The Biot-Savart law describes the magnetic field  $B$  at a point in space generated by a constant flowing current  $I$  as:

$$dB = \frac{\mu_0}{4\pi} I \frac{r \times dl}{r^3}, \quad (1)$$

where  $\mu_0$  is the magnetic constant,  $r$  is the distance from the electric circuit element to the point, and  $dl$  is a small length element of the circuit. In the simplified case of a circular current loop with radius  $a$ , the solution to this differential equation reveals that the magnetic field at the center of the ring,  $B_C$ , is given as:

$$B_C = \frac{\mu_0 I}{2a}, \quad (2)$$

which serves to highlight the directly proportional relationship between ring current  $I$  and its induced magnetic field  $B$ .

ii) The Larmor frequency  $\nu$  of a nucleus is directly proportional to the effective magnetic field strength experienced by that nucleus. The magnetic field contribution stemming from a nearby ring current,  $B_{RC}$ , may be isolated as a frequency difference  $\Delta\nu$ , assuming two states of that nucleus can be defined, one in which a ring current is on and the other one, where it is off:

$$\Delta\nu = \nu_{on} - \nu_{off} = \frac{\gamma}{2\pi} B_{RC}, \quad (3)$$

Differences in the Larmor frequency are directly translated into the experimentally observed chemical shift differences according to:

$$\Delta\delta = 10^6 \frac{\gamma}{2\pi\nu_{Inst}} B_{RC}, \quad (4)$$

where  $\nu_{Inst}$  denotes the operating frequency of the NMR instrument.

iii) In our analysis, we use the probe nuclei from templates ( $\alpha$  and  $CF_3$  resonances) and the inner THS chains to infer changes in ring current from changes in their chemical shifts. We define the chemical shift difference,  $\Delta\delta$ , as the shift difference between a state affected by the ring current and one which is not. In case of template probes, shifts corresponding to unbound template are used in order to subtract magnetic contributions inherent to the template. In case of the inner THS probe, the shift of the outer THS resonances are used to subtract magnetic contributions independent of the induced ring current.

$$\Delta\delta(template) = \delta_{Bound} - \delta_{Unbound}, \quad (5)$$

$$\Delta\delta(THS) = \delta_{THS,inner} - \delta_{THS,outer}, \quad (6)$$

According to this definition, positive chemical shift differences correspond to a paratropic ring current and an antiaromatic character, whereas negative chemical shift differences correspond to a diatropic ring current and global aromatic character of the porphyrin nanoring.

iv) The chemical shift difference ratio can be used to compare ring currents between different nanoring complexes. To compare the relative ring current strength of a partially fused nanoring complex **c-P8[b<sub>6</sub>f<sub>2</sub>](T<sub>4<sub>X,Y</sub>F)<sub>2</sub></sub>** and an all-butadiyne linked nanoring complex **c-P8[b<sub>8</sub>](T<sub>4<sub>X,Y</sub>F)<sub>2</sub></sub>**, we use their relative shift ratio,  $\varphi$ , which we define as:

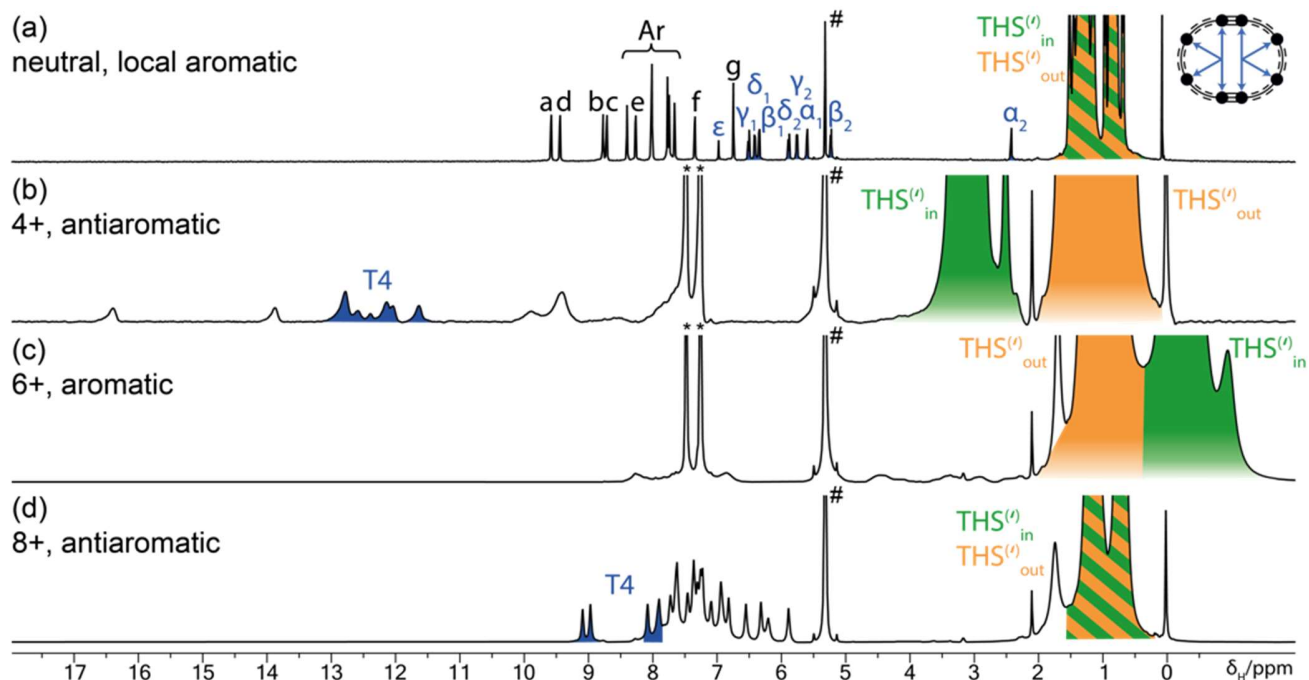
$$\varphi = \frac{\Delta\delta_{X,Y}(c-P8[b_6f_2](T_{4X,Y}F)_2)}{\Delta\delta_{X,Y}(c-P8[b_8](T_{4X,Y}F)_2)}, \quad (7)$$

with X,Y denoting either a 1,4 or 2,3 substitution pattern corresponding to the two fluorinated templates.

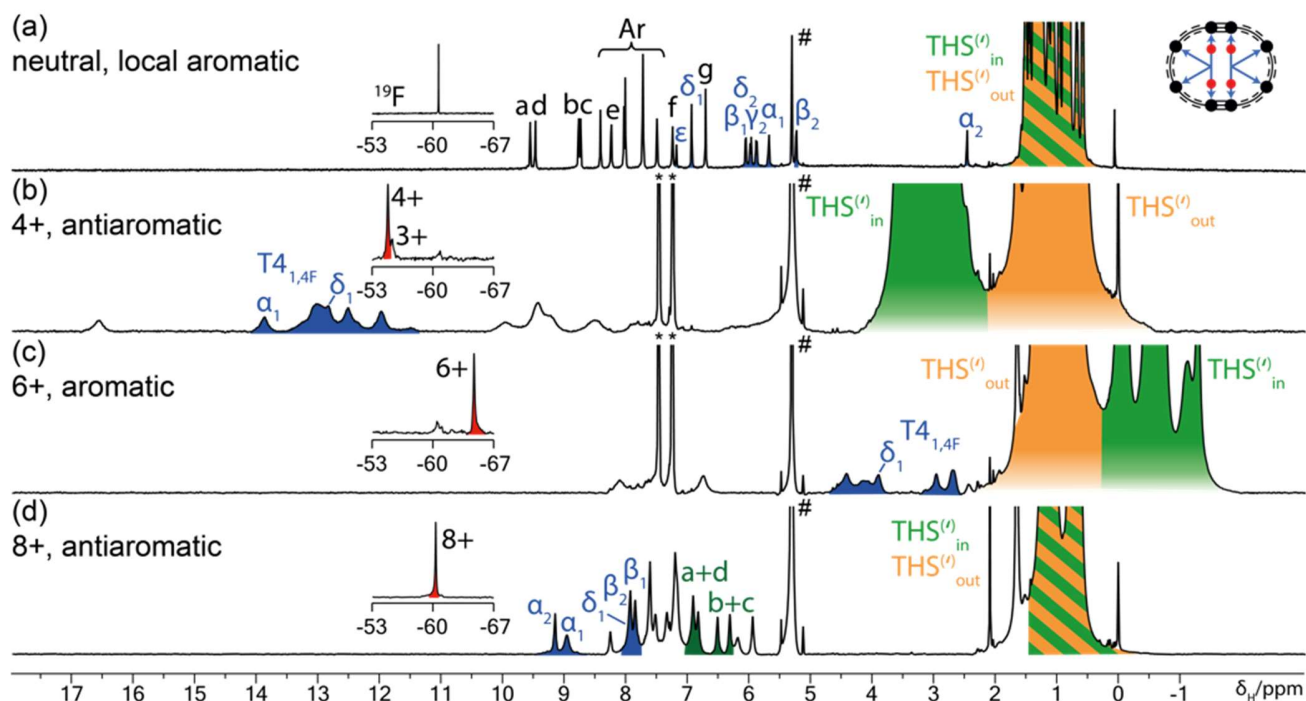
From comparison of the relative shift ratio  $\varphi$  of complexes with the same fluorination pattern, we were able to establish how the relative ring current strengths change through the oxidation states. Comparison of  $\varphi$  of complexes with different fluorination patterns in the same oxidation state allowed us to establish the global nature of the induced magnetic effects.



## 6. Overview of NMR Spectra of Nanoring Complexes



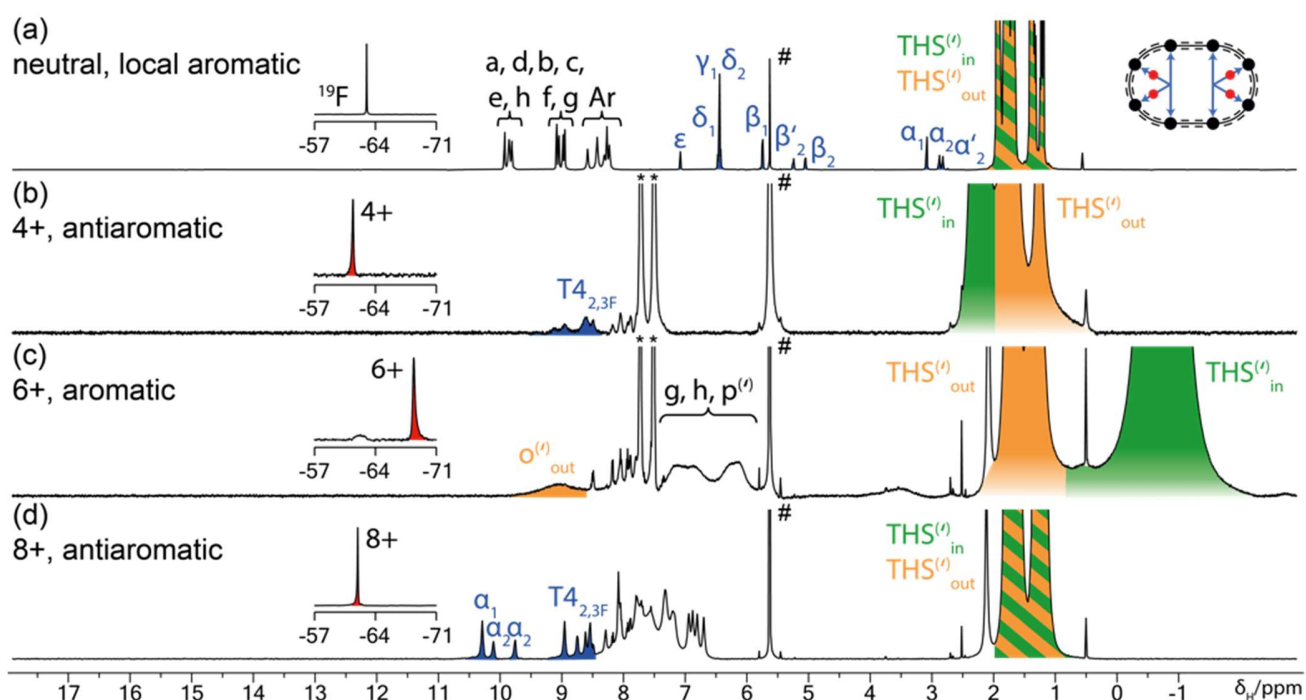
**Figure S13.** Summary of  $^1\text{H}$  NMR (500 MHz,  $\text{CD}_2\text{Cl}_2$ ) spectra of neutral (a, 298 K) and oxidized (b–d, 223 K)  $\text{c-P8}[\text{b}_6\text{f}_2]\cdot(\text{T4})_2$  generated by titration with  $\text{Thn}^+$ . Refer to **Figure S1** for labeling scheme. Peaks assigned with # and \* arise from  $\text{CH}_2\text{Cl}_2$  and neutral thianthrene, respectively. Unlabeled resonances were not unambiguously assigned.



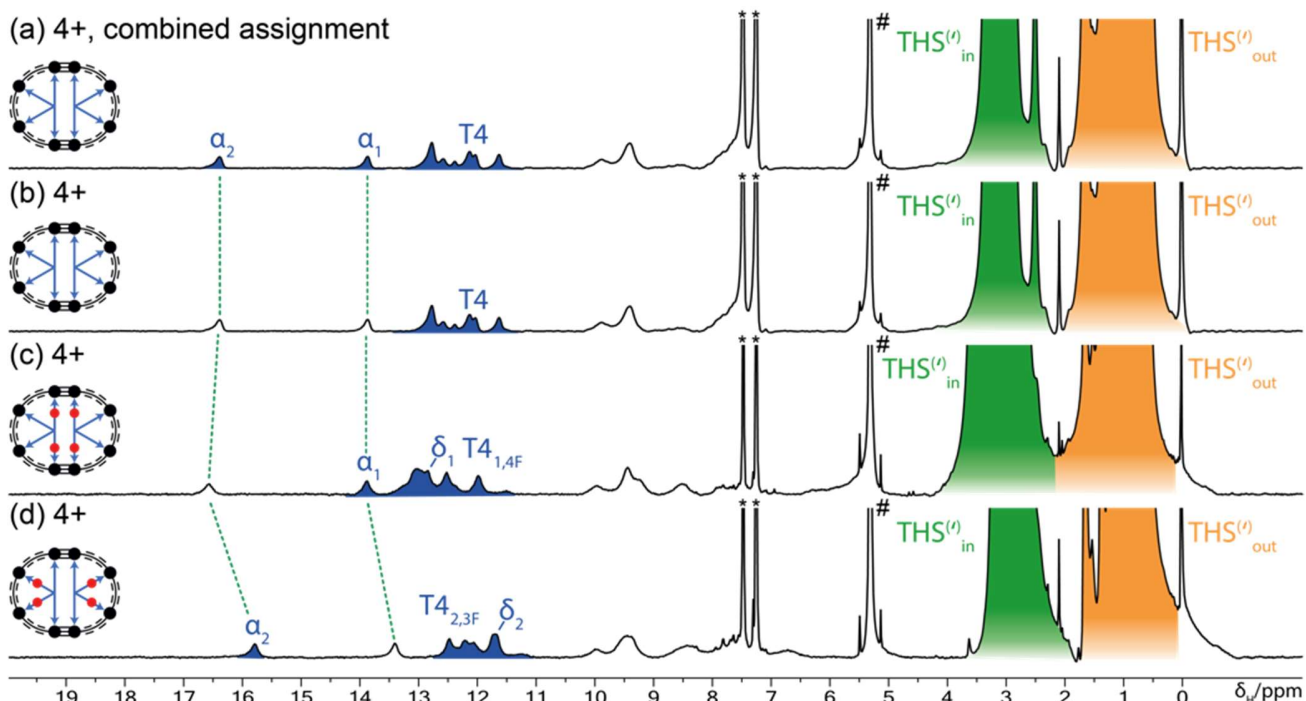
**Figure S14.** Summary of  $^1\text{H}$  NMR (500 MHz,  $\text{CD}_2\text{Cl}_2$ ) spectra of neutral (a, 298 K) and oxidized (b–d, 223 K)  $\text{c-P8}[\text{b}_6\text{f}_2]\cdot(\text{T4}_{1,4\text{F}})_2$  generated by titration with  $\text{Thn}^+$ . Inserts show concomitantly recorded  $^{19}\text{F}$  NMR (471 MHz,  $\text{CD}_2\text{Cl}_2$ ) spectra of the  $\text{CF}_3$  probes. Refer to **Figure S1** for labeling scheme. Peaks assigned with # and \* arise from  $\text{CH}_2\text{Cl}_2$  and neutral thianthrene, respectively. Unlabeled resonances were not unambiguously assigned.



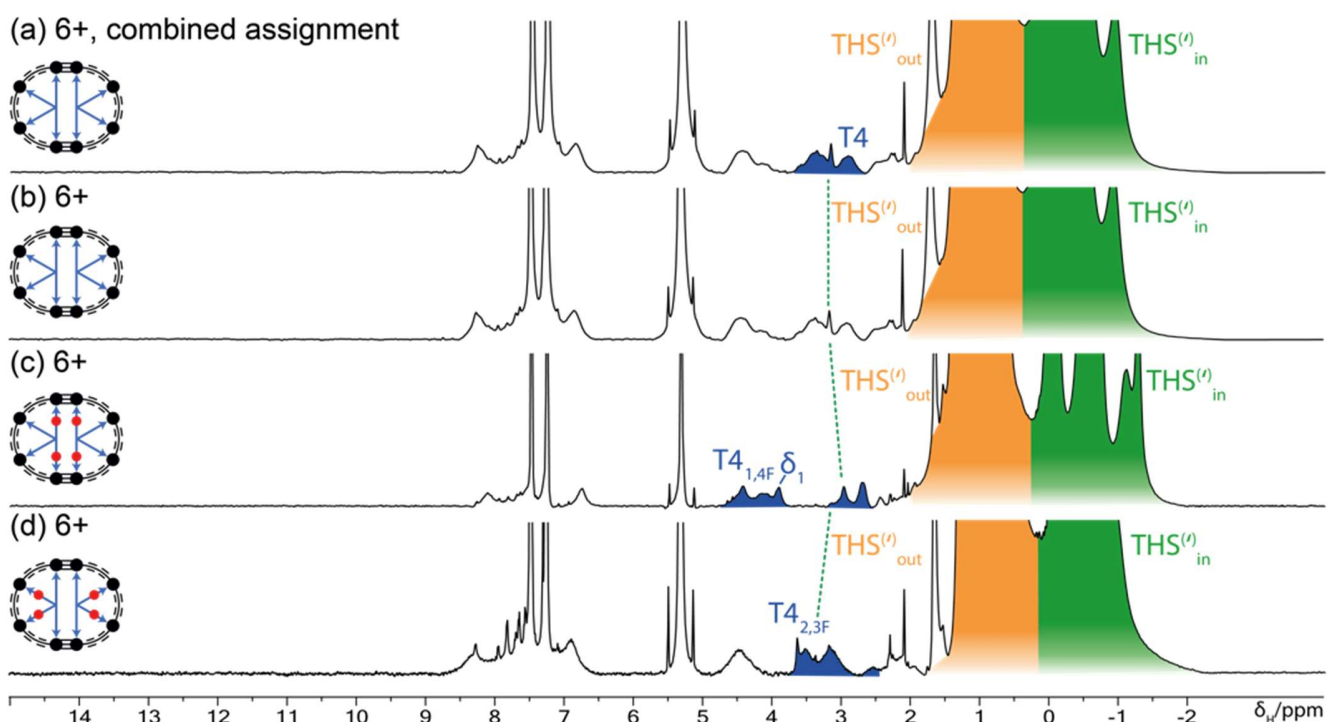




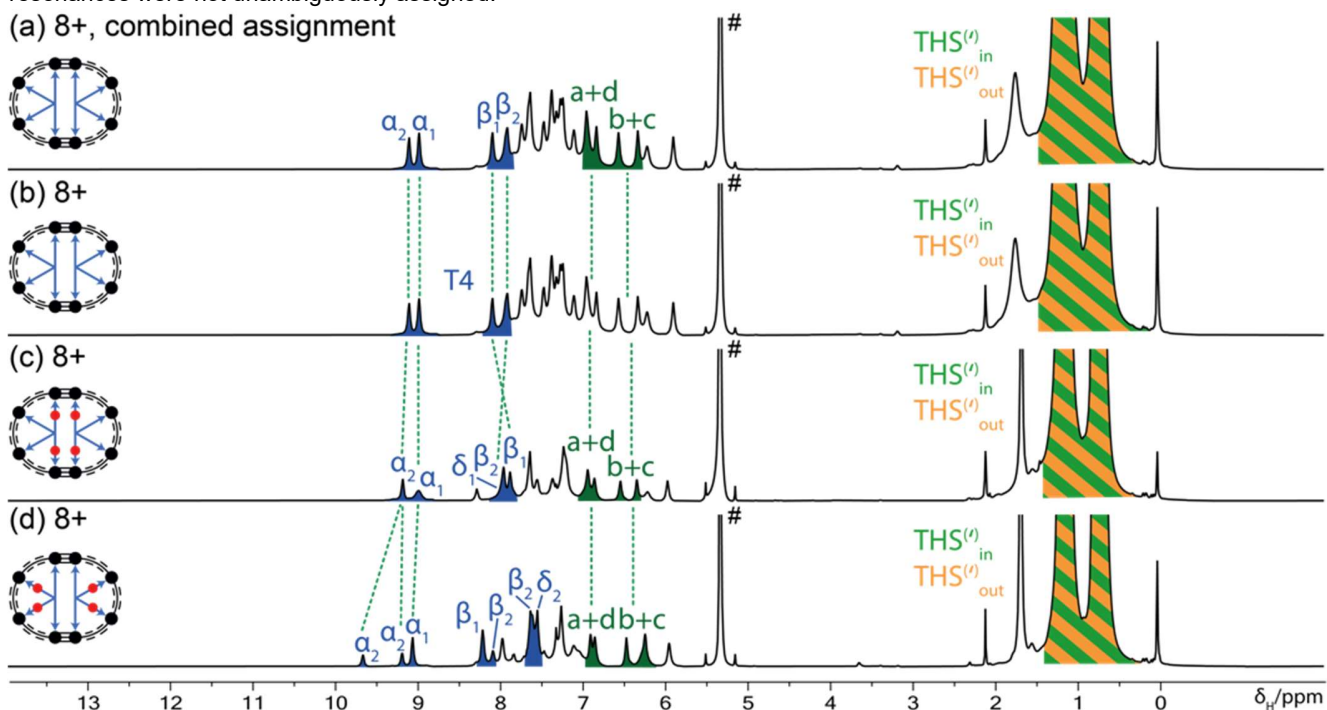
**Figure S17.** Summary of  $^1\text{H}$  NMR (500 MHz,  $\text{CD}_2\text{Cl}_2$ ) spectra of neutral (a, 298 K) and oxidized (b-d, 223 K) **c-P8[b<sub>8</sub>](T<sub>4,3F</sub>)<sub>2</sub>** generated by titration with  $\text{Thn}^+$ . Inserts show concomitantly recorded  $^{19}\text{F}$  NMR (471 MHz,  $\text{CD}_2\text{Cl}_2$ ) spectra of the  $\text{CF}_3$  probes. Refer to **Figure S1** for labeling scheme. Peaks assigned with # and \* arise from  $\text{CH}_2\text{Cl}_2$  and neutral thianthrene, respectively. Unlabeled resonances were not unambiguously assigned.



**Figure S18.** Cross-assigned  $^1\text{H}$  NMR spectrum (500 MHz,  $\text{CD}_2\text{Cl}_2$ ) of **c-P8[b<sub>6f2</sub>](T<sub>4</sub>)<sub>2</sub>** in the 4+ oxidation state (a, 223K) and individually assigned  $^1\text{H}$  NMR spectra (500 MHz,  $\text{CD}_2\text{Cl}_2$ ) of **c-P8[b<sub>6f2</sub>](T<sub>4</sub>)<sub>2</sub>** (b, 223 K), **c-P8[b<sub>6f2</sub>](T<sub>4,1,4F</sub>)<sub>2</sub>** (c, 223 K), and **c-P8[b<sub>6f2</sub>](T<sub>4,2,3F</sub>)<sub>2</sub>** (d, 223 K) in their 4+ oxidation state correlated for the overall assignment of (a). Refer to **Figure S1** for labeling scheme. Peaks assigned with # and \* arise from  $\text{CH}_2\text{Cl}_2$  and neutral thianthrene, respectively. Unlabeled resonances were not unambiguously assigned.



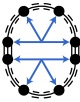
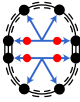
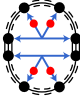
**Figure S19.** Cross-assigned  $^1\text{H}$  NMR spectrum (500 MHz,  $\text{CD}_2\text{Cl}_2$ ) of **c-P8[b<sub>6</sub>f<sub>2</sub>]•(T<sub>4</sub>)<sub>2</sub>** in the 6+ oxidation state (a, 223K) and individually assigned  $^1\text{H}$  NMR spectra (500 MHz,  $\text{CD}_2\text{Cl}_2$ ) of **c-P8[b<sub>6</sub>f<sub>2</sub>]•(T<sub>4</sub>)<sub>2</sub>** (b, 223 K), **c-P8[b<sub>6</sub>f<sub>2</sub>]•(T<sub>4</sub><sub>1,4F</sub>)<sub>2</sub>** (c, 223 K), and **c-P8[b<sub>6</sub>f<sub>2</sub>]•(T<sub>4</sub><sub>2,3F</sub>)<sub>2</sub>** (d, 223 K) in their 6+ oxidation state correlated for the overall assignment of (a). Refer to **Figure S1** for labelling scheme. Peaks assigned with # and \* arise from  $\text{CH}_2\text{Cl}_2$  and neutral thianthrene, respectively. Unlabeled resonances were not unambiguously assigned.

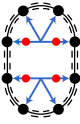
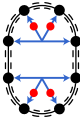


**Figure S20.** Cross-assigned  $^1\text{H}$  NMR spectrum (500 MHz,  $\text{CD}_2\text{Cl}_2$ ) of **c-P8[b<sub>6</sub>f<sub>2</sub>]•(T<sub>4</sub>)<sub>2</sub>** in the 8+ oxidation state (a, 223K) and individually assigned  $^1\text{H}$  NMR spectra (500 MHz,  $\text{CD}_2\text{Cl}_2$ ) of **c-P8[b<sub>6</sub>f<sub>2</sub>]•(T<sub>4</sub>)<sub>2</sub>** (b, 223 K), **c-P8[b<sub>6</sub>f<sub>2</sub>]•(T<sub>4</sub><sub>1,4F</sub>)<sub>2</sub>** (c, 223 K), and **c-P8[b<sub>6</sub>f<sub>2</sub>]•(T<sub>4</sub><sub>2,3F</sub>)<sub>2</sub>** (d, 223 K) in their 8+ oxidation state correlated for the overall assignment of (a). Refer to **Figure S1** for labelling scheme. Peaks assigned with # arise from  $\text{CH}_2\text{Cl}_2$ . Unlabeled resonances were not unambiguously assigned.

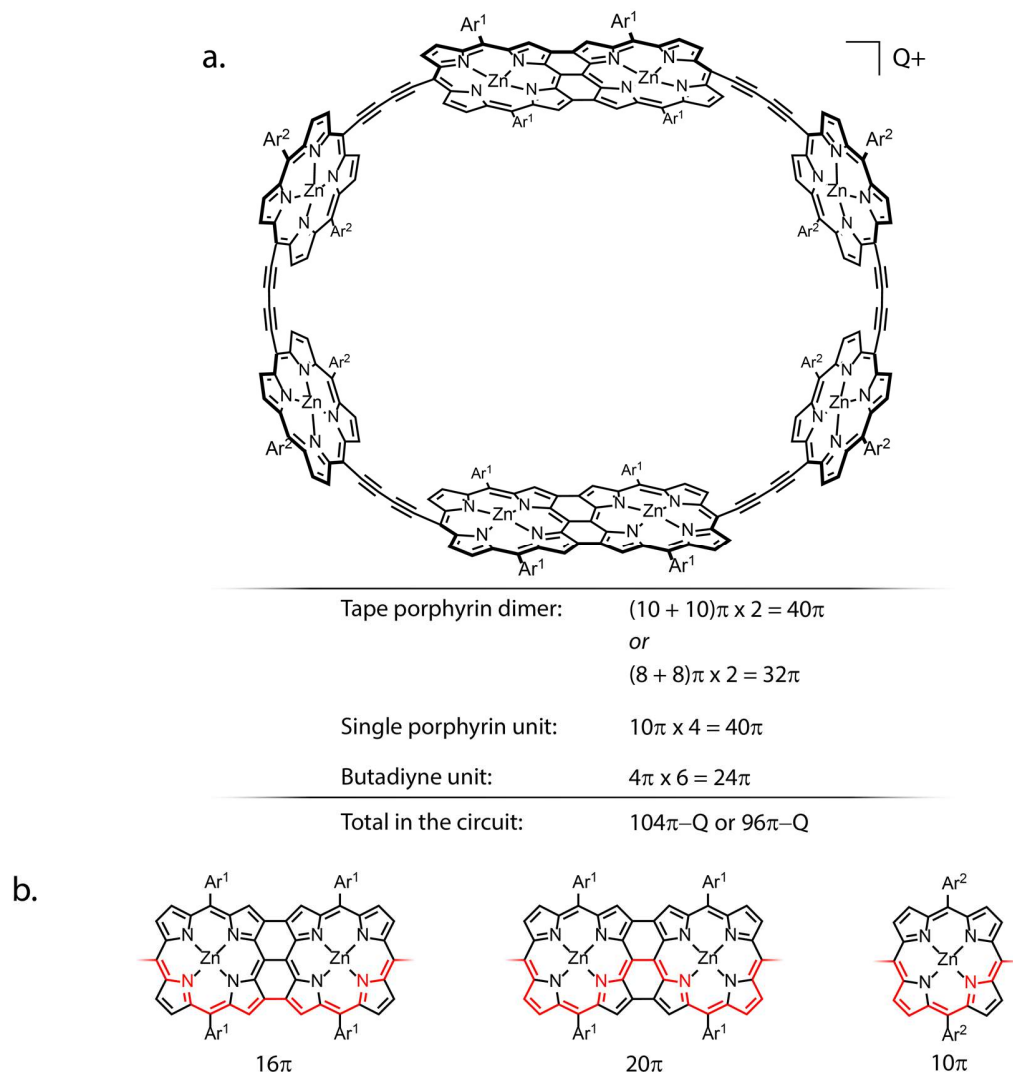
## 7. Observed NMR Shifts in Oxidation Titrations

**Table S1.**  $^1\text{H}$  and  $^{19}\text{F}$  NMR chemical shifts for oxidation states of nanoring complexes **c-P8[b<sub>6</sub>f<sub>2</sub>](T4)<sub>2</sub>**, **c-P8[b<sub>6</sub>f<sub>2</sub>](T4<sub>1,4F</sub>)<sub>2</sub>**, **c-P8[b<sub>6</sub>f<sub>2</sub>](T4<sub>2,3F</sub>)<sub>2</sub>**, **c-P8[b<sub>8</sub>](T4<sub>1,4F</sub>)<sub>2</sub>**, and **c-P8[b<sub>8</sub>](T4<sub>2,3F</sub>)<sub>2</sub>** in CD<sub>2</sub>Cl<sub>2</sub>. All chemical shifts are given in ppm. Refer to **Figure S1** for labeling scheme of the complexes. <sup>a</sup>resonance was assigned via a crossassignment approach as detailed in the strategy for the assignment of global ring currents; <sup>b</sup>referenced to hexafluorobenzene (−164.8 ppm).

<b>c-P8[b<sub>6</sub>f<sub>2</sub>](T4)<sub>2</sub></b>		<b>0 / 298 K</b>	<b>4+ / 223 K</b>	<b>6+ / 223 K</b>	<b>8+ / 223 K</b>
	<b>α<sub>1</sub></b>	5.59	13.87 <sup>a</sup>	-	8.97 <sup>a</sup>
	<b>α<sub>2</sub></b>	2.41	16.39 <sup>a</sup>	-	9.09 <sup>a</sup>
	<b>β<sub>1</sub></b>	6.34	-	-	8.08 <sup>a</sup>
	<b>β<sub>2</sub></b>	5.23	-	-	7.90 <sup>a</sup>
	<b>a + d</b>	a: 9.58 d: 9.45	-	-	6.94, 6.82 <sup>a</sup>
	<b>b + c</b>	b: 8.78 c: 8.72	-	-	6.55, 6.32 <sup>a</sup>
	<b>T4</b>	-	13.06 – 11.45	3.79 – 2.68 <sup>a</sup>	-
	<b>THS<sup>(i)</sup><sub>in</sub></b>	1.53 – 0.61	4.12 – 2.18	0.37 – -1.51	1.55 – 0.31
	<b>THS<sup>(i)</sup><sub>out</sub></b>	1.53 – 0.61	1.91 – 0.14	1.54 – 0.37	1.55 – 0.31
<b>c-P8[b<sub>6</sub>f<sub>2</sub>](T4<sub>1,4F</sub>)<sub>2</sub></b>		<b>0 / 298 K</b>	<b>4+ / 223 K</b>	<b>6+ / 223 K</b>	<b>8+ / 223 K</b>
	<b>α<sub>1</sub></b>	5.70	13.89	-	8.98
	<b>α<sub>2</sub></b>	2.51 – 2.46	16.58 <sup>a</sup>	-	9.17
	<b>β<sub>1</sub></b>	6.07	-	-	7.87
	<b>β<sub>2</sub></b>	5.25	-	-	7.94
	<b>δ<sub>1</sub></b>	6.95	12.85	3.91	7.94
	<b>CF<sub>3</sub><sup>b</sup></b>	-60.61	-54.76	-64.74	-60.30
	<b>a + d</b>	a: 9.57 d: 9.49	-	-	6.92, 6.84
	<b>b + c</b>	b: 8.79 c: 8.75	-	-	6.53, 6.33
	<b>T4<sub>1,4F</sub></b>	-	13.53 – 11.35	4.71 – 3.80, 3.20 – 2.60	-
	<b>THS<sup>(i)</sup><sub>in</sub></b>	1.64 – 0.55	4.18 – 2.12	0.27 – -1.62	1.50 – 0.41
	<b>THS<sup>(i)</sup><sub>out</sub></b>	1.64 – 0.55	1.80 – 0.09	1.59 – 0.27	1.50 – 0.41
<b>c-P8[b<sub>6</sub>f<sub>2</sub>](T4<sub>2,3F</sub>)<sub>2</sub></b>		<b>0 / 298 K</b>	<b>4+ / 223 K</b>	<b>6+ / 223 K</b>	<b>8+ / 223 K</b>
	<b>α<sub>1</sub></b>	5.70 – 5.66	13.41 <sup>a</sup>	-	9.05
	<b>α<sub>2</sub></b>	α <sub>2</sub> : 2.56–2.52 α' <sub>2</sub> : 2.46–2.42	15.80	-	9.65, 9.17
	<b>β<sub>1</sub></b>	6.39	-	-	8.20
	<b>β<sub>2</sub></b>	β <sub>2</sub> : 4.81 β' <sub>2</sub> : 5.00	-	-	8.07, 7.62
	<b>δ<sub>2</sub></b>	6.36	11.71	-	7.53
	<b>CF<sub>3</sub><sup>b</sup></b>	-61.23	-56.07	-65.41	-60.46
	<b>a + d</b>	a: 9.67 d: 9.46	-	-	6.89, 6.84
	<b>b + c</b>	b: 8.76 c: 8.67	-	-	6.46, 6.23
	<b>T4<sub>2,3F</sub></b>	-	12.67 – 11.08	3.70 – 2.44	-
	<b>THS<sup>(i)</sup><sub>in</sub></b>	1.50 – 0.67	3.49 – 1.82	0.13 – -2.05	1.47 – 0.39
	<b>THS<sup>(i)</sup><sub>out</sub></b>	1.50 – 0.67	1.72 – 0.07	1.47 – 0.13	1.47 – 0.39

<b>c-P8[b<sub>8</sub>]<sup>•</sup>(T<sub>4,4F</sub>)<sub>2</sub></b>		<b>0 / 298 K</b>	<b>4+ / 223 K</b>	<b>6+ / 223 K</b>	<b>8+ / 223 K</b>
	<b>α<sub>1</sub> + α<sub>2</sub></b>	α <sub>1</sub> : 2.57–2.52 α <sub>2</sub> : 2.50–2.44	-	-	9.94, 9.81
	<b>β<sub>1</sub> + β<sub>2</sub></b>	β <sub>1</sub> : 5.10 β <sub>2</sub> : 5.19	-	-	8.65, 8.41
	<b>CF<sub>3</sub><sup>b</sup></b>	-60.63	-59.11	-67.52	-59.86
	<b>o<sup>(i)</sup><sub>out</sub></b>	8.11	6.96 – 5.97	9.50 – 8.61	-
	<b>T<sub>4,4F</sub></b>	-	9.80 – 8.00	-	-
	<b>THS<sup>(i)</sup><sub>in</sub></b>	1.66 – 0.57	2.51 – 1.78	-0.24 – -2.51	1.58 – 0.37
	<b>THS<sup>(i)</sup><sub>out</sub></b>	1.66 – 0.57	1.78 – 0.17	1.57 – 0.35	1.58 – 0.37
<b>c-P8[b<sub>8</sub>]<sup>•</sup>(T<sub>4,3F</sub>)<sub>2</sub></b>		<b>0 / 298 K</b>	<b>4+ / 223 K</b>	<b>6+ / 223 K</b>	<b>8+ / 223 K</b>
	<b>α<sub>1</sub></b>	2.74 – 2.66	-	-	10.13
	<b>α<sub>2</sub></b>	α <sub>2</sub> : 2.52–2.46 α' <sub>2</sub> : 2.45–2.41	-	-	9.95, 9.59
	<b>CF<sub>3</sub><sup>b</sup></b>	-61.32	-59.42	-67.85	-60.08
	<b>o<sup>(i)</sup><sub>out</sub></b>	8.09	-	9.68 – 8.41	-
	<b>T<sub>4,3F</sub></b>	-	9.30 – 8.13	-	8.84 – 8.22
	<b>THS<sup>(i)</sup><sub>in</sub></b>	1.58 – 0.71	2.22 – 1.56	-0.11 – -2.61	1.57 – 0.29
	<b>THS<sup>(i)</sup><sub>out</sub></b>	1.58 – 0.71	1.56 – 0.10	1.55 – 0.40	1.57 – 0.29

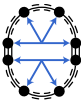
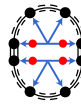
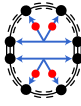
## 8. Counting of $\pi$ -Electrons in a Global c-P8[b<sub>6</sub>f<sub>2</sub>] Circuit

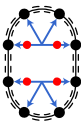


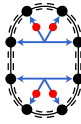
**Figure S21.**  $\pi$ -Electron count for the global ring circuit of **c-P8[b<sub>6</sub>f<sub>2</sub>]** (a) and possible delocalization pathways (in red) in the porphyrin tape dimer and single porphyrin units (b). The complete circuit consists of 2 tape dimers, 4 single porphyrin units, and 6 butadiyne links. A long and a short conjugation pathway exist for the tape dimer, contributing in total 20 $\pi$  and 16 $\pi$  electrons, respectively, per unit. This leads to two possible  $\pi$  electron counts for the global circuit: 104 $\pi$ –Q or 96 $\pi$ –Q, where Q denotes the oxidation state of the system. Ar<sup>1</sup> = Ar<sup>2</sup> = 3,5-bis(trihexylsilyl)phenyl.

## 9. Summary of Experimental Results and NICS Calculations

**Table S2.** Summary of calculated (NICS, ppm) and experimental ( $\Delta\delta$ , ppm) results for the study of global (anti)aromaticity in **c-P8[b<sub>6</sub>f<sub>2</sub>](T4)<sub>2</sub>**, **c-P8[b<sub>6</sub>f<sub>2</sub>](T4<sub>1,4F</sub>)<sub>2</sub>**, **c-P8[b<sub>6</sub>f<sub>2</sub>](T4<sub>2,3F</sub>)<sub>2</sub>**, **c-P8[b<sub>8</sub>](T4<sub>1,4F</sub>)<sub>2</sub>**, and **c-P8[b<sub>8</sub>](T4<sub>2,3F</sub>)<sub>2</sub>**. Negative NICS/ $\Delta\delta$  values and  $4n + 2$  Hückel classification correspond to aromaticity; positive NICS/ $\Delta\delta$  values and  $4n$  Hückel classification to antiaromaticity. NICS(0) values were calculated in the center of the nanoring complexes using DFT (LC-whPBE/6-31G\* (w=0.1)) without template. Chemical shift differences  $\Delta\delta_{\text{TMS}} = \delta_{\text{TMS}}(\text{in}) - \delta_{\text{TMS}}(\text{out})$  were calculated using the average chemical shift of the respective multiplets.  $\Delta\delta_{\text{X}} = \delta_{\text{X,bound}} - \delta_{\text{X,unbound}}$  values describe the chemical shift differences of template resonances X =  $\alpha_1$ ,  $\alpha_2$ ,  $\delta_1$ , and  $\delta_2$  in the nanoring complexes with respect to free template.  $\Delta\delta_{\text{F}} = \delta_{\text{F,bound}} - \delta_{\text{F,unbound}}$  values describe the  $^{19}\text{F}$  chemical shift differences of the CF<sub>3</sub> groups with respect to free template. Refer to Tables S23–S25 for unbound template resonances at room temperature. Chemical shift differences  $\Delta\delta_{\text{F}}$  for the oxidized nanoring complexes were calculated using the chemical shifts of unbound template in CD<sub>2</sub>Cl<sub>2</sub> at 223 K:  $\delta_{\text{F}}(\text{T4}_{1,4\text{F}}) = -60.59$  ppm;  $\delta_{\text{F}}(\text{T4}_{2,3\text{F}}) = -60.69$  ppm. NMR spectra of nanoring complexes were recorded in CD<sub>2</sub>Cl<sub>2</sub>. Neutral shifts: 298 K; oxidized shifts: 223 K. <sup>a</sup>local aromatic current observed; <sup>b</sup>value averaged over the respective resonance region.

<b>c-P8[b<sub>6</sub>f<sub>2</sub>](T4)<sub>2</sub></b>		<b>0</b>	<b>4+</b>	<b>6+</b>	<b>8+</b>
	$n \pi e^-$	104 / 96	100 / 92	98 / 90	96 / 88
	Hückel classification	$4n\pi^a$	$4n\pi$	$4n + 2\pi$	$4n\pi$
	NICS(0) <sub>zz</sub>	0.69	6.86	-37.51	3.97
	NICS(0) <sub>iso</sub>	-0.76	1.83	-12.69	1.37
	$\Delta\delta_{\text{TMS}}$	0	2.12	-1.53	-
	$\Delta\delta_{\alpha 1}$	-3.03	5.25	-	0.35
	$\Delta\delta_{\alpha 2}$	-6.15	7.83	-	0.53
<b>c-P8[b<sub>6</sub>f<sub>2</sub>](T4<sub>1,4F</sub>)<sub>2</sub></b>		<b>0</b>	<b>4+</b>	<b>6+</b>	<b>8+</b>
	$n \pi e^-$	104 / 96	100 / 92	98 / 90	96 / 88
	Hückel classification	$4n\pi^a$	$4n\pi$	$4n + 2\pi$	$4n\pi$
	NICS(0) <sub>zz</sub>	0.69	6.86	-37.51	3.97
	NICS(0) <sub>iso</sub>	-0.76	1.83	-12.69	1.37
	$\Delta\delta_{\text{TMS}}$	0	2.20	-1.61	-
	$\Delta\delta_{\alpha 1}$	-2.94	5.25	-	0.34
	$\Delta\delta_{\alpha 2}$	-6.12 <sup>b</sup>	7.97	-	0.56
	$\Delta\delta_{\delta 1}$	-0.79	5.11	-3.83	0.20
	$\Delta\delta_{1,4\text{F}}$	-0.12	5.83	-4.15	0.29
<b>c-P8[b<sub>6</sub>f<sub>2</sub>](T4<sub>2,3F</sub>)<sub>2</sub></b>		<b>0</b>	<b>4+</b>	<b>6+</b>	<b>8+</b>
	$n \pi e^-$	104 / 96	100 / 92	98 / 90	96 / 88
	Hückel classification	$4n\pi^a$	$4n\pi$	$4n + 2\pi$	$4n\pi$
	NICS(0) <sub>zz</sub>	0.69	6.86	-37.51	3.97
	NICS(0) <sub>iso</sub>	-0.76	1.83	-12.69	1.37
	$\Delta\delta_{\text{TMS}}$	0	1.76	-1.76	-
	$\Delta\delta_{\alpha 1}$	-3.00 <sup>b</sup>	4.73	-	0.37
	$\Delta\delta_{\delta 2}$	-1.05	4.30	-	0.12
	$\Delta\delta_{2,3\text{F}}$	-0.53	4.62	-4.72	0.23

<b>c-P8[b<sub>8</sub>](T<sub>41,4F</sub>)<sub>2</sub></b>		<b>0</b>	<b>4+</b>	<b>6+</b>	<b>8+</b>
	<i>n</i> $\pi$ e <sup>-</sup>	112	108	106	104
	Hückel classification	$4n\pi^a$	$4n\pi$	$4n + 2\pi$	$4n\pi$
	NICS(0) <sub>zz</sub>	0.53	8.64	-39.07	1.84
	NICS(0) <sub>iso</sub>	-0.68	2.12	-13.57	0.40
	$\Delta\delta_{\text{THS}}$	0	1.17	-2.34	-
	$\Delta\delta_{1,4\text{F}}$	-0.14	1.48	-6.93	0.73

<b>c-P8[b<sub>8</sub>](T<sub>42,3F</sub>)<sub>2</sub></b>		<b>0</b>	<b>4+</b>	<b>6+</b>	<b>8+</b>
	<i>n</i> $\pi$ e <sup>-</sup>	112	108	106	104
	Hückel classification	$4n\pi^a$	$4n\pi$	$4n + 2\pi$	$4n\pi$
	NICS(0) <sub>zz</sub>	0.53	8.64	-39.07	1.84
	NICS(0) <sub>iso</sub>	-0.68	2.12	-13.57	0.40
	$\Delta\delta_{\text{THS}}$	0	1.06	-2.34	-
	$\Delta\delta_{a1}$	-5.98 <sup>b</sup>	-	-	1.45
	$\Delta\delta_{2,3\text{F}}$	-0.62	1.27	-7.16	0.61



## 10. Full NMR Oxidation Titrations

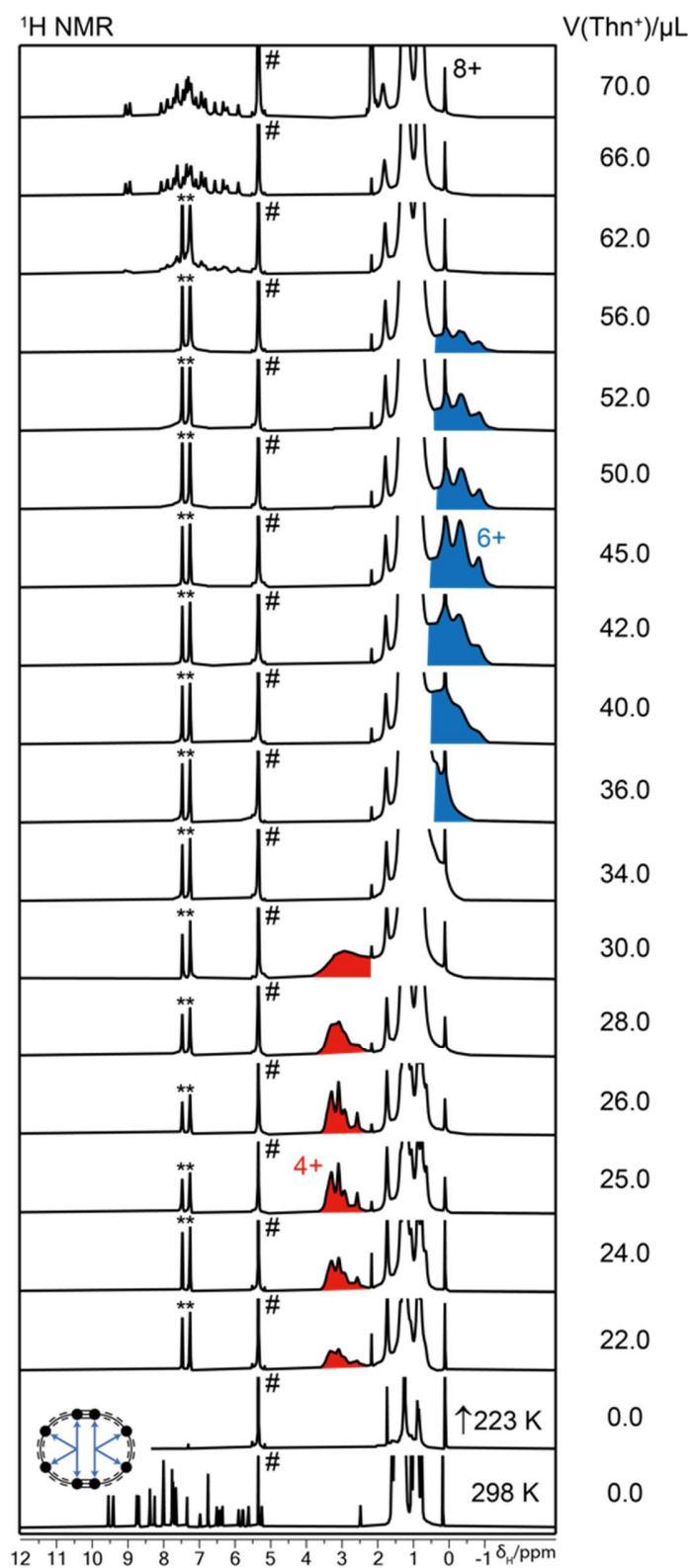


**Figure S22.** Summary of the  $^1\text{H}$  NMR titration of  $\text{c-P8}[\text{b6f2}]\bullet(\text{T4})_2$  (500 MHz, 223 K,  $\text{CD}_2\text{Cl}_2$ ) with  $\text{Thn}^+$  in  $\text{CD}_2\text{Cl}_2$ . Shifted  $\text{THS}^{(4)}_{\text{in}}$  resonances indicating global antiaromaticity are highlighted in red; those indicating global aromaticity are highlighted in blue. Peaks assigned with # and \* arise from  $\text{CH}_2\text{Cl}_2$  and neutral thianthrene, respectively.



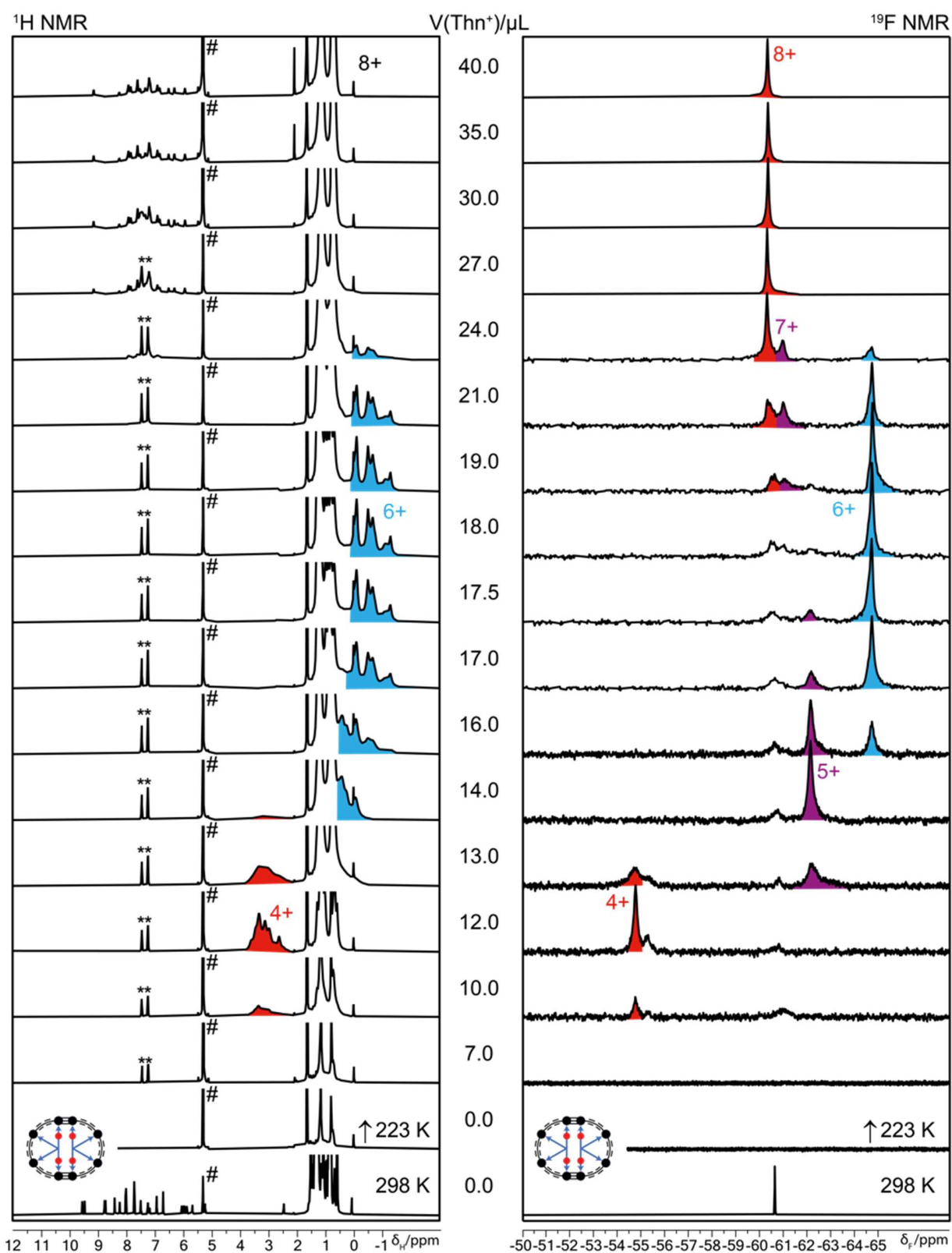


**Figure S23.** Summary of the  $^1\text{H}$  and  $^{19}\text{F}$  NMR titration of  $\text{c-P8}[\text{b6f2}]\cdot(\text{T4}_{1,4\text{F}})_2$  (500/471 MHz, 223 K,  $\text{CD}_2\text{Cl}_2$ ) with  $\text{Thn}^+$  in  $\text{CD}_2\text{Cl}_2$ . Shifted  $\text{THS}^{(\text{I})}_{\text{in}}$  and  $\text{CF}_3$  resonances indicating global antiaromaticity are highlighted in red; those indicating global aromaticity highlighted in blue. Odd-numbered oxidation states are highlighted in purple in the  $^{19}\text{F}$  NMR spectrum. Peaks assigned with # and \* arise from  $\text{CHDCl}_2$  and neutral thianthrene, respectively.

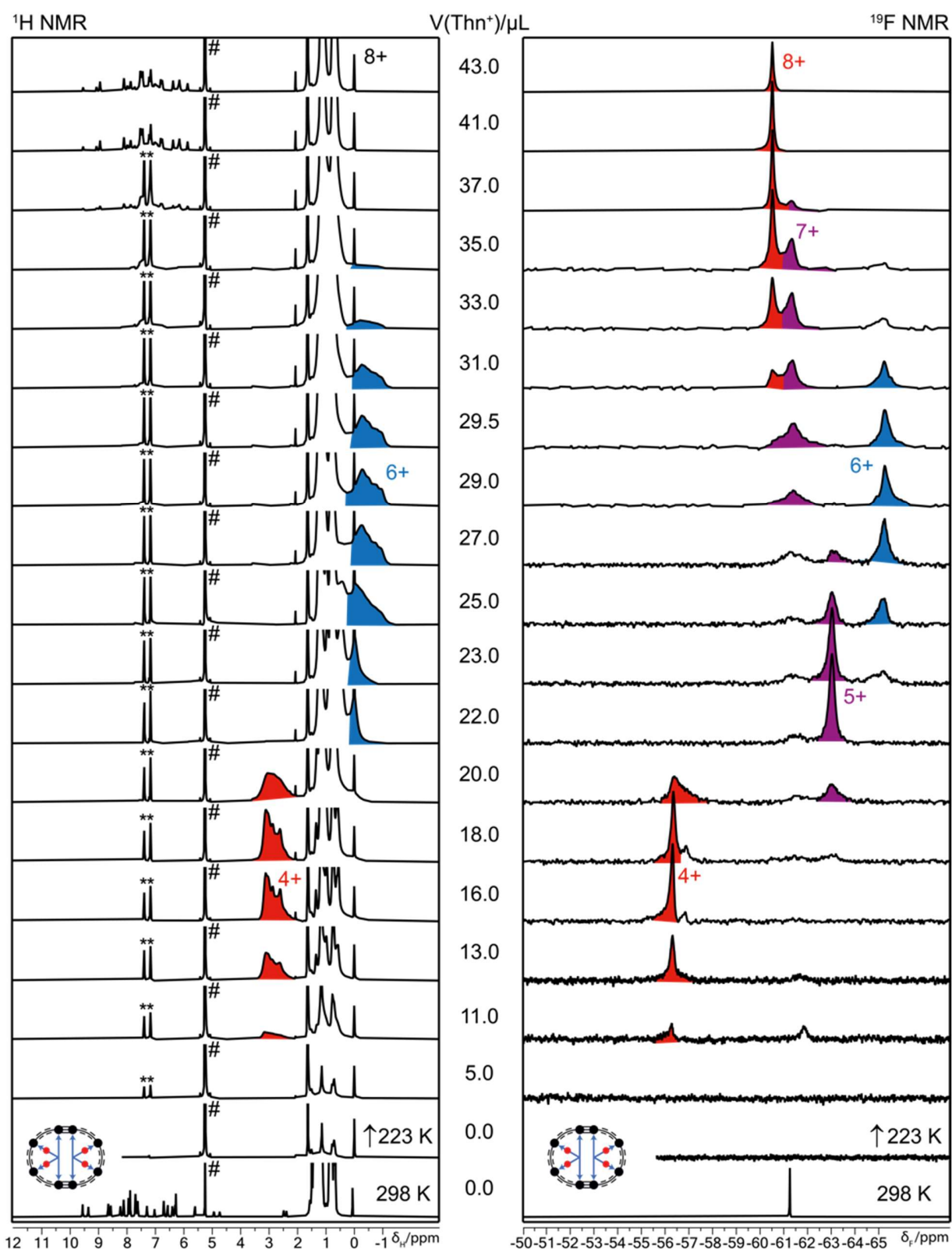


**Figure S24.** Summary of the  $^1\text{H}$  and  $^{19}\text{F}$  NMR titration of  $\text{c-P8}[\text{b}_6\text{f}_2]\cdot(\text{T}_{4,2,3\text{F}})_2$  (500/471 MHz, 223 K,  $\text{CD}_2\text{Cl}_2$ ) with  $\text{Thn}^+$  in  $\text{CD}_2\text{Cl}_2$ . Shifted  $\text{THS}^{(i)}_{\text{in}}$  and  $\text{CF}_3$  resonances indicating global antiaromaticity are highlighted in red; those indicating global aromaticity highlighted in blue. Odd-numbered oxidation states are highlighted in purple in the  $^{19}\text{F}$  NMR spectrum. Peaks assigned with # and \* arise from  $\text{CHDCl}_2$  and neutral thianthrene, respectively.

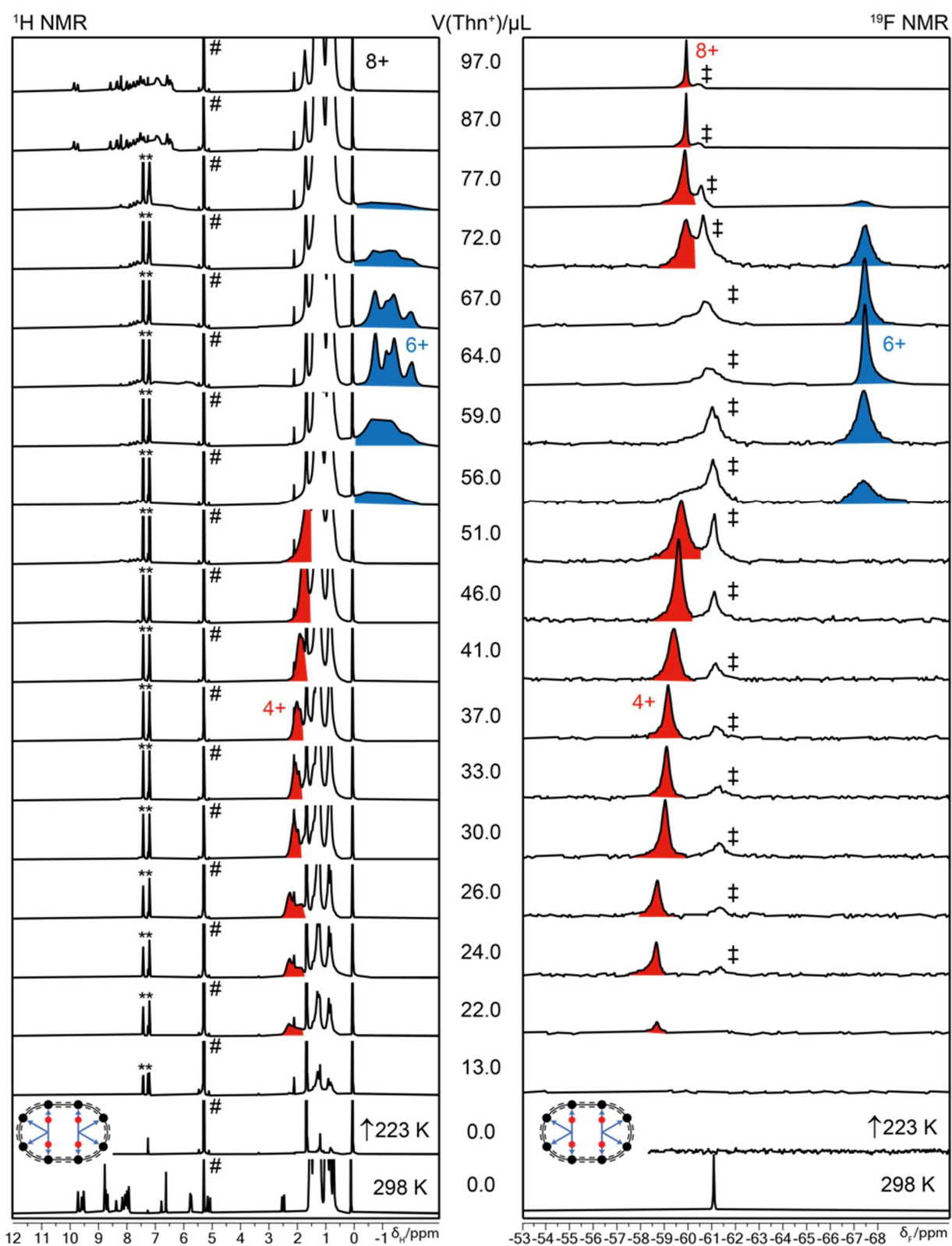


**Figure S25.** Summary of the  $^1\text{H}$  and  $^{19}\text{F}$  NMR titration of **c-P8[b<sub>8</sub>](T<sub>41,4F</sub>)<sub>2</sub> (500/471 MHz, 223 K,  $\text{CD}_2\text{Cl}_2$ ) with  $\text{Thn}^+$  in  $\text{CD}_2\text{Cl}_2$ . Shifted  $\text{THS}^{(i)}_{\text{in}}$  and  $\text{CF}_3$  resonances indicating global antiaromaticity are highlighted in red; those indicating global aromaticity are highlighted in blue. Peaks assigned with # and \* arise from  $\text{CH}_2\text{Cl}_2$  and neutral thianthrene, respectively. Residual  $^{19}\text{F}$  resonances assigned with ‡ indicate decomposed nanoring.**

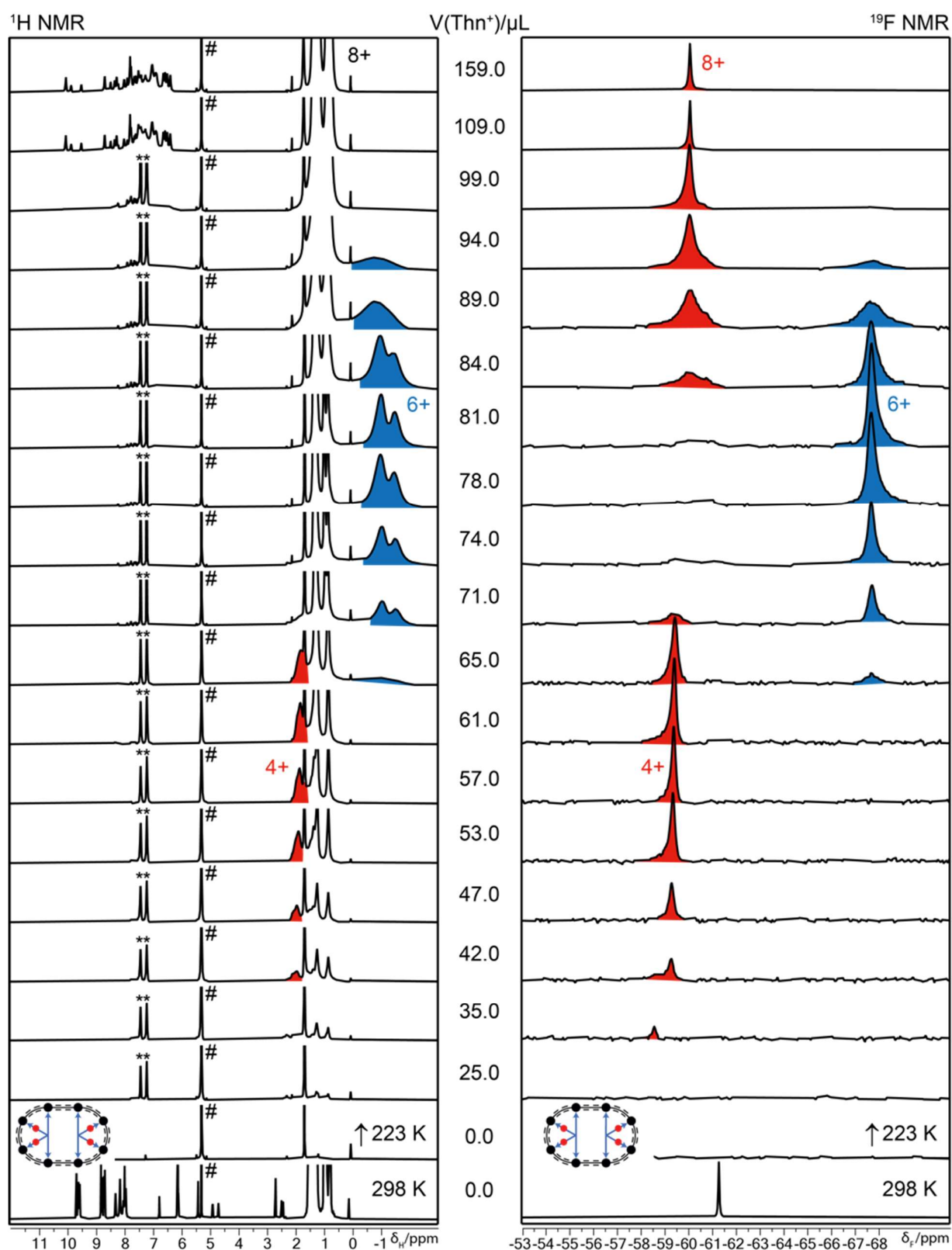


**Figure S26.** Summary of the  $^1\text{H}$  and  $^{19}\text{F}$  NMR titration of **c-P8[b<sub>8</sub>](T<sub>42,3F</sub>)<sub>2</sub> (500/471 MHz, 223 K, CD<sub>2</sub>Cl<sub>2</sub>) with Thn<sup>+</sup> in CD<sub>2</sub>Cl<sub>2</sub>. Shifted THS<sup>(i)</sup><sub>in</sub> and CF<sub>3</sub> resonances indicating global antiaromaticity are highlighted in red; those indicating global aromaticity are highlighted in blue. Peaks assigned with # and \* arise from CHDCl<sub>2</sub> and neutral thianthrene, respectively.**

## 11. Computational Chemistry Methods

Molecular models were built in HyperChem<sup>TM</sup> 8.0 using the MM+ forcefield with parameters modified for the description of porphyrins.<sup>12–15</sup> The porphyrin *meso* aryl groups were replaced with H for all calculations. The resulting geometries were subjected to further optimization in MOPAC2016 using the PM7 level of theory and in the absence of symmetry.<sup>16</sup> The optimized structures were subjected for DFT calculations. DFT geometry optimizations of nanorings **c-P8[b<sub>6</sub>f<sub>2</sub>](T4)<sub>2</sub>** and **c-P8[b<sub>8</sub>](T4)<sub>2</sub>** (*D*<sub>2</sub> initial guess), and linear oligomers **H-/P2[f<sub>1</sub>]-H**, **H-/P2[b<sub>1</sub>]-H**, **H-/P4[b<sub>2</sub>f<sub>1</sub>]-H** and **H-/P8[b<sub>5</sub>f<sub>2</sub>]-H** (*D*<sub>2h</sub> initial guess) were first performed using Gaussian 16/A.03 with the B3LYP/6-31G\* functional/basis set.<sup>17–21</sup> The minimized structures (converged to *D*<sub>2</sub> symmetry for nanorings and *D*<sub>2h</sub> for linear oligomers) were subjected to frequency calculations, revealing no imaginary frequencies. After that, the structures were further optimized for every oxidation state using the LC- $\omega$ PBE/6-31G\* ( $\omega = 0.1$ ) functional/basis set,<sup>22–25</sup> and the resulting structures were used for NICS, ACID and TD-DFT calculations.

NICS/susceptibility calculations were performed using the GIAO method, as implemented in Gaussian16/A.03 with the LC- $\omega$ PBE/6-31G\* ( $\omega = 0.1$ ) functional/basis set.<sup>26</sup> For nanorings **c-P8[b<sub>6</sub>f<sub>2</sub>](T4)<sub>2</sub>** and **c-P8[b<sub>8</sub>](T4)<sub>2</sub>**, NICS grids were calculated with 1 Å resolution on a 51 Å × 41 Å grid. For linear oligomers **H-/P2[f<sub>1</sub>]-H** and **H-/P2[b<sub>1</sub>]-H**, NICS grids were calculated with 0.25 Å resolution on a 21 Å × 11 Å grid.

ACID calculations were conducted using the CSGT method, as implemented in Gaussian09/D.01 with the LC- $\omega$ PBE/6-31G\* ( $\omega = 0.1$ ) functional/basis set.<sup>26</sup> Version 2.0 of the ACID program (external to Gaussian) was used to generate the ACID results,<sup>27</sup> and the results were visualized using POV-Ray. Templates were removed prior to NICS and ACID calculations.

TD-DFT calculations were conducted for the first 64 excited states employing Gaussian16/A.03 with the LC- $\omega$ PBE/6-31G\* ( $\omega = 0.1$ ) functional/basis set.<sup>29</sup> Natural transition orbitals (NTOs) were calculated for the excited states *S*<sub>1</sub> and *S*<sub>2</sub> for **c-P8[b<sub>6</sub>f<sub>2</sub>](T4)<sub>2</sub>** and **c-P8[b<sub>8</sub>](T4)<sub>2</sub>**, *S*<sub>2</sub> for **H-/P4[b<sub>2</sub>f<sub>1</sub>]-H**, as well as *S*<sub>3</sub> for **H-/P8[b<sub>5</sub>f<sub>2</sub>]-H**.<sup>30</sup>

## 12. Time-Dependent Density Functional Theory

**Table S3.** TD-DFT excitation energies and oscillator strengths of the **c-P8[b<sub>6</sub>f<sub>2</sub>](T4)<sub>2</sub>** calculated at LC- $\omega$ hPBE/6-31G\* ( $\omega = 0.1$ ) level of energy.

excited state	nm	eV	<i>f</i>	excited state	nm	eV	<i>f</i>
1	1347.79	0.9199	0	33	628.9	1.9714	0
2	1175.31	1.0549	2.2972	34	625.31	1.9828	0.0307
3	1030.26	1.2034	0.0003	35	612.53	2.0241	0
4	1030.25	1.2034	0	36	607.62	2.0405	0.0058
5	898.68	1.3796	2.6932	37	600.02	2.0663	0
6	859.78	1.442	0.0001	38	574.85	2.1568	0
7	749.26	1.6547	0	39	573.1	2.1634	0
8	711.07	1.7436	1.7492	40	572.82	2.1645	0.0777
9	709.94	1.7464	0	41	572.47	2.1658	0.0036
10	706.44	1.7551	0.0946	42	572	2.1676	0.0001
11	705.96	1.7563	0.4364	43	571.97	2.1677	0.0721
12	704.02	1.7611	0.0088	44	571.43	2.1697	0
13	699.89	1.7715	0	45	569.83	2.1758	0.0002
14	684.03	1.8126	0.3936	46	565.55	2.1923	0
15	680.35	1.8224	0.0099	47	565.29	2.1933	0
16	677.06	1.8312	0	48	554.47	2.2361	0.0001
17	676.5	1.8327	0.0009	49	553.47	2.2401	0.0012
18	675.35	1.8359	0	50	548.25	2.2615	0.8856
19	670.92	1.848	0.0032	51	545.36	2.2734	0
20	669.68	1.8514	0	52	533.99	2.3218	0.067
21	667.91	1.8563	0.0031	53	533.92	2.3221	0.0166
22	660.27	1.8778	0.0373	54	533.47	2.3241	0.4247
23	657.85	1.8847	0	55	524.3	2.3647	0.0013
24	651.62	1.9027	0.0024	56	524.28	2.3649	0
25	651.54	1.9029	0.0243	57	522.47	2.3731	0.0004
26	649.06	1.9102	0.0001	58	522.4	2.3733	0.0192
27	646.13	1.9189	0.0019	59	522.24	2.3741	0
28	645.3	1.9214	0.0002	60	518.93	2.3892	0.0008
29	640.78	1.9349	0	61	517.16	2.3974	1.9387
30	640.49	1.9358	0.0366	62	509.88	2.4316	0.0001
31	636.49	1.9479	0.0002	63	509.84	2.4318	0
32	636.44	1.9481	0.0005	64	509.39	2.434	0.0204

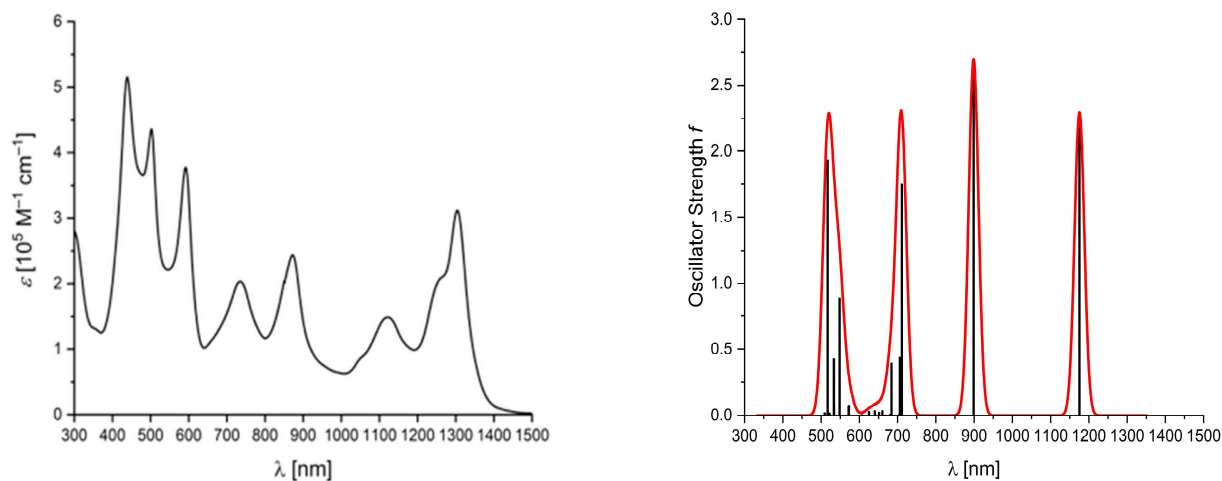


**Figure S27.** (Left) Experimental UV-Vis-NIR of **c-P8[b<sub>6</sub>f<sub>2</sub>](T4)<sub>2</sub>** measured in CHCl<sub>3</sub> at 298 K. (Right) (black bars) Calculated wavelength vs. oscillator strength of **c-P8[b<sub>6</sub>f<sub>2</sub>](T4)<sub>2</sub>**. (red) Simulated absorption spectrum assuming a Gaussian line-shape for each transition, with width 50 nm. Calculated at the LC- $\omega$ hPBE/6-31G\* ( $\omega = 0.1$ ) level of energy for the first 64 excited states.



**Table S4.** TD-DFT excitation energies and oscillator strengths of the **c-P8[b<sub>8</sub>](T4)<sub>2</sub>** calculated at LC-whPBE/6-31G\* ( $\omega = 0.1$ ) level of energy.

excited state	nm	eV	<i>f</i>	excited state	nm	eV	<i>f</i>
1	1053.31	1.1771	0	33	562.11	2.2057	0
2	893.97	1.3869	2.9308	34	556.87	2.2264	0
3	865.05	1.4333	6.1074	35	556.52	2.2278	0.0009
4	720.83	1.72	0.0003	36	556.1	2.2295	0
5	719.74	1.7226	0.0013	37	555.53	2.2318	0
6	681.35	1.8197	0.0048	38	554.65	2.2354	0
7	680.96	1.8207	0.0018	39	524.21	2.3652	0.0015
8	671.44	1.8465	0.0161	40	520.75	2.3809	0.0051
9	670.7	1.8486	0.0002	41	511.27	2.425	0.1629
10	650.43	1.9062	0.0005	42	509.66	2.4327	0.0016
11	650.32	1.9065	0.0002	43	508.85	2.4366	0.0038
12	650.09	1.9072	0.0003	44	507.43	2.4434	0.0028
13	649.62	1.9086	0.0001	45	506.63	2.4472	0.0009
14	649.18	1.9099	0.0001	46	506.18	2.4494	0.0132
15	647.25	1.9156	0.0017	47	506.17	2.4495	0.001
16	644.72	1.9231	0.0021	48	505.34	2.4535	0.0008
17	643.98	1.9253	0.003	49	504.62	2.457	0.2523
18	643.71	1.9261	0	50	503.62	2.4618	0.0214
19	643.44	1.9269	0.0004	51	503.22	2.4638	0.0019
20	642.67	1.9292	0.0007	52	503.05	2.4646	0.0062
21	631.19	1.9643	0.0046	53	503.03	2.4647	0.0072
22	623.74	1.9878	0.0248	54	502.96	2.4651	0.0107
23	623.17	1.9896	0.0139	55	502.27	2.4685	0.2279
24	614.13	2.0189	0.0002	56	499.04	2.4845	0.0066
25	613.96	2.0194	0.0001	57	498.65	2.4864	0.0036
26	600.8	2.0637	0.0002	58	495.07	2.5044	0.0288
27	590.38	2.1001	0	59	494.02	2.5097	0.0027
28	573.96	2.1602	0.0001	60	493.8	2.5108	0.0007
29	573.63	2.1614	0.0001	61	493.52	2.5123	0.0014
30	573.35	2.1624	0.0001	62	493.08	2.5145	0.0047
31	571.1	2.171	0.0001	63	490.5	2.5277	0.0047
32	563.96	2.1985	0	64	489.54	2.5327	0.0094

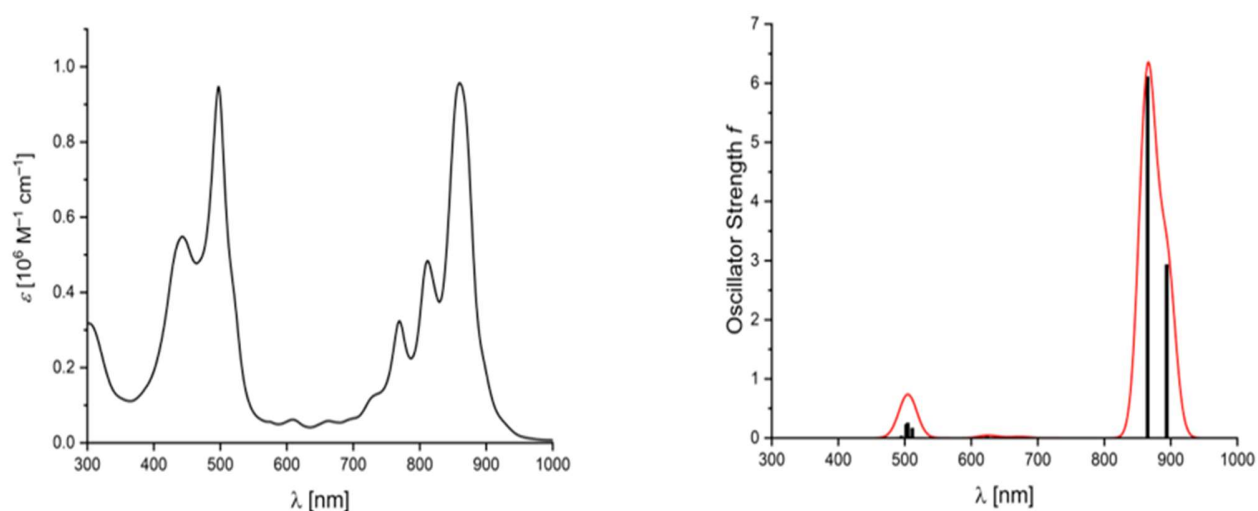
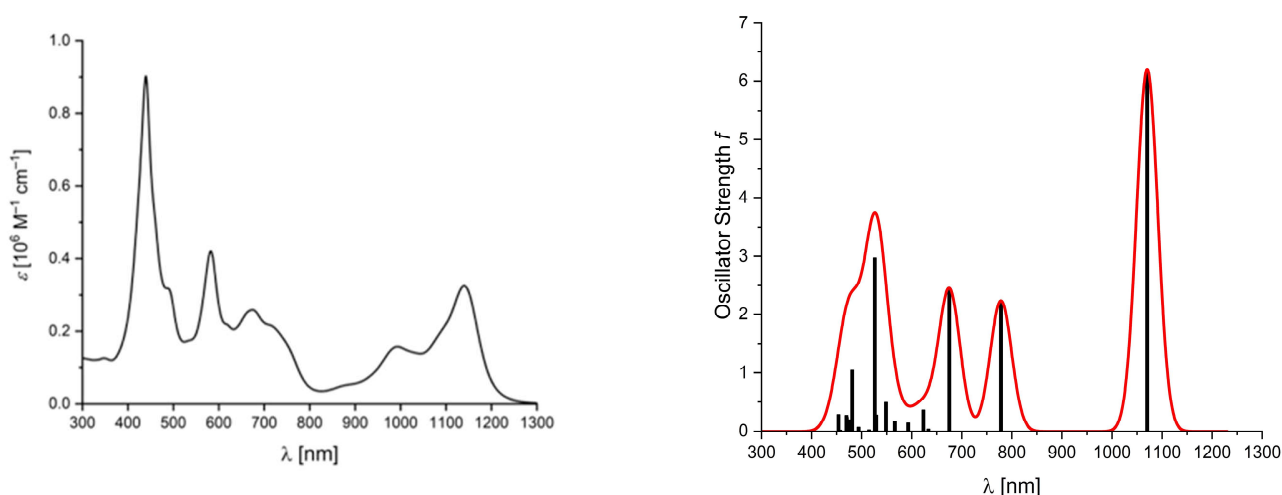


**Figure S28.** (Left) Experimental UV-Vis-NIR of **c-P8[b<sub>8</sub>](T4)<sub>2</sub>** measured in CHCl<sub>3</sub> at 298 K. (Right) (black bars) Calculated wavelength vs. oscillator strength of **c-P8[b<sub>8</sub>](T4)<sub>2</sub>**. (red) Simulated absorption spectrum assuming a Gaussian line-shape for each transition, with width 50 nm. Calculated at the LC-whPBE/6-31G\* ( $\omega = 0.1$ ) level of energy for the first 64 excited states.



**Table S5.** TD-DFT excitation energies and oscillator strengths of the **H-I-P8[bsf<sub>2</sub>]-H** calculated at LC-whPBE/6-31G\* ( $\omega = 0.1$ ) level of energy.

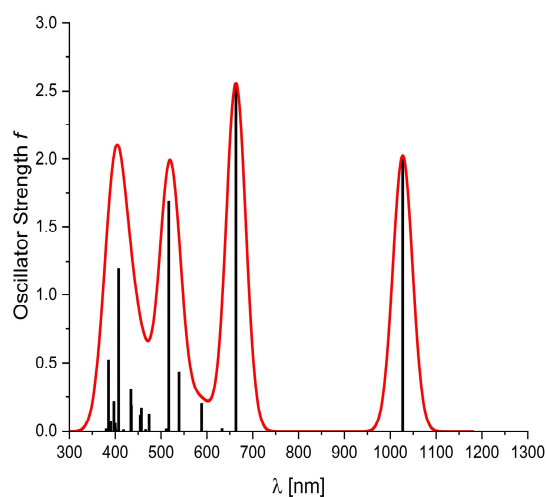
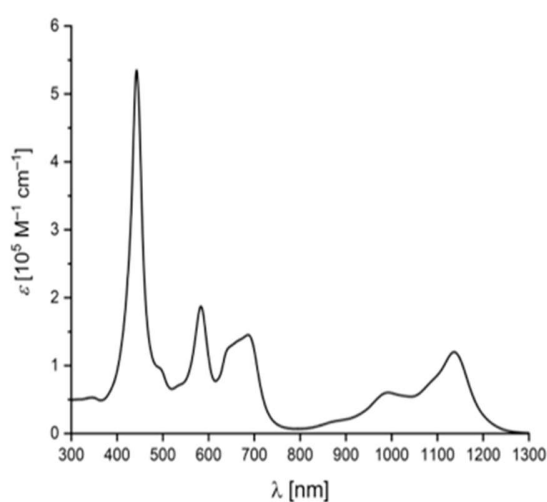
excited state	nm	eV	<i>f</i>	excited state	nm	eV	<i>f</i>
1	1070.3	1.1584	6.1995	33	530.13	2.3388	0
2	1020.2	1.2153	0	34	529.1	2.3433	0.2737
3	1003.23	1.2358	0	35	526.26	2.356	2.9716
4	1003.23	1.2358	0	36	514.64	2.4091	0
5	778.23	1.5931	2.2381	37	514.64	2.4092	0.0248
6	682.49	1.8166	0	38	511.62	2.4234	0
7	675.07	1.8366	2.4317	39	507.92	2.441	0
8	660.97	1.8758	0	40	507.92	2.441	0.0001
9	660.82	1.8762	0	41	497.83	2.4905	0
10	660.82	1.8762	0	42	495.28	2.5033	0
11	633.39	1.9575	0	43	494.04	2.5096	0.0684
12	633.38	1.9575	0.0394	44	488.99	2.5355	0
13	632.63	1.9598	0	45	488.99	2.5355	0
14	632.63	1.9598	0.0012	46	481.12	2.577	1.0396
15	629.93	1.9682	0	47	478.32	2.5921	0
16	629.93	1.9682	0	48	477.58	2.5961	0
17	623.32	1.9891	0.3605	49	476.2	2.6036	0.1893
18	618.97	2.0031	0.002	50	475.18	2.6092	0
19	618.06	2.006	0	51	475.18	2.6092	0.1118
20	610.48	2.0309	0	52	474.11	2.6151	0
21	598.26	2.0724	0	53	474.11	2.6151	0
22	598.26	2.0724	0.0038	54	472.07	2.6264	0
23	592.96	2.0909	0.1376	55	472.07	2.6264	0
24	589.57	2.103	0	56	471.04	2.6321	0.1145
25	574.7	2.1574	0	57	470.4	2.6357	0
26	566.28	2.1895	0.1628	58	470.36	2.636	0.2346
27	552.08	2.2458	0	59	469.53	2.6406	0.2666
28	552.03	2.246	0	60	467.38	2.6528	0
29	548.56	2.2602	0.4922	61	457.17	2.712	0
30	547.05	2.2664	0	62	457.17	2.712	0.0206
31	542.45	2.2856	0	63	453.75	2.7324	0
32	542.45	2.2856	0	64	453.73	2.7326	0.2833



**Figure S29.** (Left) Experimental UV-Vis-NIR of **H-I-P8[bsf<sub>2</sub>]-H** measured in CHCl<sub>3</sub> at 298 K. (Right) (black bars) Calculated wavelength vs. oscillator strength of **H-I-P8[bsf<sub>2</sub>]-H**. (red) Simulated absorption spectrum assuming a Gaussian line-shape for each transition, with width 50 nm. Calculated at the LC-whPBE/6-31G\* ( $\omega = 0.1$ ) level of energy for the first 64 excited states.

**Table S6.** TD-DFT excitation energies and oscillator strengths of the **H-I-P4[b<sub>2</sub>f<sub>1</sub>]-H** calculated at LC-whPBE/6-31G\* ( $\omega = 0.1$ ) level of energy.

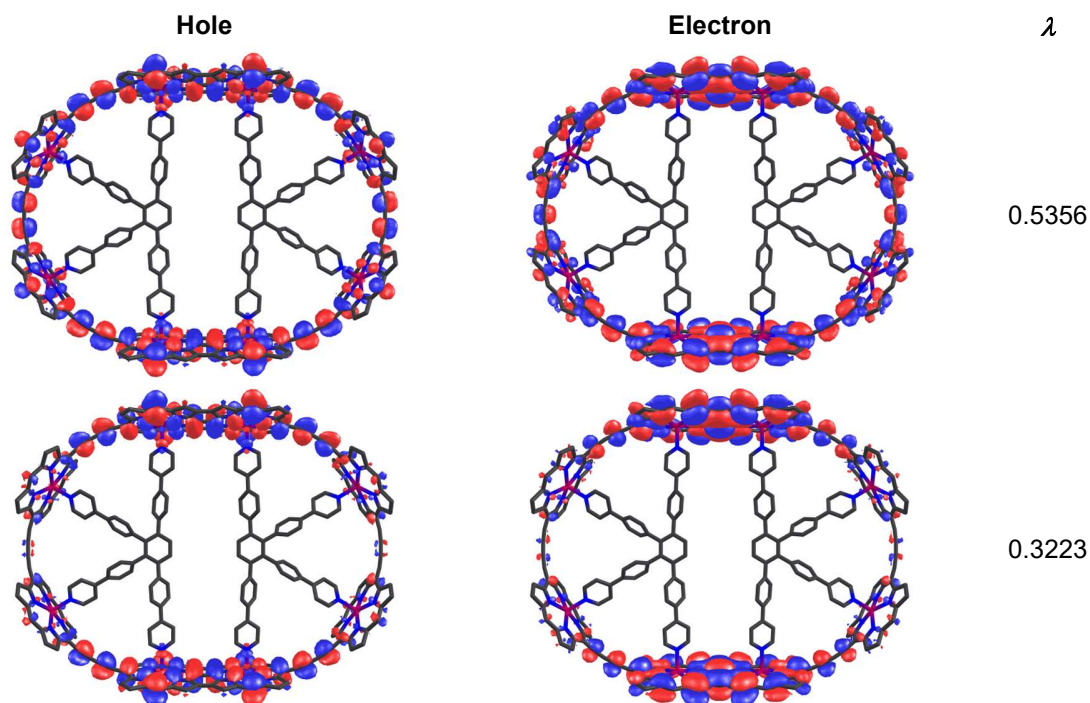
excited state	nm	eV	<i>f</i>	excited state	nm	eV	<i>f</i>
1	1027.16	1.2071	2.0243	33	436.58	2.8399	0
2	1002.11	1.2372	0	34	436.57	2.84	0
3	682.33	1.8171	0	35	436.51	2.8404	0.0027
4	663.44	1.8688	2.5494	36	435.27	2.8484	0
5	660.35	1.8775	0	37	435.22	2.8488	0.1914
6	633.08	1.9584	0.02	38	434.23	2.8553	0.3032
7	632.82	1.9592	0	39	431.3	2.8747	0
8	629.52	1.9695	0	40	431.16	2.8756	0
9	601.31	2.0619	0	41	421.76	2.9397	0
10	598.26	2.0724	0.0037	42	418.08	2.9655	0.0129
11	598.26	2.0724	0	43	412.02	3.0092	0
12	588.42	2.1071	0.2045	44	411.01	3.0166	0
13	550.7	2.2514	0	45	407.61	3.0417	0
14	542.26	2.2864	0	46	407.26	3.0444	1.1945
15	542.26	2.2864	0	47	403.48	3.0729	0
16	539.16	2.2996	0.4288	48	403.23	3.0748	0.0074
17	516.68	2.3996	1.6909	49	403.23	3.0748	0
18	511.08	2.4259	0.019	50	401.78	3.0859	0
19	507.48	2.4431	0	51	400.53	3.0955	0.0244
20	489.07	2.5351	0	52	399.99	3.0997	0.0563
21	488.35	2.5389	0	53	397.18	3.1216	0
22	481.83	2.5732	0	54	397.15	3.1219	0.2179
23	474.16	2.6148	0	55	391.08	3.1703	0.0013
24	474.16	2.6148	0	56	390.02	3.1789	0.0688
25	474.03	2.6155	0	57	389.98	3.1792	0
26	474.03	2.6155	0.1238	58	389.98	3.1792	0
27	469.26	2.6421	0	59	388.84	3.1886	0
28	466.37	2.6585	0.0142	60	388.49	3.1914	0
29	456.95	2.7133	0.1722	61	385.25	3.2183	0
30	454.58	2.7274	0.1167	62	385.15	3.2191	0.5197
31	452.34	2.741	0	63	380.26	3.2605	0.0152
32	447.1	2.7731	0	64	380.18	3.2612	0.0199



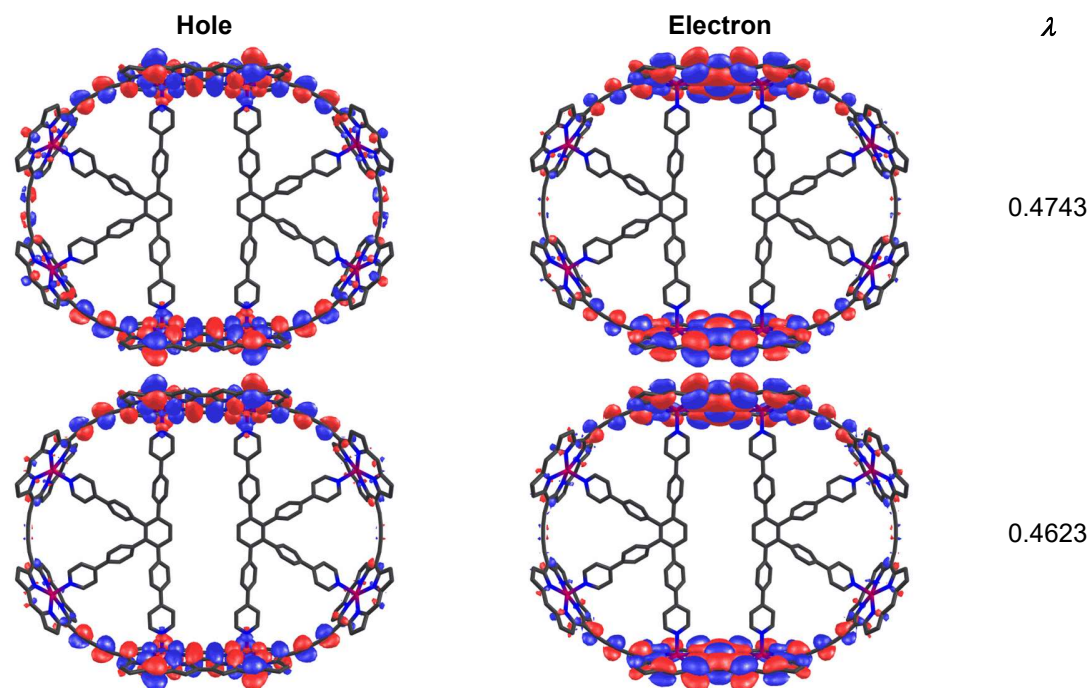
**Figure S30.** (Left) Experimental UV-Vis-NIR of **Si-I-P4[b<sub>2</sub>f<sub>1</sub>]-Si** measured in CHCl<sub>3</sub> at 298 K. (Right) (black bars) Calculated wavelength vs. oscillator strength of **H-I-P4[b<sub>2</sub>f<sub>1</sub>]-H**. (red) Simulated absorption spectrum assuming a Gaussian line-shape for each transition, with width 50 nm. Calculated at the LC-whPBE/6-31G\* ( $\omega = 0.1$ ) level of energy for the first 64 excited states.

### 13. Natural Transition Orbital Pair Calculations

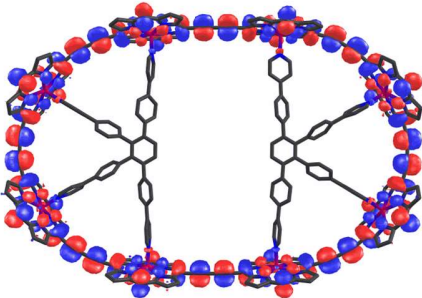
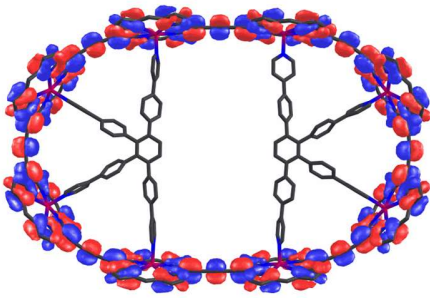
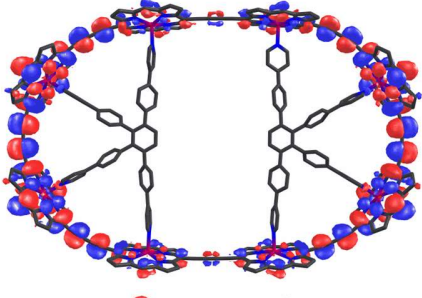
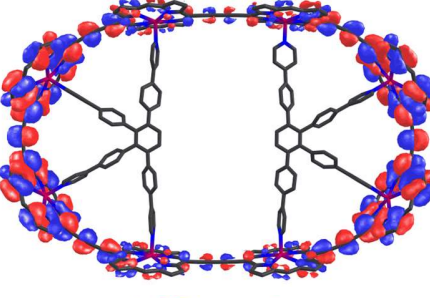
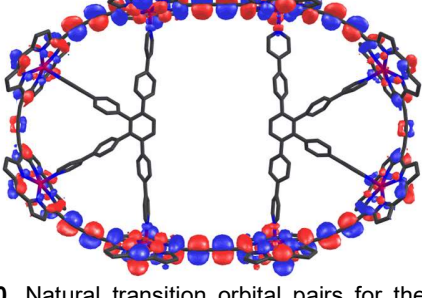
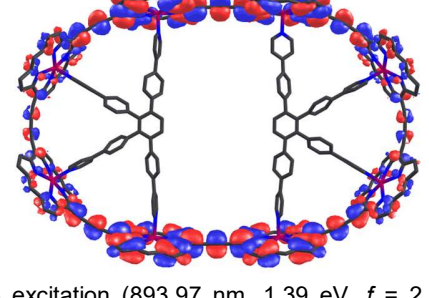
**Table S7.** Natural transition orbital pairs for the  $S_0 \rightarrow S_1$  excitation (1347.79 nm, 0.92 eV,  $f = 0.0000$ ) of **c-P8[b<sub>6</sub>f<sub>2</sub>](T4)<sub>2</sub>** calculated at the LC-whPBE/6-31G\* ( $w = 0.1$ ) level of theory. The eigenvalue associated with the natural transition orbital pair is  $\lambda$ .



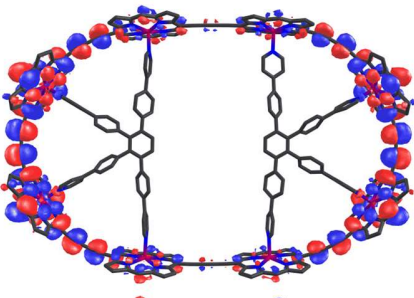
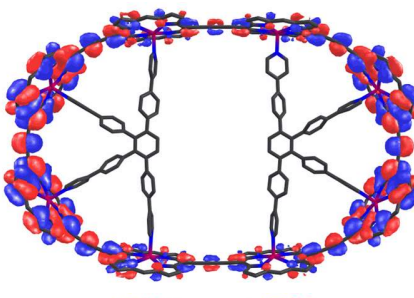
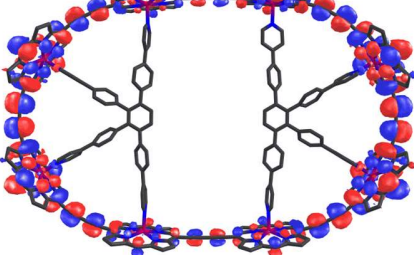
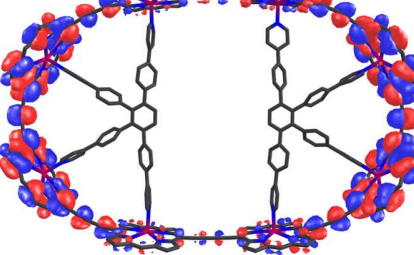
**Table S8.** Natural transition orbital pairs for the  $S_0 \rightarrow S_2$  excitation (1175.31 nm, 1.05 eV,  $f = 2.2972$ ) of **c-P8[b<sub>6</sub>f<sub>2</sub>](T4)<sub>2</sub>** calculated at the LC-whPBE/6-31G\* ( $w = 0.1$ ) level of theory. The eigenvalue associated with the natural transition orbital pairs is  $\lambda$ .



**Table S9.** Natural transition orbital pairs for the  $S_0 \rightarrow S_1$  excitation (1053.31 nm, 1.18 eV,  $f = 0.0000$ ) of **c-P8[b<sub>8</sub>](T4)<sub>2</sub>** calculated at the LC-whPBE/6-31G\* ( $w = 0.1$ ) level of theory. The eigenvalue associated with the natural transition orbital pair is  $\lambda$ .

Hole	Electron	$\lambda$
		0.4715
		0.2193
		0.1887

**Table S10.** Natural transition orbital pairs for the  $S_0 \rightarrow S_2$  excitation (893.97 nm, 1.39 eV,  $f = 2.9308$ ) of **c-P8[b<sub>8</sub>](T4)<sub>2</sub>** calculated at the LC-whPBE/6-31G\* ( $w = 0.1$ ) level of theory. The eigenvalue associated with the natural transition orbital pair is  $\lambda$ .

Hole	Electron	$\lambda$
		0.4207
		0.4155



**Table S11.** Natural transition orbital pairs for the  $S_0 \rightarrow S_1$  excitation (1027.16 nm, 1.21 eV,  $f = 2.2043$ ) of **H-/P4[b<sub>2</sub>f<sub>1</sub>]-H** calculated at the LC-whPBE/6-31G\* ( $w = 0.1$ ) level of theory. The eigenvalue associated with the natural transition orbital pair is  $\lambda$ .

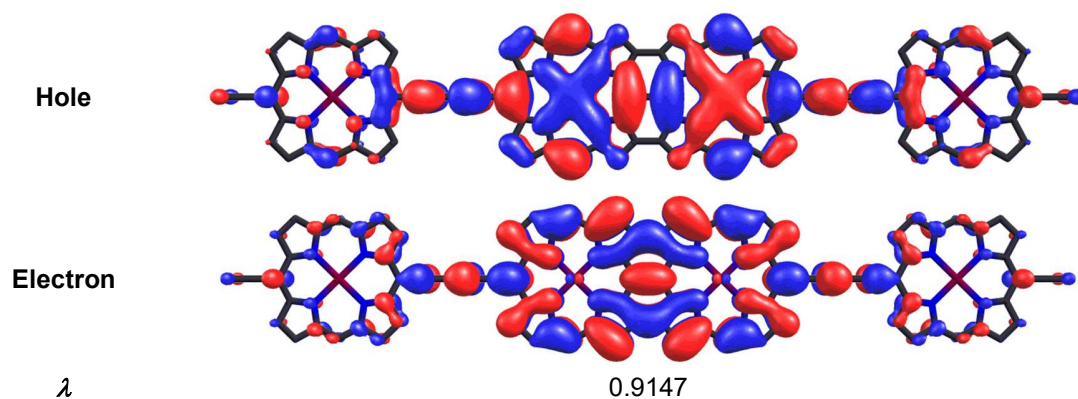
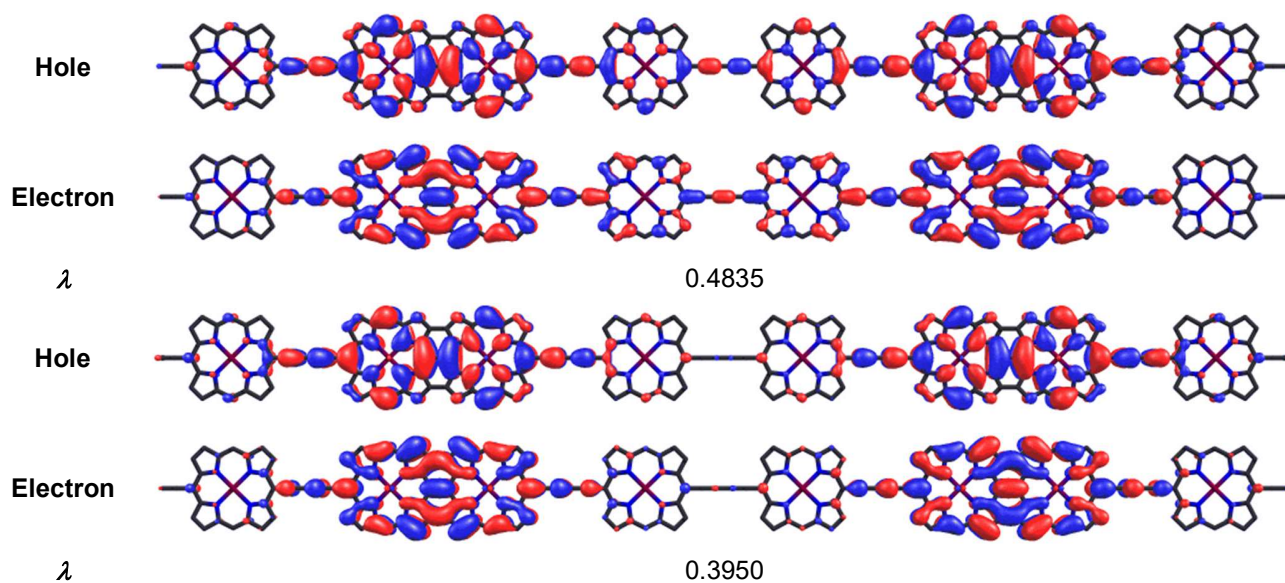


**Table S12.** Natural transition orbital pairs for the  $S_0 \rightarrow S_1$  excitation (1070.30 nm, 1.16 eV,  $f = 6.1995$ ) of **H-/P8[b<sub>5</sub>f<sub>2</sub>]-H** calculated at the LC-whPBE/6-31G\* ( $w = 0.1$ ) level of theory. The eigenvalue associated with the natural transition orbital pair is  $\lambda$ .



## 14. NICS and ACID calculations

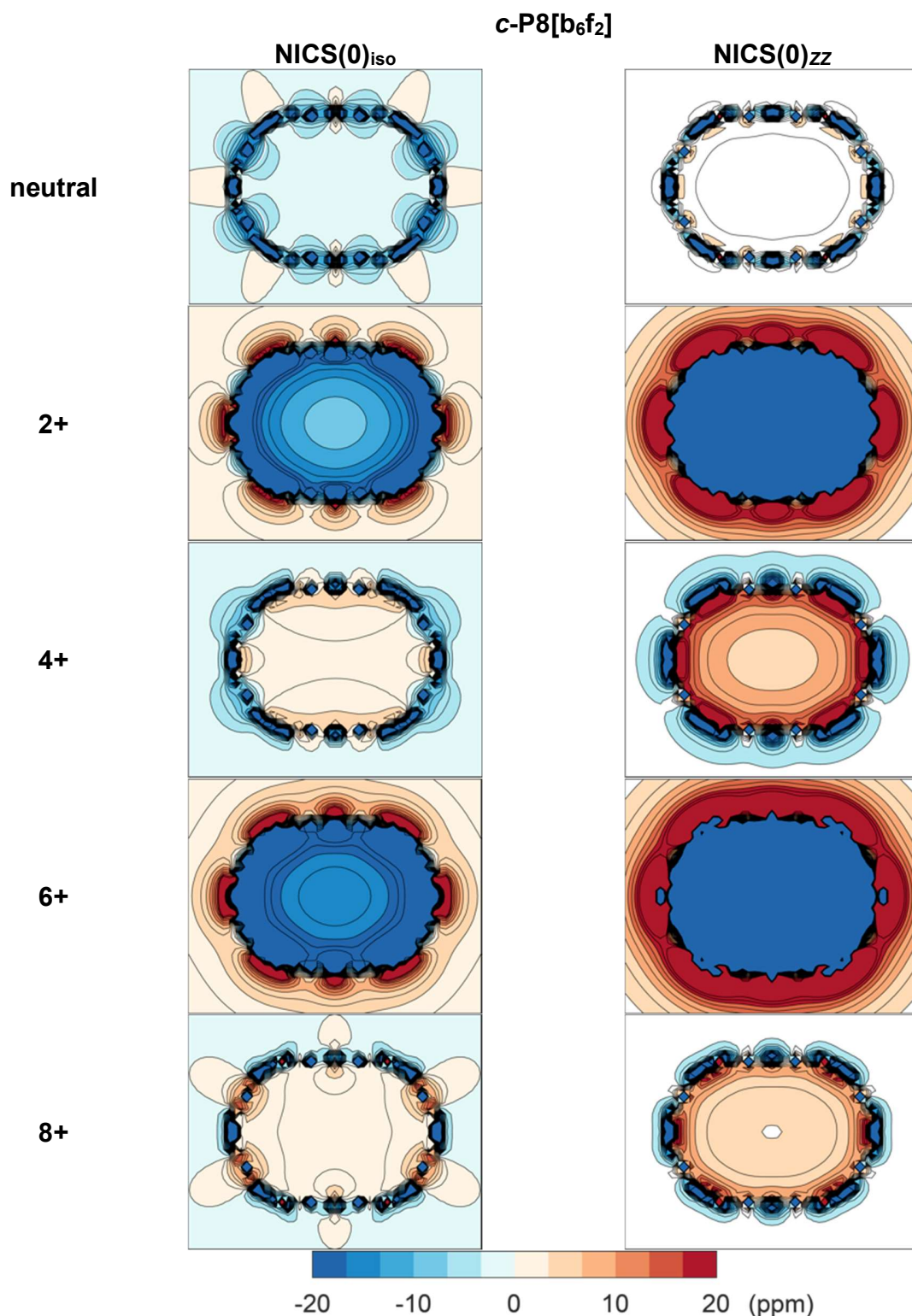


**Figure S31.** NICS(0)<sub>iso</sub> and NICS(0)<sub>zz</sub> plots of **c-P8[b<sub>6</sub>f<sub>2</sub>]** at oxidation states 0, 2+, 4+, 6+ and 8+. Geometries were optimized using LC- $\omega$ hPBE/6-31G\* ( $\omega = 0.1$ ) at every oxidation state with the templates. NICS were calculated in the absence of template on a planar grid bisecting the Zn atoms (51 Å × 41 Å, spacing 1 Å). The color axis is truncated left (blue) and right (red) -20 ppm and 20 ppm, respectively. Contours are drawn every 3.3 ppm, from -20 to 20 ppm.

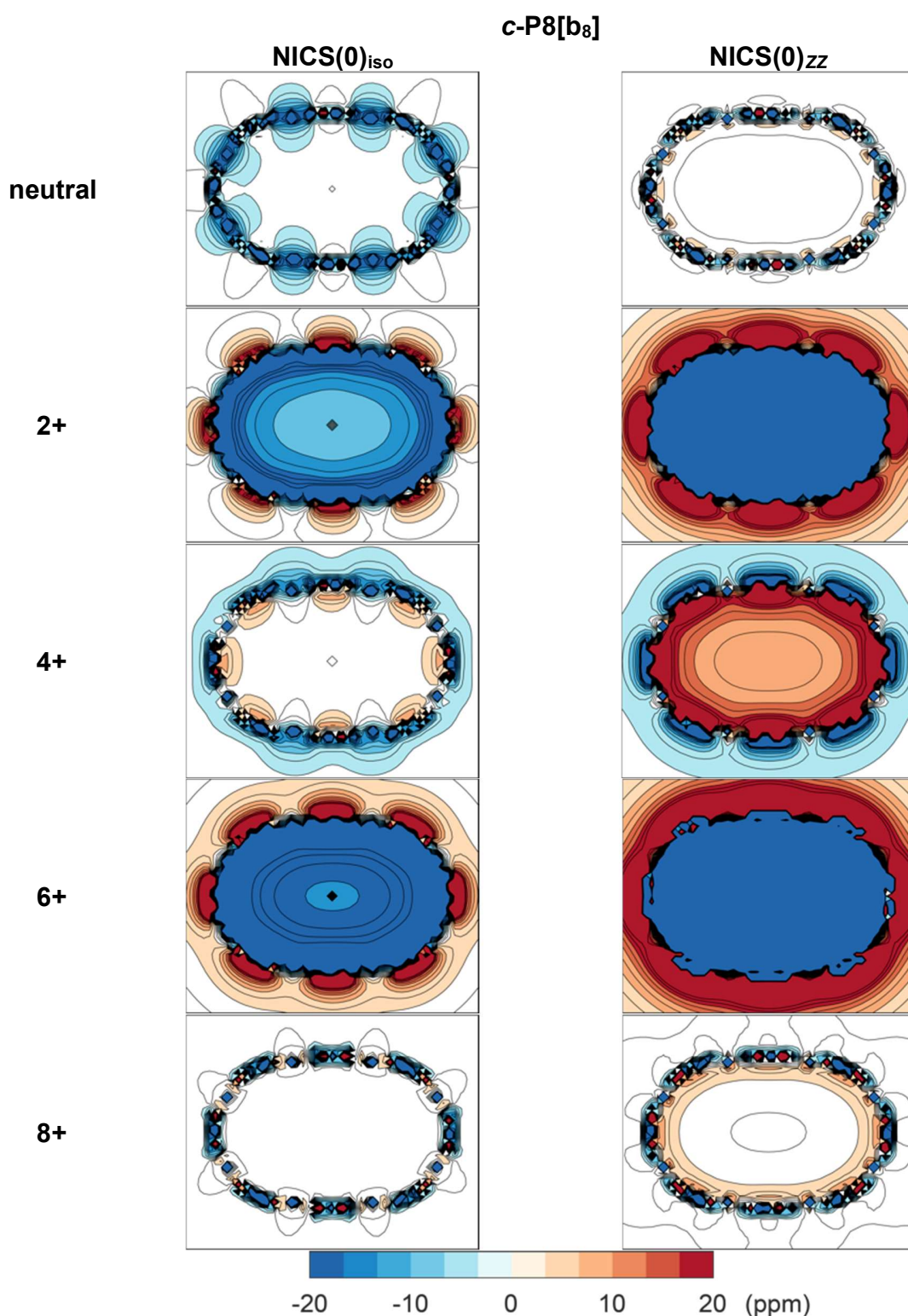


**Figure S32.** NICS(0)<sub>iso</sub> and NICS(0)<sub>zz</sub> plots of **c-P8[b<sub>8</sub>]** at oxidation states 0, 2+, 4+, 6+ and 8+. Geometries were optimized using LC- $\omega$ hPBE/6-31G\* ( $\omega = 0.1$ ) at every oxidation state with the templates. NICS were calculated in the absence of template on a planar grid bisecting the Zn atoms (51 Å  $\times$  41 Å, spacing 1 Å). The color axis is truncated left (blue) and right (red) -20 ppm and 20 ppm, respectively. Contours are drawn every 3.3 ppm, from -20 to 20 ppm.



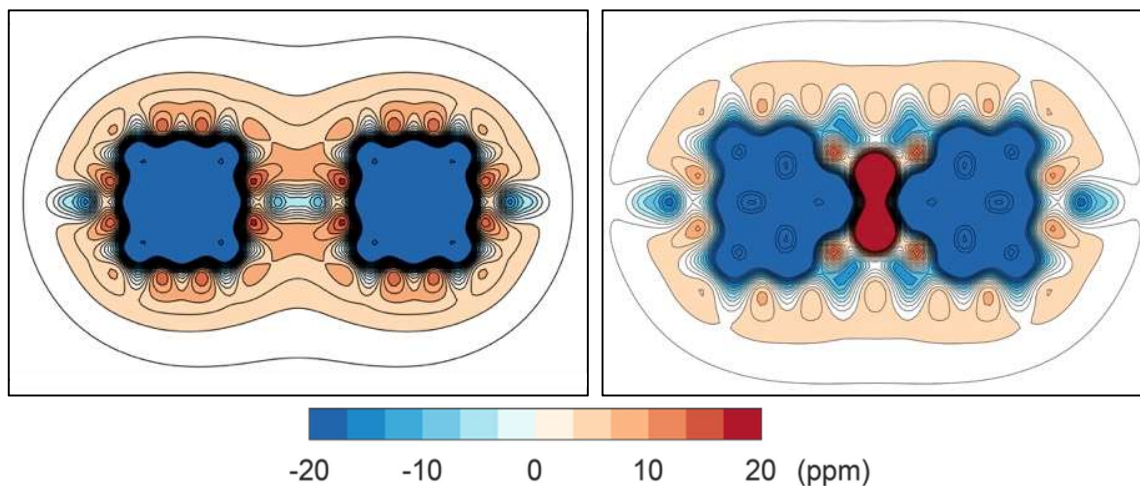


**Figure S33.** NICS(0)<sub>zz</sub> plots of linear oligomers **H-/P2[b<sub>1</sub>]-H** (left) and **H-/P2[f<sub>1</sub>]-H** (right). Geometries were optimized using LC- $\omega$ hPBE/6-31G\* ( $\omega = 0.1$ ) and NICS grids were calculated with 0.25 Å resolution on a 21 Å × 11 Å grid. The color axis is truncated left (blue) and right (red) -20 ppm and 20 ppm, respectively.

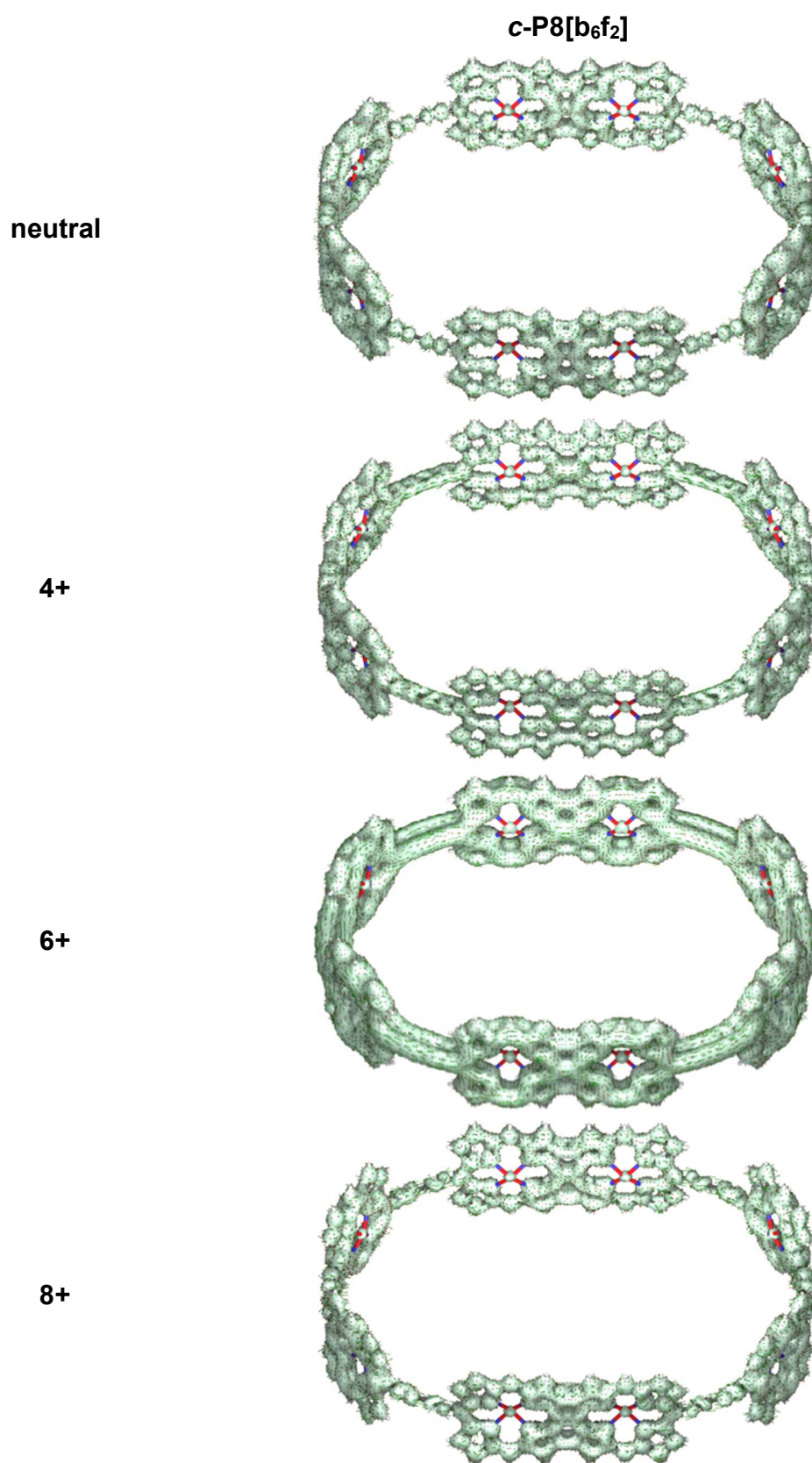


**Figure S34.** ACID plots of **c-P8[b<sub>6</sub>f<sub>2</sub>]** (top view at an angle).

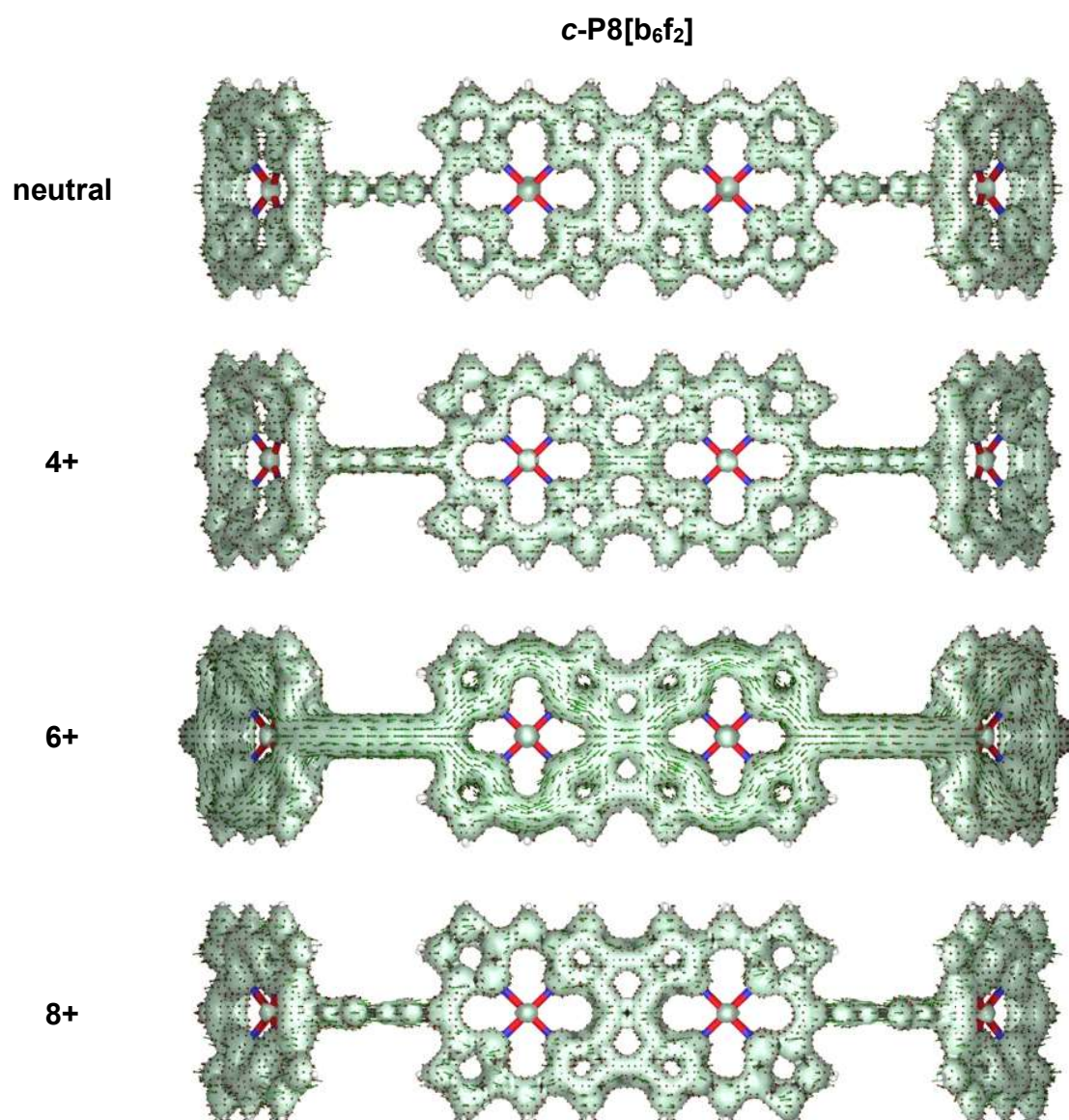


**Figure S35.** ACID plots of **c-P8[b<sub>6</sub>f<sub>2</sub>]** (porphyrin tape region).

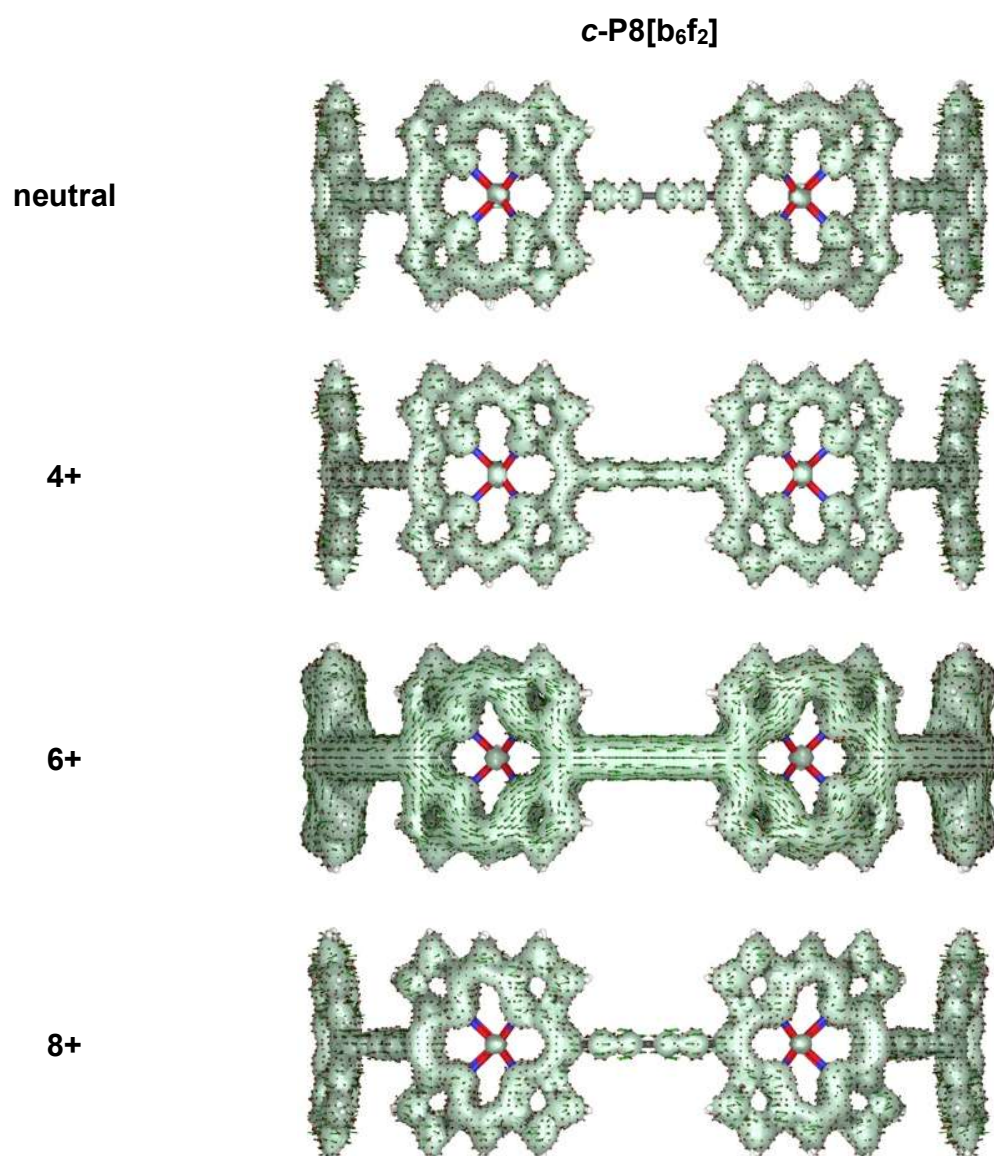


**Figure S36.** ACID plots of **c-P8[b<sub>6</sub>f<sub>2</sub>]** (butadiyne porphyrin region).



## 15. NMR and Mass Spectra of Novel Compounds

Si-*l*-P2[f<sub>1</sub>]-Si:

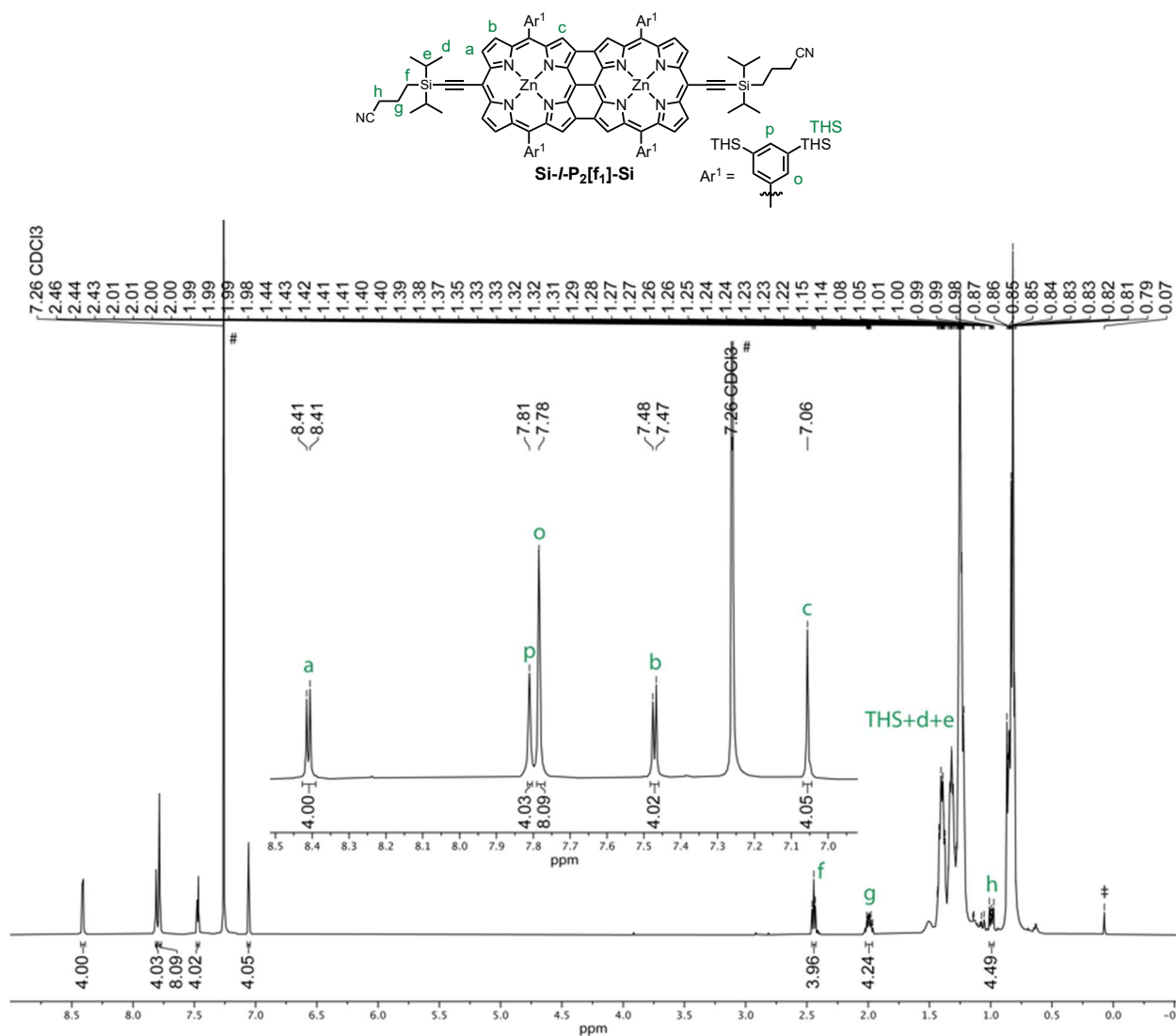


**Figure S37.** Labelled structure and  $^1\text{H}$  NMR spectrum of Si-*l*-P2[f<sub>1</sub>]-Si (500 MHz,  $\text{CDCl}_3$ , 298 K). # =  $\text{CHCl}_3$ ; ‡ = silicon grease.

**Table S13.** NMR assignment and correlations for Si-*l*-P2[f<sub>1</sub>]-Si.

#	Assign.	$^1\text{H}$	Mult. $J$ (Hz)	$^1\text{H}$ - $^1\text{H}$ COSY	$^1\text{H}$ - $^1\text{H}$ NOESY <sup>†</sup>	$^1\text{H}$ - $^{13}\text{C}$ HSQC + $^{13}\text{C}$
1	a	8.41 (4H)	d, $J$ = 4.6	4	s: 4; w: 3	129.8
2	p	7.81 (4H)	s	-	m: 9	139.4
3	o	7.78 (8H)	s	-	w: 1; s: 4, 5; m: 9	138.6
4	b	7.47 (4H)	d, $J$ = 4.6	1	s: 1, 3; m: 9	132.2
5	c	7.06 (4H)	s	-	s: 3; m: 9	127.8
6	f	2.44 (4H)	t, $J$ = 6.8	7	-	21.1
7	g	2.04–1.95 (4H)	m	6, 8	-	21.6
8	h	1.01–0.97 (4H)	m	7	-	10.1
9	TMS+d+e	1.45–0.75 (340H)	m	9	m: 2, 3, 4, 5	12.2, 12.8, 14.3, 18.3, 18.6, 22.6, 22.8, 24.1, 29.9, 31.7, 33.6

<sup>†</sup>Relative correlation intensities are designated as: s = strong, m = medium, w = weak.

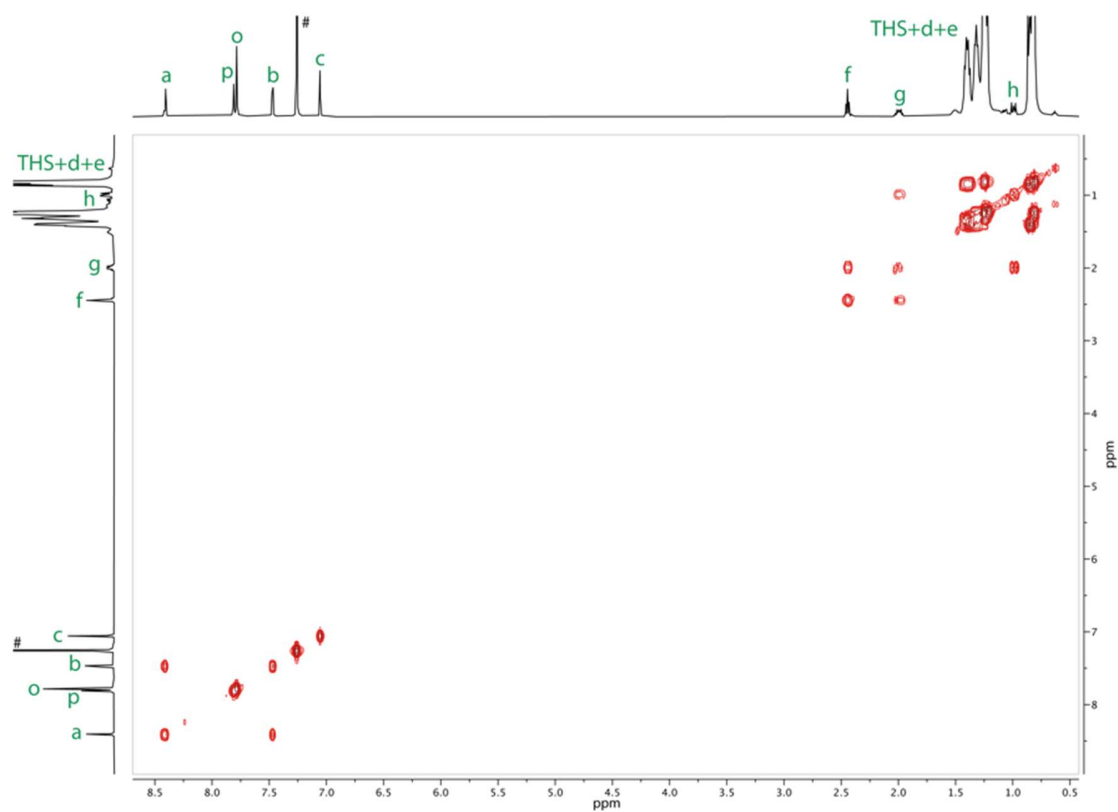


Figure S38.  $^1\text{H}$ - $^1\text{H}$  COSY spectrum of **Si-l-P2**[ $f_1$ ]-**Si** (500 MHz,  $\text{CDCl}_3$ , 298 K).

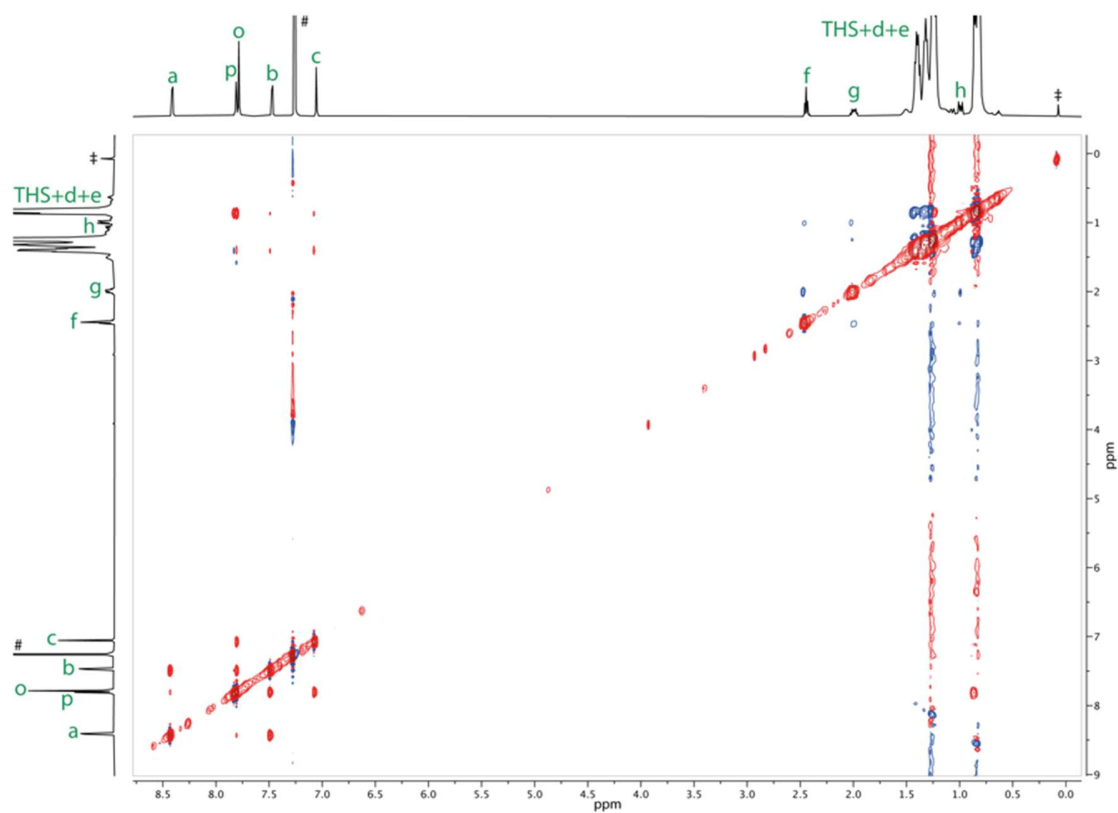
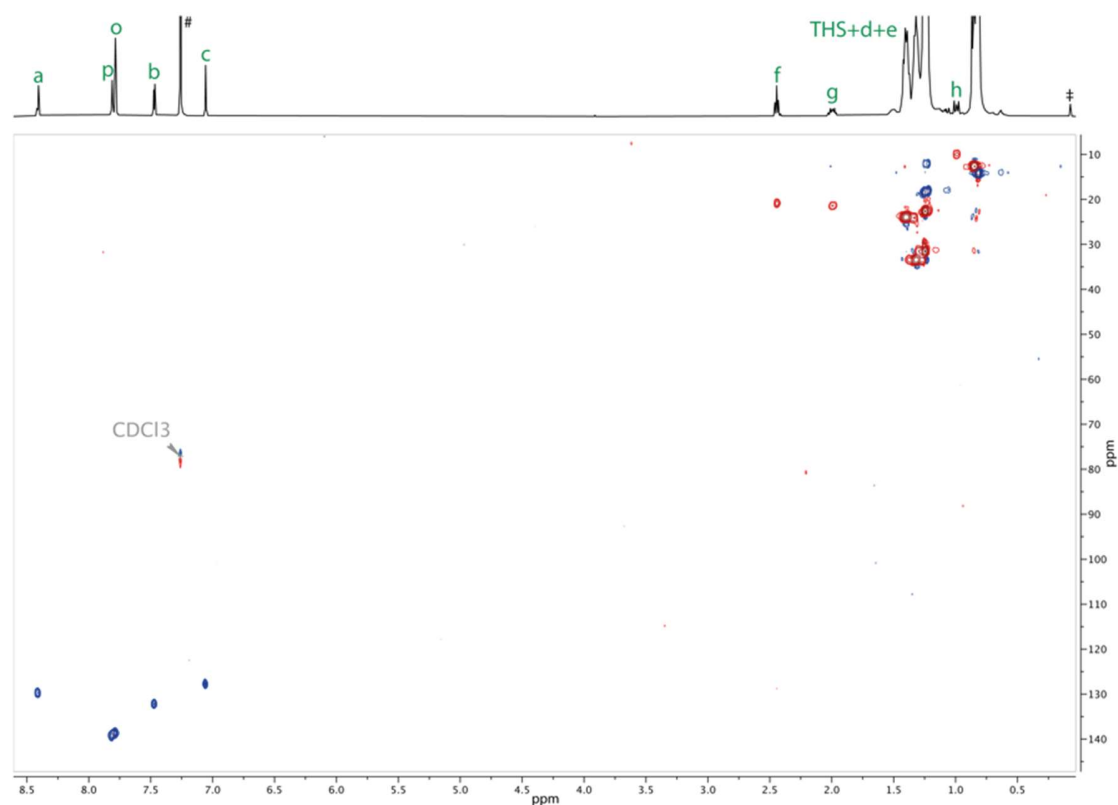
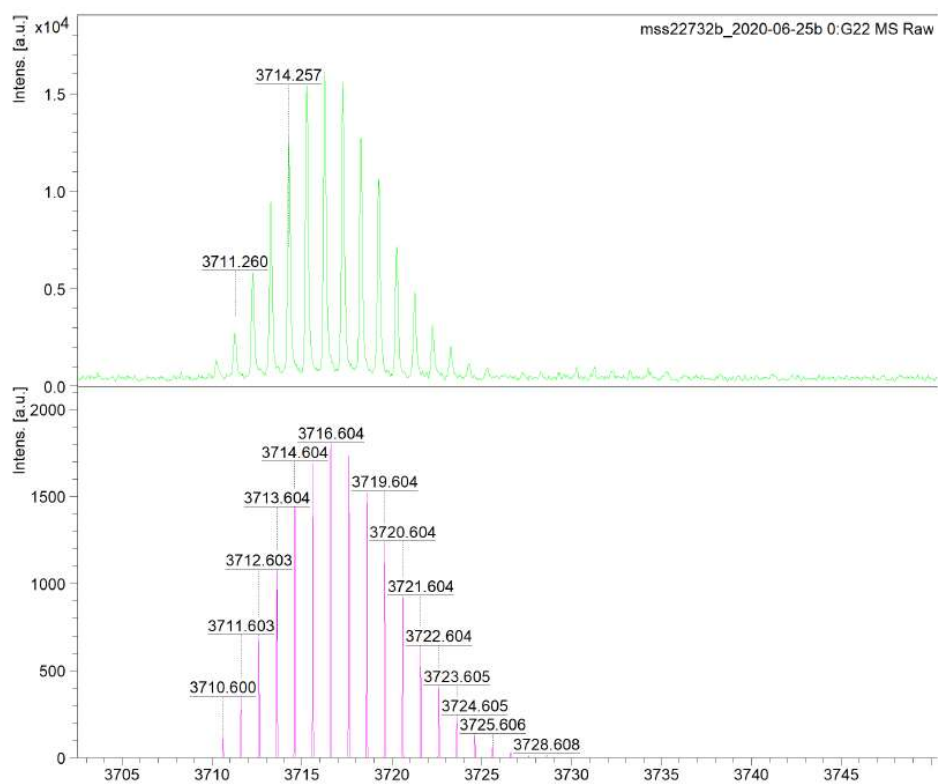


Figure S39.  $^1\text{H}$ - $^1\text{H}$  NOESY spectrum of **Si-l-P2**[ $f_1$ ]-**Si** (500 MHz,  $\text{CDCl}_3$ , 298 K).



**Figure S40.**  $^1\text{H}$ - $^{13}\text{C}$  HSQC spectrum of **Si-I-P2[f<sub>1</sub>]-Si** (500 MHz,  $\text{CDCl}_3$ , 298 K).



**Figure S41.** Experimental MALDI-ToF spectrum of **Si-I-P2[f<sub>1</sub>]-Si** (top) and simulated MALDI-ToF spectrum of **Si-I-P2[f<sub>1</sub>]-Si** [ $\text{C}_{232}\text{H}_{376}\text{N}_{10}\text{Si}_{10}\text{Zn}_2$ ] $^+$  (bottom).



**H-*I*-P2[f<sub>1</sub>]-H:**

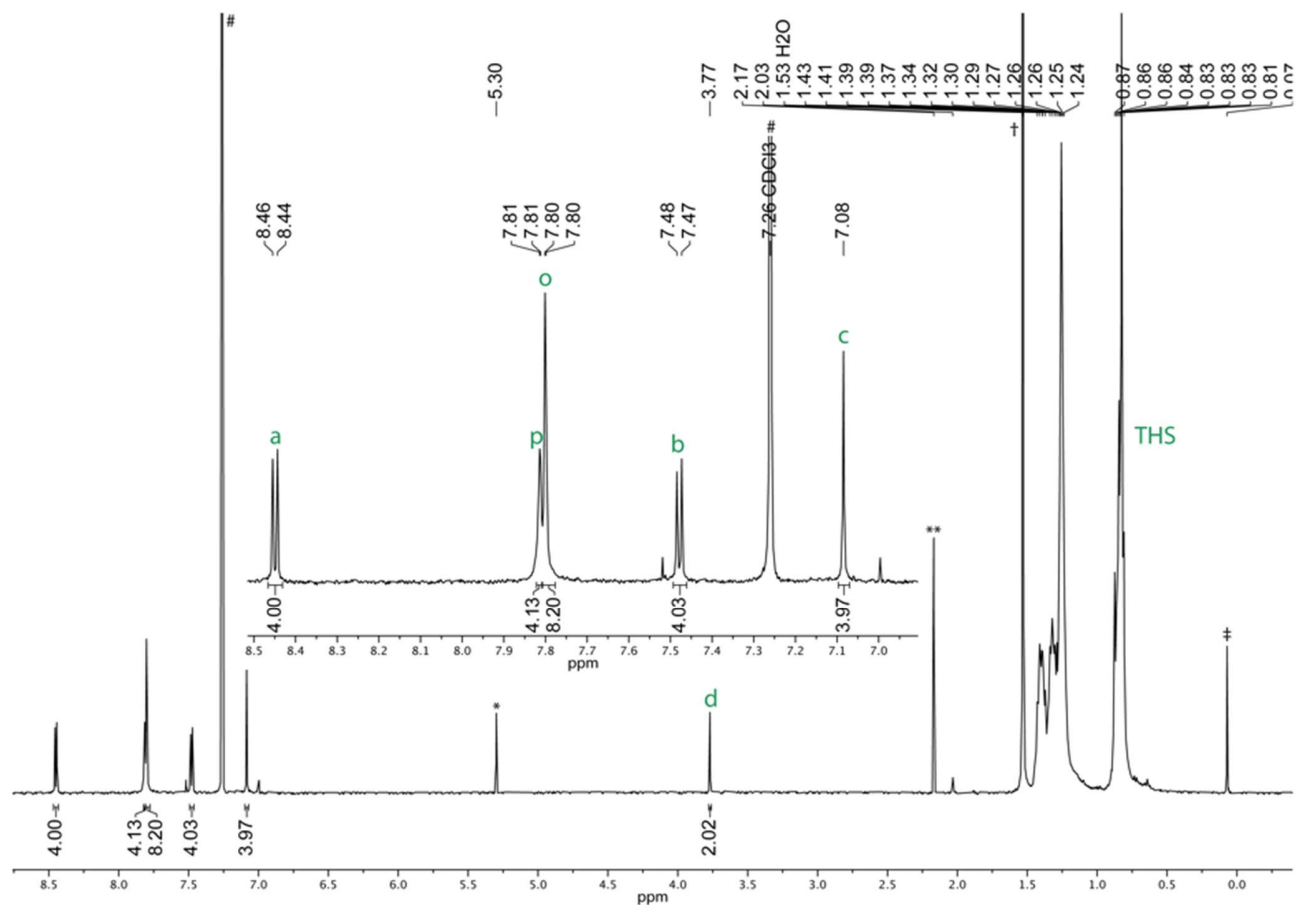
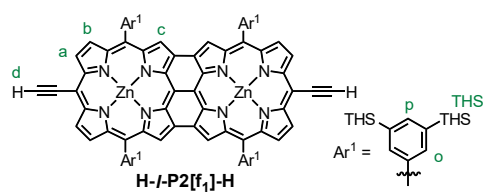


**Figure S42.** Labelled structure and <sup>1</sup>H NMR spectrum of **H-*I*-P2[f<sub>1</sub>]-H** (400 MHz, CDCl<sub>3</sub>, 298 K). # = CHCl<sub>3</sub>; \* = CH<sub>2</sub>Cl<sub>2</sub>; \*\* = acetone; † = water; ‡ = silicon grease.

**Si-*l*-P4[b<sub>2</sub>f<sub>1</sub>]-Si:**

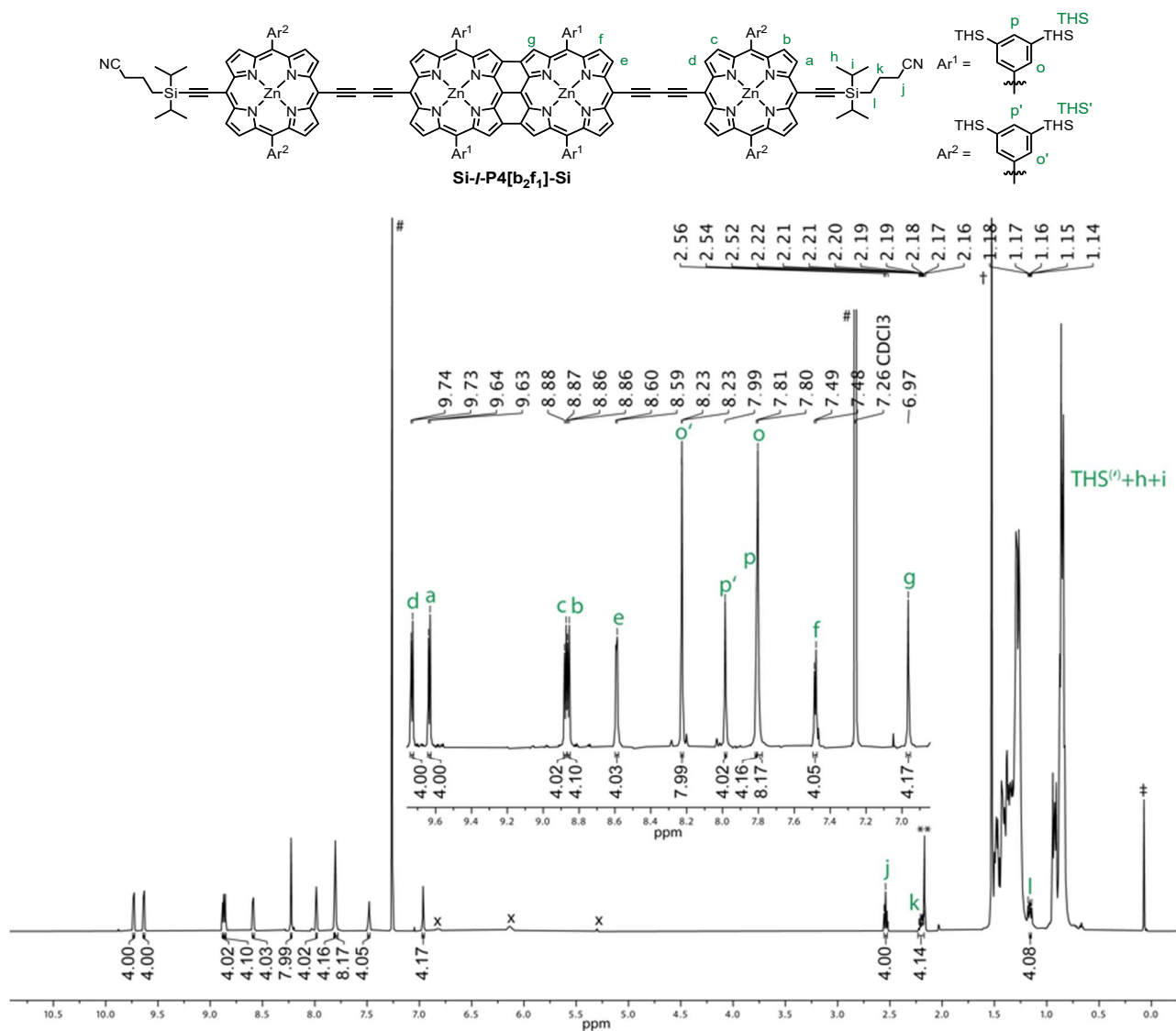


**Figure S43.** Labelled structure and <sup>1</sup>H NMR spectrum of Si-*l*-P4[b<sub>2</sub>f<sub>1</sub>]-Si (500 MHz, CDCl<sub>3</sub>, 298 K). # = CHCl<sub>3</sub>; x = pyridine; \*\* = acetone; † = water; ‡ = silicon grease.

**Table S14.** NMR assignment and correlations for tetramer **Si-*I*-P4[b<sub>2</sub>f<sub>1</sub>]-Si**.

#	Assign.	<sup>1</sup> H	Mult. <i>J</i> (Hz)	<sup>1</sup> H- <sup>1</sup> H COSY	<sup>1</sup> H- <sup>1</sup> H ROESY <sup>†</sup>	<sup>1</sup> H- <sup>13</sup> C HSQC + <sup>13</sup> C
1	d	9.73 (4H)	d, <i>J</i> = 4.6	3	s: 3; w: 5, 15	130.89
2	a	9.63 (4H)	d, <i>J</i> = 4.6	4	s: 4; m: 15	130.89
3	c	8.88 (4H)	d, <i>J</i> = 4.6	1	s: 1, 6; m: 15	133.30
4	b	8.86 (4H)	d, <i>J</i> = 4.6	2	s: 2, 6; m: 15	133.11
5	e	8.59 (4H)	d, <i>J</i> = 4.5	10	s: 10; m: 15; w: 1	129.43
6	o'	8.23 (8H)	s	7	s: 3, 4, 15	140.52
7	p'	7.99 (4H)	s	6	s: 15	139.31
8	p	7.81 (4H)	s	-	s: 15	139.00
9	o	7.80 (8H)	s	-	s: 10, 11, 15	138.79
10	f	7.48 (4H)	d, <i>J</i> = 4.5	5	s: 5, 9; w: 15	132.32
11	g	6.96 (4H)	s	-	s: 9, 15	127.67
12	j	2.54 (4H)	t, <i>J</i> = 6.82	13	w: 13, 14	21.19
13	k	2.23–2.16 (4H)	m	12, 14	w: 12, 14, 15	21.77
14	l	1.19–1.14 (4H)	m	13	w: 12, 13, 15	10.30
15	THS+THS'+h+i	1.55–0.64 (652H)	m	15	s: 6, 7, 8, 9, 11; m: 2, 3, 4, 5, 10; w: 1, 13, 14	12.46, 12.58, 12.77, 12.79, 14.30, 18.50, 18.76, 22.79, 22.82, 24.14, 24.17, 29.86, 31.71, 31.75, 33.63, 33.66

<sup>†</sup>Relative correlation intensities are designated as: s = strong, m = medium, w = weak.

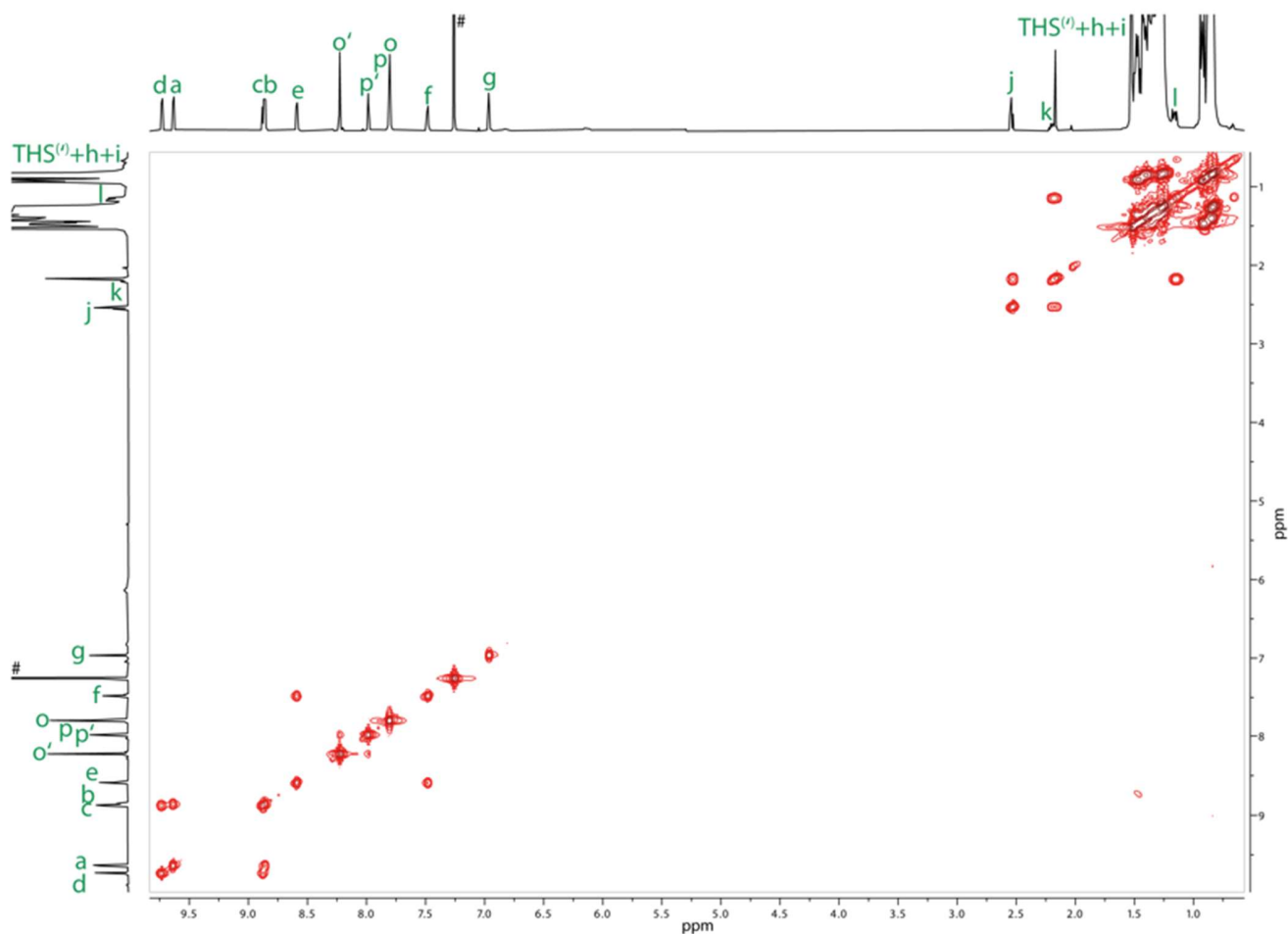


**Figure S44.** <sup>1</sup>H-<sup>1</sup>H COSY spectrum of **Si-*I*-P4[b<sub>2</sub>f<sub>1</sub>]-Si** (500 MHz, CDCl<sub>3</sub>, 298 K).

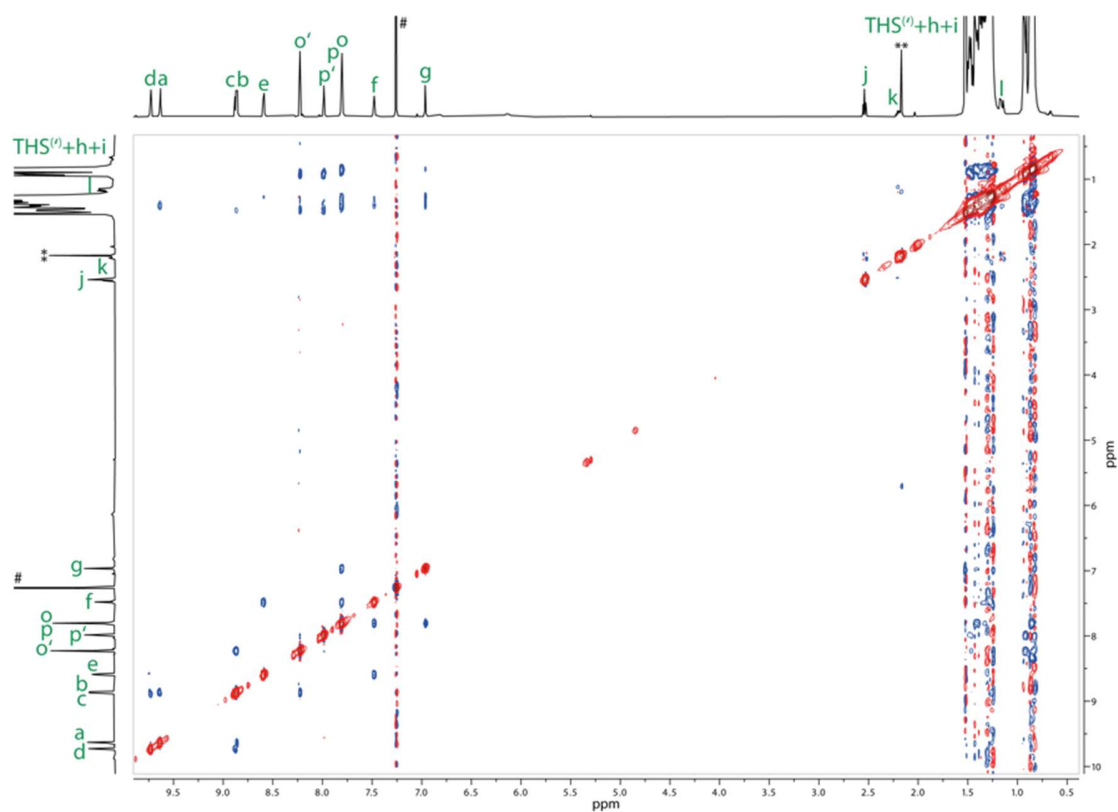


Figure S45.  $^1\text{H}$ - $^1\text{H}$  ROESY spectrum of  $\text{Si-}I\text{-P4}[\text{b}_2\text{f}_1]\text{-Si}$  (500 MHz,  $\text{CDCl}_3$ , 298 K).

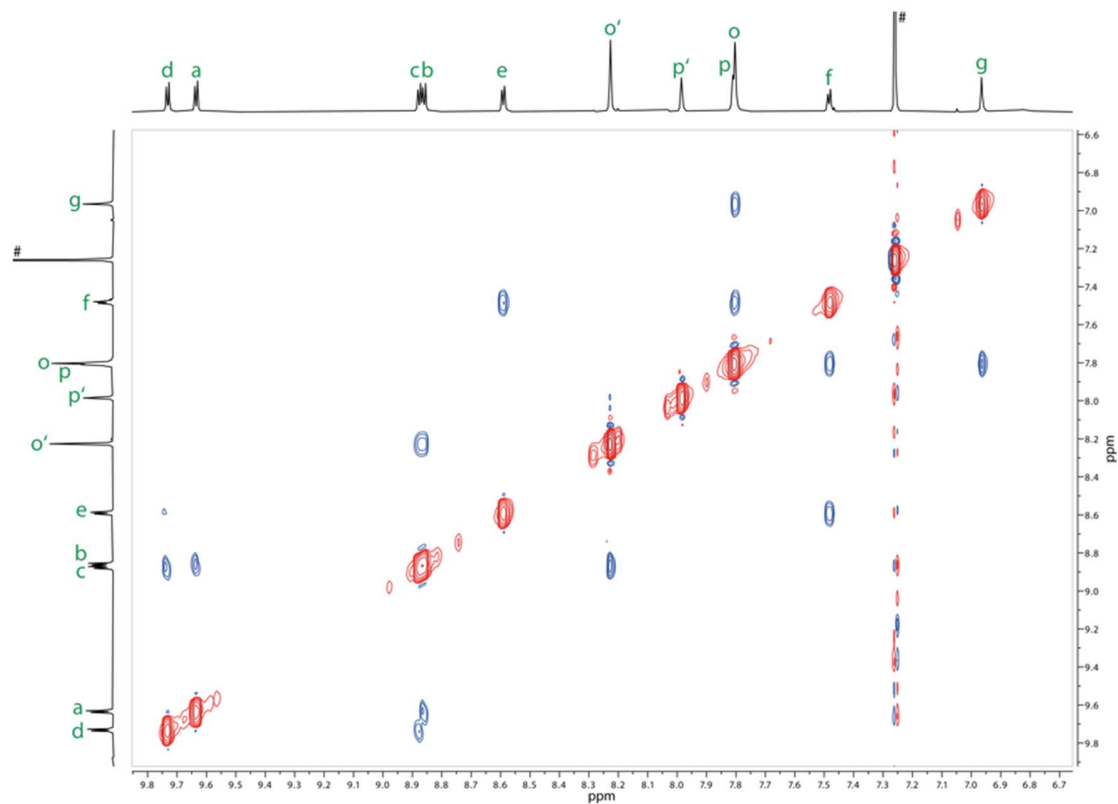


Figure S46. Enlarged region of the ROESY spectrum of  $\text{Si-}I\text{-P4}[\text{b}_2\text{f}_1]\text{-Si}$  (500 MHz,  $\text{CDCl}_3$ , 298 K).

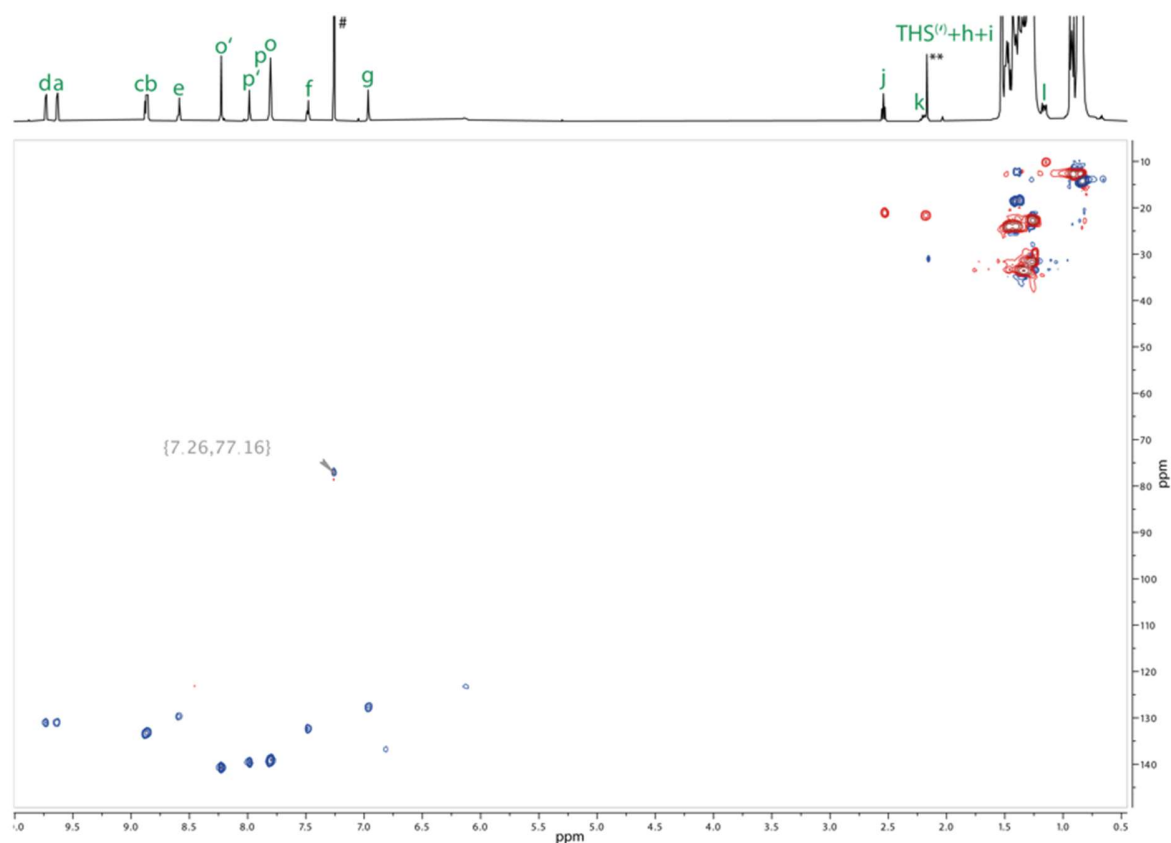


Figure S47.  $^1\text{H}$ - $^{13}\text{C}$  HSQC spectrum of **Si-I-P4[b<sub>2</sub>f<sub>1</sub>]-Si** (500 MHz,  $\text{CDCl}_3$ , 298 K).

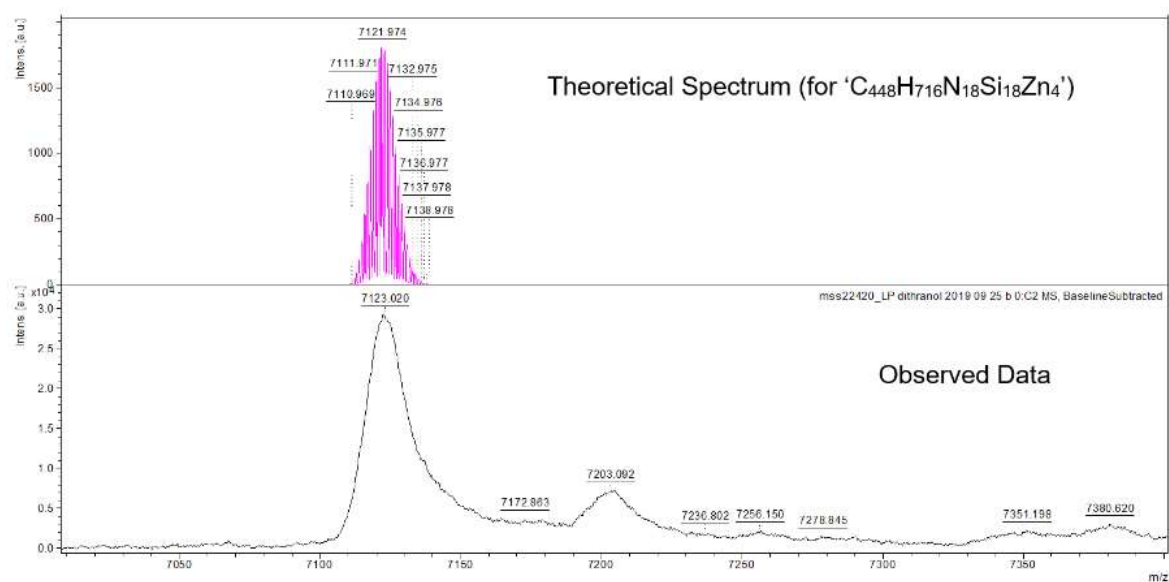
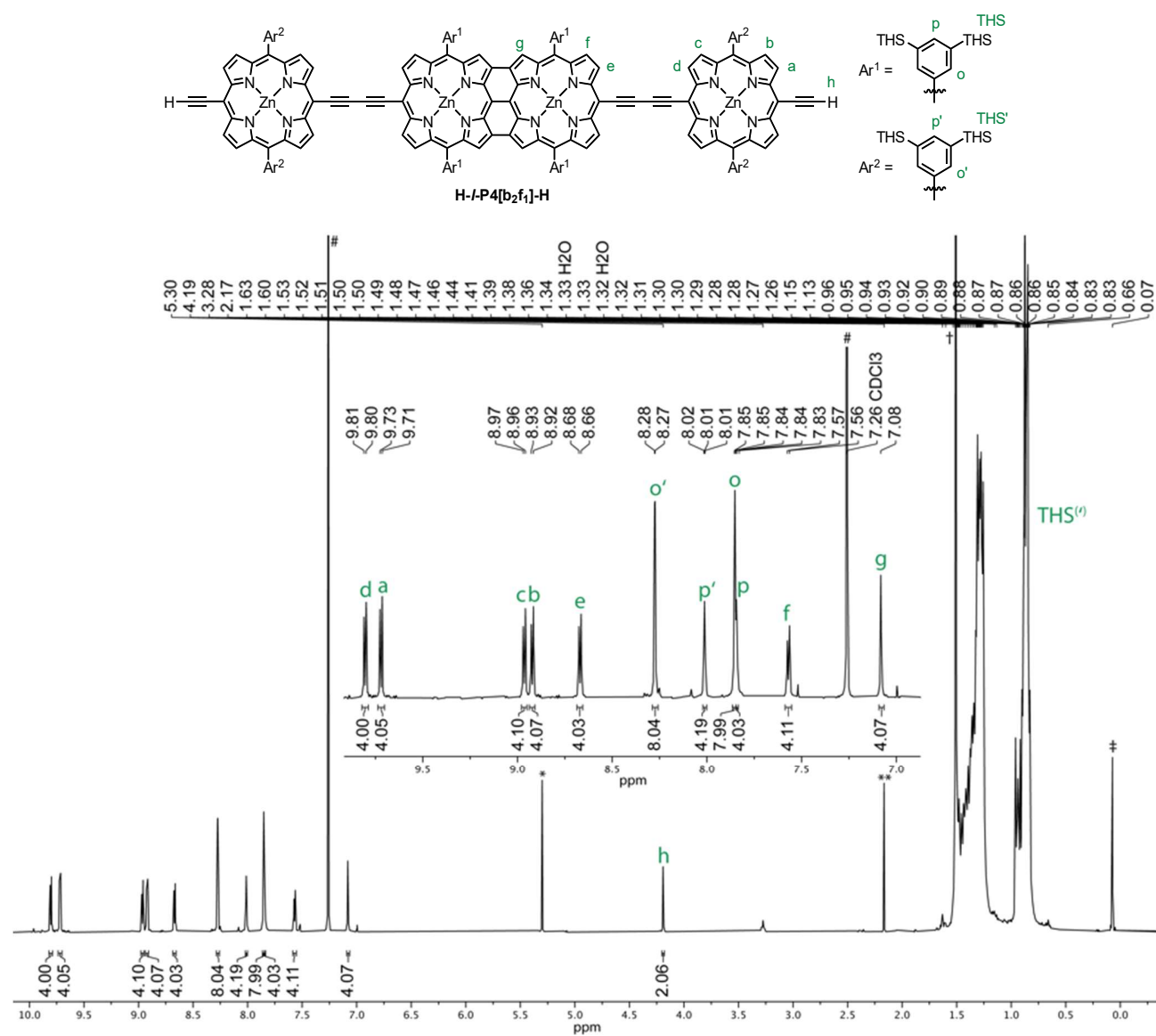


Figure S48. Experimental MALDI-ToF spectrum of **Si-I-P4[b<sub>2</sub>f<sub>1</sub>]-Si** (bottom) and simulated MALDI-ToF spectrum of **Si-I-P4[b<sub>2</sub>f<sub>1</sub>]-Si<sup>+</sup>** [ $\text{C}_{448}\text{H}_{716}\text{N}_{18}\text{Si}_{18}\text{Zn}_4$ ]<sup>+</sup> (top).

**H-*I*-P4[b<sub>2</sub>f<sub>1</sub>]-H:**



**Figure S49.** Labelled structure and <sup>1</sup>H NMR spectrum of H-*I*-P4[b<sub>2</sub>f<sub>1</sub>]-H (400 MHz, CDCl<sub>3</sub>, 298 K). # = CHCl<sub>3</sub>; \* = CH<sub>2</sub>Cl<sub>2</sub>; \*\* = acetone; † = water; ‡ = silicon grease.

Complex  $c\text{-P8}[\text{b}_6\text{f}_2]\bullet(\text{T4})_2$ :

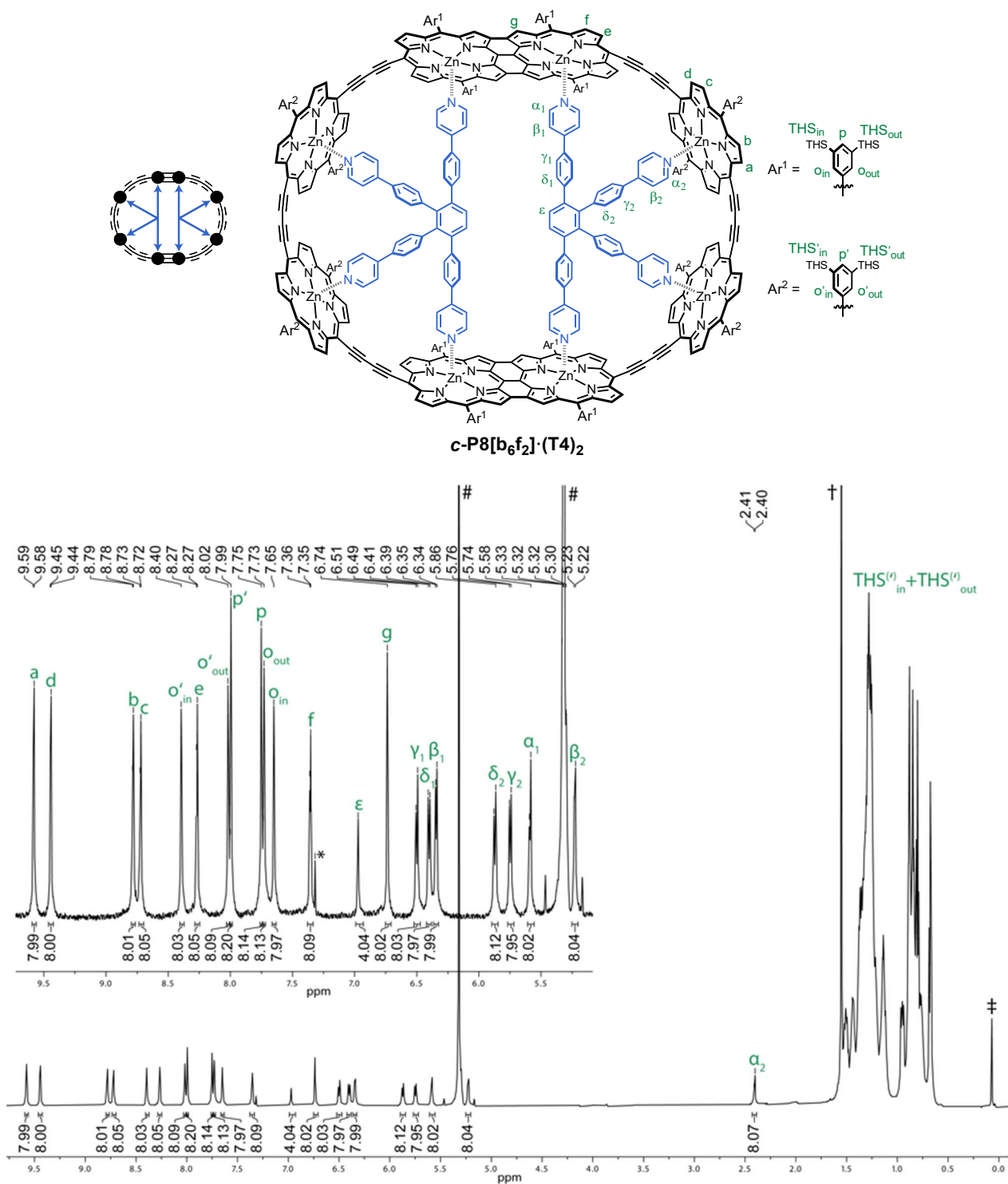


**Figure S50.** Assigned structure and  $^1\text{H}$  NMR spectrum of  $c\text{-P8}[\text{b}_6\text{f}_2]\bullet(\text{T4})_2$  (600 MHz,  $\text{CD}_2\text{Cl}_2$ , 298 K). # =  $\text{CHDCl}_2$ ; \* =  $\text{CHCl}_3$ ; † = water; ‡ = silicon grease.



**Table S15.** Complete <sup>1</sup>H NMR assignment and correlations for complex **c-P8[b<sub>6</sub>f<sub>2</sub>](T4)<sub>2</sub>**.

#	Assign.	<sup>1</sup> H	Mult. <i>J</i> (Hz)	<sup>1</sup> H– <sup>1</sup> H COSY	<sup>1</sup> H– <sup>1</sup> H NOESY <sup>†</sup>	<sup>1</sup> H– <sup>13</sup> C HSQC
1	a	9.58 (8H)	d, <i>J</i> = 4.3	3	s: 3; m: 5, 7, 23; w: 21, 22	-
2	d	9.45 (8H)	d, <i>J</i> = 4.3	4	s: 4; m: 5, 6, 7, 23; w: 22	130.6
3	b	8.78 (8H)	d, <i>J</i> = 4.3	1	s: 1, 5, 7, 23; m: 22; w: 21	133.2
4	c	8.72 (8H)	d, <i>J</i> = 4.3	2	s: 2, 5, 7, 23; m: 22; w: 21	-
5	o' <sub>in</sub>	8.40 (8H)	s	7	s: 3, 4, 7, 23; m: 1, 2, 8, 22; w: 21	140.6
6	e	8.27 (8H)	d, <i>J</i> = 4.3	12	s: 12; m: 2, 10, 11, 23; w: 9, 20	128.7
7	o' <sub>out</sub>	8.02 (8H)	s	5	s: 3, 4, 5, 23; m: 1, 2; w: 22	141.7
8	p'	7.99 (8H)	s	-	m: 5; s: 23	139.7
9	p	7.75 (8H)	s	-	s: 23, m: 11, 12, 14; w: 6	139.6
10	o <sub>out</sub>	7.73 (8H)	s	-	s: 12, 14, 23; m: 6	-
11	o <sub>in</sub>	7.65 (8H)	s	-	s: 12, 14, 23; m: 6, 9, 20; w: 17	-
12	f	7.36 (8H)	d, <i>J</i> = 4.3	6	s: 6, 10, 11, 23; m: 9, 14; w: 17, 20	132.1
13	ε	6.97 (4H)	s	-	s: 16; m: 15; w: 18	-
14	g	6.74 (8H)	s	-	s: 10, 11, 23; m: 9, 12; w: 20	-
15	γ <sub>1</sub>	6.50 (8H)	d, <i>J</i> = 8.7	16	s: 16, 17; m: 13, 18, 20; w: 19, 23	125.9
16	δ <sub>1</sub>	6.40 (8H)	d, <i>J</i> = 8.7	15	s: 13, 15, 18; m: 17, 19; w: 20, 23	130.2
17	β <sub>1</sub>	6.34 (8H)	d, <i>J</i> = 6.4	20	s: 15, 20; m: 16; w: 11, 12, 23	121.3
18	δ <sub>2</sub>	5.87 (8H)	d, <i>J</i> = 8.8	19	s: 16, 19; m: 15, 21; w: 13, 22, 23	131.5
19	γ <sub>2</sub>	5.75 (8H)	d, <i>J</i> = 8.8	18	s: 18; m: 16, 21, 22; w: 15, 23	-
20	α <sub>1</sub>	5.59 (8H)	d, <i>J</i> = 6.4	17	s: 17; m: 11, 15; w: 6, 12, 16, 20, 23	145.7
21	β <sub>2</sub>	5.23 (8H)	d, <i>J</i> = 6.2	22	s: 22; m: 18, 19; w: 1, 3, 4, 5, 23	119.9
22	α <sub>2</sub>	2.41 (8H)	d, <i>J</i> = 6.2	21	s: 21; m: 3, 4, 5, 19; w: 1, 2, 7, 18, 23	143.0
23	THS <sub>in</sub> + THS <sub>out</sub> + THS' <sub>in</sub> + THS' <sub>out</sub>	1.53–0.61 (1248H)	m	23	s: 3, 4, 5, 7, 8, 9, 10, 11, 12, 14, 23; m: 1, 2; w: 15, 16, 17, 18, 19, 20, 21, 22	12.66, 12.69, 12.8, 14.25, 14.33, 14.4, 22.92, 22.93, 23.00, 23.01, 24.17, 24.21, 24.24, 24.4, 30.0, 31.76, 31.84, 31.88, 31.92, 32.0, 33.75, 33.83, 33.86, 33.93

<sup>†</sup>Relative correlation intensities are designated as: s = strong, m = medium, w = weak.

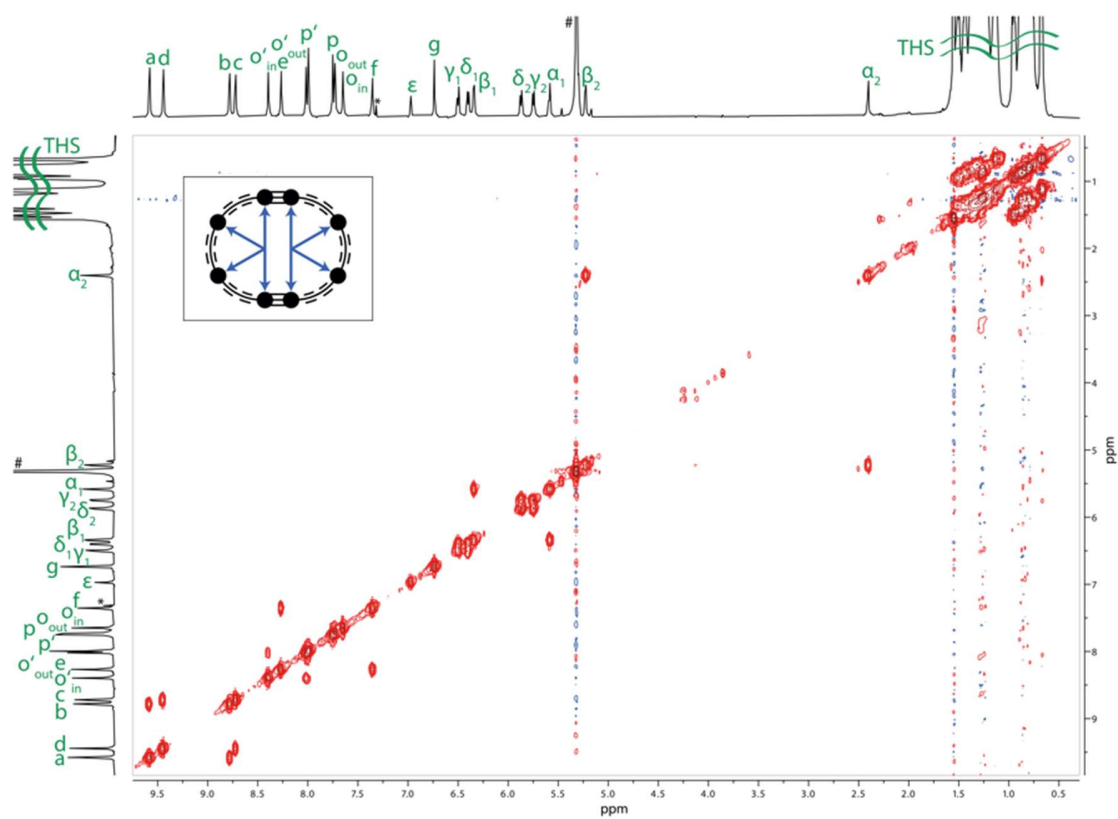


Figure S51.  $^1\text{H}$ - $^1\text{H}$  COSY spectrum of  $c\text{-P8}[\text{b}_6\text{f}_2]\bullet(\text{T4})_2$  (600 MHz,  $\text{CD}_2\text{Cl}_2$ , 298 K).

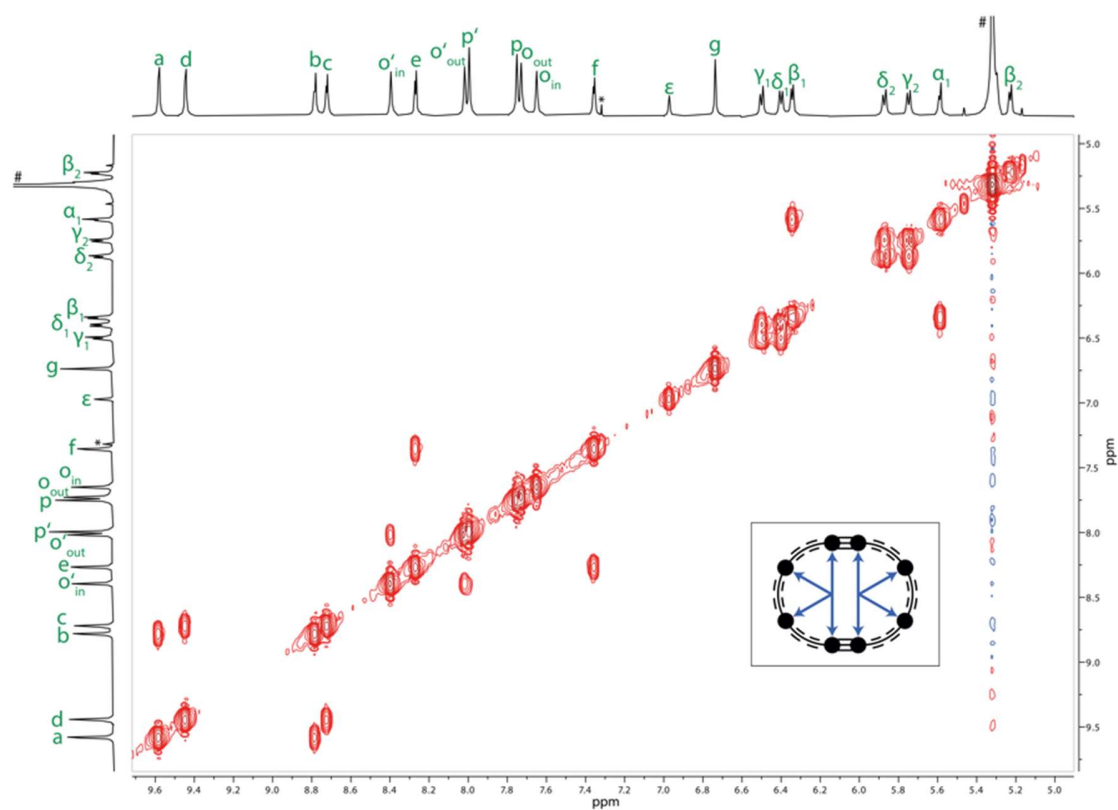


Figure S52. Enlarged region of the COSY spectrum of  $c\text{-P8}[\text{b}_6\text{f}_2]\bullet(\text{T4})_2$  (600 MHz,  $\text{CD}_2\text{Cl}_2$ , 298 K).

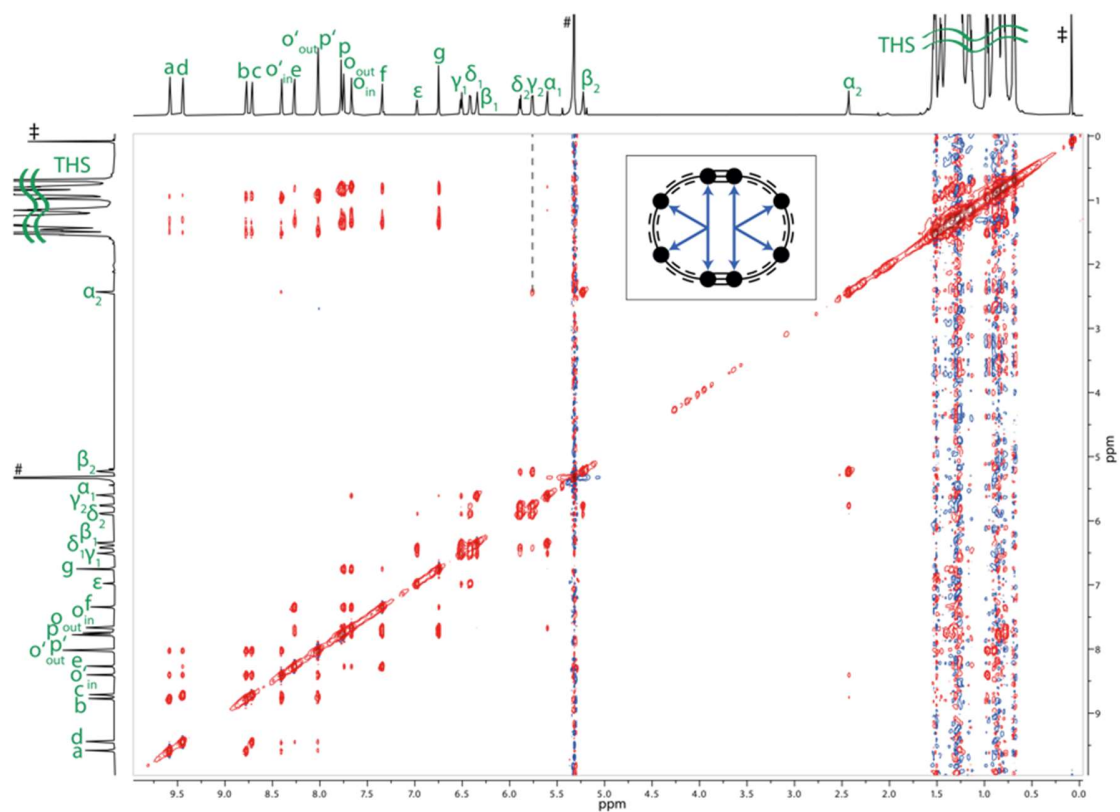


Figure S53.  $^1\text{H}$ - $^1\text{H}$  NOESY spectrum of  $c\text{-P8}[\text{b}_6\text{f}_2]\bullet(\text{T4})_2$  (600 MHz,  $\text{CD}_2\text{Cl}_2$ , 298 K).

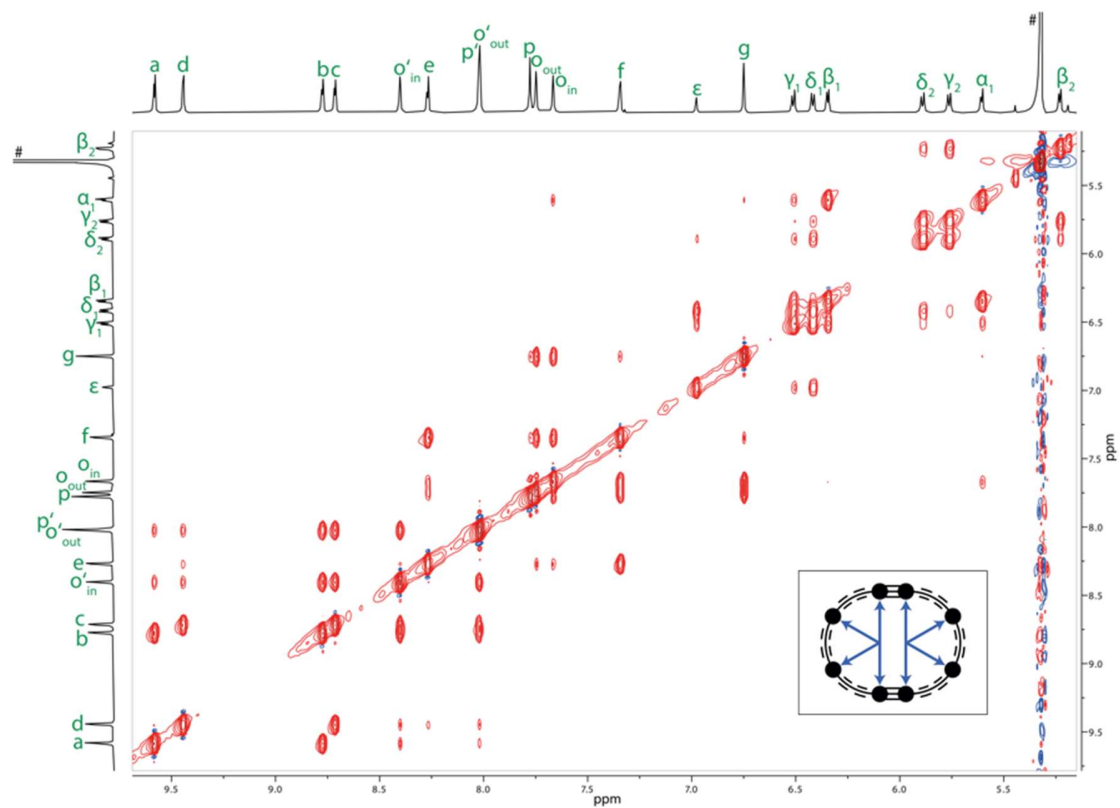


Figure S54. Enlarged region of the NOESY spectrum of  $c\text{-P8}[\text{b}_6\text{f}_2]\bullet(\text{T4})_2$  (600 MHz,  $\text{CD}_2\text{Cl}_2$ , 298 K).

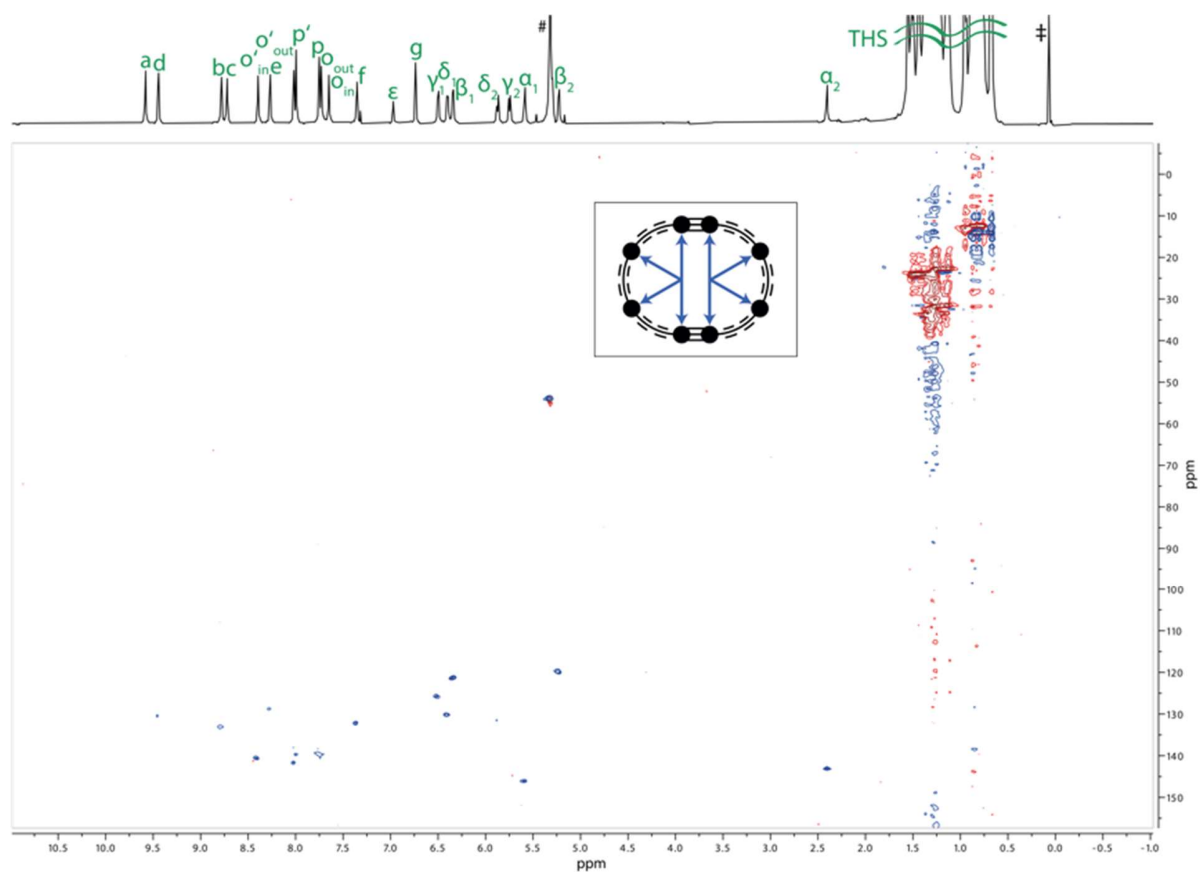


Figure S55.  $^1\text{H}$ - $^{13}\text{C}$  HSQC spectrum of  $\text{c-P8}[\text{b}_6\text{f}_2]\bullet(\text{T4})_2$  (600 MHz,  $\text{CD}_2\text{Cl}_2$ , 298 K).

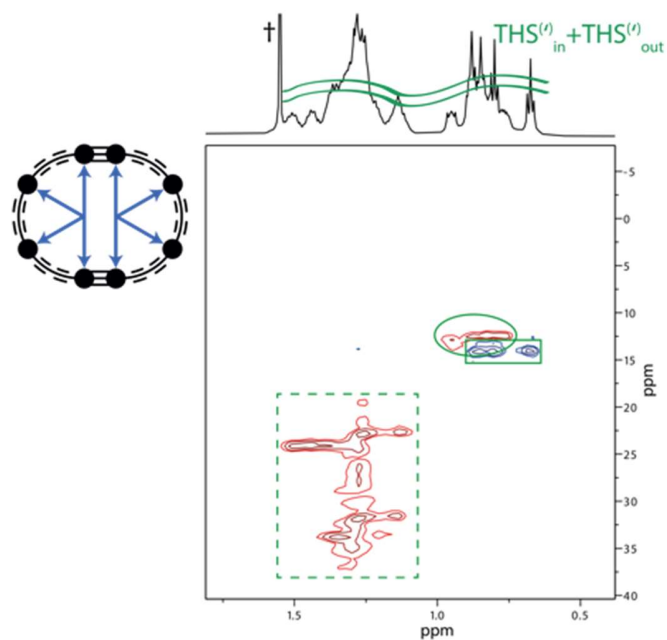
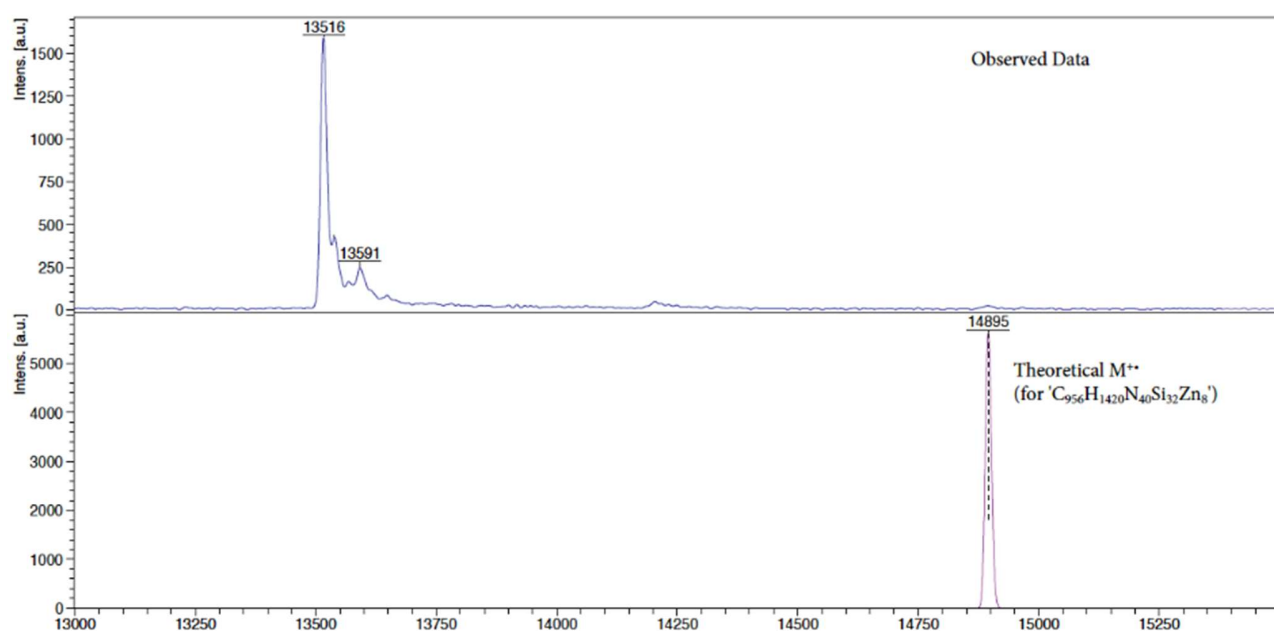
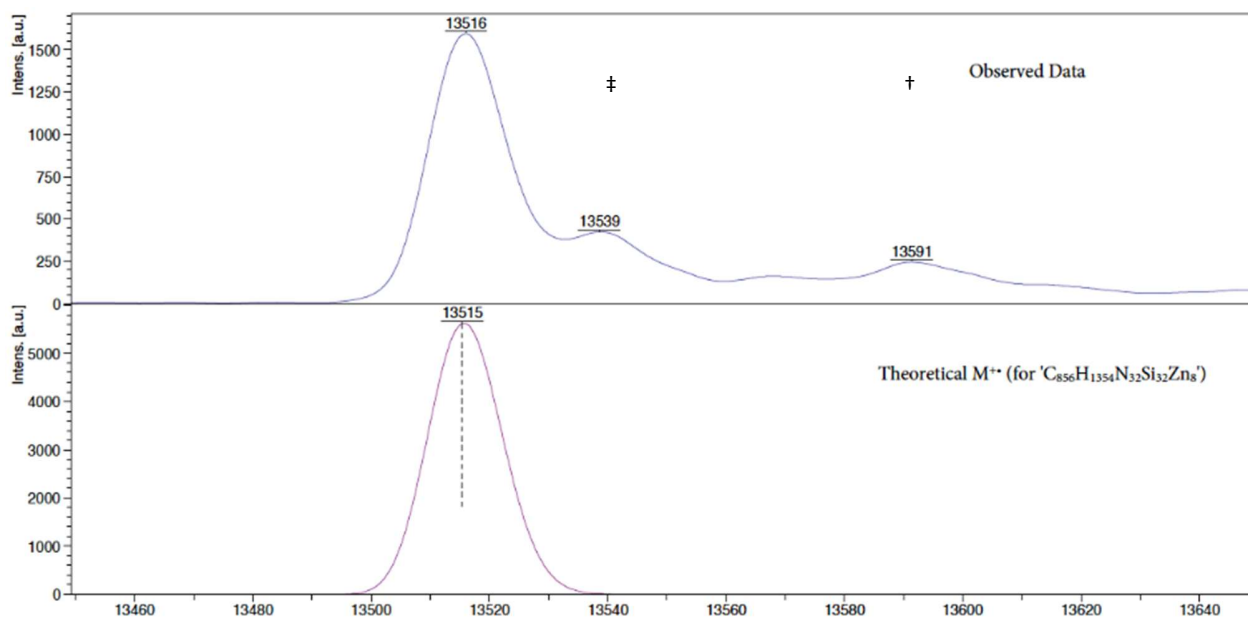


Figure S56. THS region of the  $^1\text{H}$ - $^{13}\text{C}$  HSQC spectrum of  $\text{c-P8}[\text{b}_6\text{f}_2]\bullet(\text{T4})_2$  (600 MHz,  $\text{CD}_2\text{Cl}_2$ , 298 K). Si-R- $\text{CH}_3$  resonances are indicated with a solid box, Si- $\text{CH}_2$ -R resonances with a solid circle, and Si- $\text{CH}_2$ - $\text{C}_4\text{H}_8$ - $\text{CH}_3$  resonances with a dashed box.



**Figure S57.** Experimental MALDI-ToF spectrum of  $c\text{-P8}[\text{b}_6\text{f}_2]\bullet(\text{T4})_2$  (top) and simulated MALDI-ToF spectrum of  $c\text{-P8}[\text{b}_6\text{f}_2]\bullet(\text{T4})_2^+$  [ $C_{956}H_{1420}N_{40}Si_{32}Zn_8$ ] $^+$  (bottom). † and ‡ indicate residual signals of  $c\text{-P8}[\text{b}_6\text{f}_2]\bullet(\text{T4})_2^+$  and  $c\text{-P8}[\text{b}_6\text{f}_2]\bullet(\text{T4})^+$  before and after onefold fragmentation, respectively.



**Figure S58.** Enlarged region of the experimental MALDI-ToF spectrum of  $c\text{-P8}[\text{b}_6\text{f}_2]\bullet(\text{T4})_2$  (top) and simulated spectrum of  $c\text{-P8}[\text{b}_6\text{f}_2]+2\text{H}^+$  [ $C_{856}H_{1352}N_{32}Si_{32}Zn_8$ ] $^+$  (bottom).

**H-*I*-P8[b<sub>5</sub>f<sub>2</sub>]-H:**

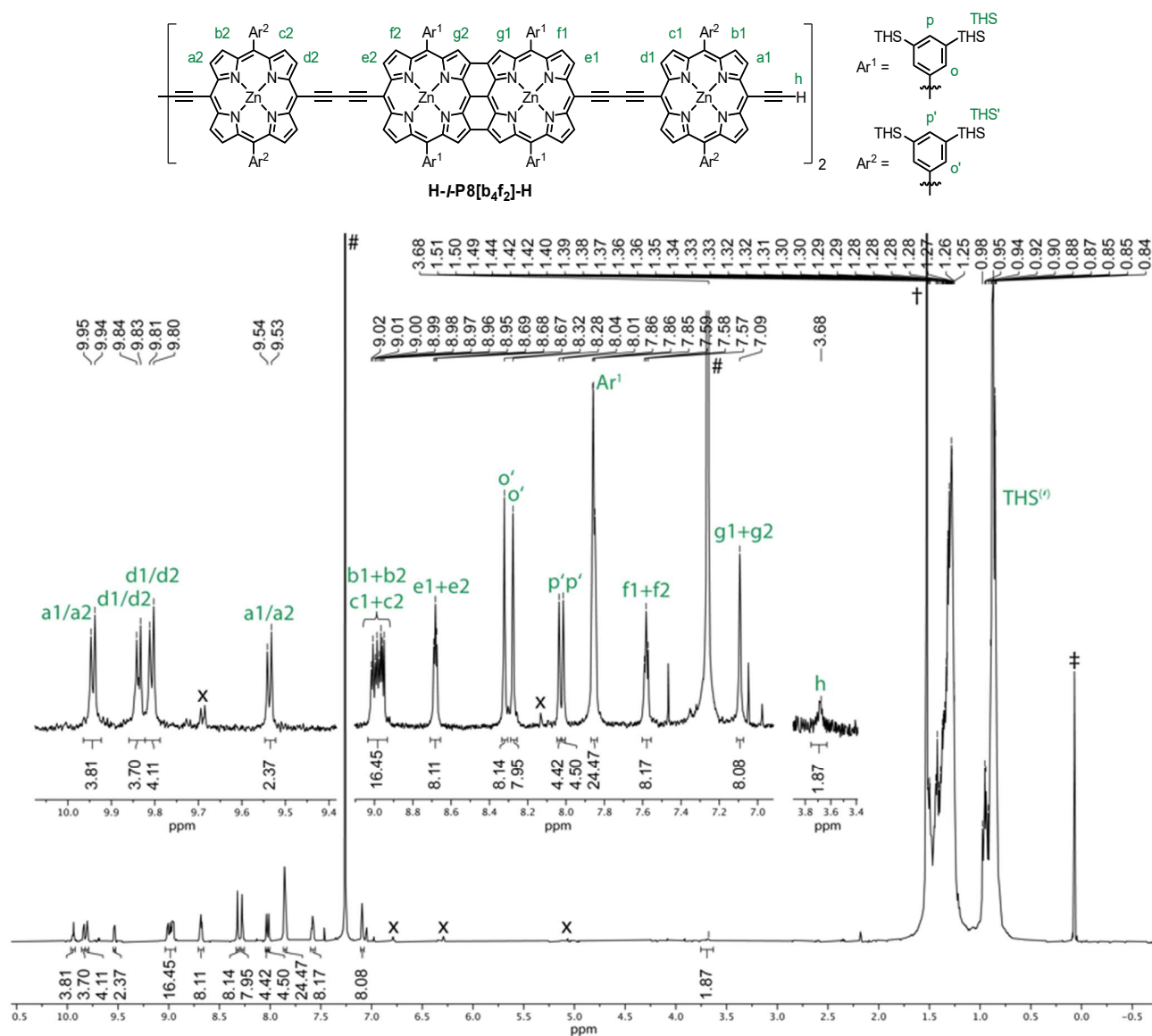


**Figure S59.** Assigned structure and <sup>1</sup>H NMR spectrum of **H-*I*-P8[b<sub>5</sub>f<sub>2</sub>]-H** (500 MHz, CDCl<sub>3</sub>, 298 K). # = CHCl<sub>3</sub>; + = water; ‡ = silicon grease; x = decomposition products.



**Table S16.** Complete  $^1\text{H}$  NMR assignment and correlations for complex **H-*I*-P8[b<sub>5</sub>f<sub>2</sub>]-H**.

#	Assign.	$^1\text{H}$	Mult. $J$ (Hz)	$^1\text{H}$ - $^1\text{H}$ COSY	$^1\text{H}$ - $^1\text{H}$ NOESY <sup>†</sup>
1	a1/a2	9.94 (4H)	d, $J$ = 4.6	5	s: 5; m: 10; w: 18
2	d1/d2	9.85–9.82 (4H)	m	6	s: 6; m: 11; w: 9
3	d1/d2	9.81 (4H)	d, $J$ = 4.5	7	s: 7; m: 10; w: 9, 18
4	a1/a2	9.54 (4H)	d, $J$ = 4.6	8	s: 8; w: 11
5	b1/b2	9.01 (4H)	d, $J$ = 4.6	1	s: 1, 10, 11; m: 18
6	c1/c2	8.99 (4H)	d, $J$ = 4.5	2	s: 2, 10, 11; m: 18
7	c1/c2	8.97 (4H)	d, $J$ = 4.5	3	s: 3, 10, 11; m: 18
8	b1/b2	8.95 (4H)	d, $J$ = 4.6	4	s: 4, 10, 11; m: 18
9	e1+e2	8.70–8.66 (8H)	m	15	s: 15, 18; m: 14; w: 2, 3, 16
10	Ar <sup>2</sup> , o'	8.32 (8H)	s	12	s: 5, 6, 7, 8, 18; m: 1, 3; w: 12
11	Ar <sup>2</sup> , o'	8.28 (8H)	s	13	s: 5, 6, 7, 8, 18; m: 2; w: 4, 13
12	Ar <sup>2</sup> , p'	8.04 (4H)	s	10	s: 18; w: 10
13	Ar <sup>2</sup> , p'	8.01 (4H)	s	11	s: 18; w: 11
14	Ar <sup>1</sup>	7.88–7.83 (24H)	m	-	s: 15, 16, 18; m: 9
15	f1+f2	7.60–7.56 (8H)	m	9	s: 14, 18; m: 16
16	g1+g2	7.09 (8H)	s	-	s: 14, 18; m: 15; w: 9
17	h	3.73–3.63 (2H)	m	-	-
18	THS+THS'	1.56–0.69 (1248H)	m	18	s: 9, 10, 11, 12, 13, 14, 15, 16; m: 5, 6, 7, 8; w: 1, 3

<sup>†</sup>Relative correlation intensities are designated as: s = strong, m = medium, w = weak.

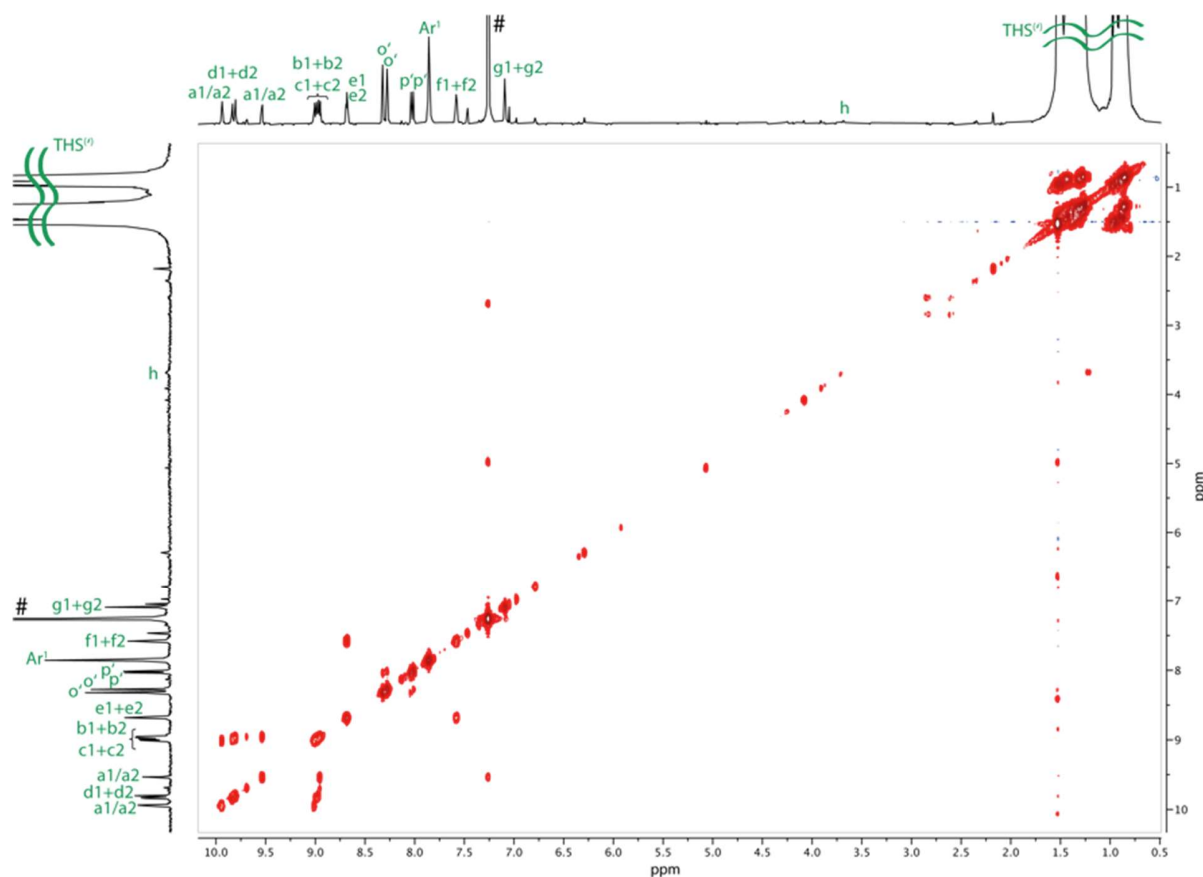


**Figure S60.**  $^1\text{H}$ - $^1\text{H}$  COSY spectrum of **H-*I*-P8[b<sub>5</sub>f<sub>2</sub>]-H** (500 MHz,  $\text{CDCl}_3$ , 298 K).

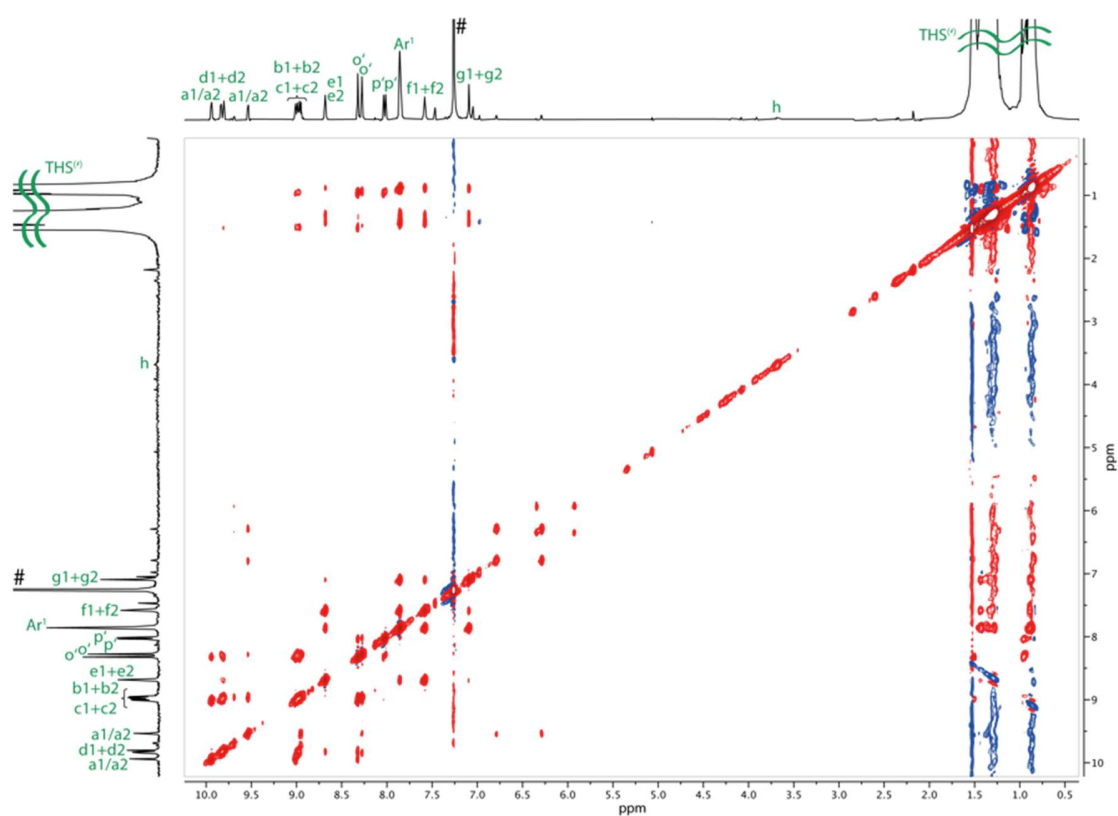


**Figure S61.**  $^1\text{H}$ - $^1\text{H}$  NOESY spectrum of **H-I-P8[b<sub>5</sub>f<sub>2</sub>]-H** (500 MHz,  $\text{CDCl}_3$ , 298 K).

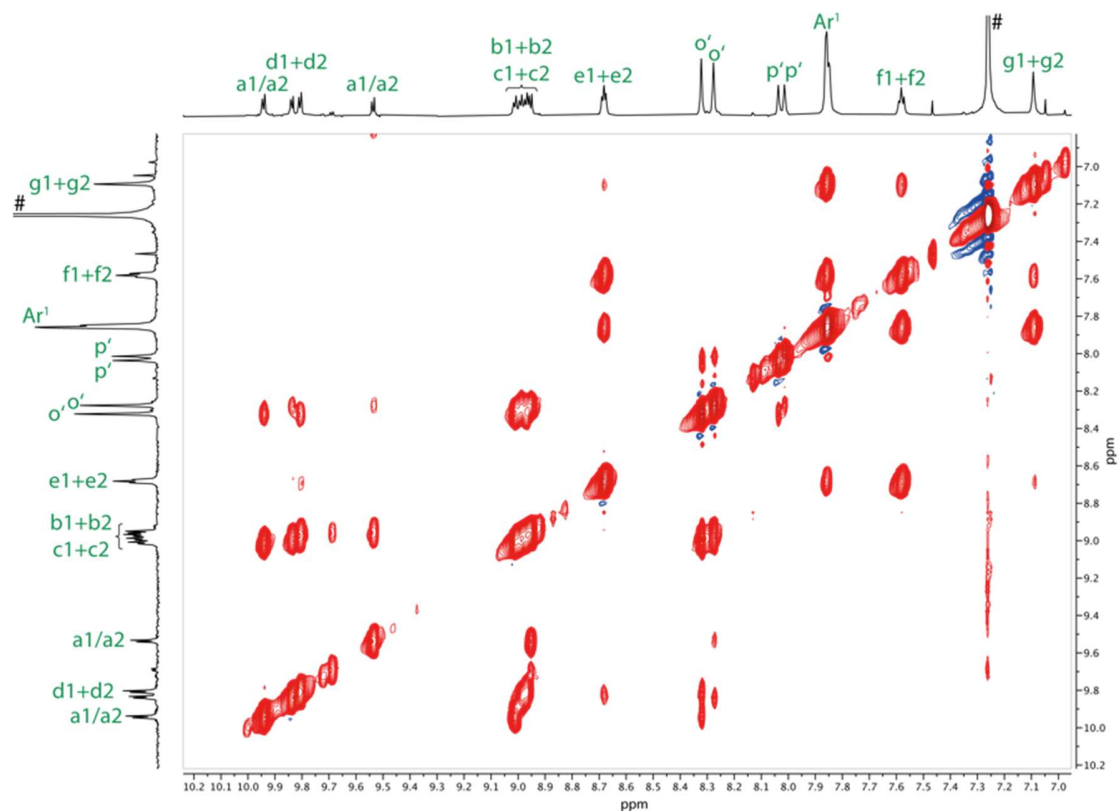


**Figure S62.** Enlarged region of the NOESY spectrum of **H-I-P8[b<sub>5</sub>f<sub>2</sub>]-H** (500 MHz,  $\text{CDCl}_3$ , 298 K).

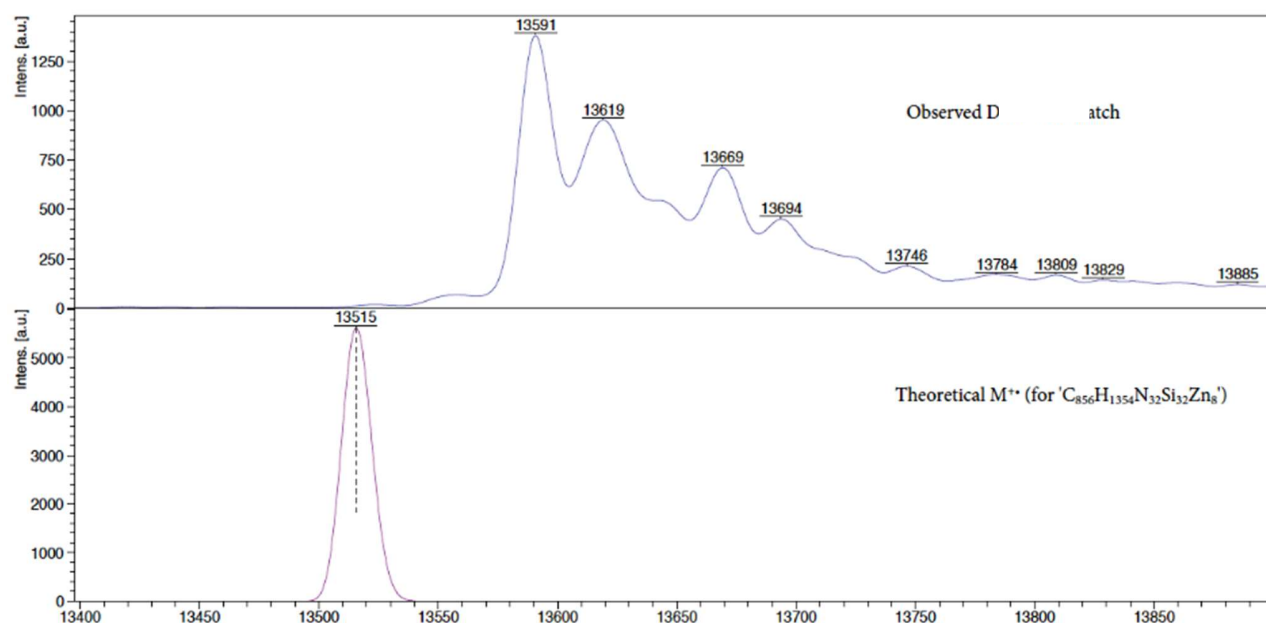


**Figure S63.** Experimental MALDI-ToF spectrum of **H-/P8[b<sub>5</sub>f<sub>2</sub>]-H** (top) and simulated MALDI-ToF spectrum of **H-/P8[b<sub>5</sub>f<sub>2</sub>]-H<sup>+</sup>** [C<sub>856</sub>H<sub>1354</sub>N<sub>32</sub>Si<sub>32</sub>Zn<sub>8</sub>]<sup>+</sup> (bottom). The observed signal in the experimental spectrum corresponds to **[H-/P8[b<sub>5</sub>f<sub>2</sub>]-H+pyridine]<sup>+</sup>** with a theoretical *m/z* value for [C<sub>861</sub>H<sub>1359</sub>N<sub>33</sub>Si<sub>32</sub>Zn<sub>8</sub>]<sup>+</sup> = 13595.

Free ring *c*-P8[b<sub>6</sub>f<sub>2</sub>]:

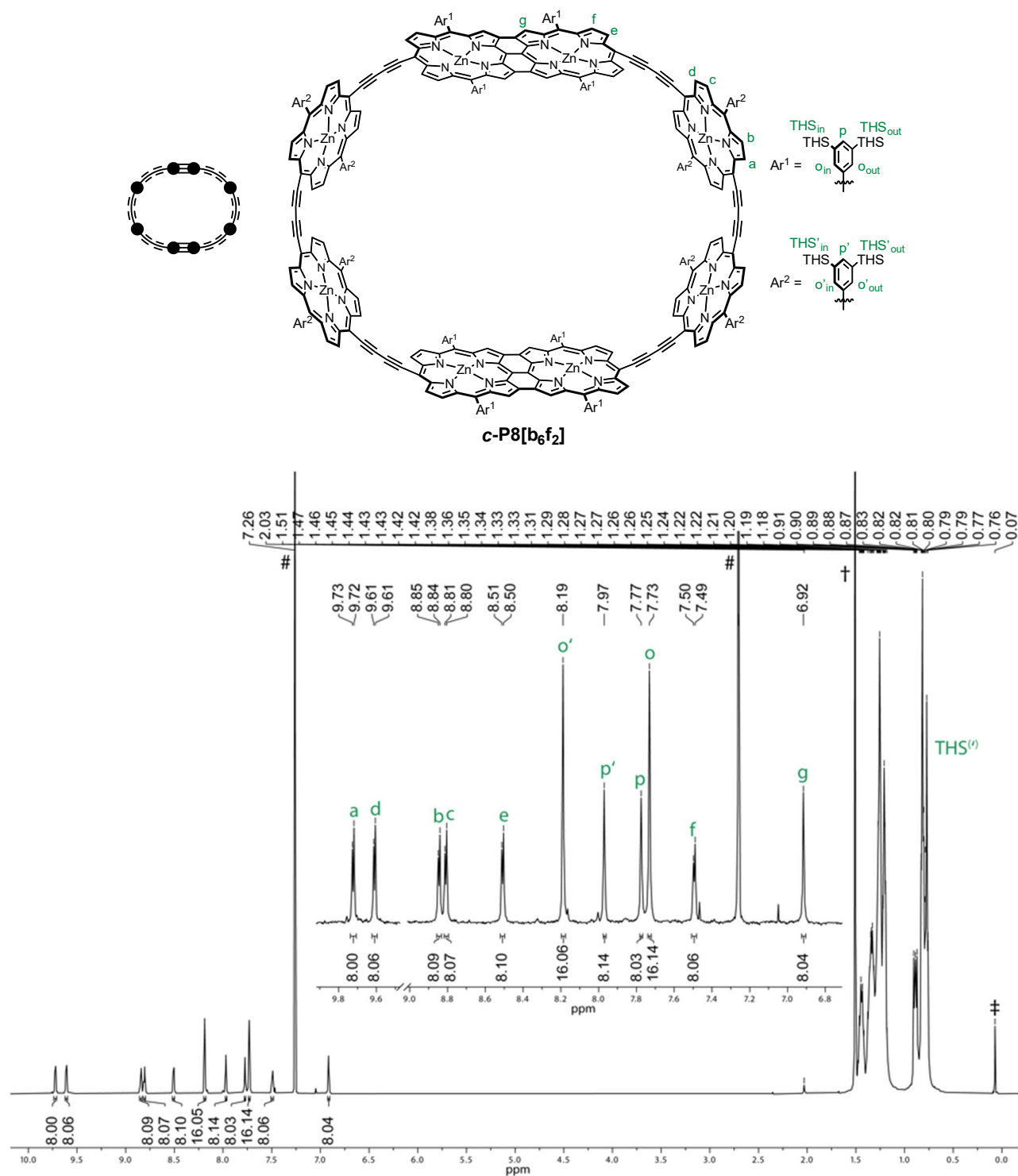


**Figure S64.** Assigned structure and <sup>1</sup>H NMR spectrum of *c*-P8[b<sub>6</sub>f<sub>2</sub>] (500 MHz, CDCl<sub>3</sub>, 298 K). # = CHCl<sub>3</sub>; † = water; ‡ = silicon grease.

**Table S17.** Complete  $^1\text{H}$  NMR assignment and correlations for **c-P8[b<sub>6</sub>f<sub>2</sub>]**

#	Assign.	$^1\text{H}$	Mult. $J$ (Hz)	$^1\text{H}$ - $^1\text{H}$ COSY	$^1\text{H}$ - $^1\text{H}$ NOESY <sup>†</sup>	$^1\text{H}$ - $^{13}\text{C}$ HSQC
1	a	9.72 (8H)	d, $J = 4.5$	3	s: 3; m: 6, 12	131.3
2	d	9.61 (8H)	d, $J = 4.5$	4	s: 4; m: 6, 12; w: 5	131.3
3	b	8.85 (8H)	d, $J = 4.5$	1	s: 1, 6; m: 12; w: 7	133.6
4	c	8.81 (8H)	d, $J = 4.5$	2	s: 2, 6; m: 12; w: 7	133.6
5	e	8.51 (8H)	d, $J = 4.5$	10	s: 10; m: 9, 12; w: 2, 11	129.4
6	o'	8.19 (16H)	s	7	s: 3, 4, 12; m: 1, 2, 7	140.5
7	p'	7.97 (8H)	s	6	s: 12; m: 6; w: 3, 4	139.5
8	p	7.77 (8H)	s	-	s: 12; m: 10, 11	139.4
9	o	7.73 (16H)	s	-	s: 10, 11; 12; m: 5	138.7
10	f	7.49 (8H)	d, $J = 4.5$	5	s: 5, 9; m: 8, 11, 12	132.4
11	g	6.92 (8H)	s	-	s: 9, 12; m: 8, 10; w: 5	128.0
12	THS+THS'	1.48–0.72 (1248H)	m	12	s: 6, 7, 8, 9, 11; m: 1, 2, 3, 4, 5, 10	12.7, 12.8, 14.2, 14.3, 22.76, 22.77, 24.1, 24.2, 29.9, 31.66, 31.73, 33.57, 33.63

<sup>†</sup>Relative correlation intensities are designated as: s = strong, m = medium, w = weak.

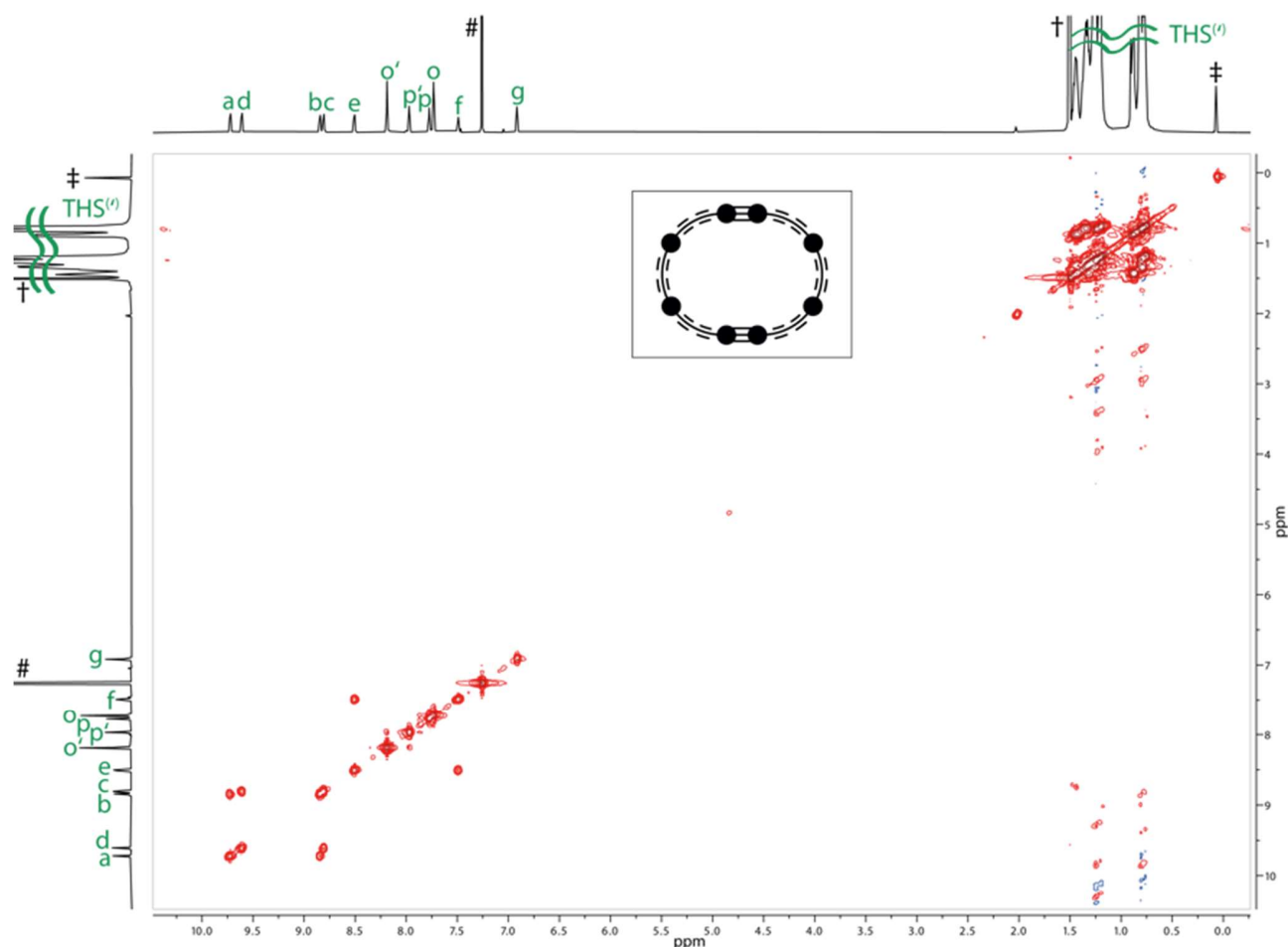


**Figure S65.**  $^1\text{H}$ - $^1\text{H}$  COSY spectrum of **c-P8[b<sub>6</sub>f<sub>2</sub>]** (500 MHz,  $\text{CDCl}_3$ , 298 K).

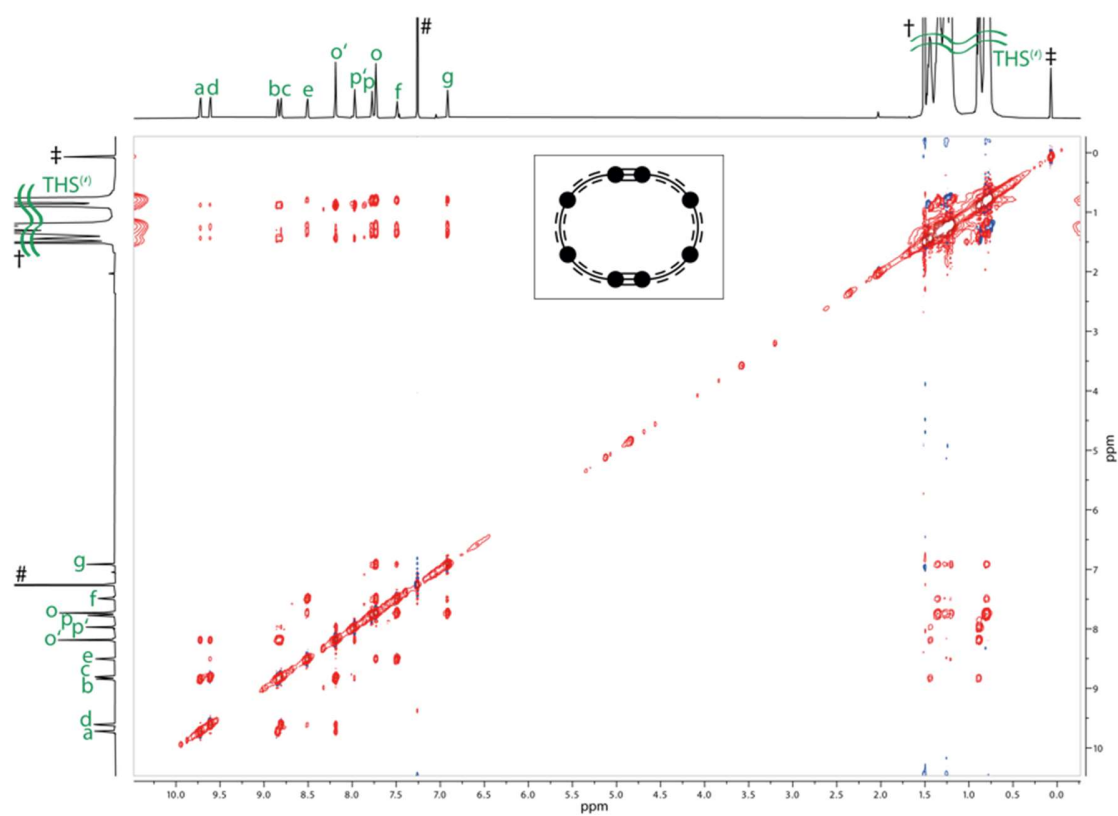


Figure S66.  $^1\text{H}$ - $^1\text{H}$  NOESY spectrum of *c*-P8[b<sub>6</sub>f<sub>2</sub>] (500 MHz, CDCl<sub>3</sub>, 298 K).

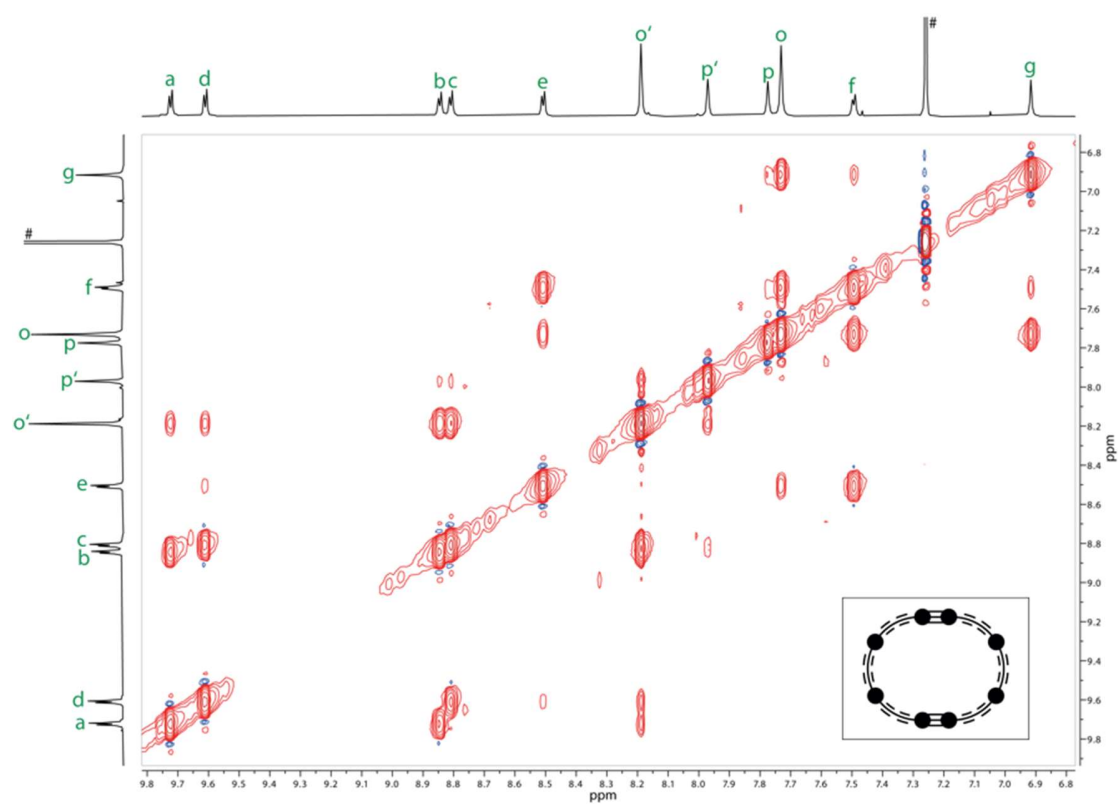
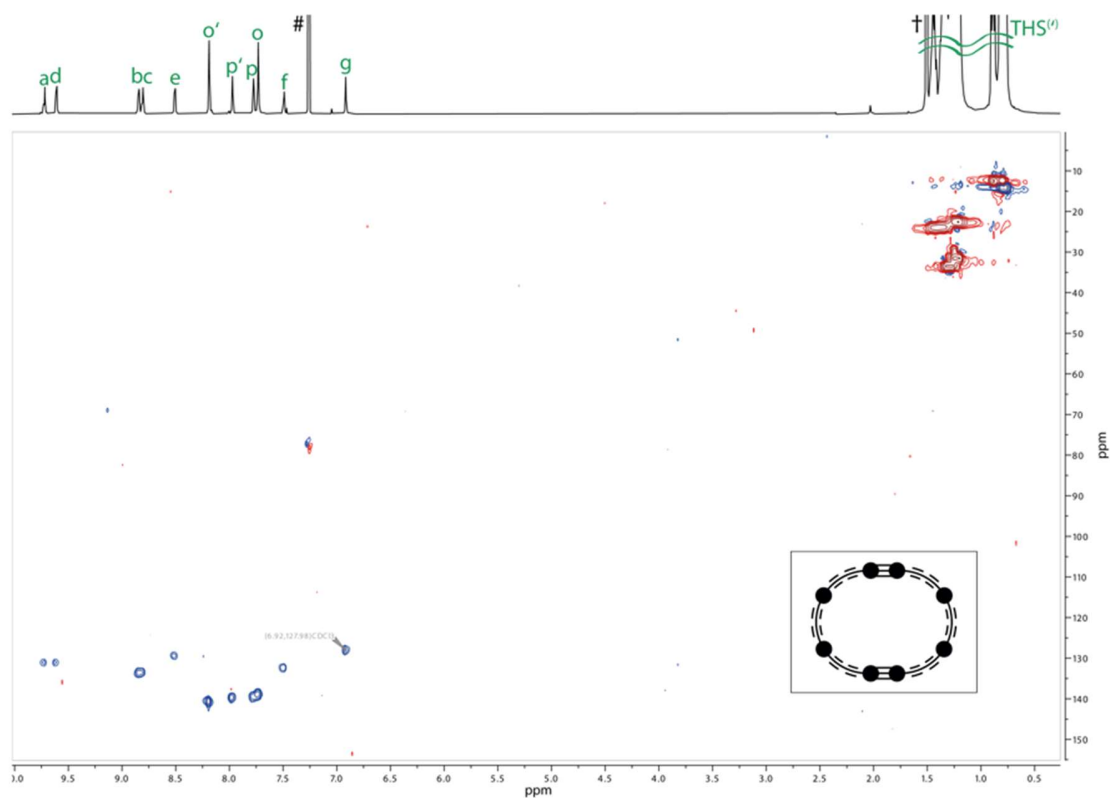
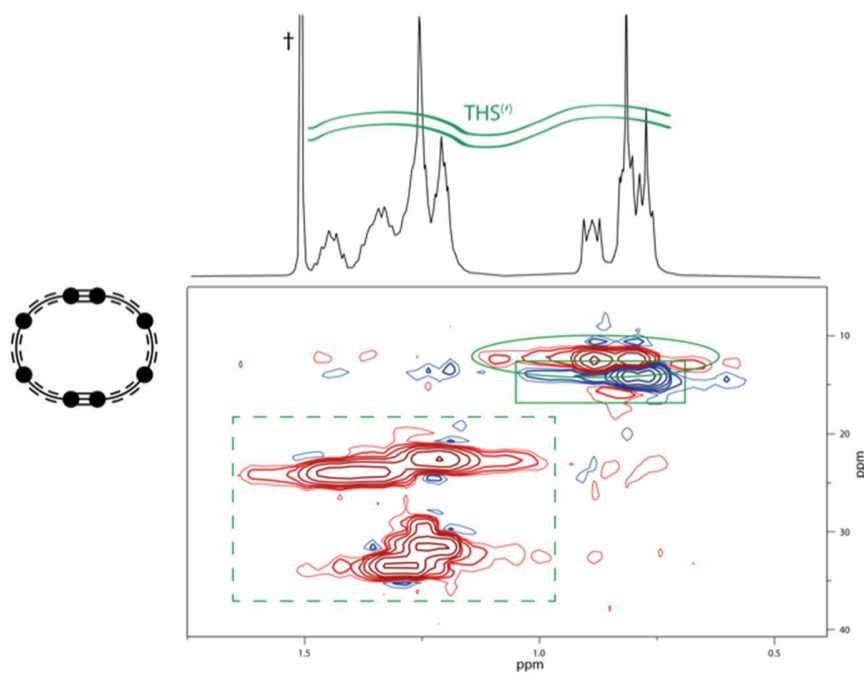


Figure S67. Enlarged region of the NOESY spectrum of *c*-P8[b<sub>6</sub>f<sub>2</sub>] (500 MHz, CDCl<sub>3</sub>, 298 K).





**Figure S68.**  $^1\text{H}$ - $^{13}\text{C}$  HSQC spectrum of **c-P8[b<sub>6</sub>f<sub>2</sub>]** (500 MHz,  $\text{CDCl}_3$ , 298 K).



**Figure S69.** THS region of the  $^1\text{H}$ - $^{13}\text{C}$  HSQC spectrum of **c-P8[b<sub>6</sub>f<sub>2</sub>]** (500 MHz,  $\text{CD}_2\text{Cl}_2$ , 298 K). Si-R- $\text{CH}_3$  resonances are indicated with a solid box, Si- $\text{CH}_2$ -R resonances with a solid circle, and Si- $\text{CH}_2$ - $\text{C}_4\text{H}_8$ - $\text{CH}_3$  resonances with a dashed box.

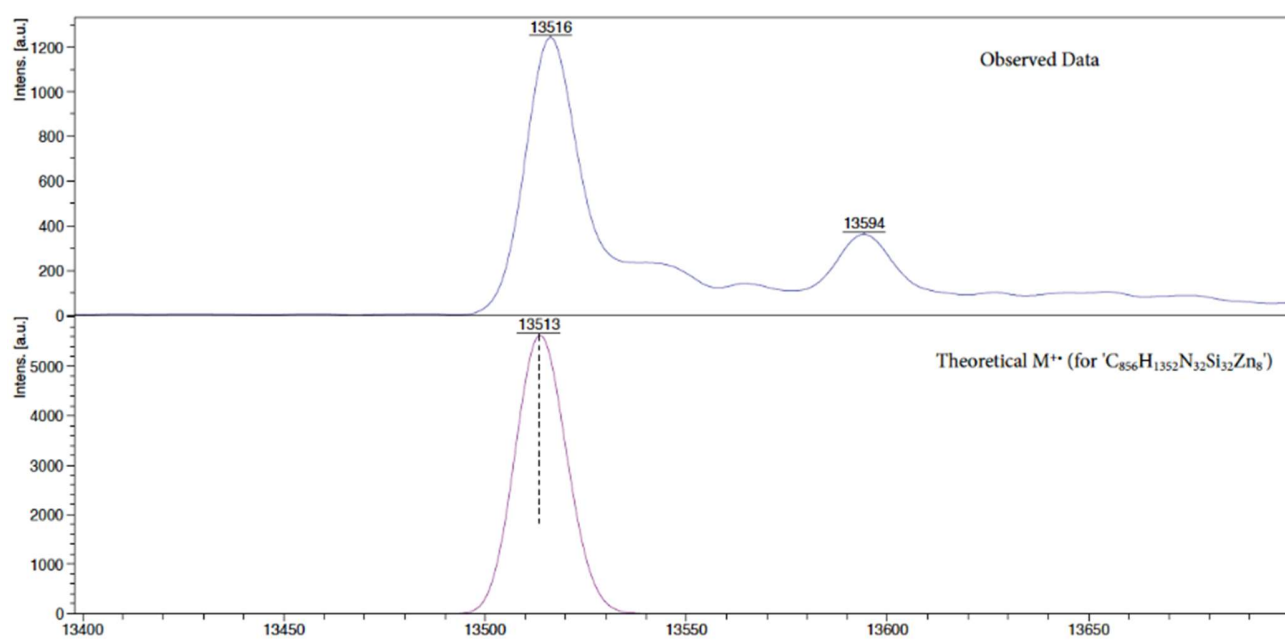


**Figure S70.** Experimental MALDI-ToF spectrum of **c-P8[b<sub>6</sub>f<sub>2</sub>]** (top) and simulated MALDI-TOF spectrum of **c-P8[b<sub>6</sub>f<sub>2</sub>]<sup>+</sup>** [C<sub>856</sub>H<sub>1352</sub>N<sub>32</sub>Si<sub>32</sub>Zn<sub>8</sub>]<sup>+</sup> (bottom).

**Complex  $c\text{-P8}[\text{b}_6\text{f}_2] \cdot (\text{T4}_{1,4\text{F}})_2$ :**

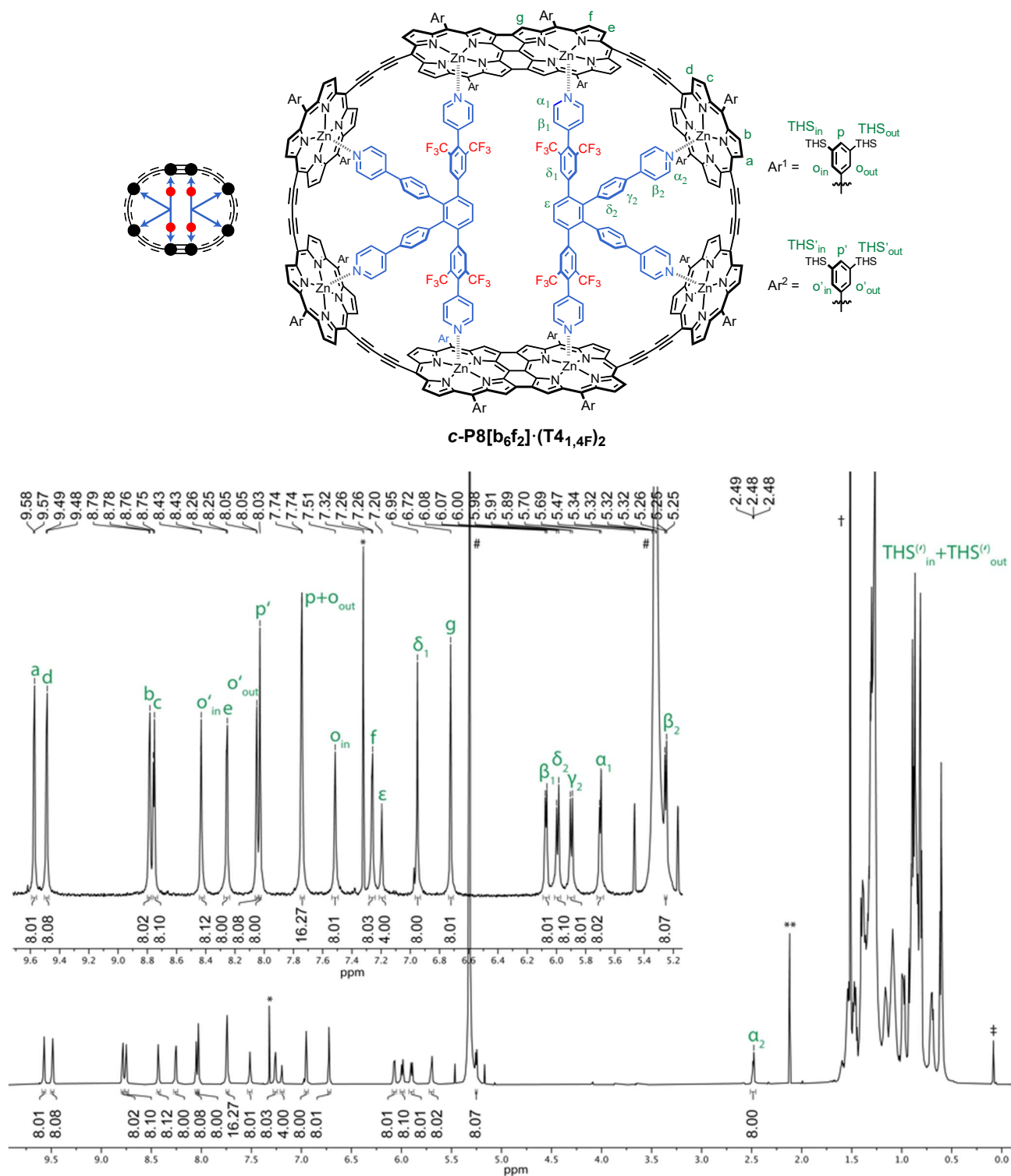


**Table S18.** Complete  $^1\text{H}$  NMR assignment and correlations for complex  $c\text{-P8}[\text{b}_6\text{f}_2]\bullet(\text{T4}_{1,4\text{F}})_2$ .

#	Assign.	$^1\text{H}$	Mult. $J$ (Hz)	$^1\text{H}$ - $^1\text{H}$ COSY	$^1\text{H}$ - $^1\text{H}$ NOESY <sup>†</sup>	$^1\text{H}$ - $^{19}\text{F}$ HOESY <sup>†</sup>	$^1\text{H}$ - $^{13}\text{C}$ HSQC
1	a	9.57 (8H)	d, $J = 4.3$	3	s: 3; w: 5, 7, 20, 21	-	130.5
2	d	9.49 (8H)	d, $J = 4.4$	4	s: 4; w: 5, 6, 7, 20, 21	-	130.8
3	b	8.79 (8H)	d, $J = 4.3$	1	s: 1, 5, 7; m: 21, w: 20	-	133.7
4	c	8.75 (8H)	d, $J = 4.4$	2	s: 2, 5, 7; m: 21; w: 20	-	133.7
5	$\text{o}'_{\text{in}}$	8.43 (8H)	s	7	s: 3, 4, 7, 8, 21; w: 1, 2, 20	-	140.8
6	e	8.26 (8H)	d, $J = 4.4$	11	s: 11; m: 21; w: 2, 9, 10, 18	-	-
7	$\text{o}'_{\text{out}}$	8.05 (8H)	s	5	s: 3, 4, 5, 21; w: 1, 2	-	141.8
8	$\text{p}'$	8.03 (8H)	s	-	s: 5, 21	-	139.8
9	$\text{p} + \text{o}_{\text{out}}$	7.74 (16H)	s	10	s: 11, 14, 21; m: 10; w: 6	-	139.5
10	$\text{o}_{\text{in}}$	7.51 (8H)	s	9	s: 9, 14, 21; m: 11; w: 6, 18	-	138.9
11	f	7.26 (8H)	d, $J = 4.4$	6	s: 6, 9, 10, 21; w: 14	-	132.4
12	$\epsilon$	7.20 (4H)	s	-	s: 13; w: 16	w	-
13	$\delta_1$	6.95 (8H)	s	-	s: 12; m: 16; w: 17, 21	s	130.5
14	g	6.72 (8H)	s	-	s: 9, 10, 21; w: 11, 18	-	127.6
15	$\beta_1$	6.07 (8H)	d, $J = 6.2$	18	s: 18; m: 21	m	125.0
16	$\delta_2$	5.99 (8H)	d, $J = 8.8$	17	s: 17; m: 13; w: 12, 19	vw	131.4
17	$\gamma_2$	5.90 (8H)	d, $J = 8.8$	16	s: 16; m: 19; w: 13, 20	-	126.0
18	$\alpha_1$	5.70 (8H)	d, $J = 6.2$	15	s: 15; m: 21; w: 6, 10, 14	w	145.0
19	$\beta_2$	5.25 (8H)	d, $J = 6.9$	20	s: 20; m: 17; w: 16	-	120.5
20	$\alpha_2$	2.51–2.46 (8H)	m	19	s: 19; w: 1, 2, 3, 4, 5, 17	-	143.4
21	$\text{THS}_{\text{in}} + \text{THS}_{\text{out}} + \text{THS}'_{\text{in}} + \text{THS}'_{\text{out}}$	1.64–0.55 (1248H)	m	21	s: 5, 7, 8, 9, 10, 11, 14; m: 3, 4, 6, 15, 18; w: 1, 2, 13	vw	12.8, 13.0, 13.1, 14.2, 14.37, 14.40, 22.9, 23.1, 24.3, 24.38, 24.41, 24.5, 30.1, 31.9, 32.00, 32.04, 32.1, 33.8, 33.90, 33.94, 34.0

<sup>†</sup>Relative correlation intensities are designated as: s = strong, m = medium, w = weak, vw = very weak.

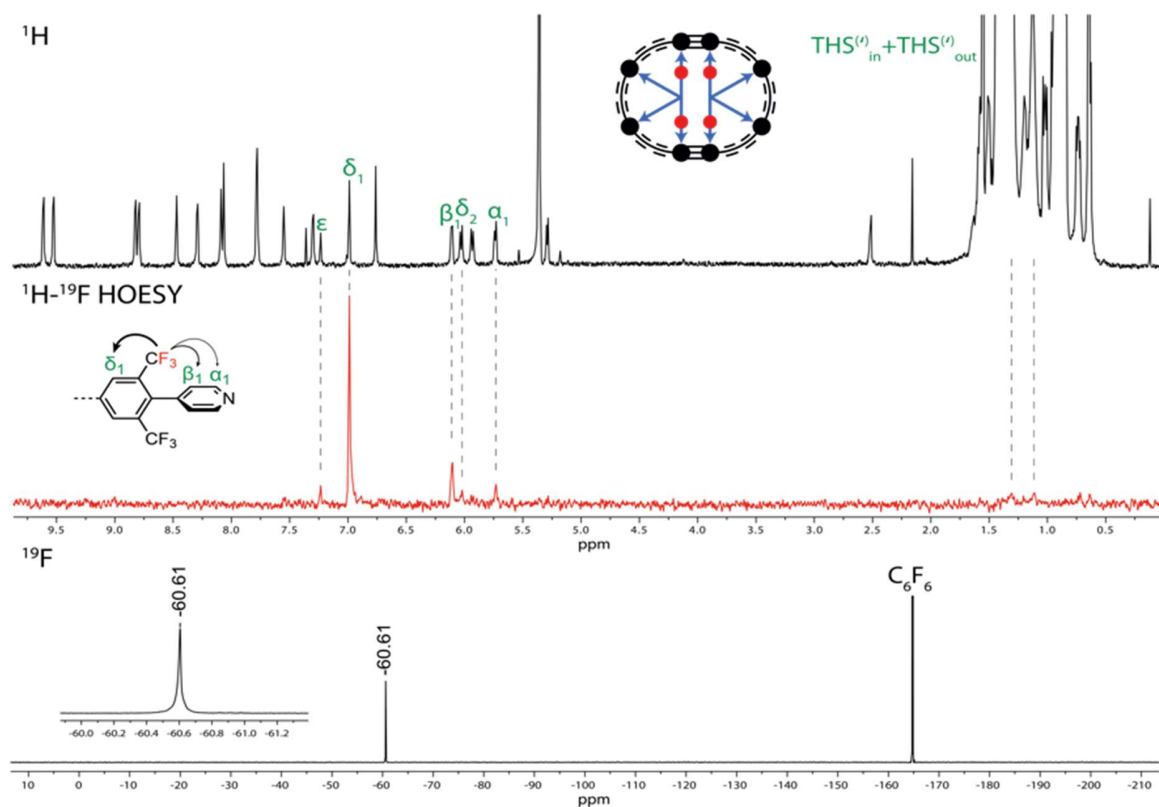


Figure S72. Combined  $^1\text{H}$  (top), 1D  $^1\text{H}$ - $^{19}\text{F}$  HOESY (middle, red), and  $^{19}\text{F}$  (bottom) spectra of  $c\text{-P8}[\text{b}_6\text{f}_2]\bullet(\text{T4}_{1,4\text{F}})_2$  (500 MHz,  $\text{CD}_2\text{Cl}_2$ , 298 K).

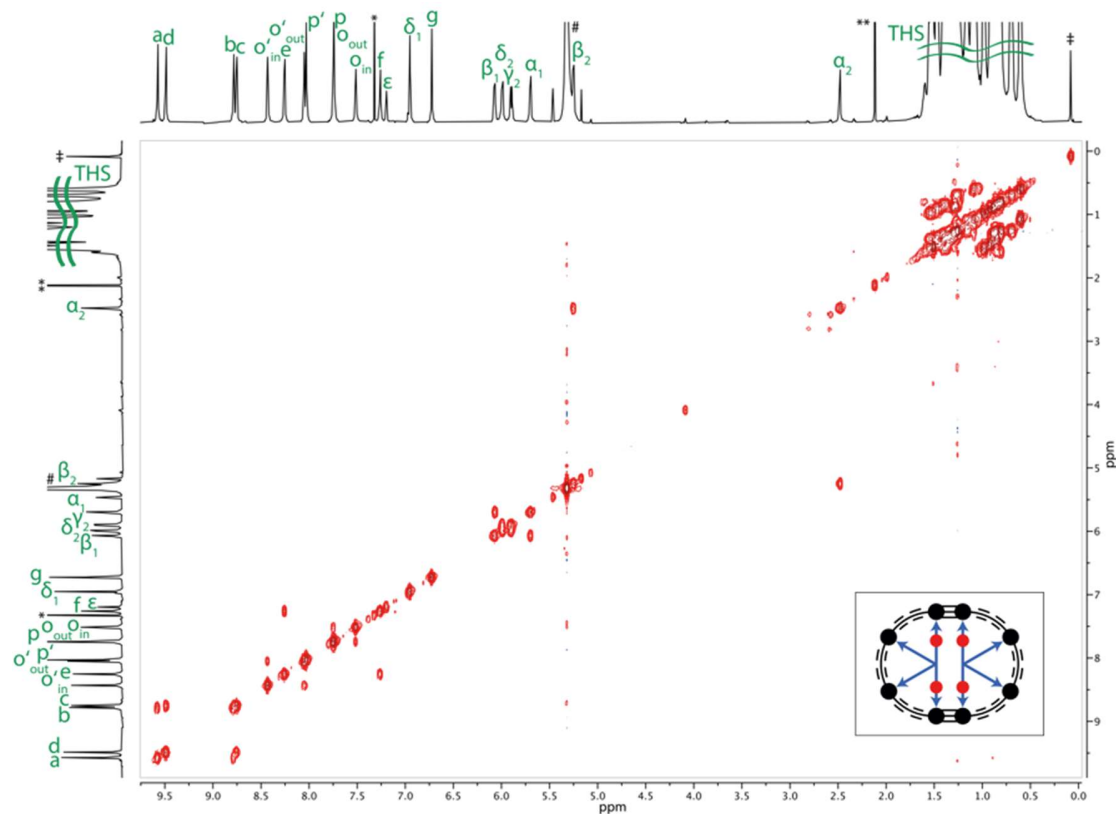


Figure S73.  $^1\text{H}$ - $^1\text{H}$  COSY spectrum of  $c\text{-P8}[\text{b}_6\text{f}_2]\bullet(\text{T4}_{1,4\text{F}})_2$  (600 MHz,  $\text{CD}_2\text{Cl}_2$ , 298 K).

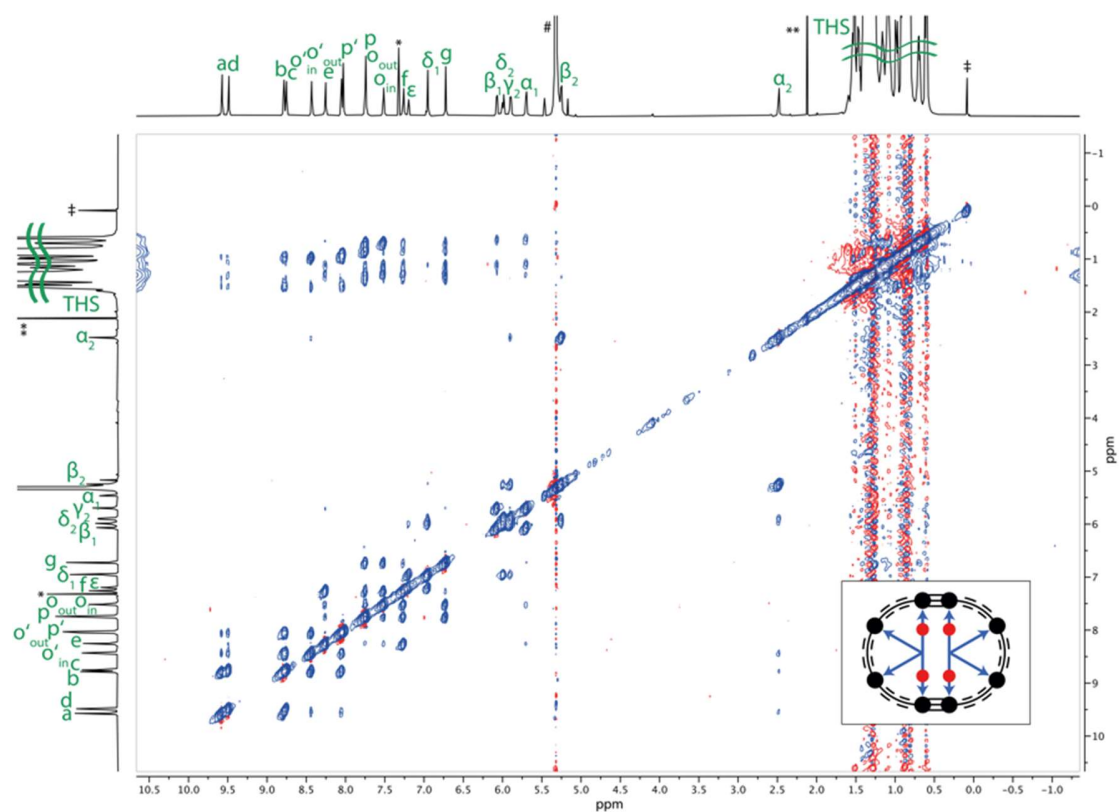


Figure S74.  $^1\text{H}$ - $^1\text{H}$  NOESY spectrum of  $c\text{-P8}[\text{b}_6\text{f}_2]\bullet(\text{T4}_{1,4\text{F}})_2$  (600 MHz,  $\text{CD}_2\text{Cl}_2$ , 298 K).

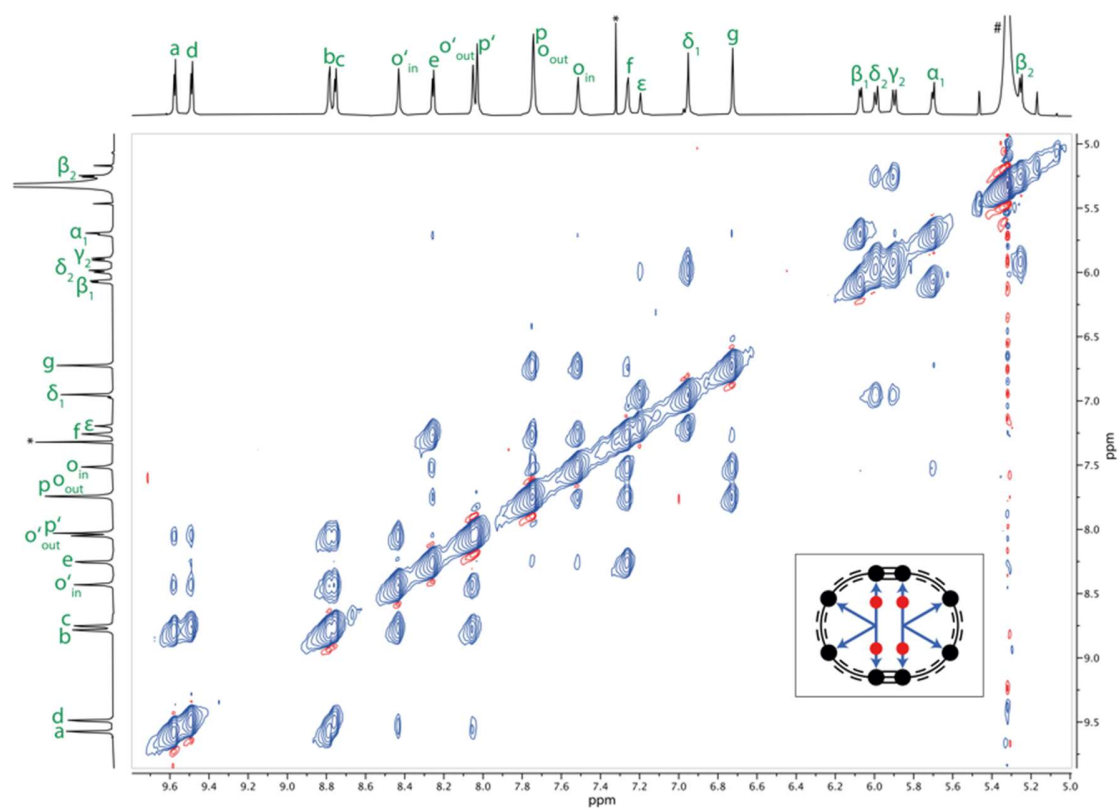


Figure S75. Enlarged region of the NOESY spectrum of  $c\text{-P8}[\text{b}_6\text{f}_2]\bullet(\text{T4}_{1,4\text{F}})_2$  (600 MHz,  $\text{CD}_2\text{Cl}_2$ , 298 K).



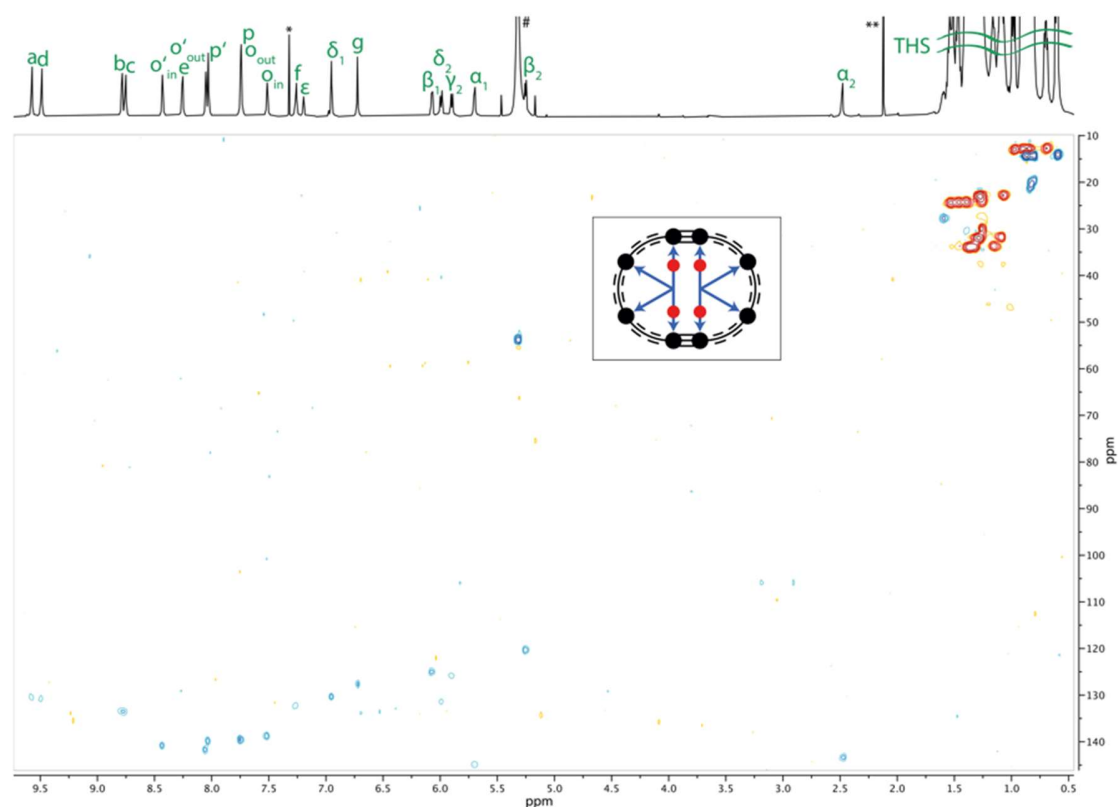


Figure S76.  $^1\text{H}$ - $^{13}\text{C}$  HSQC spectrum of  $\text{c-P8}[\text{b}_6\text{f}_2]\bullet(\text{T4}_{1,4\text{F}})_2$  (600 MHz,  $\text{CD}_2\text{Cl}_2$ , 298 K).

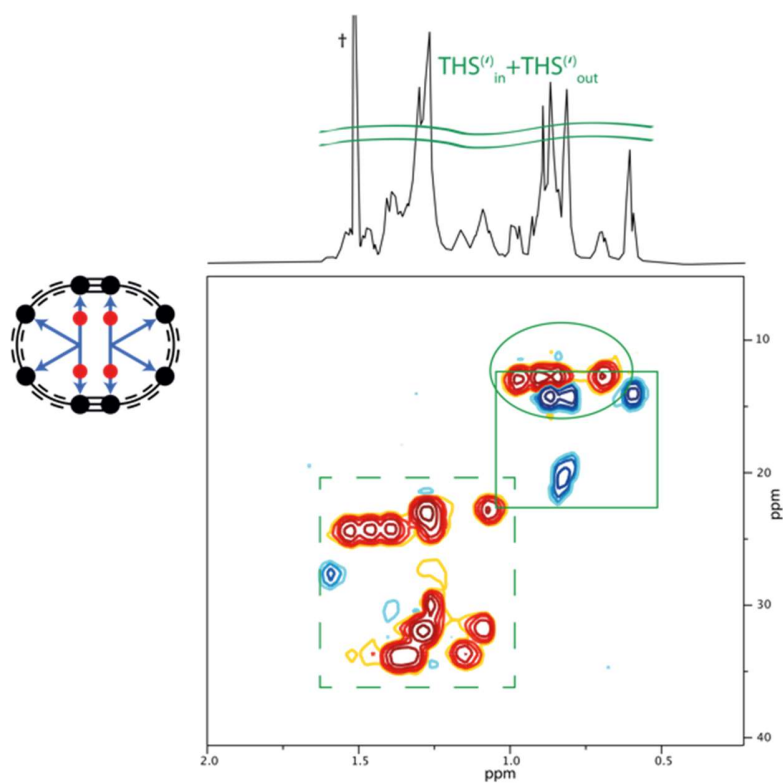
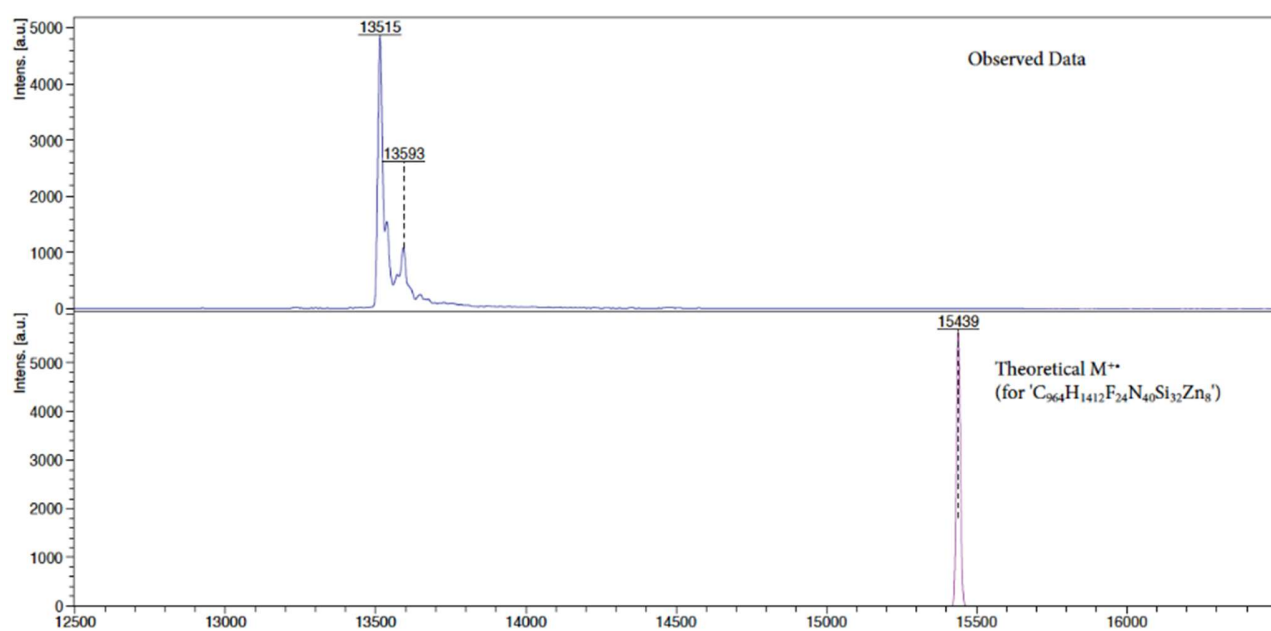
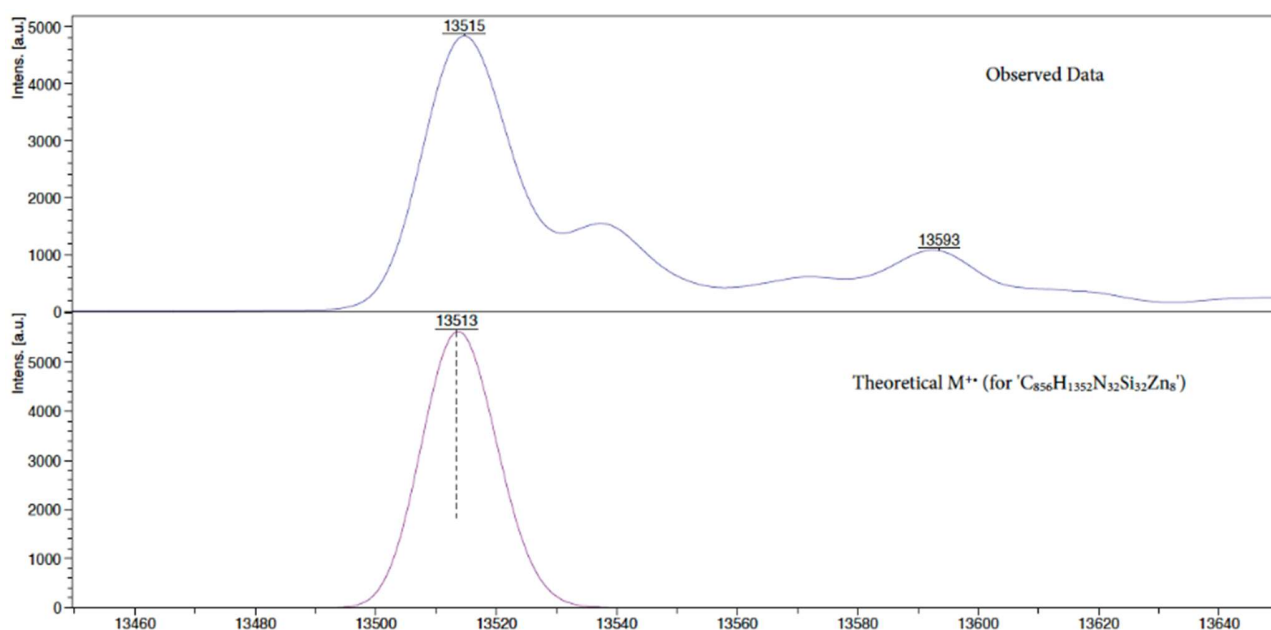


Figure S77. TMS region of the  $^1\text{H}$ - $^{13}\text{C}$  HSQC spectrum of  $\text{c-P8}[\text{b}_6\text{f}_2]\bullet(\text{T4}_{1,4\text{F}})_2$  (600 MHz,  $\text{CD}_2\text{Cl}_2$ , 298 K). Si-R- $\text{CH}_3$  resonances are indicated with a solid box, Si- $\text{CH}_2$ -R resonances with a solid circle, and Si- $\text{CH}_2$ - $\text{C}_4\text{H}_8$ - $\text{CH}_3$  resonances with a dashed box.



**Figure S78.** Experimental MALDI-ToF spectrum of  $c\text{-P8}[\text{b}_6\text{f}_2] \bullet (\text{T}_{4,4\text{F}})_2$  (top) and simulated MALDI-ToF spectrum of  $c\text{-P8}[\text{b}_6\text{f}_2] \bullet (\text{T}_{4,4\text{F}})_2^+ [\text{C}_{964}\text{H}_{1412}\text{F}_{24}\text{N}_{40}\text{Si}_{32}\text{Zn}_8]^+$  (bottom).



**Figure S79.** Enlarged region of the experimental MALDI-ToF spectrum of  $c\text{-P8}[\text{b}_6\text{f}_2] \bullet (\text{T}_{4,4\text{F}})_2$  (top) and simulated spectrum of  $c\text{-P8}[\text{b}_6\text{f}_2] \bullet (\text{T}_{4,4\text{F}})_2^+ [\text{C}_{856}\text{H}_{1352}\text{N}_{32}\text{Si}_{32}\text{Zn}_8]^+$  (bottom).

Complex  $c\text{-P8}[\text{b}_6\text{f}_2] \cdot (\text{T4}_{2,3\text{F}})_2$ :

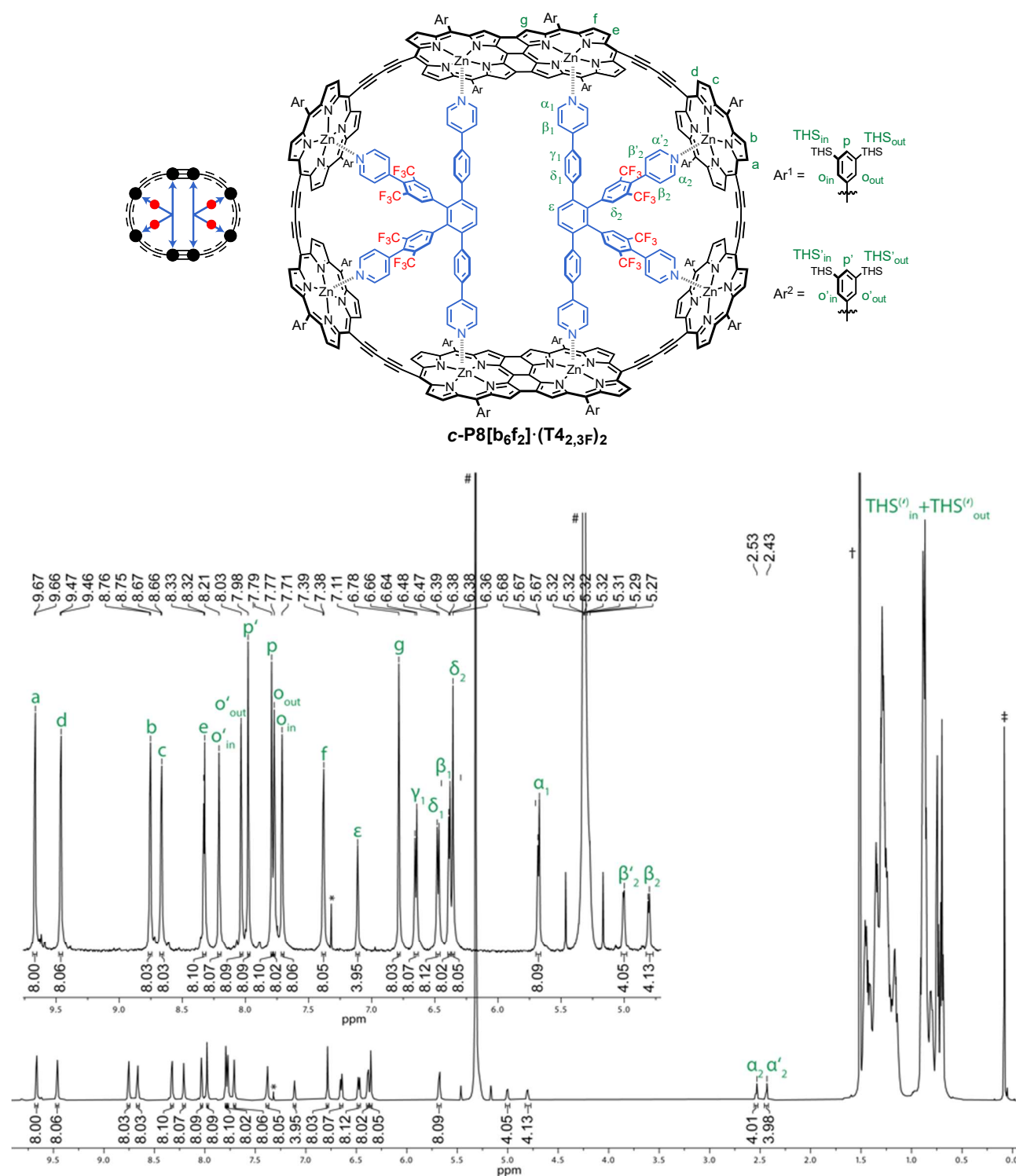


**Figure S80.** Labelled structure and  $^1\text{H}$  NMR spectrum of  $c\text{-P8}[\text{b}_6\text{f}_2] \cdot (\text{T4}_{2,3\text{F}})_2$  (600 MHz,  $\text{CD}_2\text{Cl}_2$ , 298 K). # =  $\text{CH}_2\text{Cl}_2$ ; \* =  $\text{CHCl}_3$ ; † = water; ‡ = silicon grease.

**Table S19.** Complete  $^1\text{H}$  NMR assignment and correlations for complex  $c\text{-P8}[\text{b}_6\text{f}_2]\bullet(\text{T4}_{2,3\text{F}})_2$ .

#	Assign.	$^1\text{H}$	Mult. $J$ (Hz)	$^1\text{H}$ – $^1\text{H}$ COSY	$^1\text{H}$ – $^1\text{H}$ NOESY <sup>†</sup>	$^1\text{H}$ – $^{19}\text{F}$ HOESY <sup>†</sup>	$^1\text{H}$ – $^{13}\text{C}$ HSQC
1	a	9.67 (8H)	d, $J = 4.4$	3	s: 3; m: 24; w: 6, 7, 22	-	130.7
2	d	9.46 (8H)	d, $J = 4.3$	4	s: 4; m: 24; w: 5, 6, 7, 23	-	130.6
3	b	8.76 (8H)	d, $J = 4.4$	1	s: 1, 6, 7, 24; w: 22	-	133.6
4	c	8.67 (8H)	d, $J = 4.3$	2	s: 2, 6, 7, 24; w: 23	-	133.6
5	e	8.33 (8H)	d, $J = 4.4$	12	s: 12; m: 24; w: 2, 10, 11	-	129.1
6	$\text{o}'_{\text{in}}$	8.21 (8H)	s	7, 8	s: 3, 4, 24; m: 7, 8; w: 1, 2, 22	-	140.8
7	$\text{o}'_{\text{out}}$	8.03 (8H)	s	6	s: 3, 4, 24; m: 6; w: 1, 2	-	141.7
8	$\text{p}'$	7.98 (8H)	s	6	s: 24; m: 6	-	139.9
9	p	7.79 (8H)	s	-	s: 24	-	139.7
10	$\text{o}_{\text{out}}$	7.77 (8H)	s	-	s: 12, 14, 24; w: 5	-	-
11	$\text{o}_{\text{in}}$	7.71 (8H)	s	-	s: 12, 14, 24; m: 19; w: 5, 17	-	139.0
12	f	7.38 (8H)	d, $J = 4.4$	5	s: 5, 10, 11; m: 24; w: 14, 19	-	132.4
13	$\epsilon$	7.11 (4H)	s	-	m: 16; w: 15, 18	-	-
14	g	6.78 (8H)	s	-	s: 10, 11 24; w: 12, 19	-	127.5
15	$\gamma_1$	6.65 (8H)	d, $J = 8.4$	16	s: 16, 17; m: 24; w: 13, 19	vw	126.7
16	$\delta_1$	6.47 (8H)	d, $J = 8.4$	15	s: 15; m: 13, 17, 19, 24	vw	130.4
17	$\beta_1$	6.39 (8H)	d, $J = 6.7$	19	s: 15, 19; m: 16, 24; w: 11		121.8
18	$\delta_2$	6.36 (8H)	s	-	m: 24; w: 13, 20, 21	s	132.1
19	$\alpha_1$	5.70–5.66 (8H)	m	17	s: 17; m: 11, 16, 24; w: 12, 14, 15	-	146.6
20	$\beta'_2$	5.00 (4H)	d, $J = 6.6$	23	s: 23; m: 21; w: 18	m	124.0
21	$\beta_2$	4.81 (4H)	d, $J = 6.5$	22	s: 22; m: 20; w: 18, 24	m	123.2
22	$\alpha_2$	2.56–2.52 (4H)	m	21	s: 21; w: 1, 3, 6, 24	w	142.7
23	$\alpha'_2$	2.46–2.42 (4H)	m	20	s: 20; w: 2, 4, 24	w	142.6
24	$\text{THS}_{\text{in}} + \text{THS}_{\text{out}} + \text{THS}'_{\text{in}} + \text{THS}'_{\text{out}}$	1.50–0.67 (1248H)	m	24	s: 4, 6, 7, 8, 9, 10, 11, 14; m: 1, 2, 5, 12, 15, 16, 17, 18, 19; w: 21, 22, 23	w	12.9, 13.0, 14.3, 14.4, 23.0, 23.08, 23.11, 24.3, 24.40, 24.43, 31.9, 32.00, 32.03, 33.8, 33.87, 33.90, 33.93

<sup>†</sup>Relative correlation intensities are designated as: s = strong, m = medium, w = weak, vw = very weak.



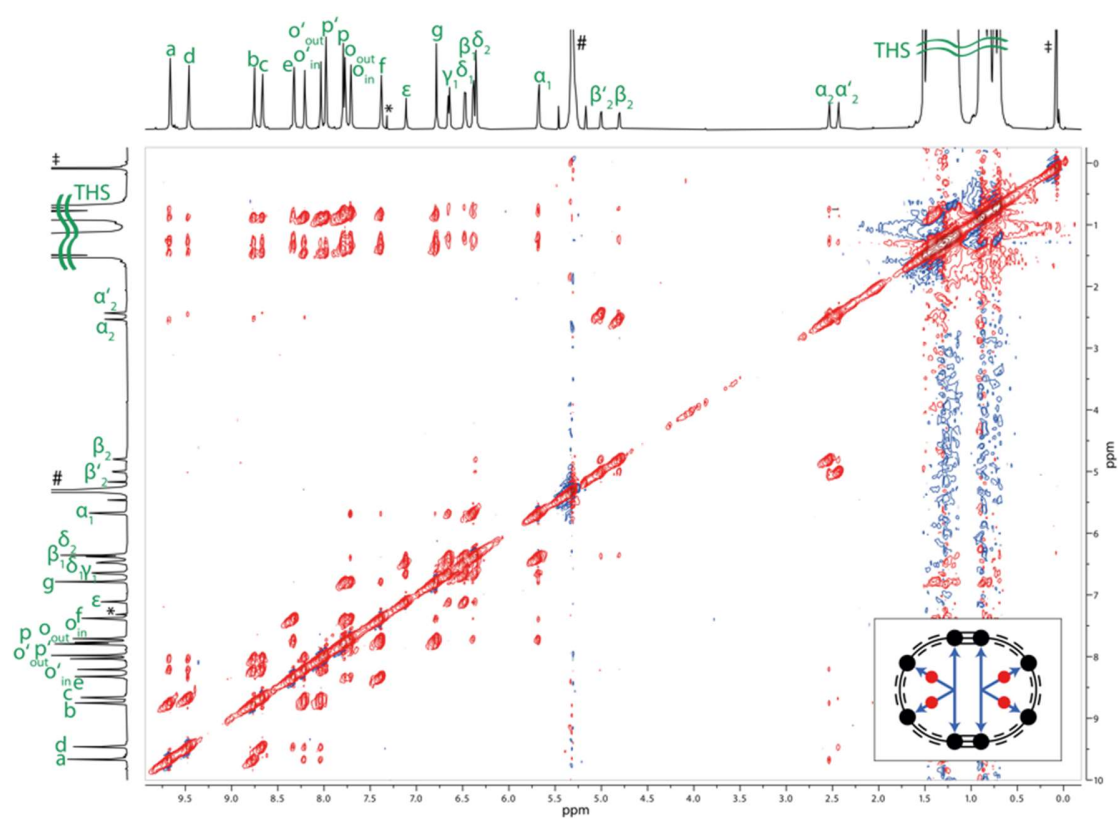


Figure S83.  $^1\text{H}$ - $^1\text{H}$  NOESY spectrum of  $c\text{-P8}[\text{b}_6\text{f}_2]\bullet(\text{T4}_{2,3\text{F}})_2$  (600 MHz,  $\text{CD}_2\text{Cl}_2$ , 298 K).

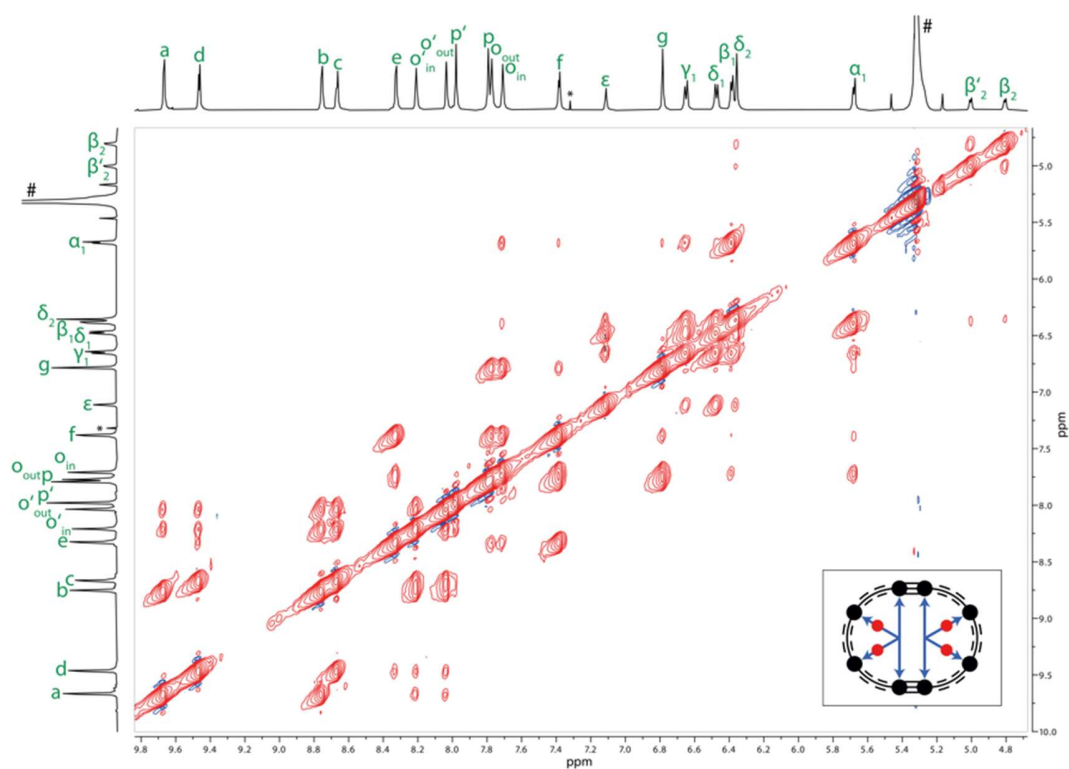
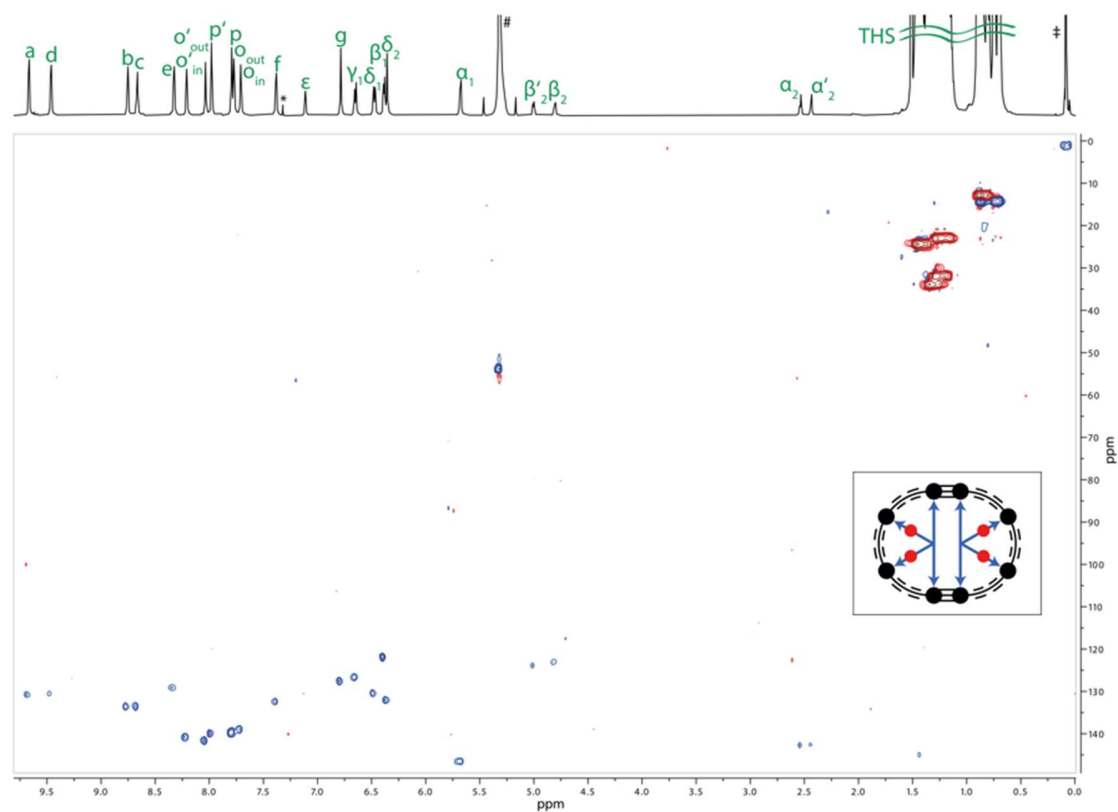
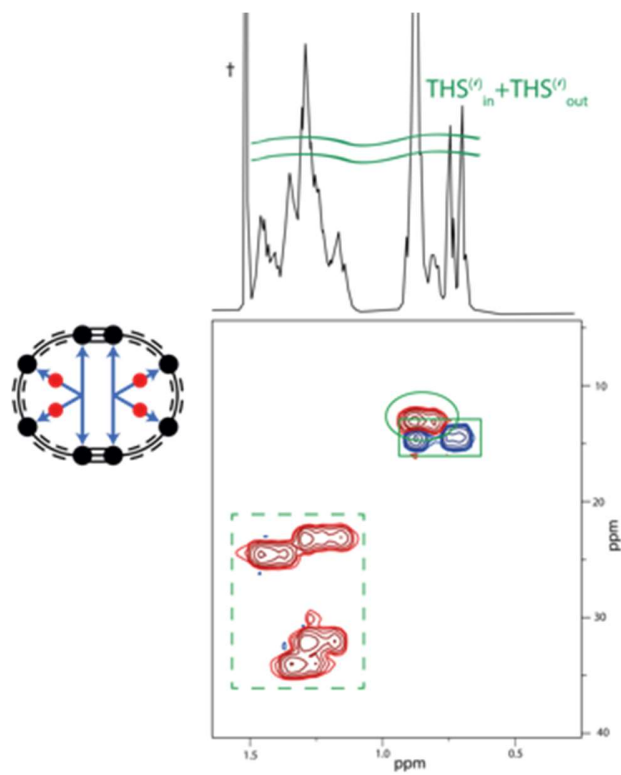


Figure S84. Enlarged region of the NOESY spectrum of  $c\text{-P8}[\text{b}_6\text{f}_2]\bullet(\text{T4}_{2,3\text{F}})_2$  (600 MHz,  $\text{CD}_2\text{Cl}_2$ , 298 K).





**Figure S85.**  $^1\text{H}$ - $^{13}\text{C}$  HSQC spectrum of **c-P8[b<sub>6</sub>f<sub>2</sub>]•(T<sub>4,3</sub>F)<sub>2</sub>** (600 MHz,  $\text{CD}_2\text{Cl}_2$ , 298 K).



**Figure S86.** TMS region of the  $^1\text{H}$ - $^{13}\text{C}$  HSQC spectrum of **c-P8[b<sub>6</sub>f<sub>2</sub>]•(T<sub>4,3</sub>F)<sub>2</sub>** (600 MHz,  $\text{CD}_2\text{Cl}_2$ , 298 K). Si-R- $\text{CH}_3$  resonances are indicated with a solid box, Si- $\text{CH}_2$ -R resonances with a solid circle, and Si- $\text{CH}_2$ - $\text{C}_4\text{H}_8$ - $\text{CH}_3$  resonances with a dashed box.

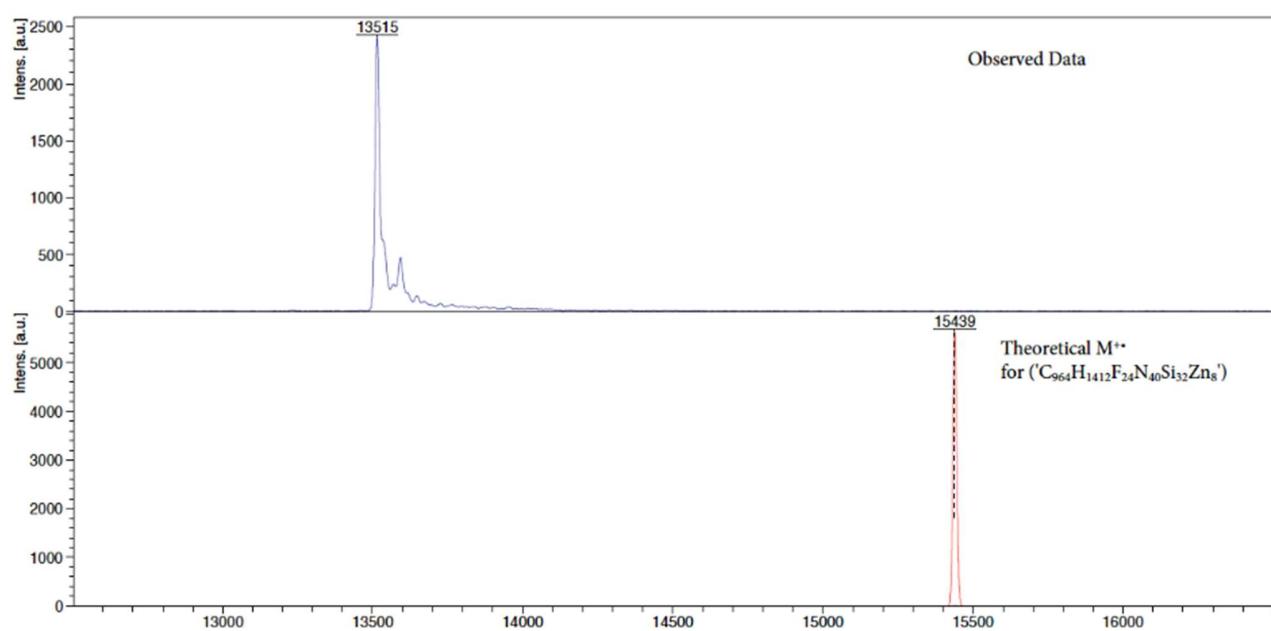


**Figure S87.** Experimental MALDI-ToF spectrum of *c*-P8[b<sub>6</sub>f<sub>2</sub>]•(T<sub>42,3F</sub>)<sub>2</sub> (top) and simulated MALDI-ToF spectrum of *c*-P8[b<sub>6</sub>f<sub>2</sub>]•(T<sub>42,3F</sub>)<sub>2</sub><sup>+</sup> [C<sub>964</sub>H<sub>1412</sub>F<sub>24</sub>N<sub>40</sub>Si<sub>32</sub>Zn<sub>8</sub>]<sup>+</sup> (bottom).

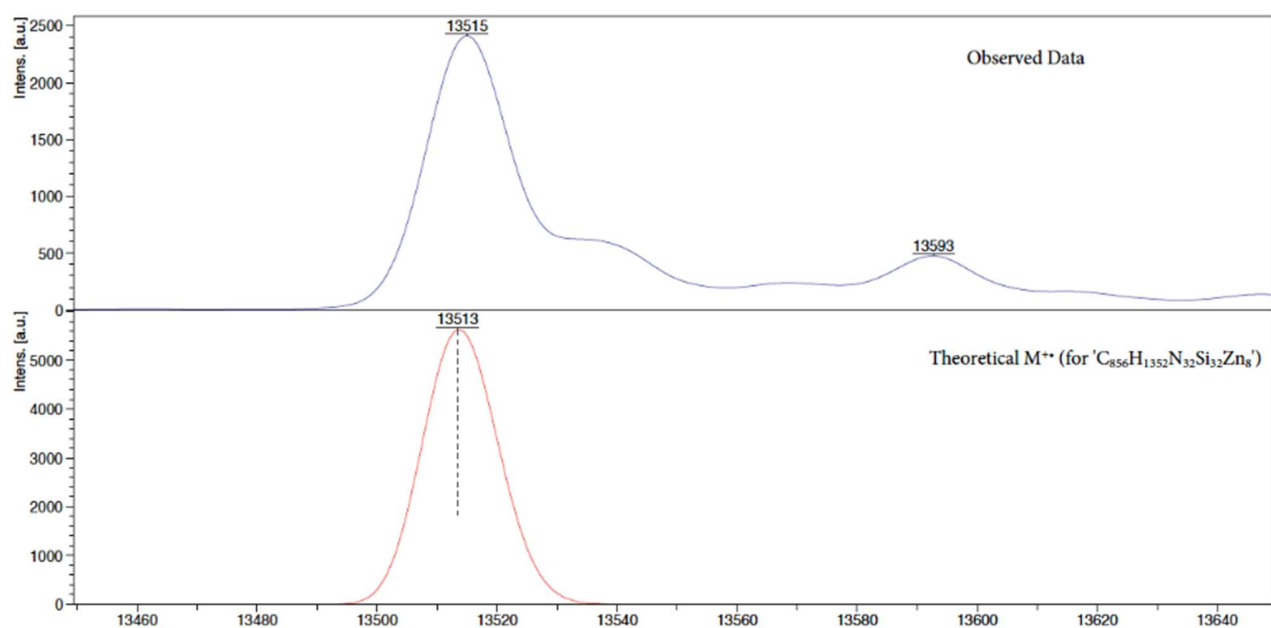


**Figure S88.** Enlarged region of the experimental MALDI-ToF spectrum of *c*-P8[b<sub>6</sub>f<sub>2</sub>]•(T<sub>42,3F</sub>)<sub>2</sub> (top) and simulated spectrum of *c*-P8[b<sub>6</sub>f<sub>2</sub>]•(T<sub>42,3F</sub>)<sub>2</sub><sup>+</sup> [C<sub>856</sub>H<sub>1352</sub>N<sub>32</sub>Si<sub>32</sub>Zn<sub>8</sub>]<sup>+</sup> (bottom).

Complex  $c\text{-P8}[\text{b}_8]\bullet(\text{T4})_2$ :

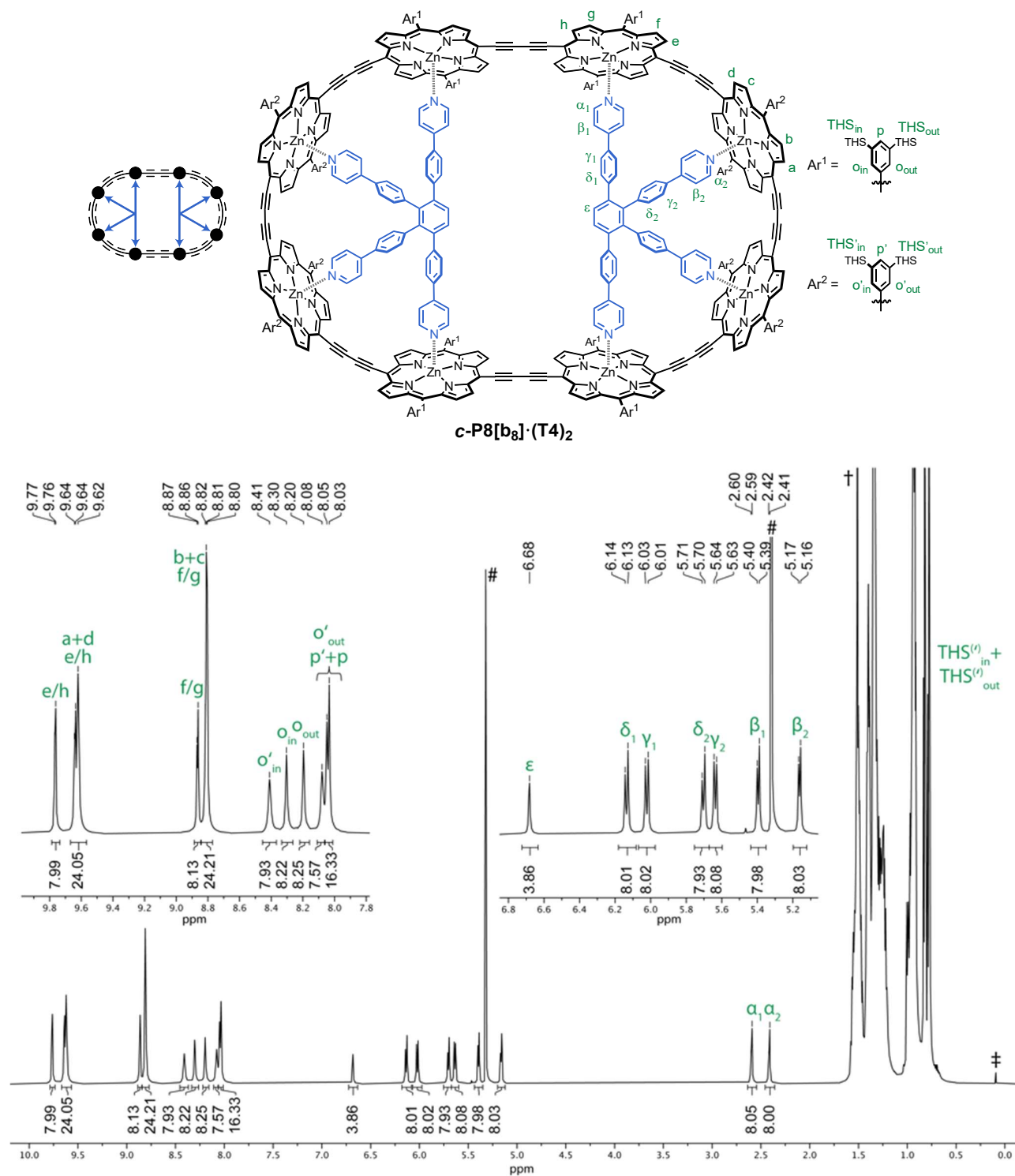


**Figure S89.** Assigned structure and  $^1\text{H}$  NMR spectrum of  $c\text{-P8}[\text{b}_8]\bullet(\text{T4})_2$  (600 MHz,  $\text{CD}_2\text{Cl}_2$ , 298 K). # =  $\text{CH}_2\text{Cl}_2$ ; † = water; ‡ = silicon grease.

**Table S20.** Complete  $^1\text{H}$  NMR assignment and correlations for complex  $\text{c-P8}[\text{b}_8]\bullet(\text{T4})_2$ .

#	Assign.	$^1\text{H}$	Mult. $J$ (Hz)	$^1\text{H}$ - $^1\text{H}$ COSY	$^1\text{H}$ - $^1\text{H}$ NOESY <sup>†</sup>	$^1\text{H}$ - $^{13}\text{C}$ HSQC + $^{13}\text{C}$
1	e/h	9.76 (8H)	d, $J = 4.0$	4	s: 4; m: 5, 7, 8, 19, 21; w: 11, 17	130.8
2	a/d	9.64 (8H)	d, $J = 4.1$	5	s: 5; m: 6, 9, 20, 21; w: 16, 18	130.8
3	a/d + e/h	9.63–9.60 (16H)	m	5	m: 4, 6, 7, 8, 9, 19, 20, 21; w: 10, 13, 14, 15, 16, 17, 18	131.0, 131.0
4	f/g	8.87 (8H)	d, $J = 4.0$	1	s: 1; m: 3, 7, 8, 17, 19, 21	133.6
5	b + c + f/g	8.84–8.77 (24H)	m	2, 3	s: 2, 21; m: 1, 6, 7, 8, 9, 17, 18, 19, 20; w: 15, 16	133.6, 133.6, 133.6
6	$\text{o}'_{\text{in}}$	8.41 (8H)	s	-	s: 21; m: 2, 3, 5, 9, 18, 20; w: 7, 10, 15, 16	-
7	$\text{o}_{\text{in}}$	8.30 (8H)	s	-	s: 21; m: 1, 3, 4, 5, 17, 19; w: 8, 11, 13, 14	-
8	$\text{o}_{\text{out}}$	8.20 (8H)	s	-	s: 21; m: 1, 3, 4, 5; w: 7, 11, 17, 19	-
9	$\text{o}'_{\text{out}}$	8.08 (8H)	s	-	s: 21; m: 2, 3, 5, 6, 20; w: 16, 18	-
10	$\text{p}'$	8.05 (8H)	s	-	s: 21; w: 3, 6	140.1
11	p	8.03 (8H)	s	-	s: 21; w: 1, 7, 8	140.1
12	$\epsilon$	6.68 (4H)	s	-	s: 13; m: 14, 15; w: 16, 21.	129.2
13	$\delta_1$	6.14 (8H)	d, $J = 9.5$	14	s: 12, 14; m: 15, 17; w: 3, 7, 16, 19, 21	130.1
14	$\gamma_1$	6.02 (8H)	d, $J = 9.5$	13	s: 13; m: 12, 17, 19; w: 3, 7, 15, 16, 21	125.5
15	$\delta_2$	5.70 (8H)	d, $J = 8.7$	16	s: 16; m: 12, 13, 18, 20; w: 3, 5, 6, 14, 21	131.6
16	$\gamma_2$	5.64 (8H)	d, $J = 8.7$	15	s: 15, 18; m: 20; w: 2, 3, 5, 6, 9, 12, 13, 14, 21	124.7
17	$\beta_1$	5.39 (8H)	d, $J = 7.3$	19	s: 19; m: 4, 5, 13, 14; w: 1, 3, 7, 8, 21	120.0
18	$\beta_2$	5.16 (8H)	d, $J = 6.6$	20	s: 16, 20; m: 5, 6, 15; w: 2, 3, 9, 21	119.9
19	$\alpha_1$	2.64–2.55 (8H)	m	17	s: 17; m: 1, 3, 4, 5, 7, 14; w: 8, 13, 21	143.7
20	$\alpha_2$	2.46–2.36 (8H)	m	18	s: 18; m: 2, 3, 5, 6, 9, 15, 16; w: 21	143.3
21	$\text{THS}_{\text{in}} + \text{THS}_{\text{out}} + \text{THS}'_{\text{in}} + \text{THS}'_{\text{out}}$	1.59–0.71 (1248H)	m	21	s: 5, 6, 7, 8, 9, 10, 11; m: 1, 2, 3, 4; w: 12, 13, 14, 15, 16, 17, 18, 19, 20	34.2, 34.14, 34.10, 32.3, 32.24, 32.23, 32.17, 24.7, 24.63, 24.61, 23.29, 23.27, 23.2, 14.59, 14.57, 14.5, 13.3, 13.21, 13.18, 13.18

<sup>†</sup>Relative correlation intensities are designated as: s = strong, m = medium, w = weak.

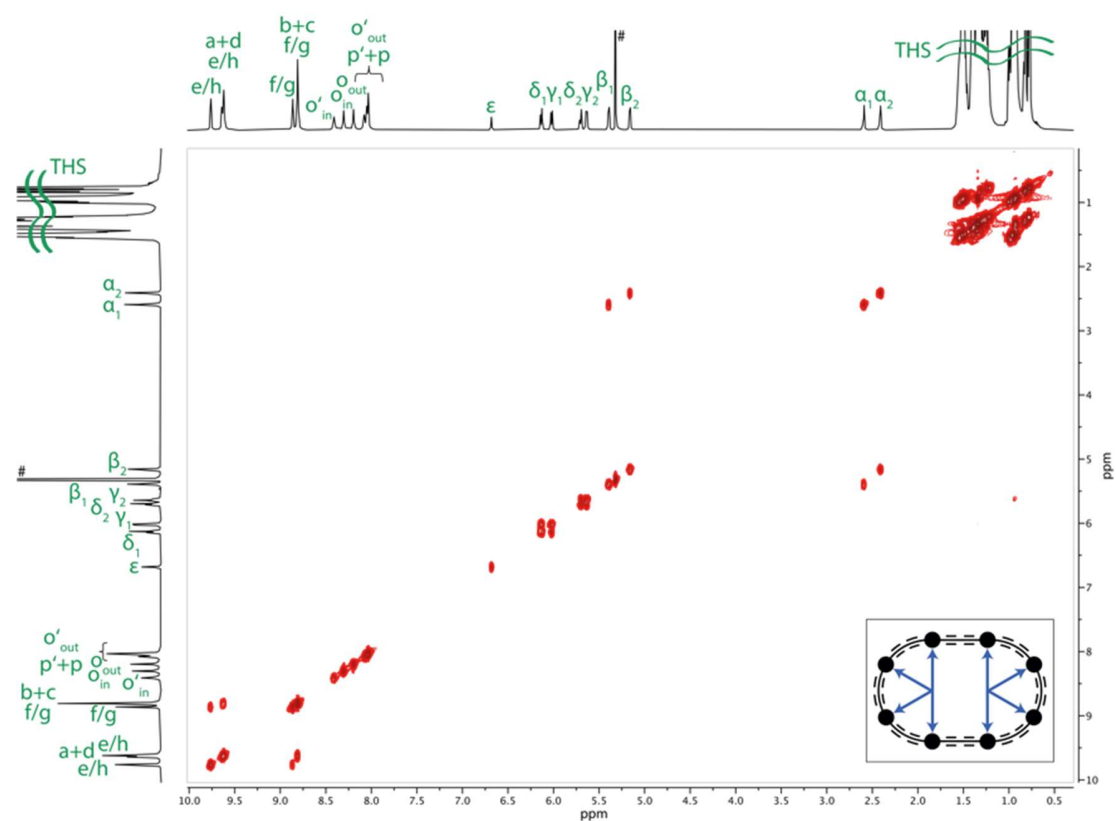


Figure S90.  $^1\text{H}$ - $^1\text{H}$  COSY spectrum of  $c\text{-P8}[\text{b}_8]\bullet(\text{T4})_2$  (600 MHz,  $\text{CD}_2\text{Cl}_2$ , 298 K).

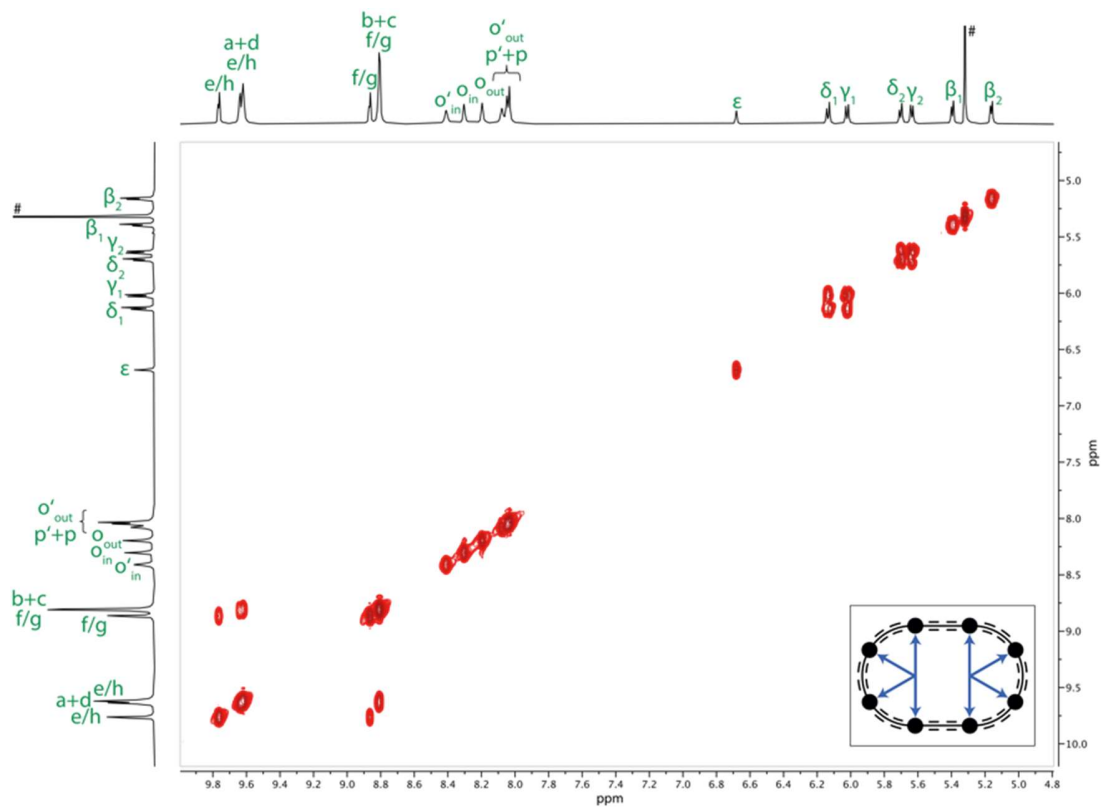


Figure S91. Enlarged region of the COSY spectrum of  $c\text{-P8}[\text{b}_8]\bullet(\text{T4})_2$  (600 MHz,  $\text{CD}_2\text{Cl}_2$ , 298 K).

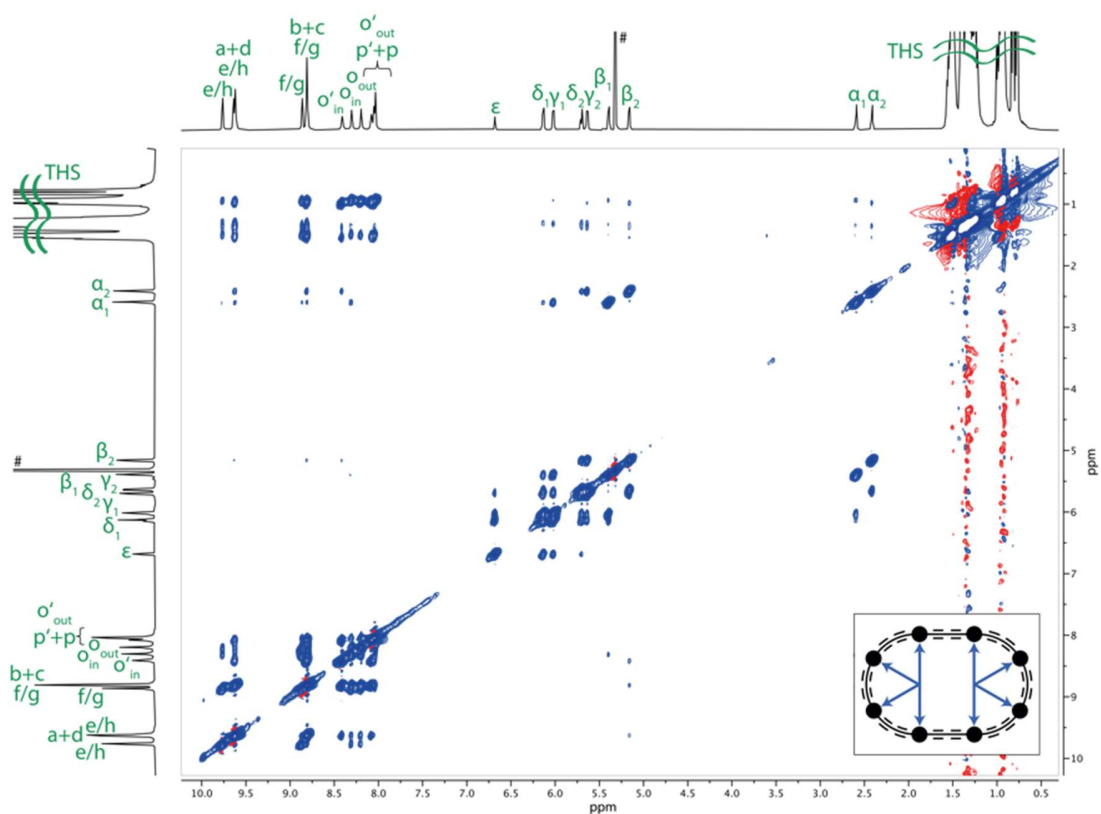


Figure S92.  $^1\text{H}$ - $^1\text{H}$  NOESY spectrum of  $c\text{-P8}[\text{b}_8]\bullet(\text{T4})_2$  (600 MHz,  $\text{CD}_2\text{Cl}_2$ , 298 K).

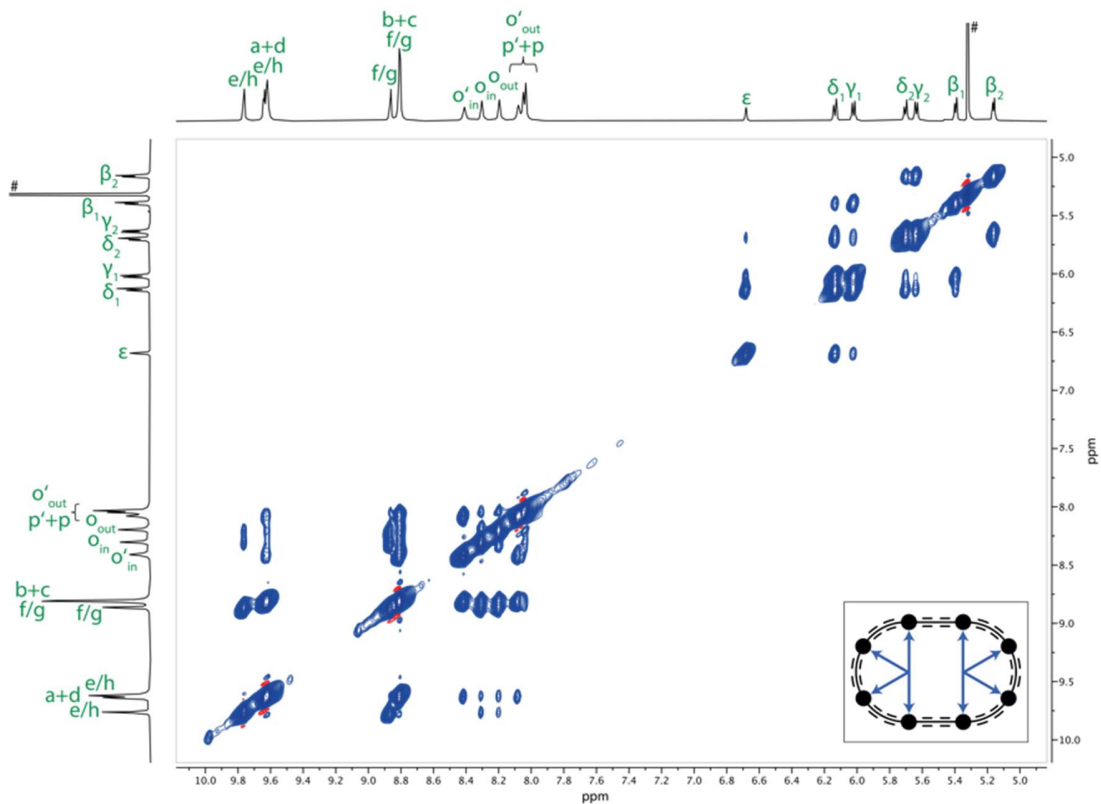


Figure S93. Enlarged region of the NOESY spectrum of  $c\text{-P8}[\text{b}_8]\bullet(\text{T4})_2$  (600 MHz,  $\text{CD}_2\text{Cl}_2$ , 298 K).



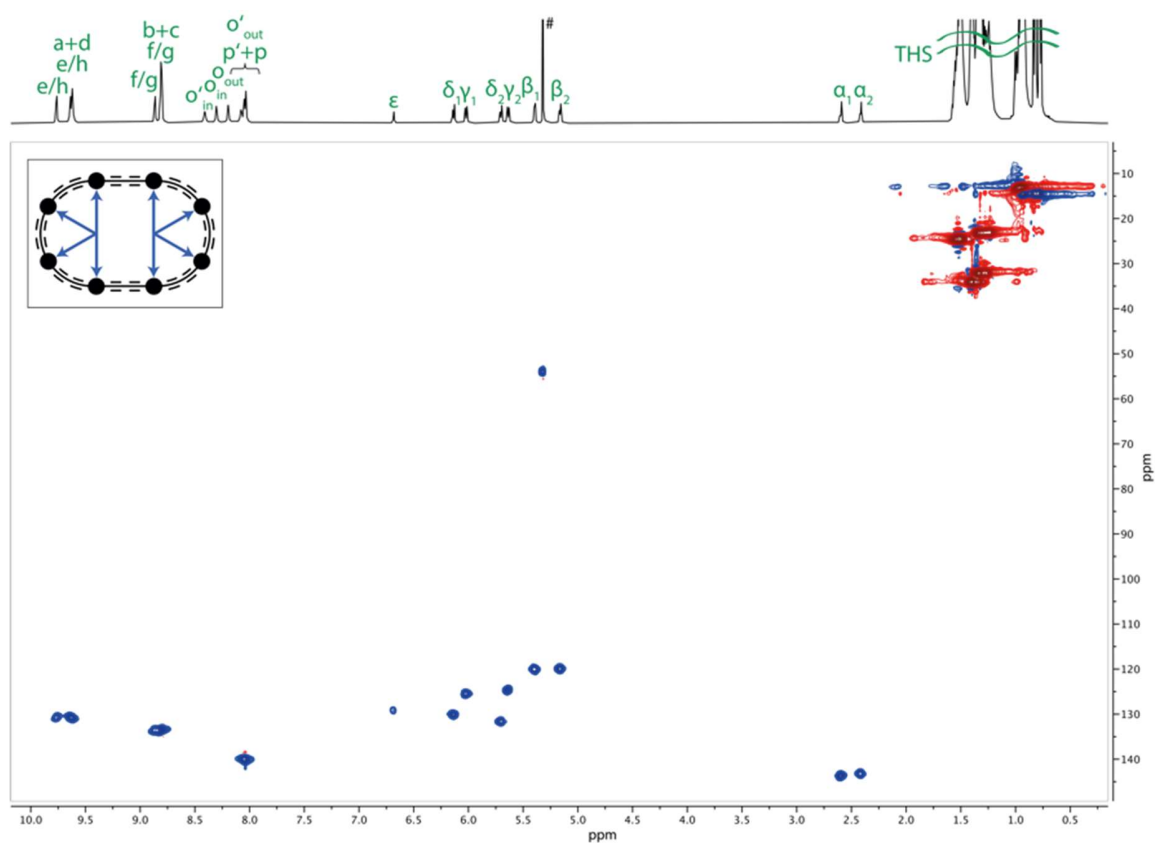


Figure S94.  $^1\text{H}$ - $^{13}\text{C}$  HSQC spectrum of  $c\text{-P8}[\text{b}_8]\bullet(\text{T4})_2$  (600 MHz,  $\text{CD}_2\text{Cl}_2$ , 298 K).

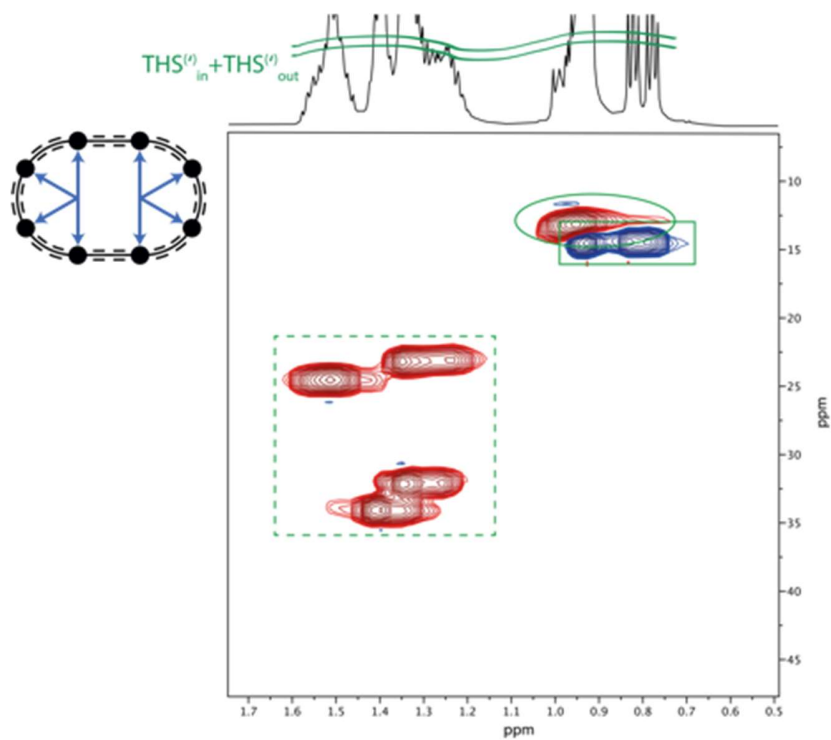
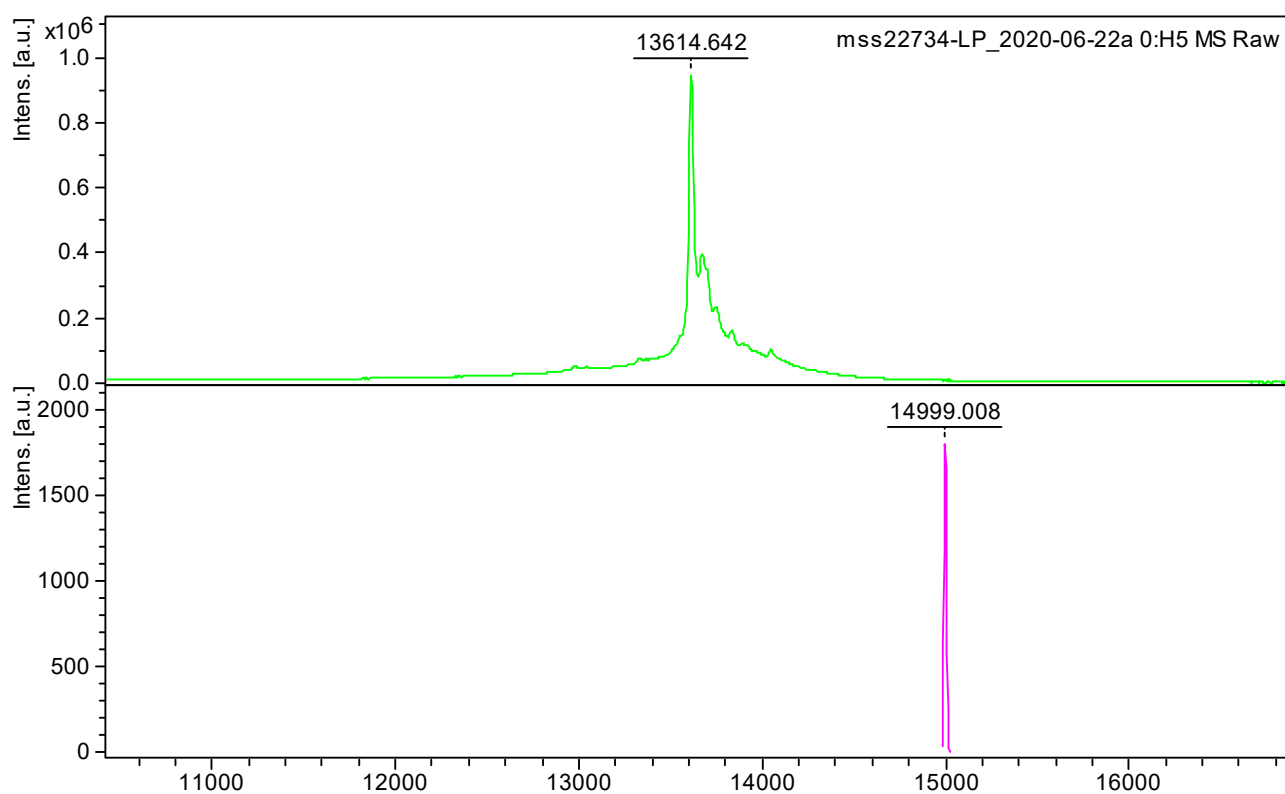
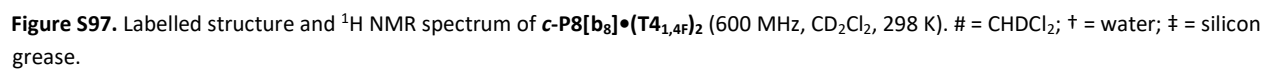


Figure S95. THS region of the  $^1\text{H}$ - $^{13}\text{C}$  HSQC spectrum of  $c\text{-P8}[\text{b}_8]\bullet(\text{T4})_2$  (600 MHz,  $\text{CD}_2\text{Cl}_2$ , 298 K). Si-R- $\text{CH}_3$  resonances are indicated with a solid box, Si- $\text{CH}_2$ -R resonances with a solid circle, and Si- $\text{CH}_2$ - $\text{C}_4\text{H}_8$ - $\text{CH}_3$  resonances with a dashed box.



**Figure S96.** Experimental MALDI-ToF spectrum of *c*-P8[b<sub>8</sub>]•(T4)<sub>2</sub> (top) and simulated MALDI-TOF spectrum of *c*-P8[b<sub>8</sub>]•(T4)<sub>2</sub><sup>+</sup> [C<sub>964</sub>H<sub>1412</sub>F<sub>24</sub>N<sub>40</sub>Si<sub>32</sub>Zn<sub>8</sub>]<sup>+</sup> (bottom). Major peak corresponds to free *c*-P8[b<sub>8</sub>]<sup>+</sup> [C<sub>864</sub>H<sub>1360</sub>N<sub>32</sub>Si<sub>32</sub>Zn<sub>8</sub>]<sup>+</sup> (calculated: 13618).

[illegible]

**Table S21.** Complete  $^1\text{H}$  NMR assignment and correlations for complex  $c\text{-P8}[\text{b}_8]\bullet(\text{T4}_{1,4\text{F}})_2$ .

#	Assign.	$^1\text{H}$	Mult. $J$ (Hz)	$^1\text{H}$ – $^1\text{H}$ COSY	$^1\text{H}$ – $^1\text{H}$ NOESY	$^1\text{H}$ – $^{19}\text{F}$ HOESY <sup>†</sup>	$^1\text{H}$ – $^{13}\text{C}$ HSQC + $^{13}\text{C}$
1	e/h	9.81 (8H)	d, $J$ = 4.1	4	s: 4; m: 8, 9, 19, w: 18, 21	-	130.7
2	a/d	9.68 (8H)	d, $J$ = 4.2	4	s: 4s; m: 7, 10, 20; w: 17, 21	-	130.9
3	a/d + e/h	9.64–9.58 (16H)	m	5, 6	s: 5, 6; m: 7, 8, 9, 10, 19, 20; w: 17, 18	vw	130.7
4	b/c + f/g	8.87–8.83 (16H)	m	1, 2	s: 1, 2, 7, 8, 9, 10, 21; m: 11, 19, 20; w: 12, 17	-	133.6
5	b/c	8.82 (8H)	d, $J$ = 4.2	3	s: 3, 7, 10, 21; m: 11, 20; w: 17	-	133.4
6	f/g	8.75 (8H)	d, $J$ = 4.1	3	s: 3, 8, 9, 21; m: 19; w: 8, 12, 18	-	133.5
7	$\text{o}'_{\text{in}}$	8.44 (8H)	s	10	s: 4, 5, 21; m: 2, 3, 10, 20; w: 11, 17	-	140.8
8	$\text{o}_{\text{out}}$	8.22 (8H)	s	12	s: 4, 6, 21; m: 1, 3, 12; w: 19	-	141.4
9	$\text{o}_{\text{in}}$	8.13 (8H)	s	-	s: 4, 6, 21; m: 1, 3, 12, 19; w: 18	w	140.9
10	$\text{o}'_{\text{out}}$	8.11 (8H)	s	7	s: 4, 5, 21; m: 2, 3, 7; w: 20	-	141.7
11	$\text{p}'$	8.06 (8H)	s	-	s: 21, m: 4, 5; w: 7	-	139.9
12	p	8.00 (8H)	s	8	s: 21; m: 8, 9; w: 4, 6	-	139.8
13	$\epsilon$	6.83 (4H)	s	-	s: 14; m: 15; w: 16, 18	w-m	-
14	$\delta_1$	6.67 (8H)	s	-	s: 13, 15, 16; m: 18 w: 17, 19	s	130.0
15	$\delta_2$	5.82 (8H)	d, $J$ = 8.7	16	s: 14, 16; m: 13, 17, 20; w: 18	w-m	131.3
16	$\gamma_2$	5.77 (8H)	d, $J$ = 8.7	15	s: 14, 15, 17; m: 20; w: 13, 18	w-m	125.4
17	$\beta_2$	5.19 (8H)	d, $J$ = 6.6	20	s: 16, 20; m: 15; w: 2, 3, 4, 5, 7, 14	-	120.2
18	$\beta_1$	5.10 (8H)	d, $J$ = 7.6	19	s: 19; m: 14; w: 1, 3, 6, 9, 13, 14, 15, 16, 21	m	123.7
19	$\alpha_1$	2.57–2.52 (8H)	m	18	s: 18; m: 1, 3, 4, 6, 9; w: 8, 14, 21	w-m	142.3
20	$\alpha_2$	2.50–2.44 (8H)	m	17	s: 17; m: 2, 3, 4, 5, 7, 15, 16; w: 2, 9, 10, 21	-	143.3
21	$\text{THS}_{\text{in}}+$ $\text{THS}_{\text{out}}+$ $\text{THS}'_{\text{in}}+$ $\text{THS}'_{\text{out}}$	1.66–0.57 (1248H)	m	21	s: 4, 5, 6, 7, 8, 9, 10, 11, 12; m: 2; w: 1, 18, 19, 20	w	34.2, 34.1, 34.0, 32.24, 32.24, 32.1, 24.7, 24.6, 24.5, 23.28, 23.27, 23.1, 14.58, 14.57, 14.4, 13.3, 13.2, 13.0

<sup>†</sup>Relative correlation intensities are designated as: s = strong, m = medium, w = weak, vw = very weak.

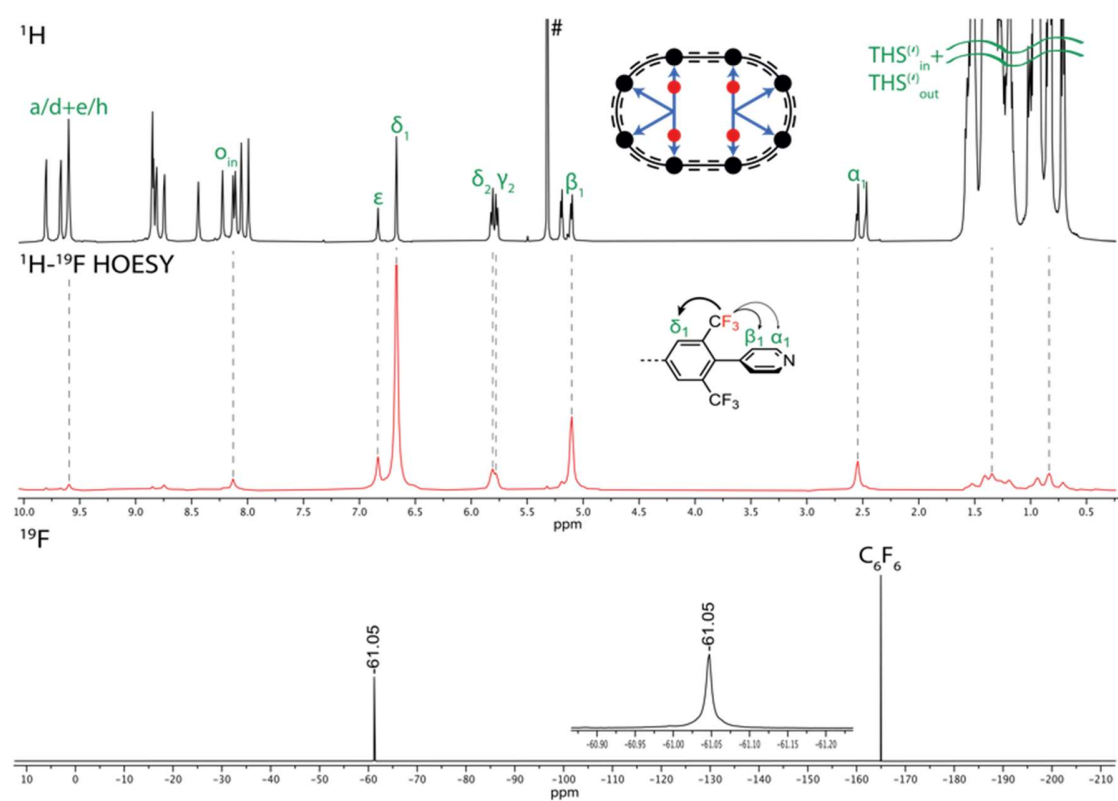


Figure S98. Combined  $^1\text{H}$  (top), 1D  $^1\text{H}$ - $^{19}\text{F}$  HOESY (middle, red), and  $^{19}\text{F}$  (bottom) spectra of  $c\text{-P8}[\text{b}_8]\bullet(\text{T}_{4,4}\text{F})_2$  (500 MHz,  $\text{CD}_2\text{Cl}_2$ , 298 K).

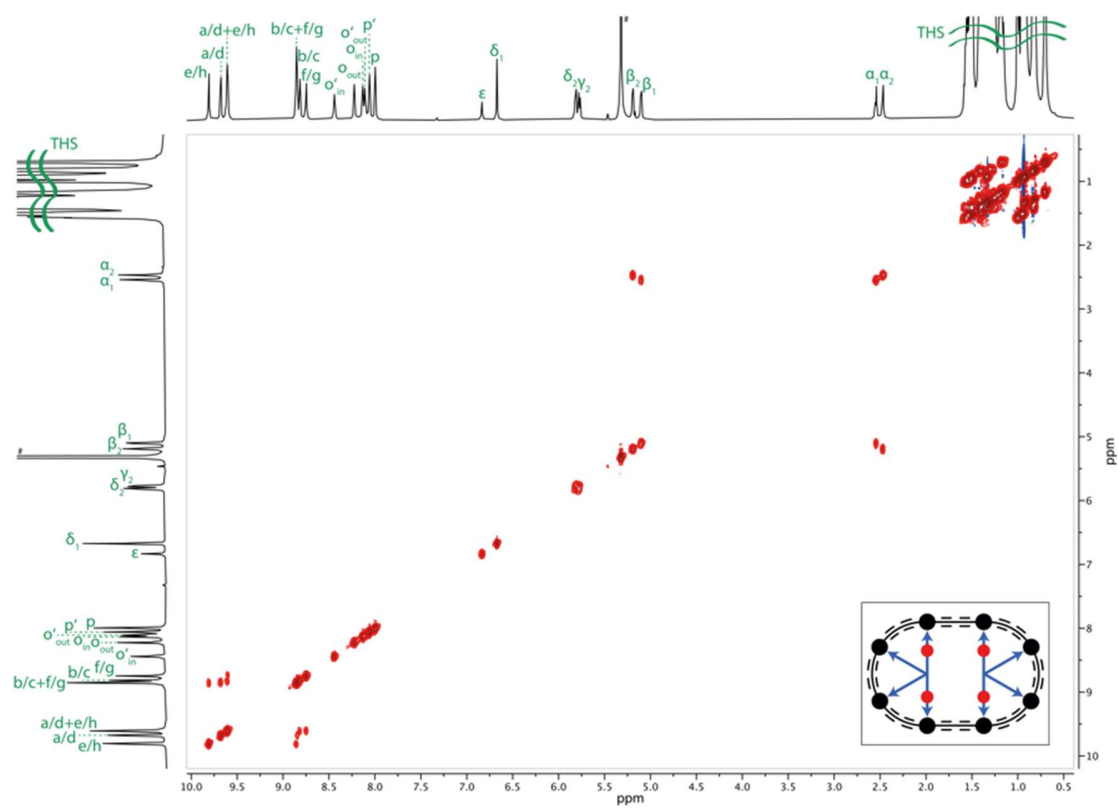


Figure S99.  $^1\text{H}$ - $^1\text{H}$  COSY spectrum of  $c\text{-P8}[\text{b}_8]\bullet(\text{T}_{4,4}\text{F})_2$  (600 MHz,  $\text{CD}_2\text{Cl}_2$ , 298 K).

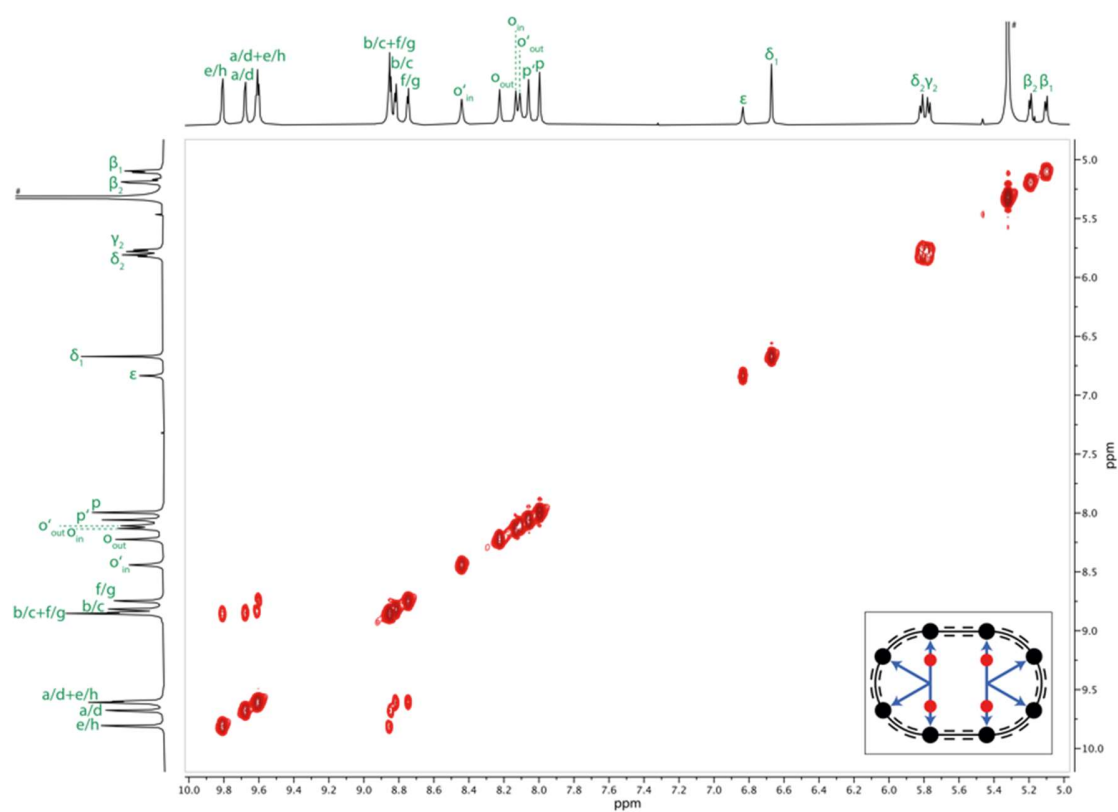


Figure S100. Enlarged region of the COSY spectrum of **c-P8[b<sub>8</sub>]•(T<sub>4,4</sub>F)<sub>2</sub>** (600 MHz, CD<sub>2</sub>Cl<sub>2</sub>, 298 K).

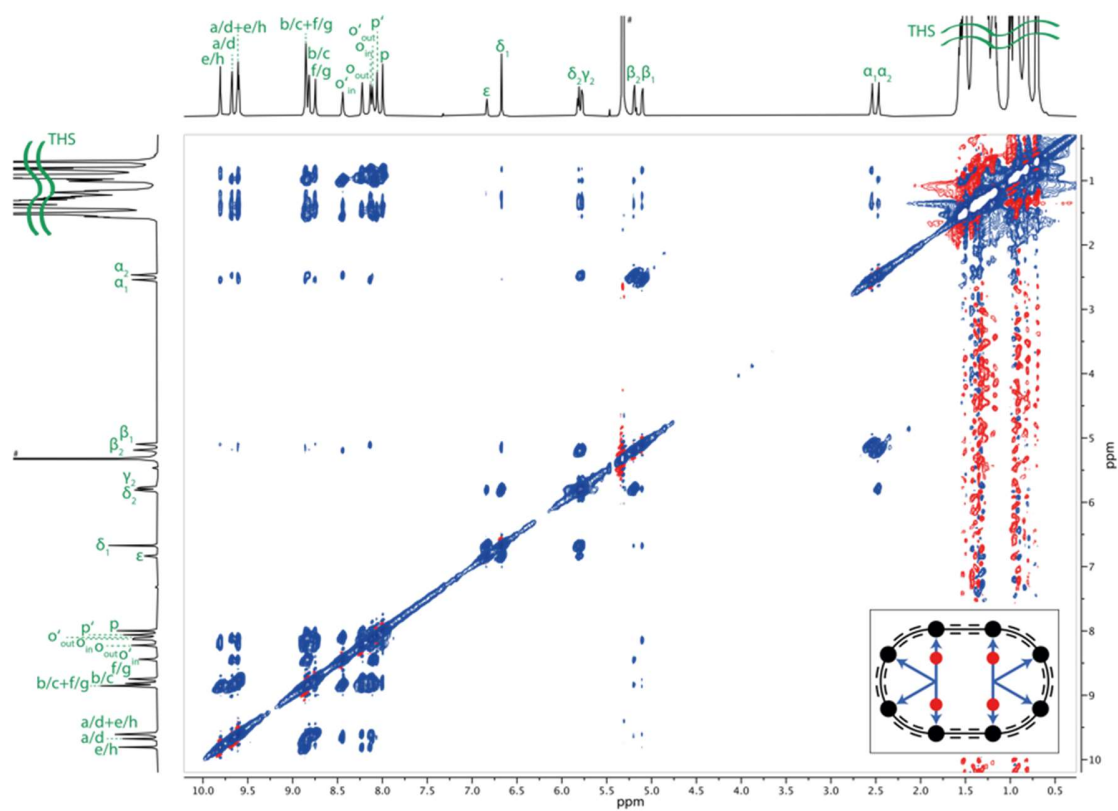


Figure S101. <sup>1</sup>H-<sup>1</sup>H NOESY spectrum of **c-P8[b<sub>8</sub>]•(T<sub>4,4</sub>F)<sub>2</sub>** (600 MHz, CD<sub>2</sub>Cl<sub>2</sub>, 298 K).

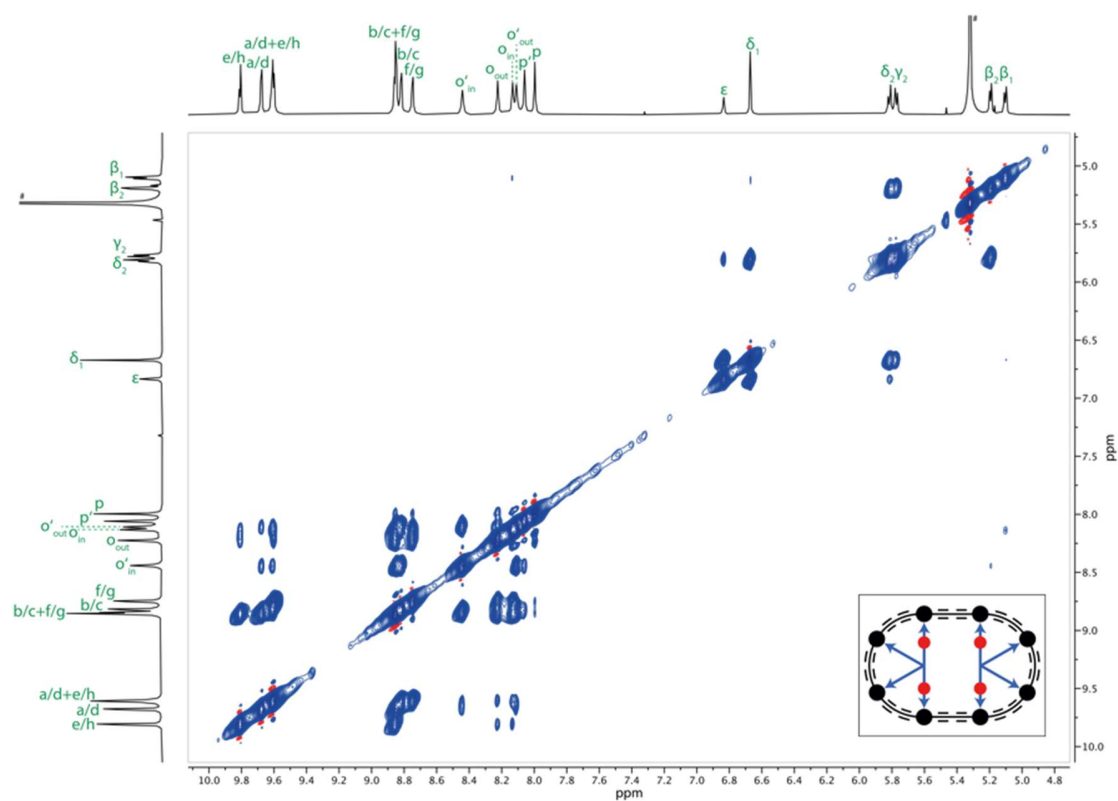


Figure S102. Enlarged region of the NOESY spectrum of **c-P8[b<sub>8</sub>]•(T<sub>41,4F</sub>)<sub>2</sub>** (600 MHz, CD<sub>2</sub>Cl<sub>2</sub>, 298 K).

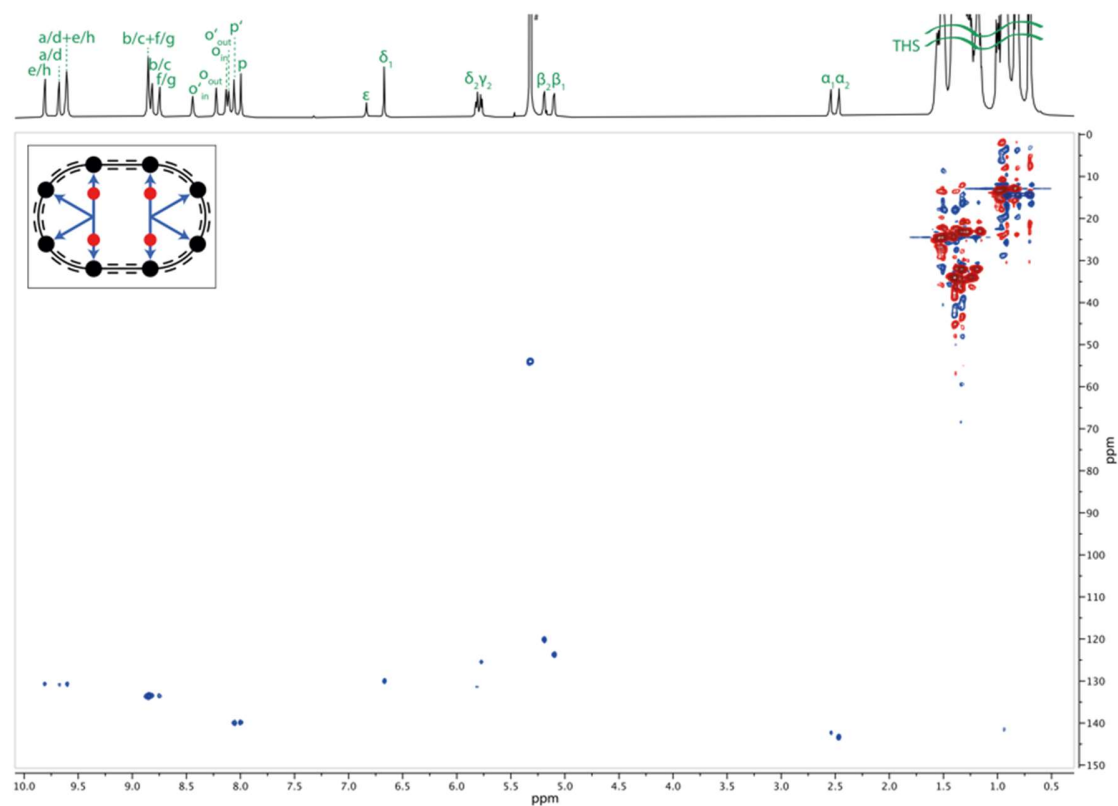
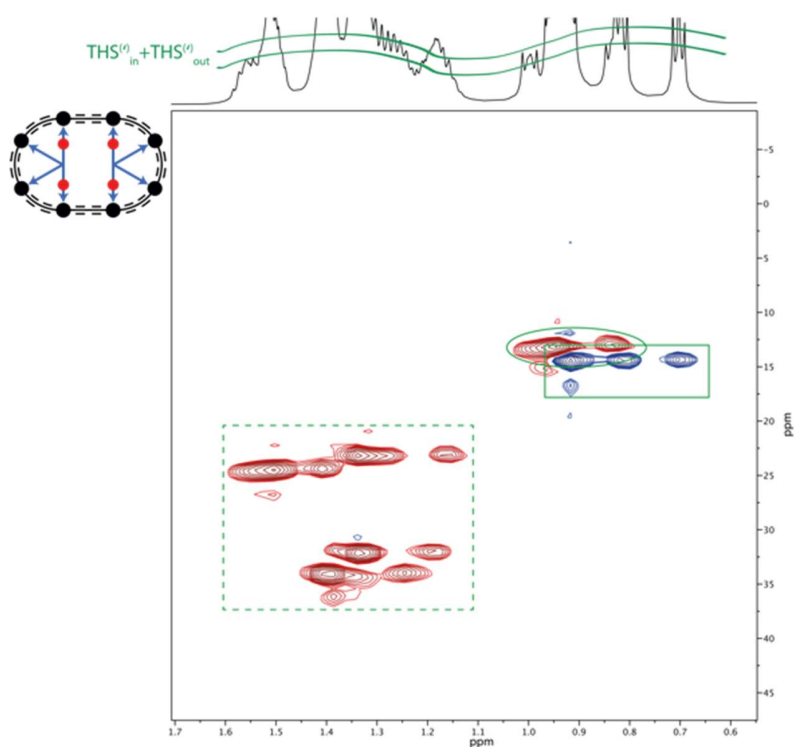
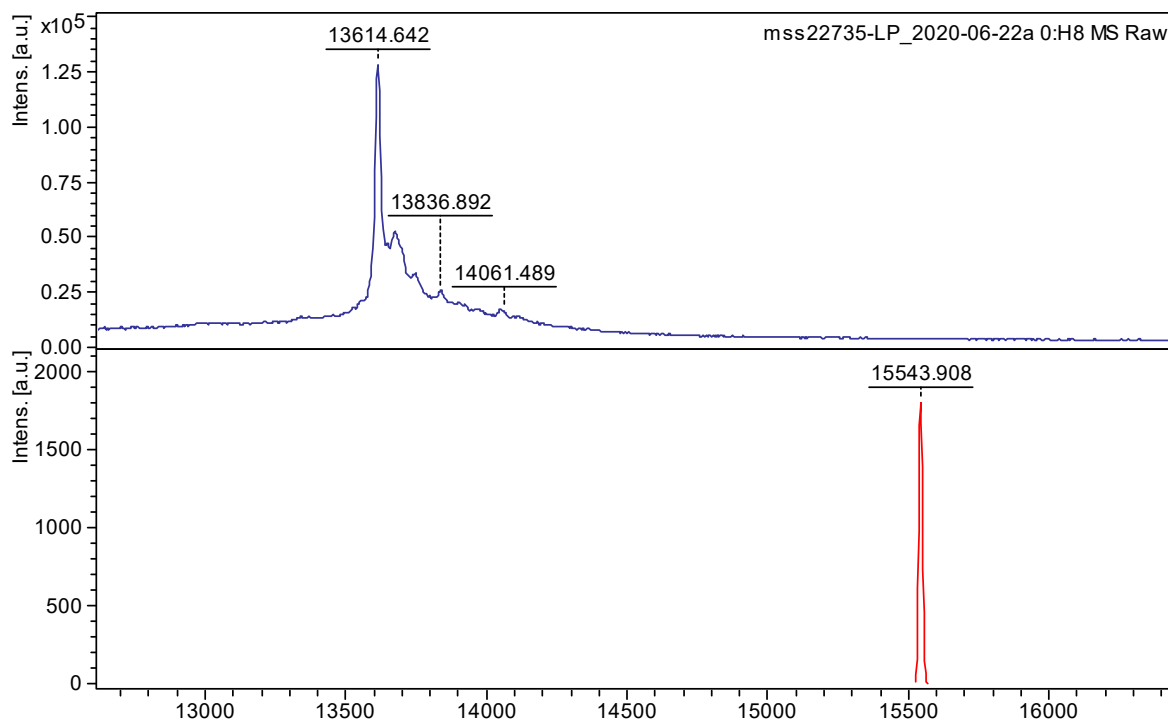


Figure S103. <sup>1</sup>H-<sup>13</sup>C HSQC spectrum of **c-P8[b<sub>8</sub>]•(T<sub>41,4F</sub>)<sub>2</sub>** (600 MHz, CD<sub>2</sub>Cl<sub>2</sub>, 298 K).





**Figure S104.** THS region of the  $^1\text{H}$ - $^{13}\text{C}$  HSQC spectrum of *c*-P8[b<sub>8</sub>]•(T<sub>41,4F</sub>)<sub>2</sub> (600 MHz, CD<sub>2</sub>Cl<sub>2</sub>, 298 K). Si-R-CH<sub>3</sub> resonances are indicated with a solid box, Si-CH<sub>2</sub>-R resonances with a solid circle, and Si-CH<sub>2</sub>-C<sub>4</sub>H<sub>8</sub>-CH<sub>3</sub> resonances with a dashed box.



**Figure S105.** Experimental MALDI-TOF spectrum of *c*-P8[b<sub>8</sub>]•(T<sub>41,4F</sub>)<sub>2</sub> (top) and simulated MALDI-TOF spectrum of *c*-P8[b<sub>8</sub>]•(T<sub>41,4F</sub>)<sub>2</sub> [C<sub>972</sub>H<sub>1420</sub>F<sub>24</sub>N<sub>40</sub>Si<sub>32</sub>Zn<sub>8</sub>]<sup>+</sup> (bottom). Major peak corresponds to free *c*-P8[b<sub>8</sub>]<sup>+</sup> [C<sub>864</sub>H<sub>1360</sub>N<sub>32</sub>Si<sub>32</sub>Zn<sub>8</sub>]<sup>+</sup> (calculated: 13618).

**Complex  $c\text{-P8}[\text{b}_8] \cdot (\text{T4}_{2,3\text{F}})_2$ :**

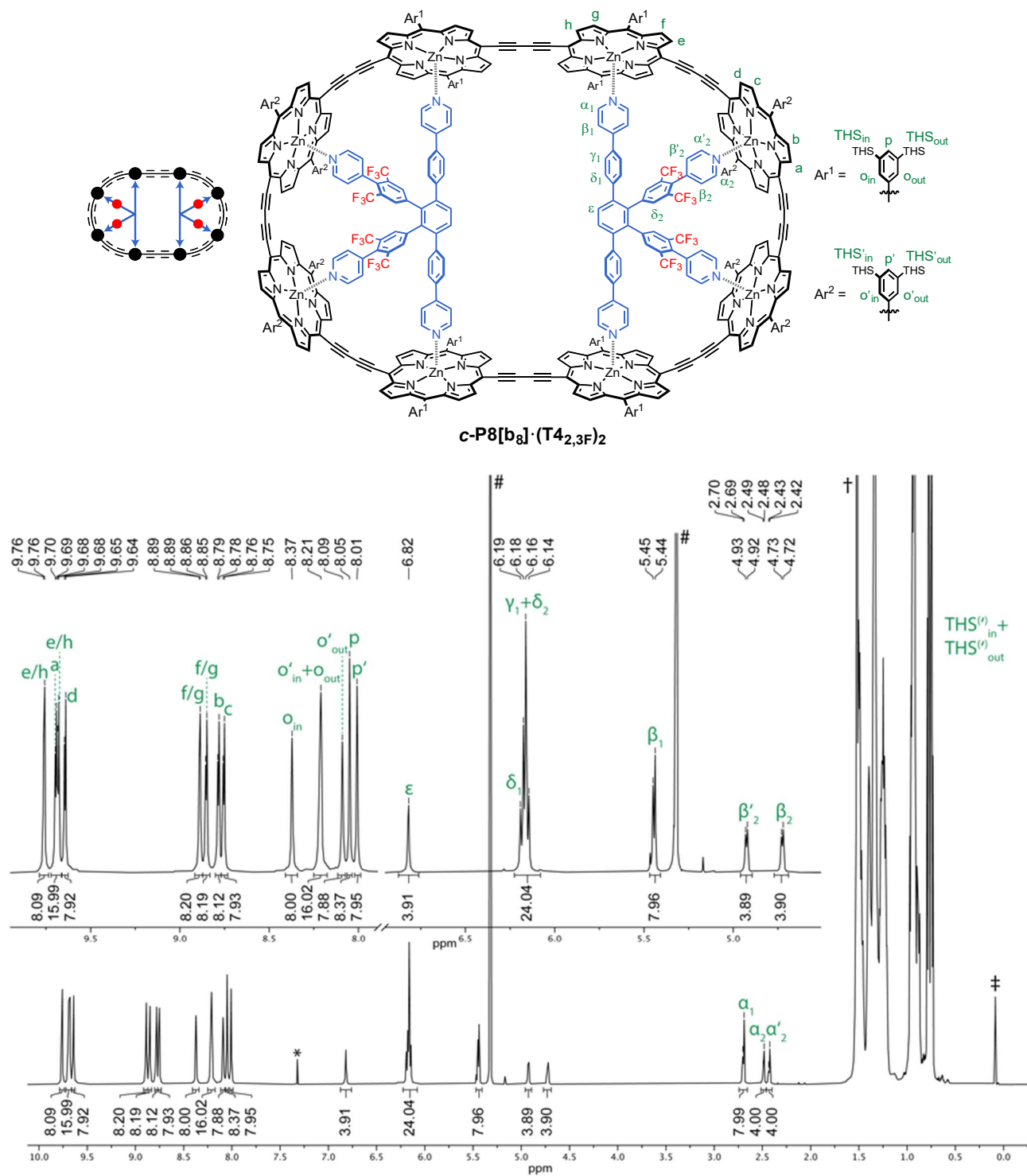


**Figure S106.** Labelled structure and  $^1\text{H}$  NMR spectrum of  $c\text{-P8}[\text{b}_8] \cdot (\text{T4}_{2,3\text{F}})_2$  (600 MHz,  $\text{CD}_2\text{Cl}_2$ , 298 K). # =  $\text{CHDCl}_2$ ; \* =  $\text{CHCl}_3$ ; + = water; ‡ = silicon grease.

**Table 22.** Complete <sup>1</sup>H NMR assignment and correlations for complex **c-P8[b<sub>8</sub>](T4<sub>2,3F</sub>)<sub>2</sub>**.

#	Assign.	<sup>1</sup> H	Mult. J (Hz)	<sup>1</sup> H– <sup>1</sup> H COSY	<sup>1</sup> H– <sup>1</sup> H NOESY <sup>†</sup>	<sup>1</sup> H– <sup>19</sup> F HOESY <sup>†</sup>	<sup>1</sup> H– <sup>13</sup> C HSQC + <sup>13</sup> C
1	e/h	9.76 (8H)	d, J = 4.0	5	s: 5; m: 9, 10, 20; w: 17, 12	-	130.8
2	a	9.69 (8H)	d, J = 4.4	7	s: 7; m: 10, 11, 21; w: 19, 23	-	130.7
3	e/h	9.68 (8H)	d, J = 4.0	6	s: 6; m: 9, 10, 20; w: 15, 17, 23	-	130.7
4	d	9.64 (8H)	d, J = 4.3	8	s: 8; m: 10, 11, 22; w: 18	-	130.7
5	f/g	8.89 (8H)	d, J = 4.0	1	s: 1; m: 9, 10, 20, 23; w: 12, 17	-	133.6
6	f/g	8.85 (8H)	d, J = 4.0	3	s: 3; m: 9, 10, 20, 23; w: 12, 17	-	133.6
7	b	8.78 (8H)	d, J = 4.4	2	s: 2; m: 10, 11, 21, 22, 23; w: 9, 13, 18, 19	vw	133.5
8	c	8.75 (8H)	d, J = 4.3	4	s: 4; m: 10, 11, 21, 22, 23; w: 9, 13, 18, 19	vw	133.5
9	o <sub>in</sub>	8.37 (8H)	s	10	s: 10, 23; m: 1, 3, 5, 6, 12, 20; w: 7, 8, 16, 17	-	140.8
10	o' <sub>in</sub> + o <sub>out</sub>	8.21 (16H)	s	9, 11	s: 9, 23; m: 1, 2, 3, 4, 5, 6, 7, 8, 11, 21, 22; w: 12, 13, 18, 19, 20	vw	141.3, 141.3
11	o' <sub>out</sub>	8.09 (8H)	s	10	s: 23; m: 2, 4, 7, 8, 10; w: 21	-	141.4
12	p	8.05 (8H)	s	-	s: 23, m: 9, w: 1, 5, 6, 10	-	139.9
13	p'	8.01 (8H)	s	-	s: 23; w: 7, 8, 10	-	139.8
14	ε	6.82 (4H)	s	-	s: 15; w: 17	-	130.5
15	δ <sub>1</sub>	6.18 (8H)	d, J = 9.7	-	s: 14; m: 17; w: 3	-	129.9
16	γ <sub>1</sub> + δ <sub>2</sub>	6.17–6.13 (16H)	m	-	s: 17; m: 20; w: 9, 18, 19, 21, 22, 23	s	131.7, 126.1
17	β <sub>1</sub>	5.44 (8H)	d, J = 7.3	20	s: 16, 20; m: 15; w: 1, 3, 5, 6, 9, 14, 18	-	120.4
18	β' <sub>2</sub>	4.93 (4H)	d, J = 6.3	22, 19	s: 21, 22; m: 19; w: 4, 7, 8, 10, 16, 17	w-m	123.8
19	β <sub>2</sub>	4.73 (4H)	d, J = 6.0	21, 18	s: 21, 22; m: 18; w: 2, 7, 8, 10, 16	m	123.0
20	α <sub>1</sub>	2.74–2.66 (8H)	m	17	s: 17; m: 1, 3, 5, 6, 9; w: 10	-	143.8
21	α <sub>2</sub>	2.52–2.46 (4H)	m	19	s: 18, 19; m: 2, 7, 8, 10; w: 11	w	142.6
22	α' <sub>2</sub>	2.45–2.41 (4H)	m	18	s: 18, 19; m: 4, 7, 8, 10	w	142.2
23	THS <sub>in</sub> + THS <sub>out</sub> + THS' <sub>in</sub> + THS' <sub>out</sub>	1.58–0.71 (1248H)	m	-	s: 9, 10, 11, 12, 13; m: 5, 6, 7, 8; w: 2, 3, 16	w	34.13, 34.10, 34.0, 32.3, 32.23, 32.16, 24.62, 24.61, 24.60, 23.3, 23.19, 23.18, 14.58, 14.57, 14.49, 14.47, 13.21, 13.17, 13.1.

<sup>†</sup>Relative correlation intensities are designated as: s = strong, m = medium, w = weak, vw = very weak.

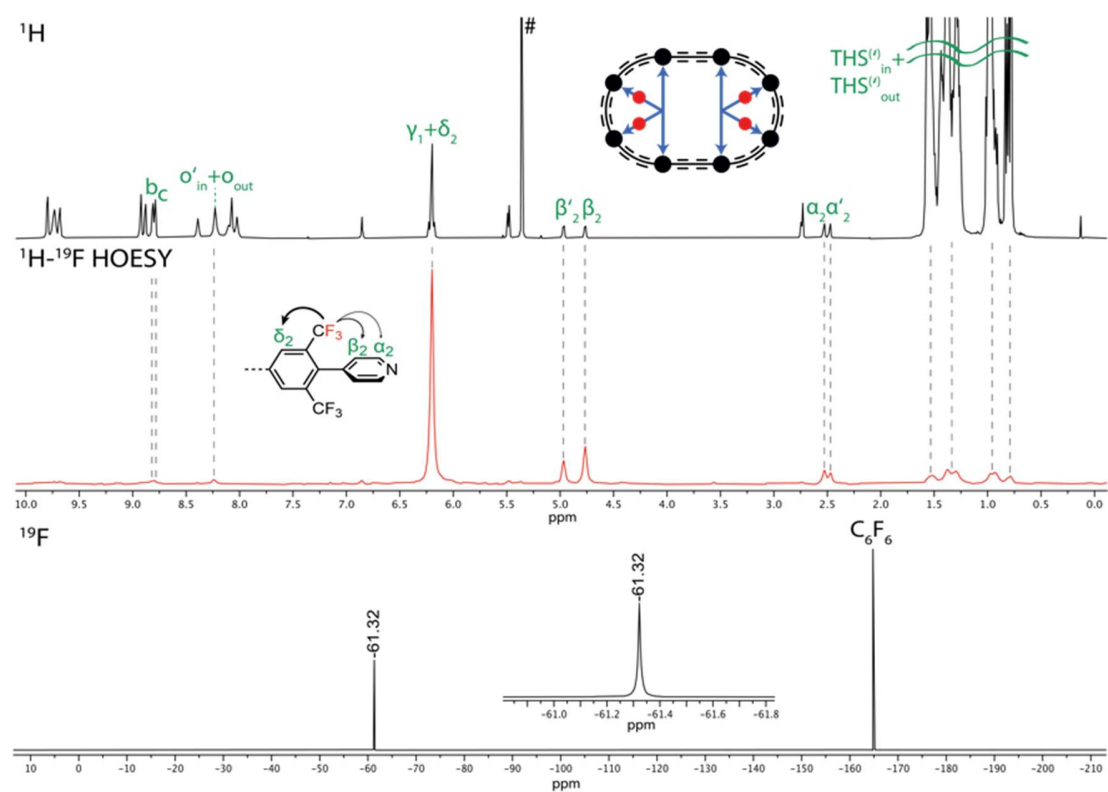


Figure S107. Combined  $^1\text{H}$  (top), 1D  $^1\text{H}$ - $^{19}\text{F}$  HOESY (middle, red), and  $^{19}\text{F}$  (bottom) spectra of *c*-P8[b<sub>8</sub>]•(T<sub>4,3F</sub>)<sub>2</sub> (500 MHz, CD<sub>2</sub>Cl<sub>2</sub>, 298 K).

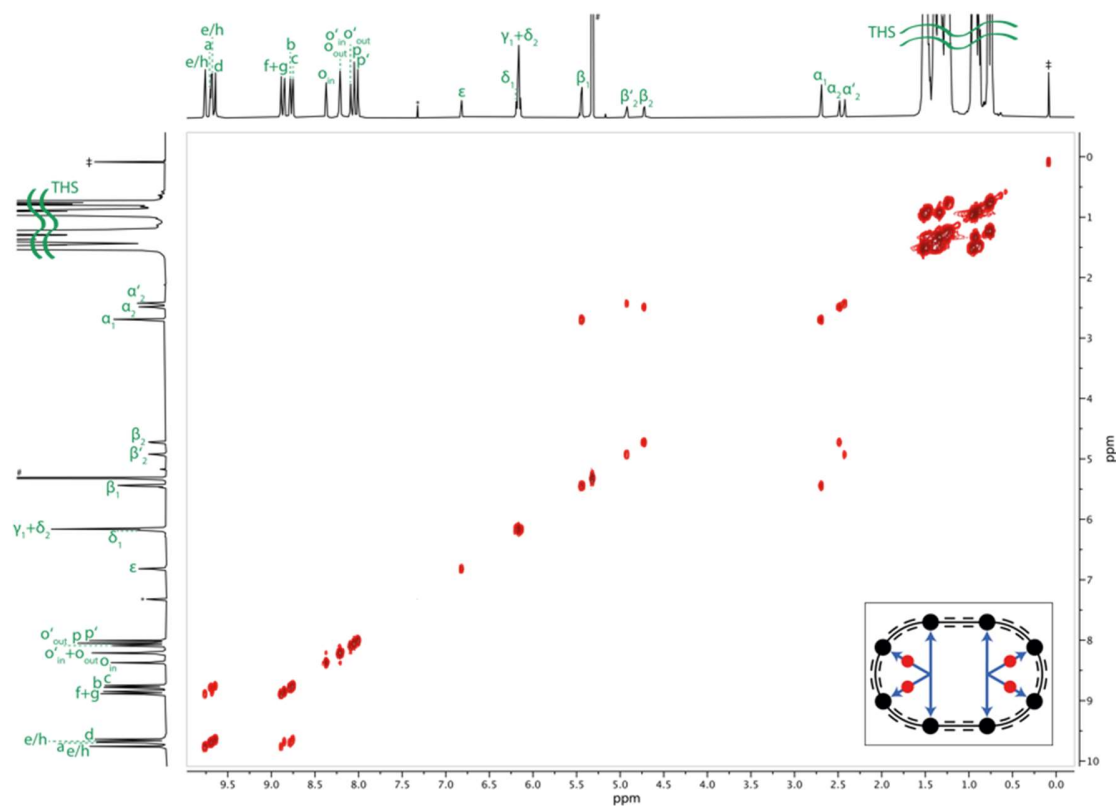


Figure S108.  $^1\text{H}$ - $^1\text{H}$  COSY spectrum of *c*-P8[b<sub>8</sub>]•(T<sub>4,3F</sub>)<sub>2</sub> (600 MHz, CD<sub>2</sub>Cl<sub>2</sub>, 298 K).

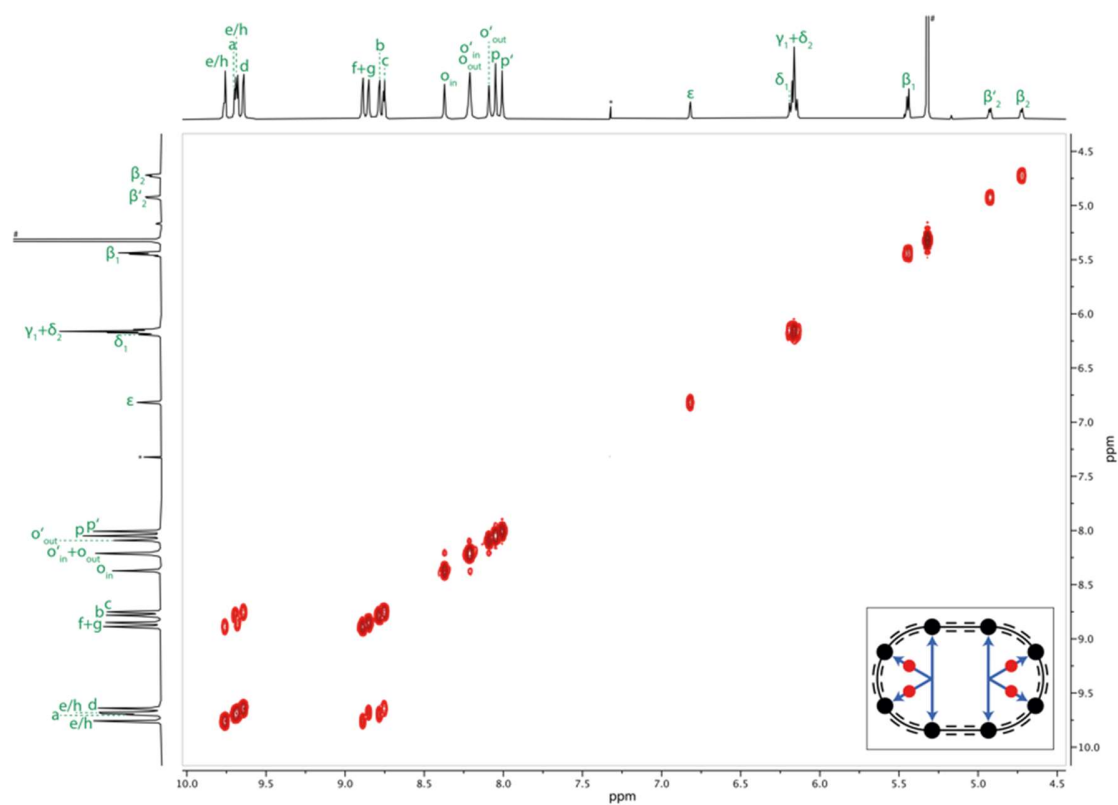


Figure S109. Enlarged region of the COSY spectrum of *c*-P8[b<sub>8</sub>]•(T<sub>42,3F</sub>)<sub>2</sub> (600 MHz, CD<sub>2</sub>Cl<sub>2</sub>, 298 K).

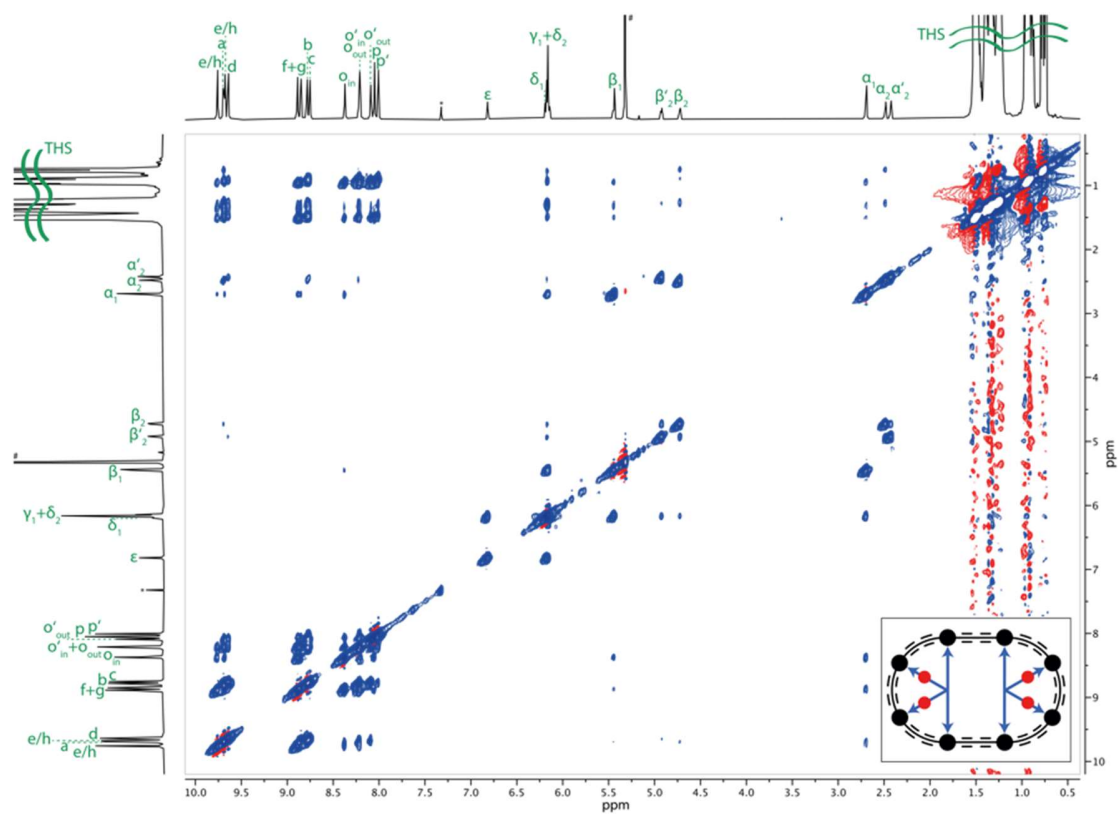


Figure S110. <sup>1</sup>H-<sup>1</sup>H NOESY spectrum of *c*-P8[b<sub>8</sub>]•(T<sub>42,3F</sub>)<sub>2</sub> (600 MHz, CD<sub>2</sub>Cl<sub>2</sub>, 298 K).

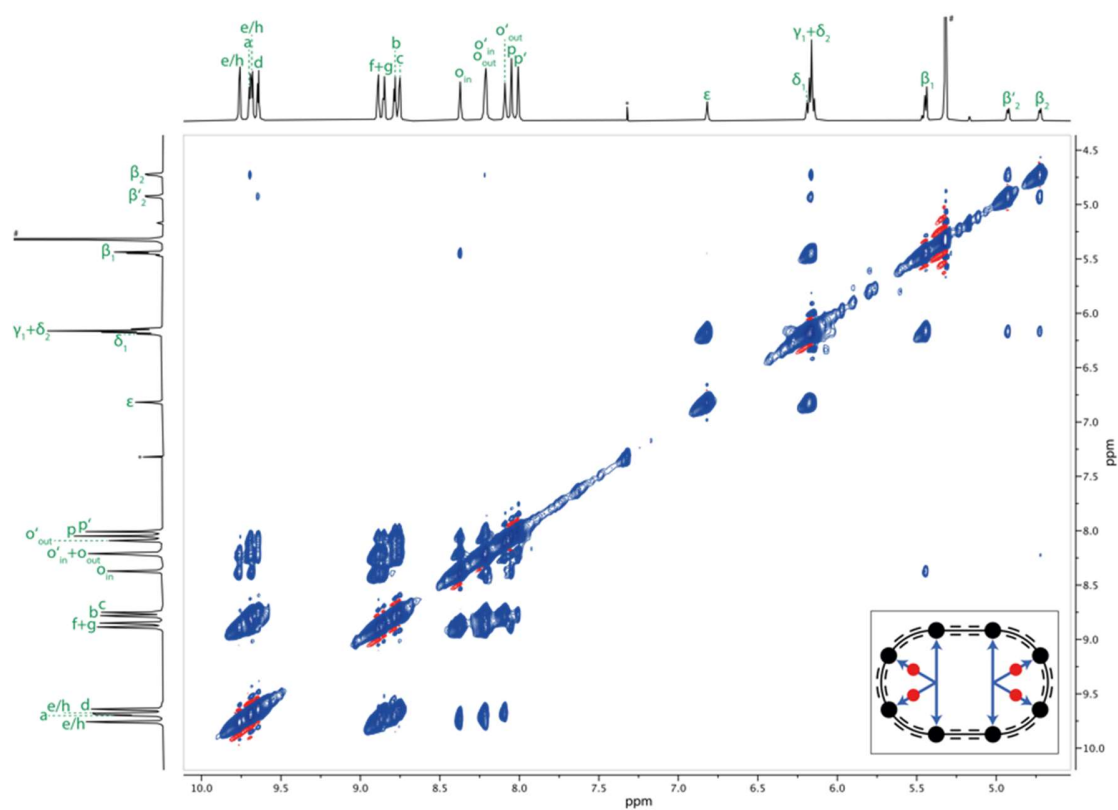


Figure S111. Enlarged region of the NOESY spectrum of **c-P8[b<sub>8</sub>]•(T<sub>42,3F</sub>)<sub>2</sub>** (600 MHz, CD<sub>2</sub>Cl<sub>2</sub>, 298 K).

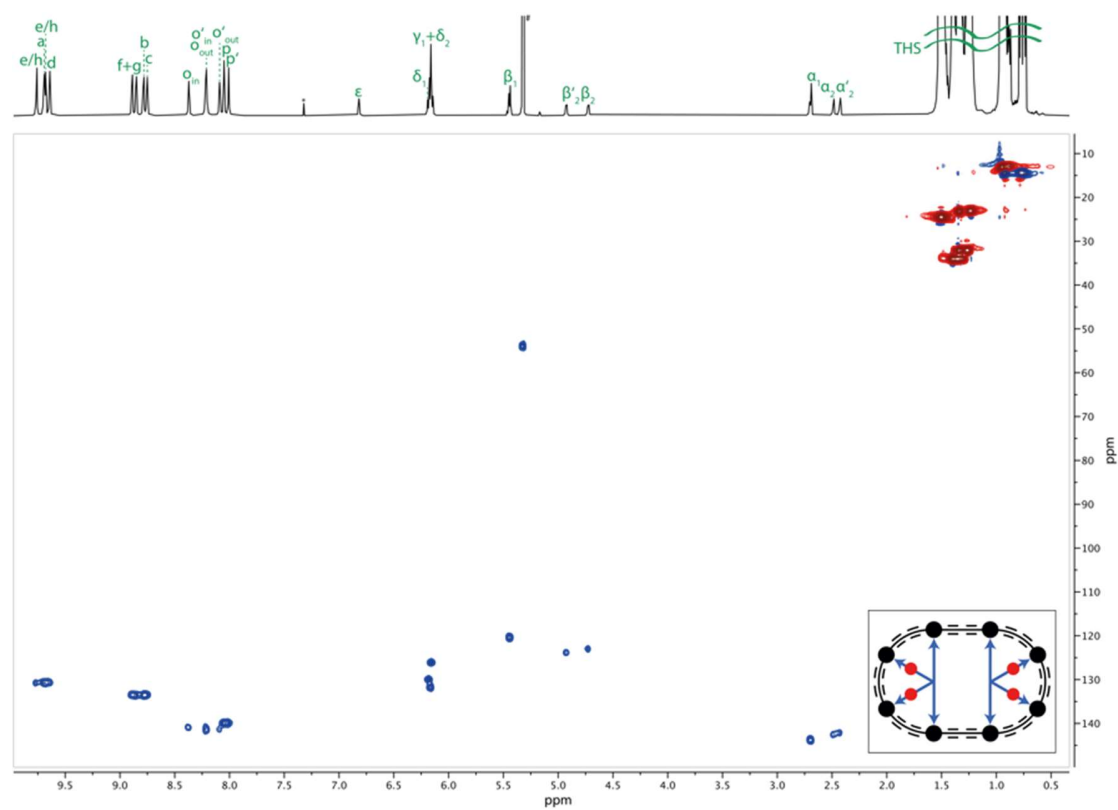
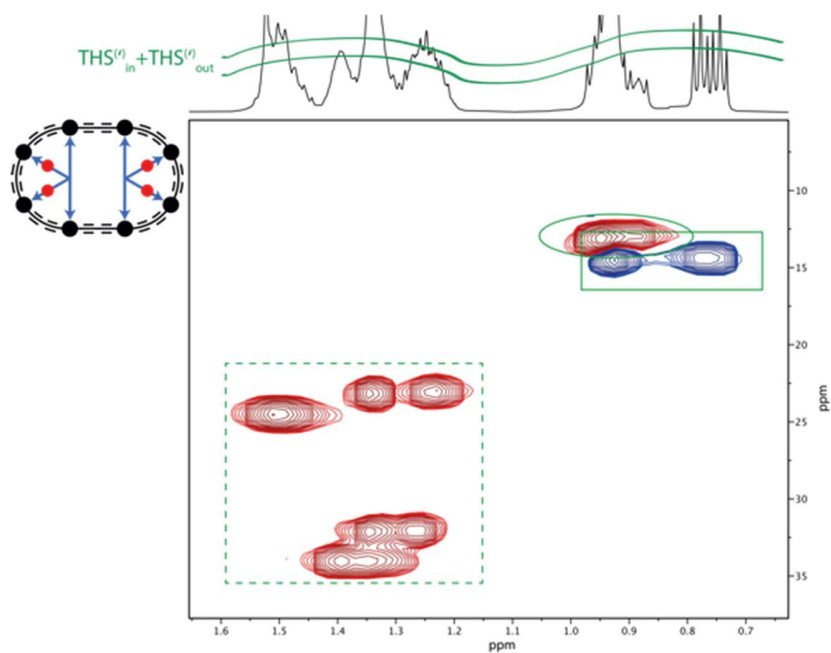
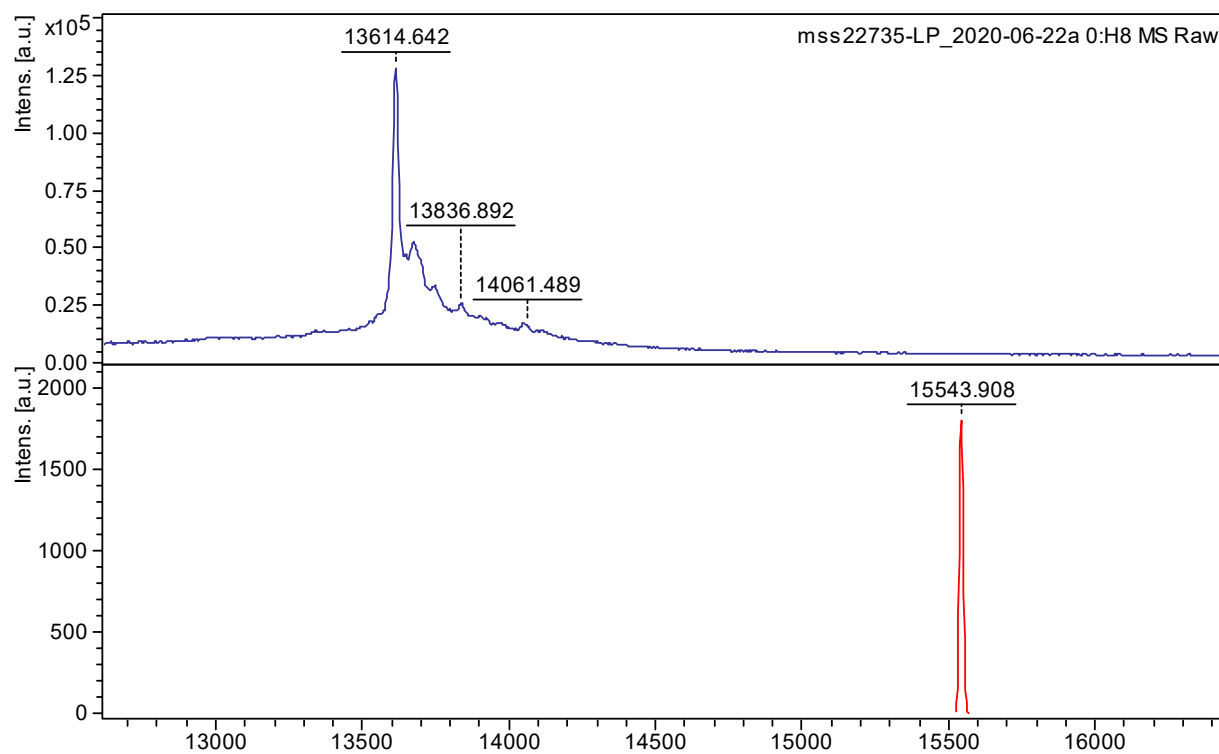


Figure S112. <sup>1</sup>H-<sup>13</sup>C HSQC spectrum of **c-P8[b<sub>8</sub>]•(T<sub>42,3F</sub>)<sub>2</sub>** (600 MHz, CD<sub>2</sub>Cl<sub>2</sub>, 298 K).



**Figure S113.** THS region of the  $^1\text{H}$ - $^{13}\text{C}$  HSQC spectrum of **c-P8[b<sub>8</sub>](T4<sub>2,3F</sub>)<sub>2</sub>** (600 MHz,  $\text{CD}_2\text{Cl}_2$ , 298 K). Si-R-CH<sub>3</sub> resonances are indicated with a solid box, Si-CH<sub>2</sub>-R resonances with a solid circle, and Si-CH<sub>2</sub>-C<sub>4</sub>H<sub>8</sub>-CH<sub>3</sub> resonances with a dashed box.



**Figure S114.** Experimental MALDI-TOF spectrum of **c-P8[b<sub>8</sub>](T4<sub>2,3F</sub>)<sub>2</sub>** (top) and simulated MALDI-TOF spectrum of **c-P8[b<sub>8</sub>](T4<sub>2,3F</sub>)<sub>2</sub>** [ $\text{C}_{972}\text{H}_{1420}\text{F}_{24}\text{N}_{40}\text{Si}_{32}\text{Zn}_8$ ]<sup>+</sup> (bottom). Major peak corresponds to free **c-P8[b<sub>8</sub>]<sup>+</sup>** [ $\text{C}_{864}\text{H}_{1360}\text{N}_{32}\text{Si}_{32}\text{Zn}_8$ ]<sup>+</sup> (calculated: 13618).



Template T4:

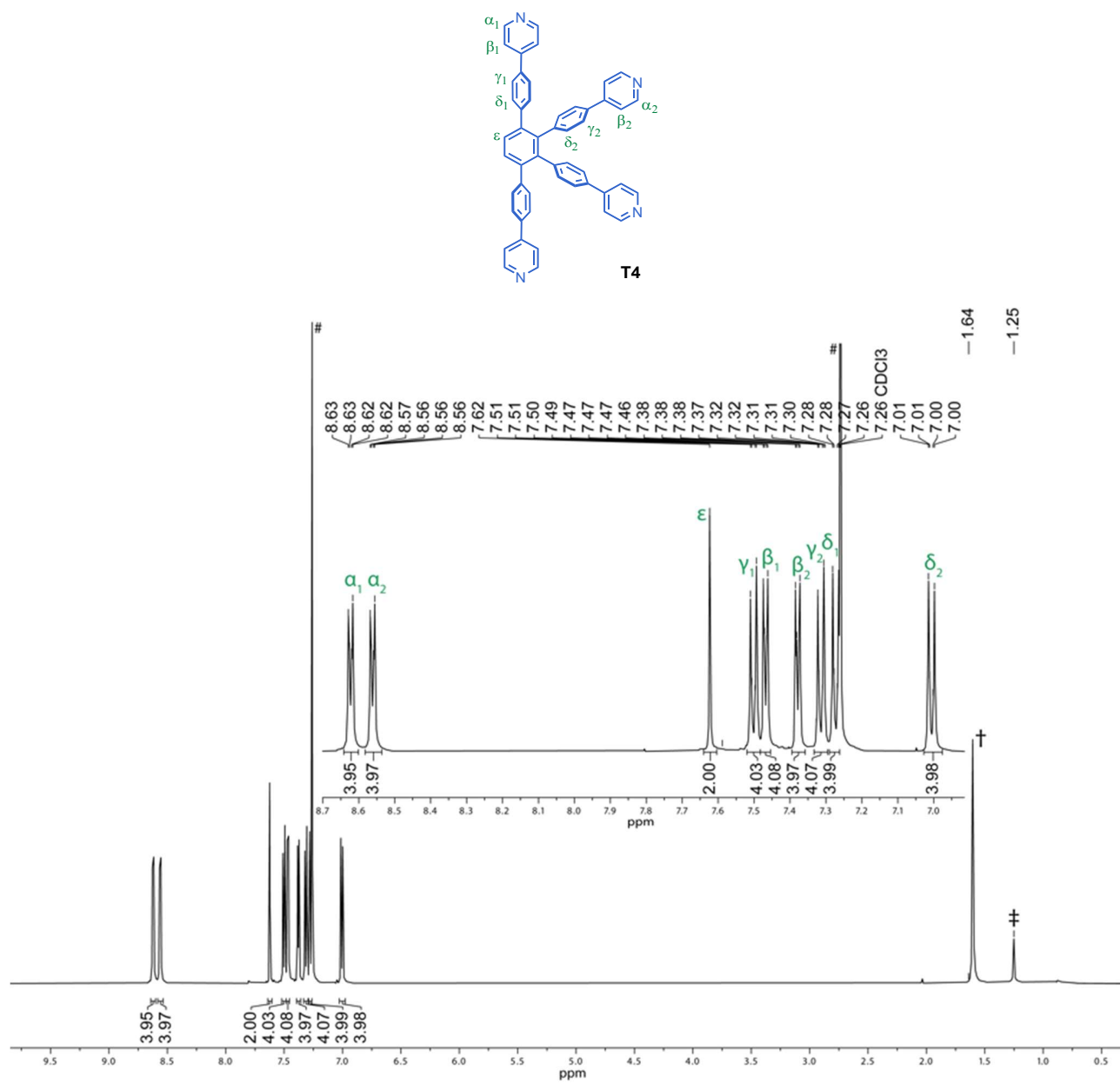
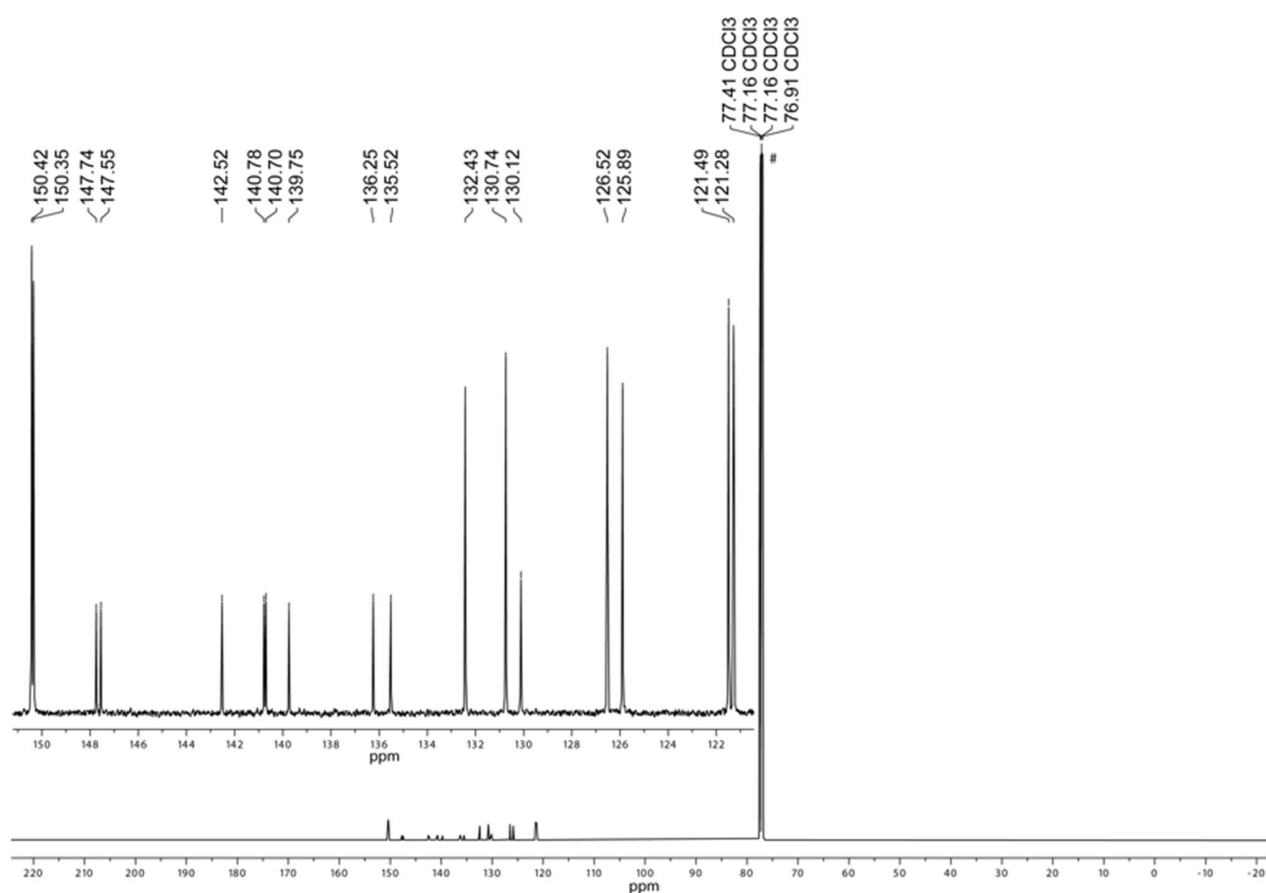


Figure S115. Assigned structure and  $^1\text{H}$  NMR spectrum of **T4** (500 MHz,  $\text{CDCl}_3$ , 298 K). # =  $\text{CHCl}_3$ ; + = water; ‡ = silicon grease.

**Table S23.**  $^1\text{H}$  NMR assignment and correlations for template **T4**.

#	Assign.	$^1\text{H}$	Mult. $J$ (Hz)	$^1\text{H}$ - $^1\text{H}$ COSY	$^1\text{H}$ - $^1\text{H}$ NOESY	$^1\text{H}$ - $^{13}\text{C}$ HSQC	$^1\text{H}$ - $^{13}\text{C}$ HMBC <sup>†</sup>
1	$\alpha_1$	8.64–8.60 (4H)	m	5	5	150.4	121.5, 147.7, 150.4
2	$\alpha_2$	8.58–8.54 (4H)	m	6	6	150.4	121.3, 147.6, 150.4
3	$\epsilon$	7.62 (2H)	s	-	8	130.1	140.7/140.8, 142.5
4	$\gamma_1$	7.50 (4H)	d, $J = 8.4$	8	8	126.5	126.5, 142.5, 147.7
5	$\beta_1$	7.48–7.45 (4H)	m	1	1	121.5	121.5, 136.3, 150.4
6	$\beta_2$	7.39–7.36 (4H)	m	2	2	121.3	121.3, 135.5, 150.4
7	$\gamma_2$	7.31 (4H)	d, $J = 8.4$	9	9	125.9	125.9, 140.7/140.8, 147.6/147.7
8	$\delta_1$	7.27 (4H)	d, $J = 8.4$	4	9, 4, 3	130.7	126.5, 130.7, 136.3, 140.7/140.8
9	$\delta_2$	7.00 (4H)	d, $J = 8.4$	7	7	132.4	125.9, 132.4, 135.5, 139.8

<sup>†</sup>When signals are separated by / this should be interpreted as 'or' since these signals were too close to distinguish.



**Figure S116.**  $^{13}\text{C}$  NMR spectrum of **T4** (500 MHz,  $\text{CDCl}_3$ , 298 K). # =  $\text{CHCl}_3$ .

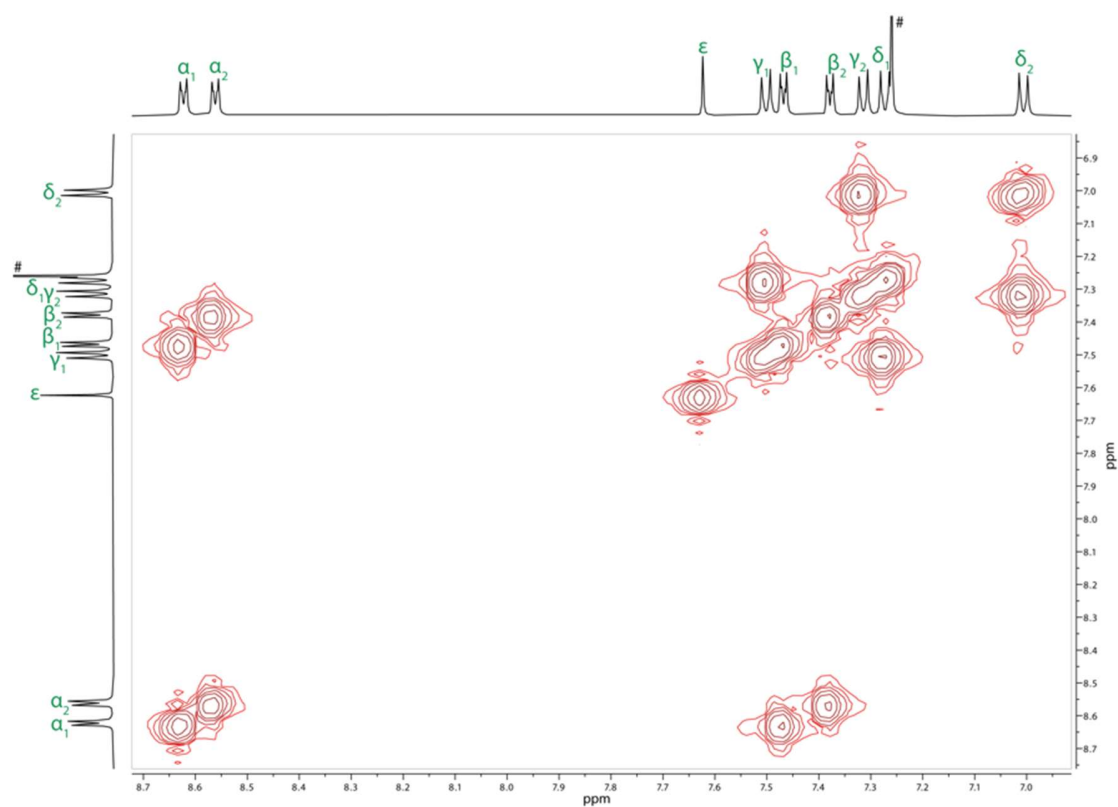


Figure S117.  $^1\text{H}$ - $^1\text{H}$  COSY spectrum of **T4** (500 MHz,  $\text{CDCl}_3$ , 298 K).

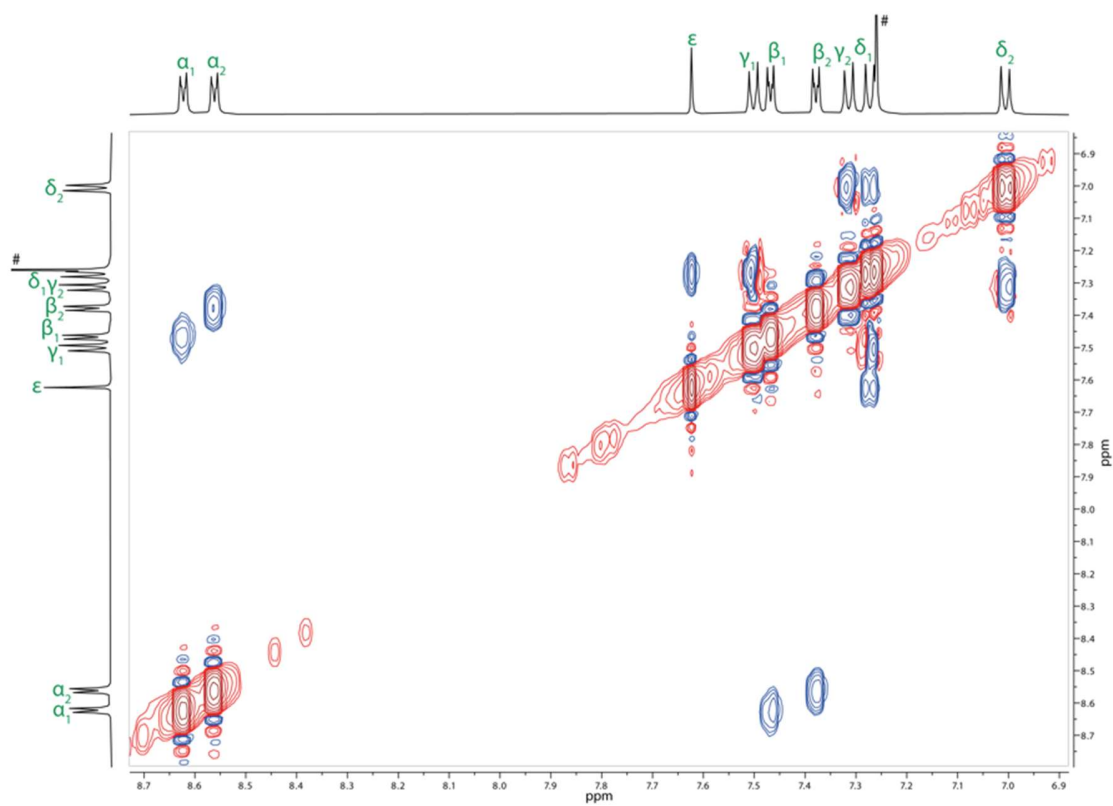
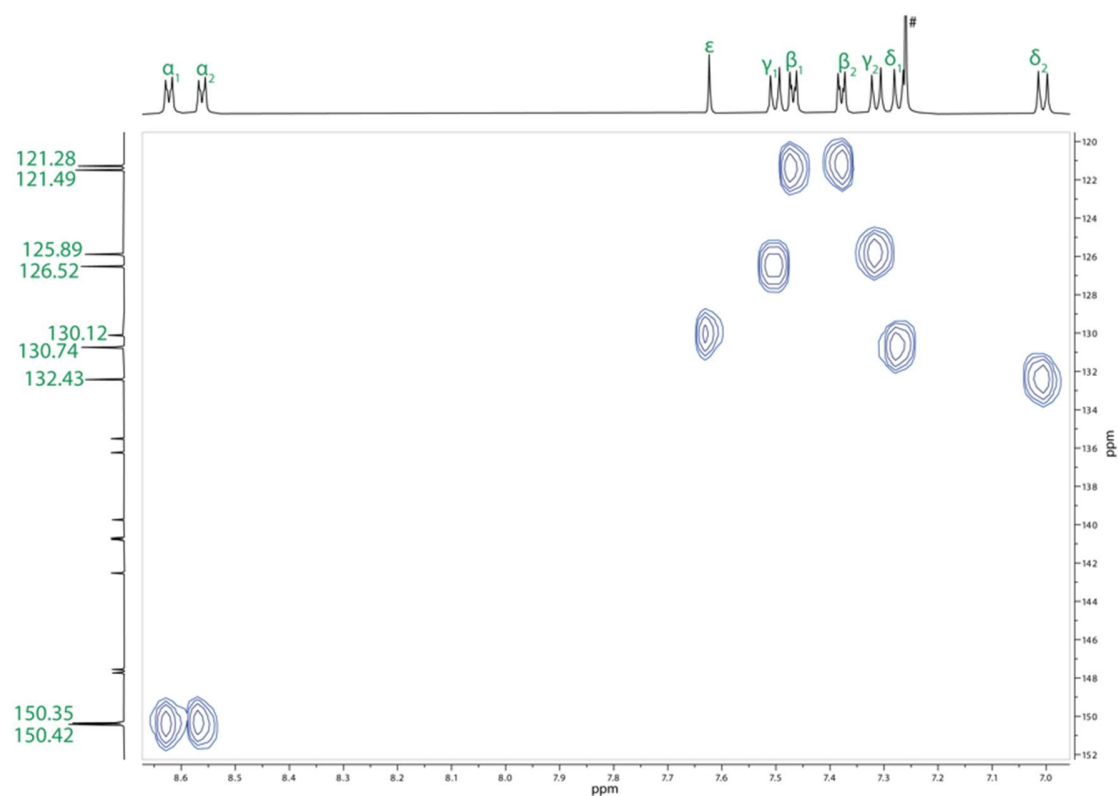
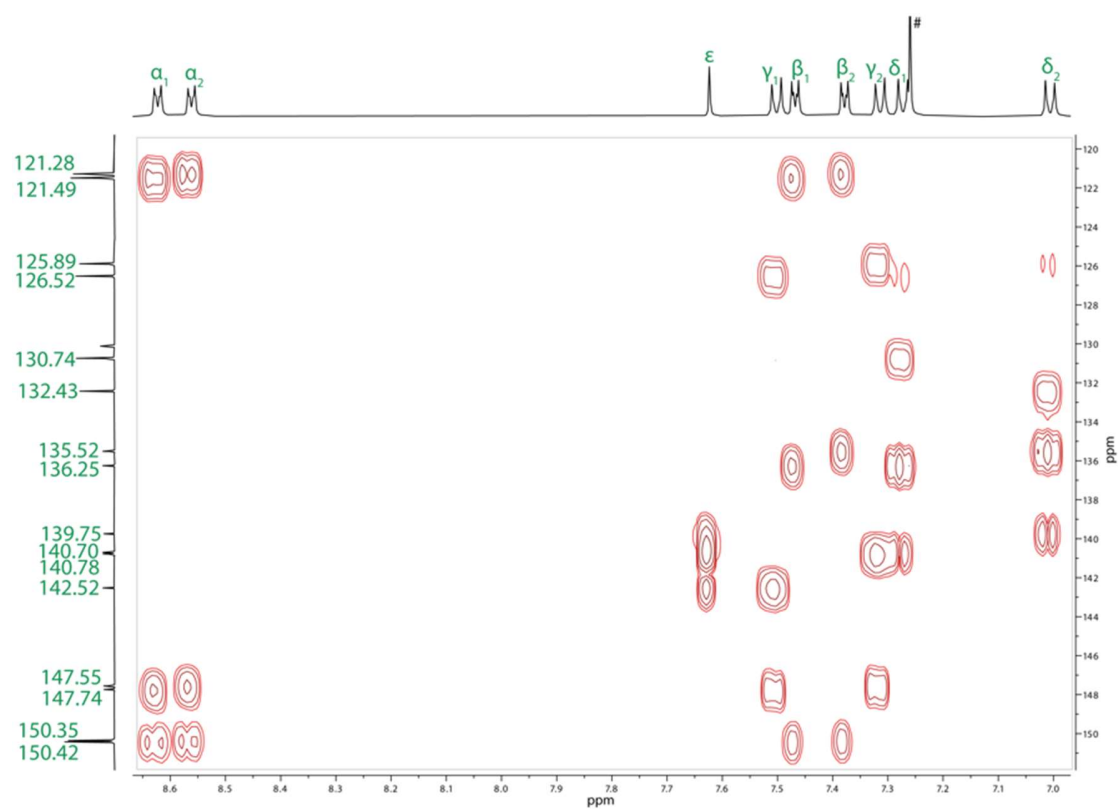


Figure S118.  $^1\text{H}$ - $^1\text{H}$  NOESY spectrum of **T4** (500 MHz,  $\text{CDCl}_3$ , 298 K).



**Figure S119.**  $^1\text{H}$ - $^{13}\text{C}$  HSQC spectrum of **T4** (500 MHz,  $\text{CDCl}_3$ , 298 K).



**Figure S120.**  $^1\text{H}$ - $^{13}\text{C}$  HMBC spectrum of **T4** (500 MHz,  $\text{CDCl}_3$ , 298 K).

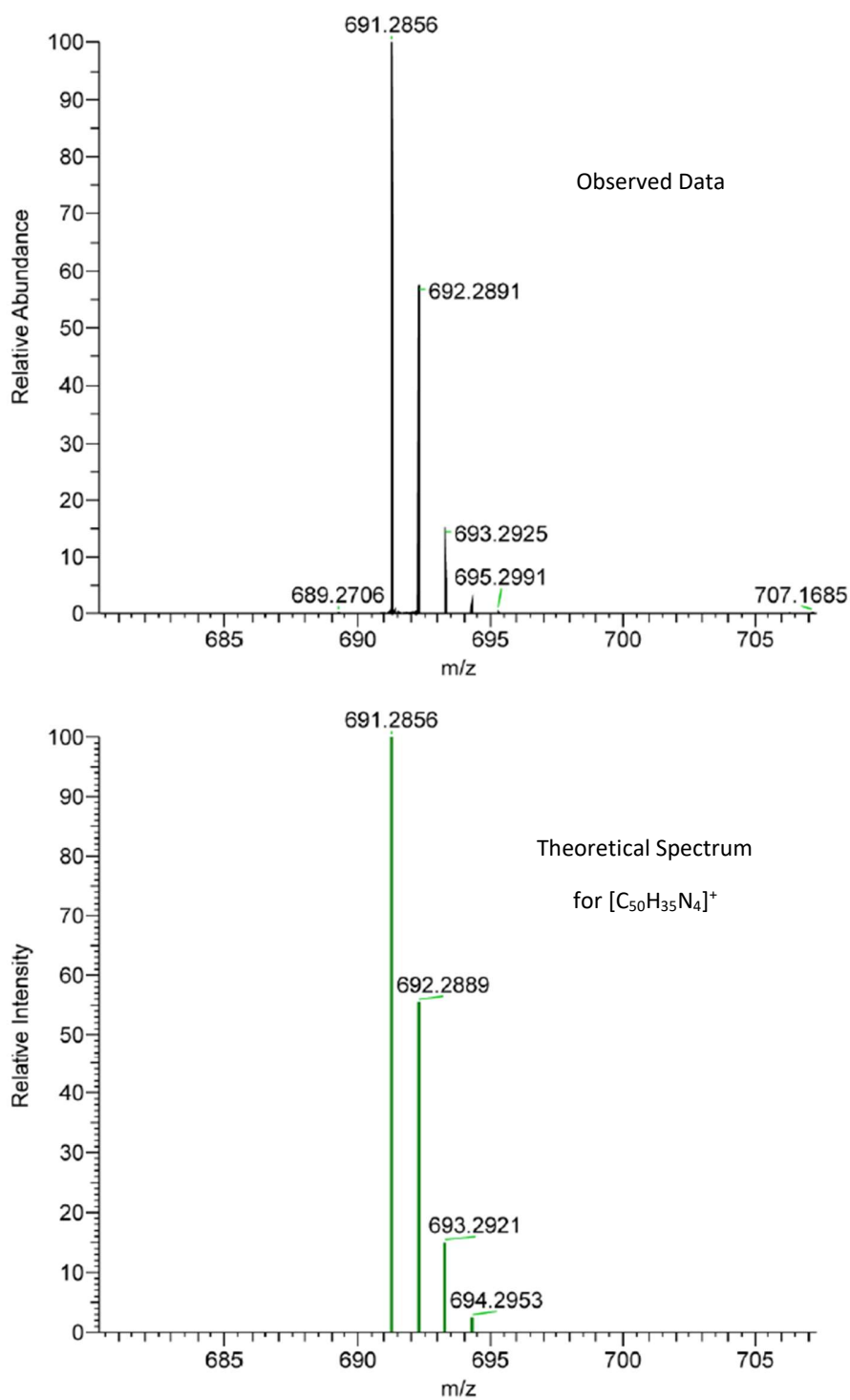


**Figure S121.** Experimental HR-ESI spectrum of **T4** (top) and simulated HR-ESI spectrum of **[T4+H]<sup>+</sup>**  $[C_{50}H_{35}N_4]^+$  (bottom).

Template T4<sub>1,4F</sub>:

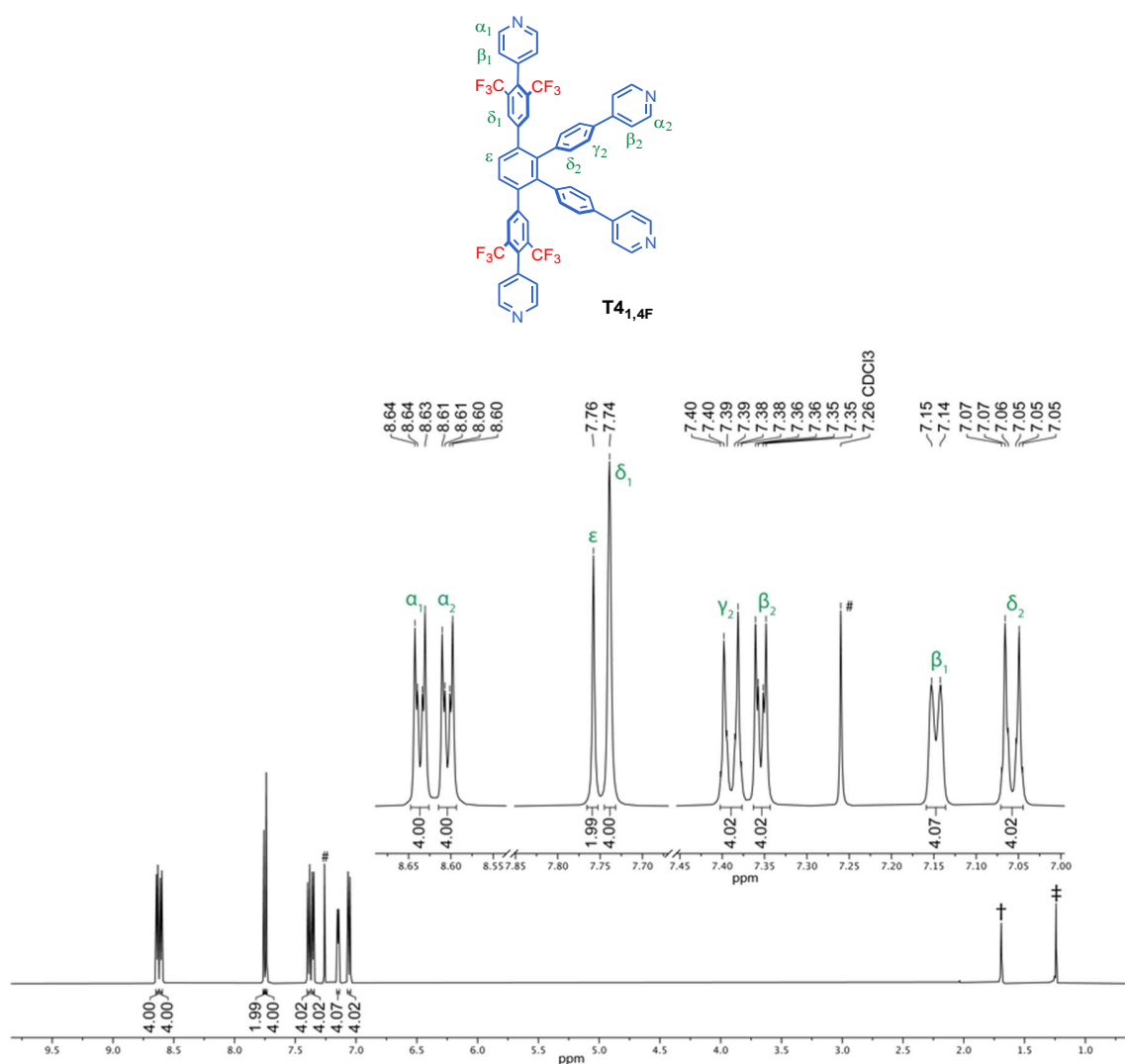


**Figure S122.** Assigned structure and <sup>1</sup>H NMR spectrum of T4<sub>1,4F</sub> (500 MHz, CDCl<sub>3</sub>, 298 K). # = CHCl<sub>3</sub>; † = water; ‡ = silicon grease.

**Table S24.** <sup>1</sup>H NMR assignment and correlations for template T4<sub>1,4F</sub>.

#	Assign.	<sup>1</sup> H	Mult. <i>J</i> (Hz)	<sup>1</sup> H- <sup>1</sup> H COSY	<sup>1</sup> H- <sup>1</sup> H NOESY	<sup>1</sup> H- <sup>19</sup> F HOESY <sup>†</sup>	<sup>1</sup> H- <sup>13</sup> C HSQC	<sup>1</sup> H- <sup>13</sup> C HMBC <sup>‡</sup>
1	α <sub>1</sub>	8.66–8.62 (4H)	m	7	7	w	148.9	148.9, 142.3, 124.9,
2	α <sub>2</sub>	8.62–8.59 (4H)	m	6	6	-	150.5	150.5, 147.5, 121.5
3	ε <sub>1</sub>	7.76 (2H)	s	-	-	(vw)	130.1	141.9, 139.2/139.1
4	δ <sub>1</sub>	7.74 (4H)	s	-	8	s	130.6	139.2/139.1, 135.3, 130.62/130.59, 122.9
5	γ <sub>2</sub>	7.39 (4H)	d <i>J</i> = 8.2	8	8	vw	126.6	147.5, 139.1, 126.6
6	β <sub>2</sub>	7.37–7.34 (4H)	m	2	2	vw	121.5	150.5, 137.3, 121.5
7	β <sub>1</sub>	7.15 (4H)	br d <i>J</i> = 5.4	1	1	m	124.9	148.9, 135.3, 124.9
8	δ <sub>2</sub>	7.06 (4H)	d <i>J</i> = 8.2	5	4, 5	vw	132.1	140.7, 137.3, 132.1

<sup>†</sup>Relative correlation intensities are classified as: s = strong, m = medium, w = weak, vw = very weak. <sup>‡</sup>When signals are separated by / this should be interpreted as 'or' since these signals were too close to distinguish.

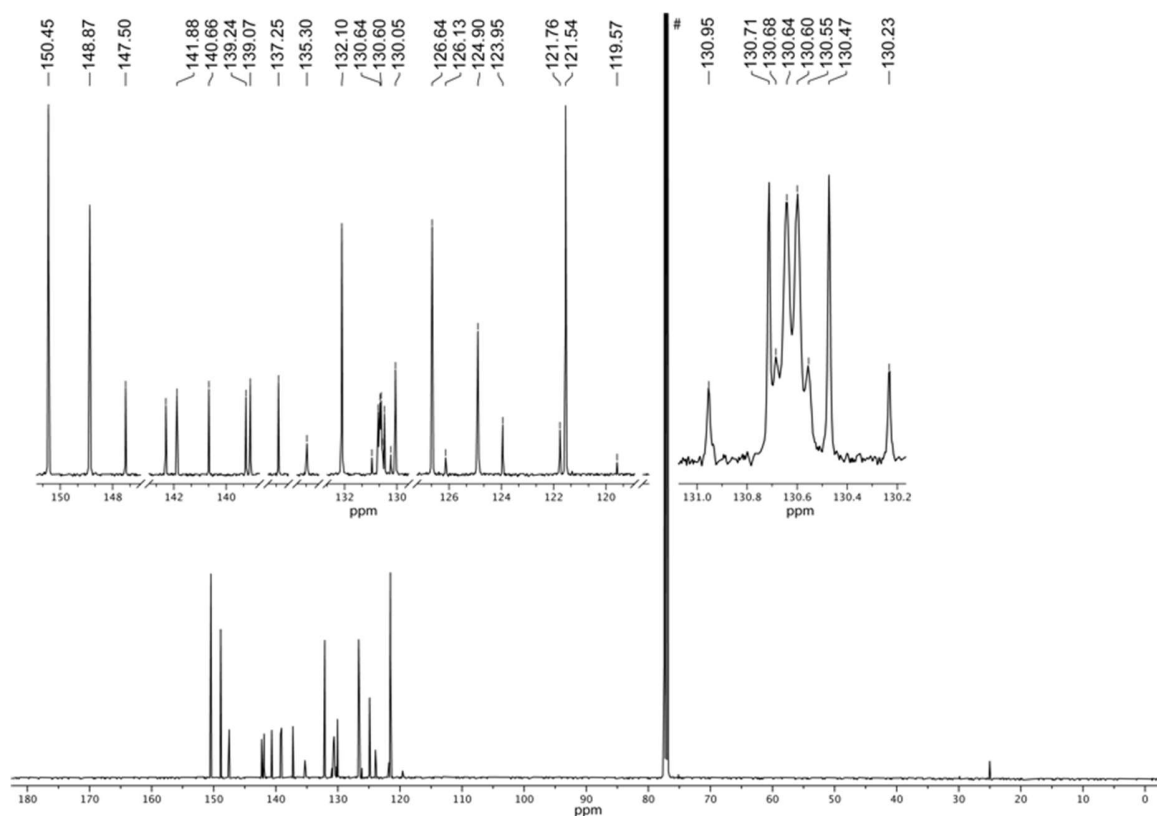


Figure S123.  $^{13}\text{C}$  NMR spectrum of **T4<sub>1,4F</sub>** (500 MHz,  $\text{CDCl}_3$ , 298 K). # =  $\text{CHCl}_3$ .

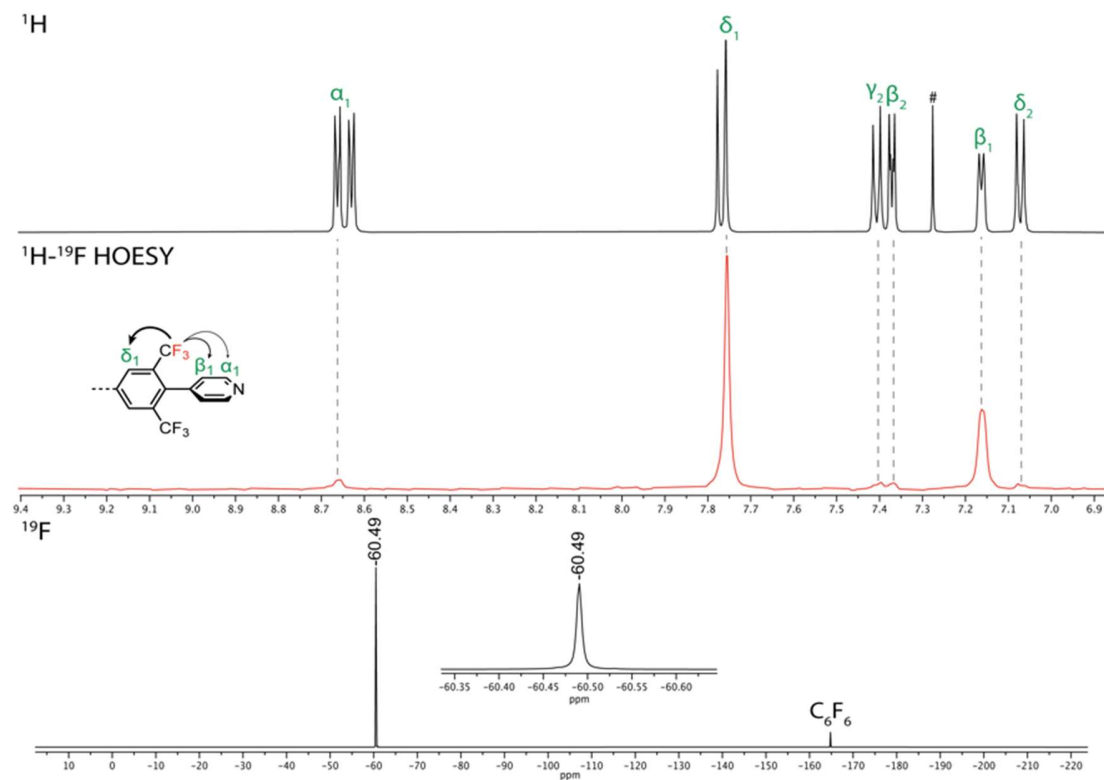


Figure S124. Combined  $^1\text{H}$  (top), 1D  $^1\text{H}$ - $^{19}\text{F}$  HOESY (middle, red), and  $^{19}\text{F}$  (bottom) spectra of **T4<sub>1,4F</sub>** (500 MHz,  $\text{CDCl}_3$ , 298 K).



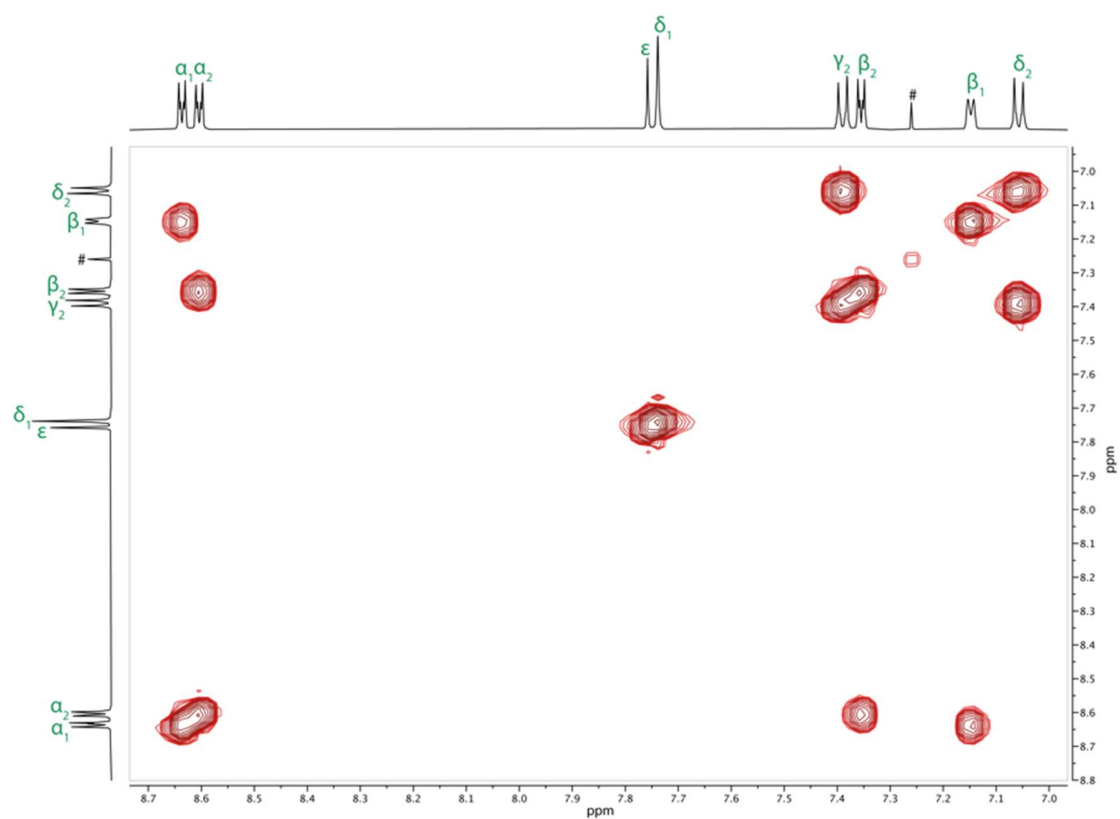


Figure S125.  $^1\text{H}$ - $^1\text{H}$  COSY spectrum of **T4<sub>1,4F</sub>** (500 MHz,  $\text{CDCl}_3$ , 298 K).

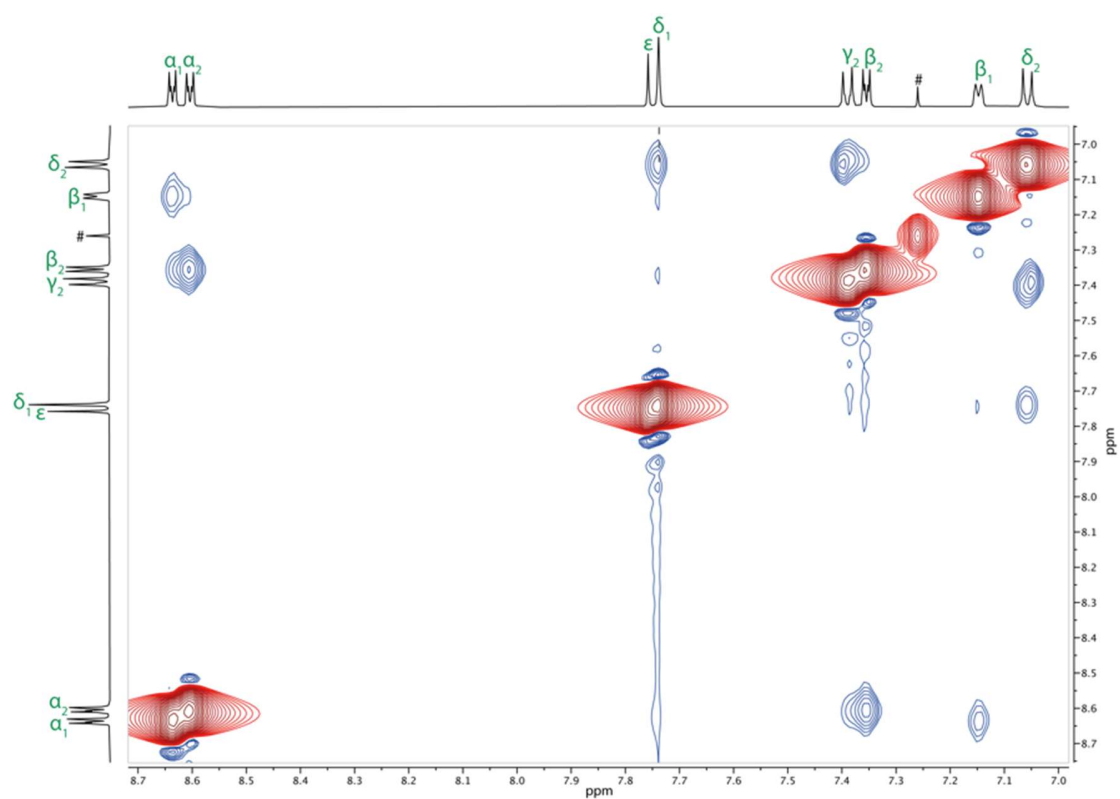


Figure S126.  $^1\text{H}$ - $^1\text{H}$  NOESY spectrum of **T4<sub>1,4F</sub>** (500 MHz,  $\text{CDCl}_3$ , 298 K).

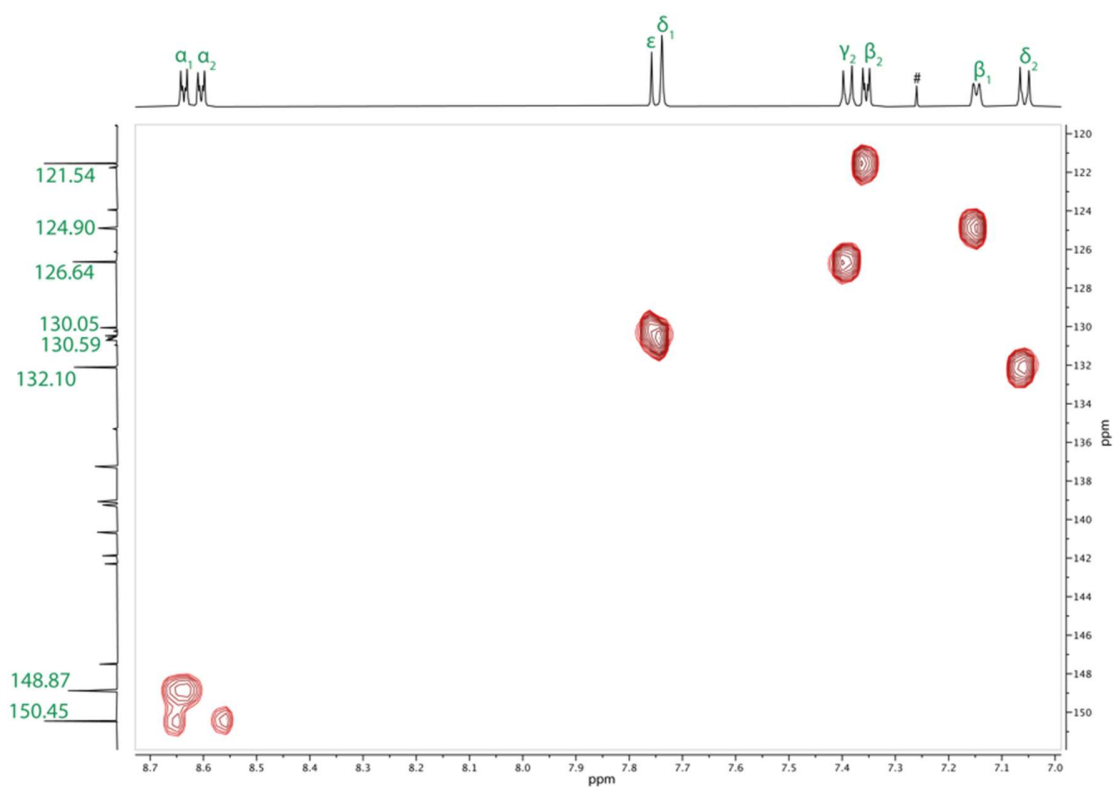


Figure S127.  $^1\text{H}$ - $^{13}\text{C}$  HSQC spectrum of **T4<sub>1,4F</sub>** (500 MHz,  $\text{CDCl}_3$ , 298 K).

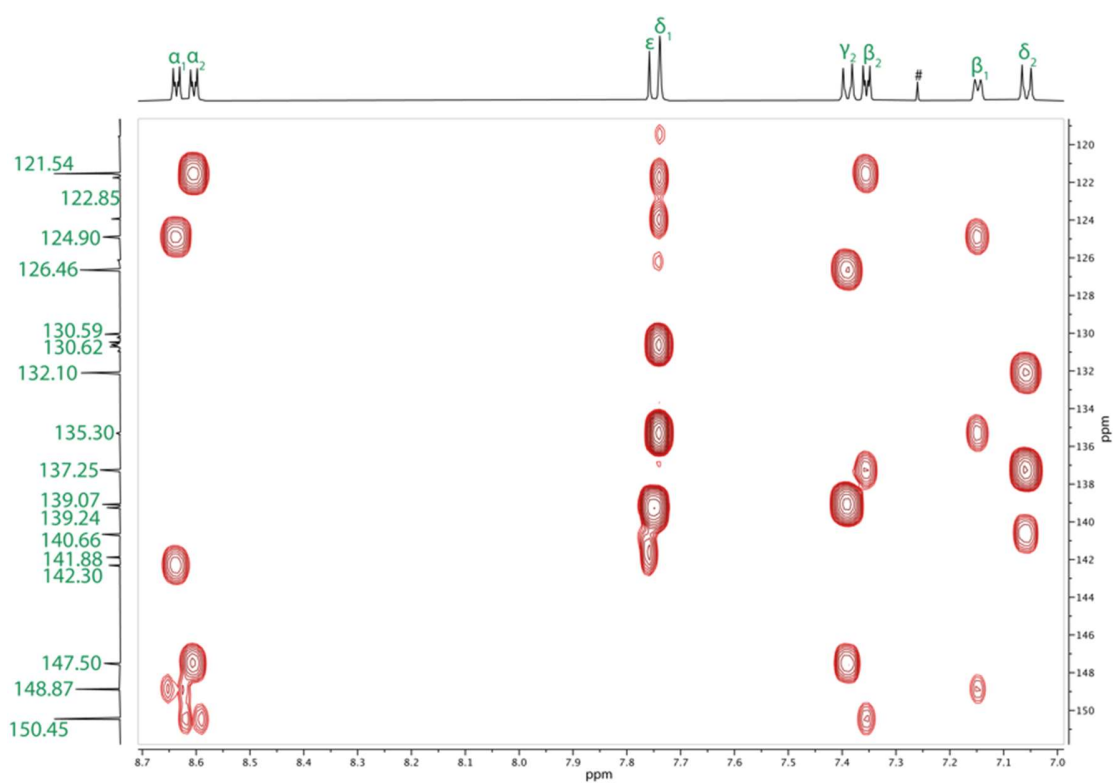
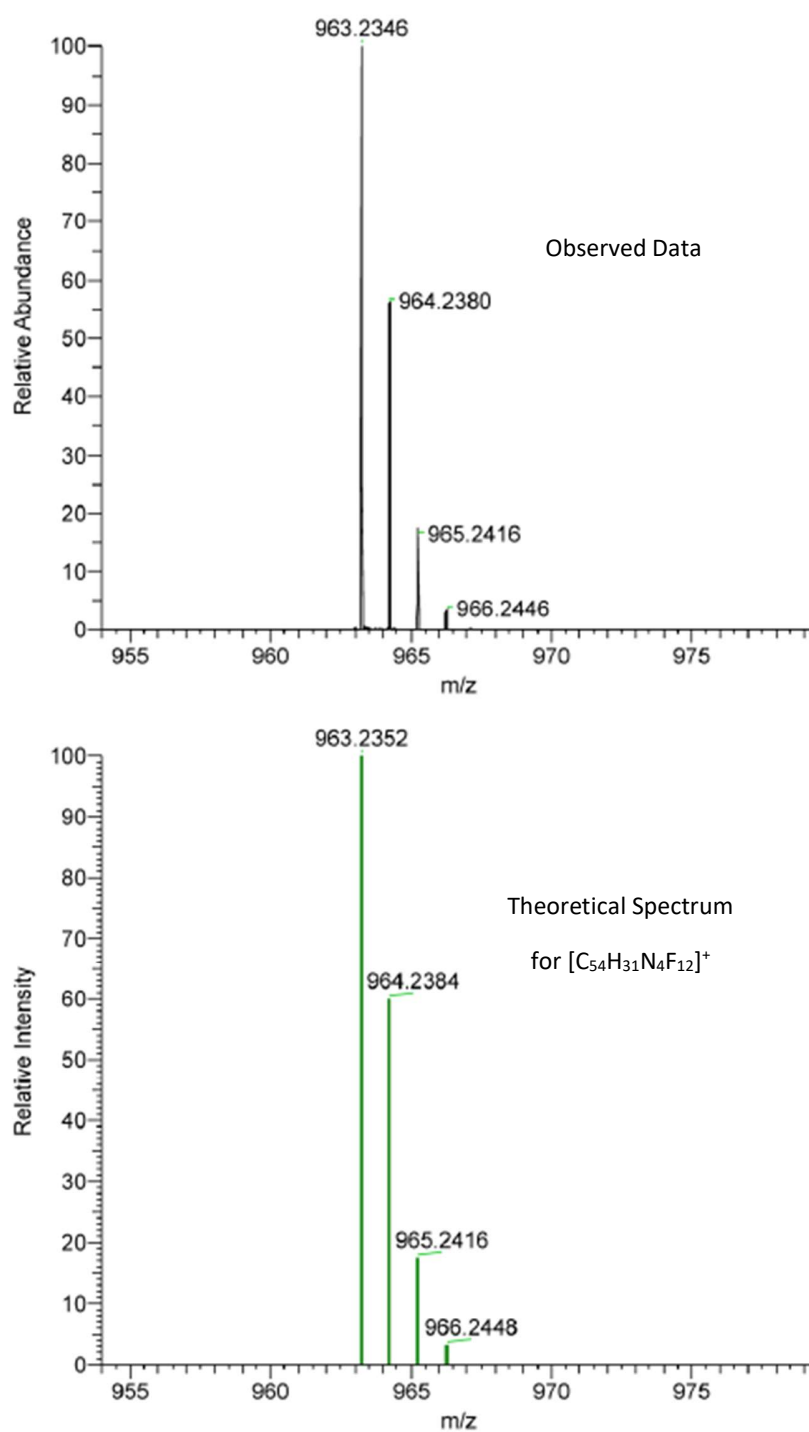


Figure S128.  $^1\text{H}$ - $^{13}\text{C}$  HMBC spectrum of **T4<sub>1,4F</sub>** (500 MHz,  $\text{CDCl}_3$ , 298 K).



**Figure S129.** Experimental HR-ESI spectrum of **T4<sub>1,4F</sub>** (top) and simulated HR-ESI spectrum of **[T4<sub>1,4F</sub>+H]<sup>+</sup>** [C<sub>54</sub>H<sub>31</sub>N<sub>4</sub>F<sub>12</sub>]<sup>+</sup> (bottom).

Template T4<sub>2,3F</sub>:

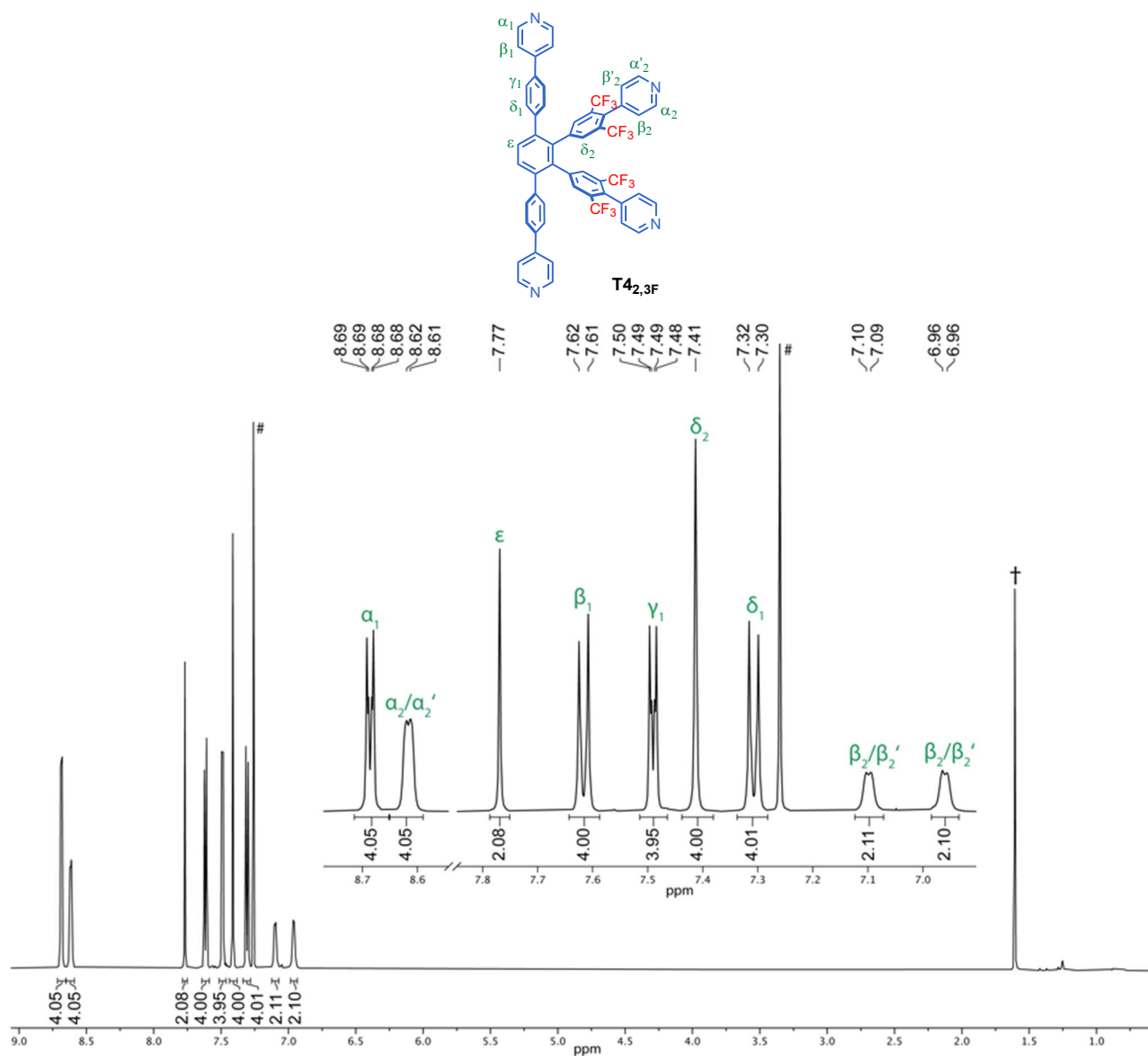
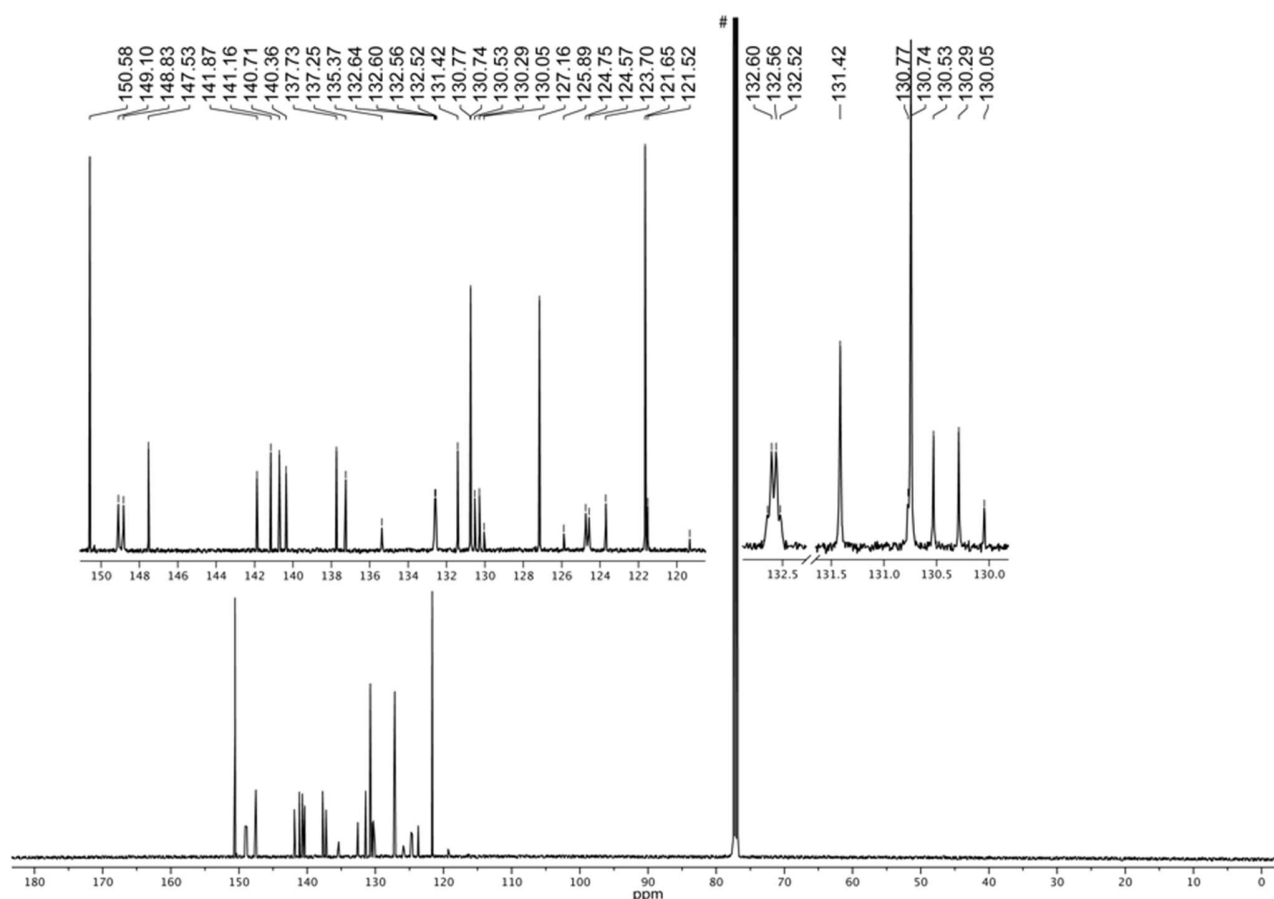


Figure S130. Assigned structure and <sup>1</sup>H NMR spectrum of T4<sub>2,3F</sub> (500 MHz, CDCl<sub>3</sub>, 298 K). # = CHCl<sub>3</sub>; † = water.

**Table S25.**  $^1\text{H}$  NMR assignment and correlations for template **T4<sub>2,3F</sub>**.

#	Assign.	$^1\text{H}$	Mult. $J$ (Hz)	$^1\text{H}$ - $^1\text{H}$ COSY	$^1\text{H}$ - $^1\text{H}$ NOESY	$^1\text{H}$ - $^{19}\text{F}$ HOESY <sup>†</sup>	$^1\text{H}$ - $^{13}\text{C}$ HSQC	$^1\text{H}$ - $^{13}\text{C}$ HMBC <sup>‡</sup>
1	$\alpha_1$	8.71–8.65 (4H)	m	5	5	-	150.6	150.6, 147.5, 121.7
2	$\alpha_2/\alpha_2'$	8.62 (4H)	br d $J = 3.8$	8, 9	8, 9	w	149.1/148.8	149.1/148.8, 141.9, 124.8, 124.6
3	$\epsilon_1$	7.77 (2H)	s	-	7	-	131.4	141.2, 137.3
4	$\gamma_1$	7.62 (4H)	d $J = 8.3$	7	5, 7	-	127.2	147.5, 140.7, 127.2, 130.7
5	$\beta_1$	7.51–7.46 (4H)	m	1	1, 4	-	121.7	150.6, 137.7, 121.7
6	$\delta_2$	7.41 (4H)	s	-	-	s	132.6	141.9, 140.4, 137.3, 135.4, 132.6, 130.4, 122.6
7	$\delta_1$	7.31 (4H)	d $J = 8.3$	4	3, 4	vw	130.7	141.2, 137.7, 130.7, 127.2
8	$\beta_2/\beta_2'$	7.10 (2H)	br d $J = 3.8$	2	2	m	124.8	135.4, 124.6
9	$\beta_2/\beta_2'$	6.96 (2H)	br d $J = 3.8$	2	2	m	124.6	135.4, 124.8

<sup>†</sup>Relative correlation intensities are classified as: s = strong, m = medium, w = weak, vw = very weak. <sup>‡</sup>When signals are separated by / this should be interpreted as 'or' since these signals were too close to distinguish.



**Figure S131.**  $^{13}\text{C}$  NMR spectrum of **T4<sub>2,3F</sub>** (500 MHz,  $\text{CDCl}_3$ , 298 K). # =  $\text{CHCl}_3$ .

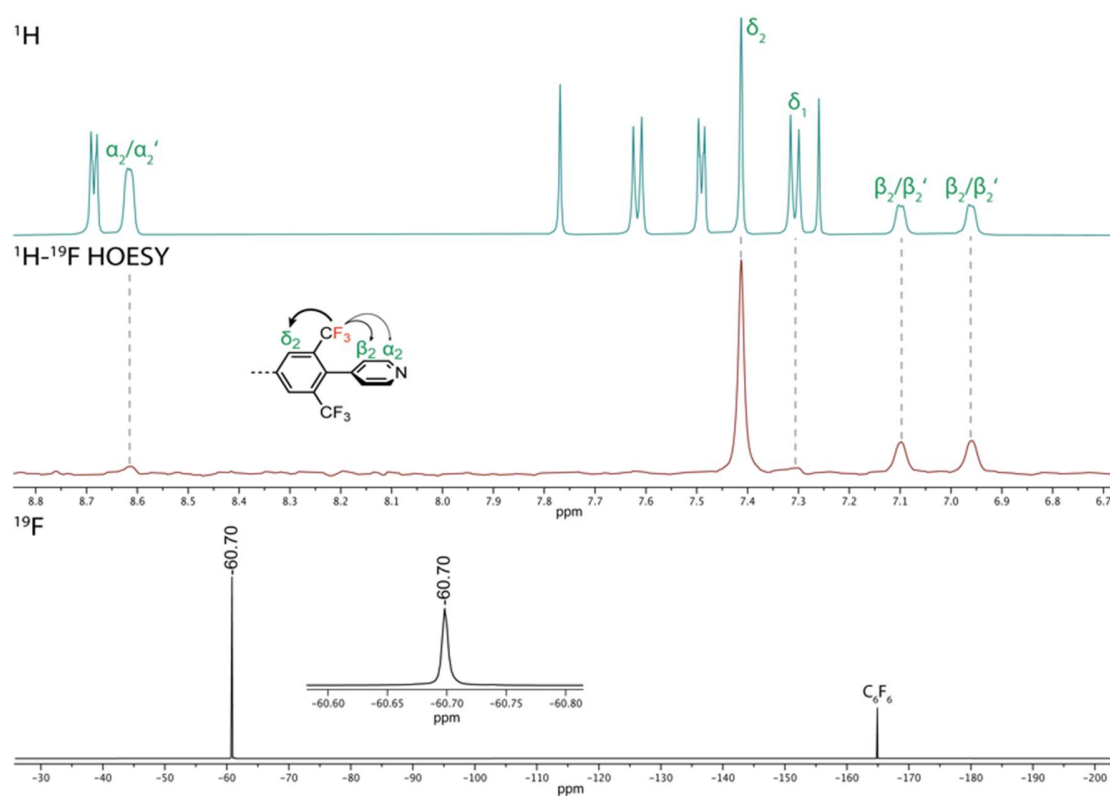


**Figure S132.** Combined <sup>1</sup>H (top), 1D <sup>1</sup>H-<sup>19</sup>F HOESY (middle, red), and <sup>19</sup>F (bottom) spectra of **T4<sub>2,3F</sub>** (500 MHz, CDCl<sub>3</sub>, 298 K).

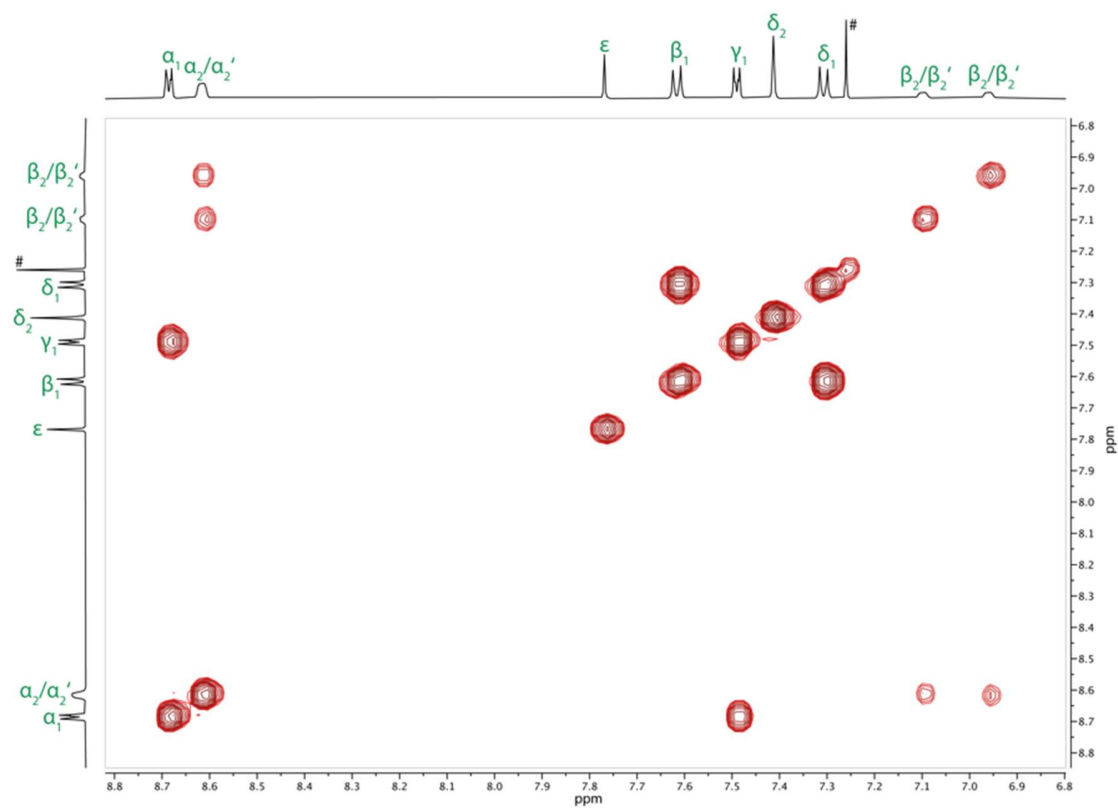


**Figure S133.** <sup>1</sup>H-<sup>1</sup>H COSY spectrum of **T4<sub>2,3F</sub>** (500 MHz, CDCl<sub>3</sub>, 298 K).

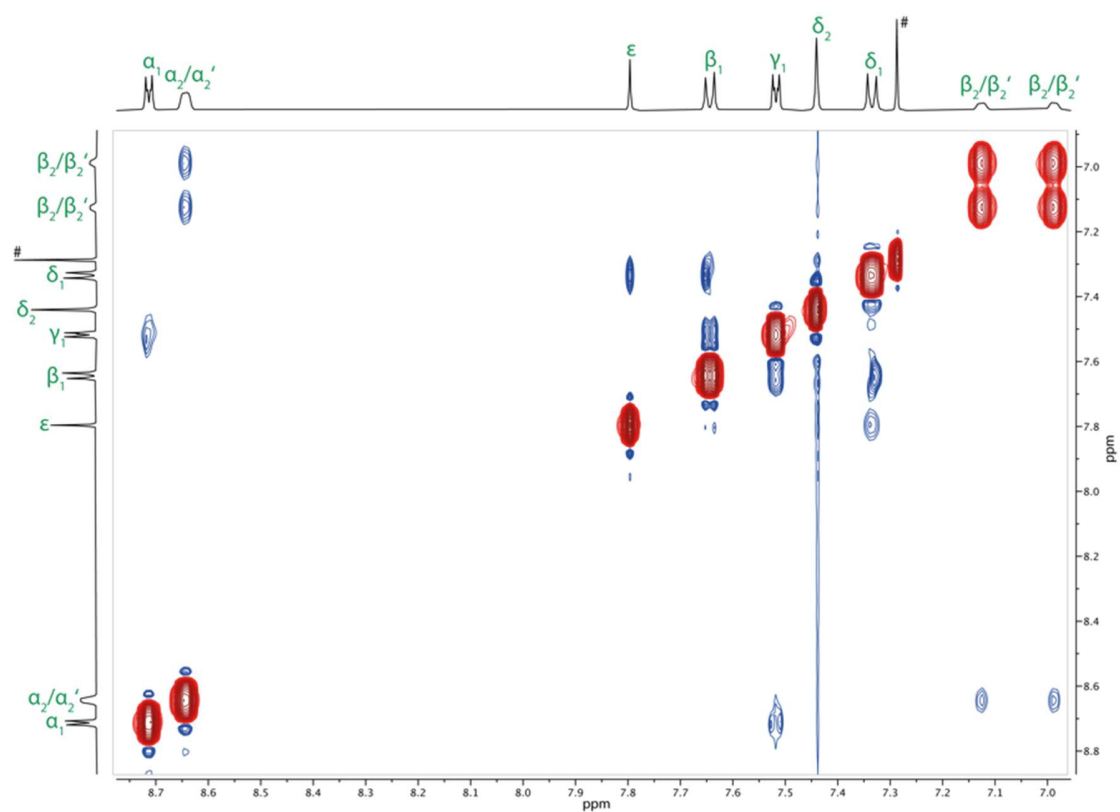


Figure S134.  $^1\text{H}$ - $^1\text{H}$  NOESY spectrum of  $\text{T4}_{2,3\text{F}}$  (500 MHz,  $\text{CDCl}_3$ , 298 K).

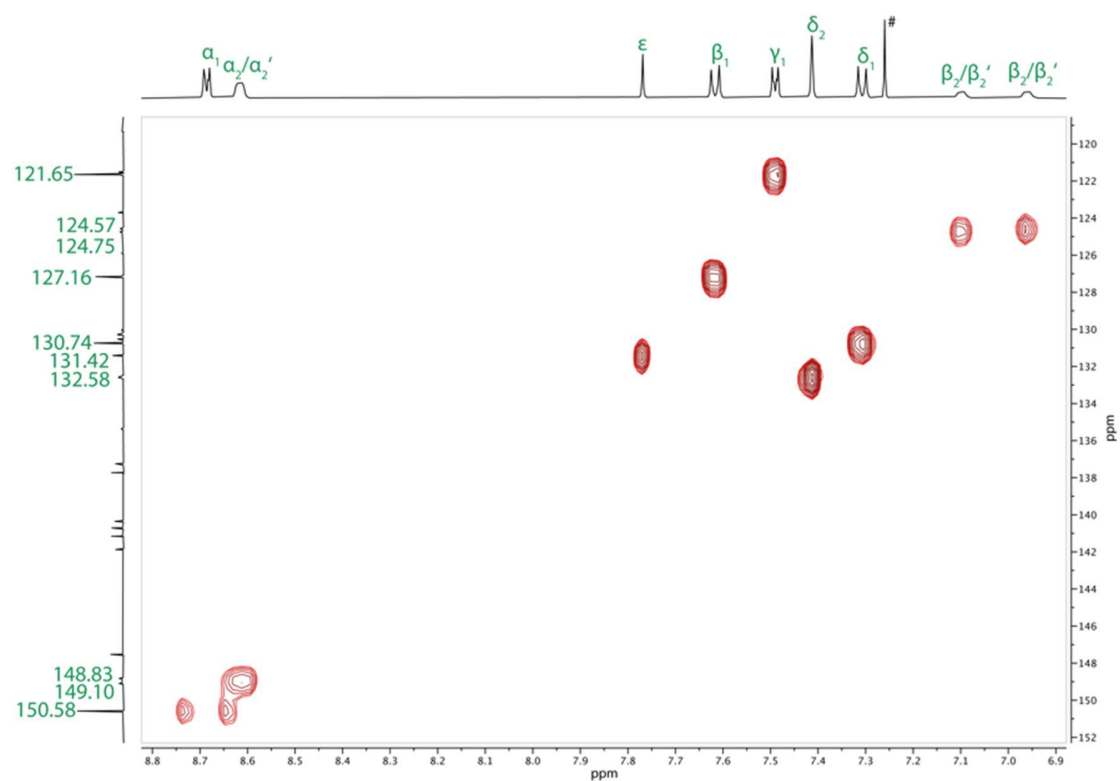
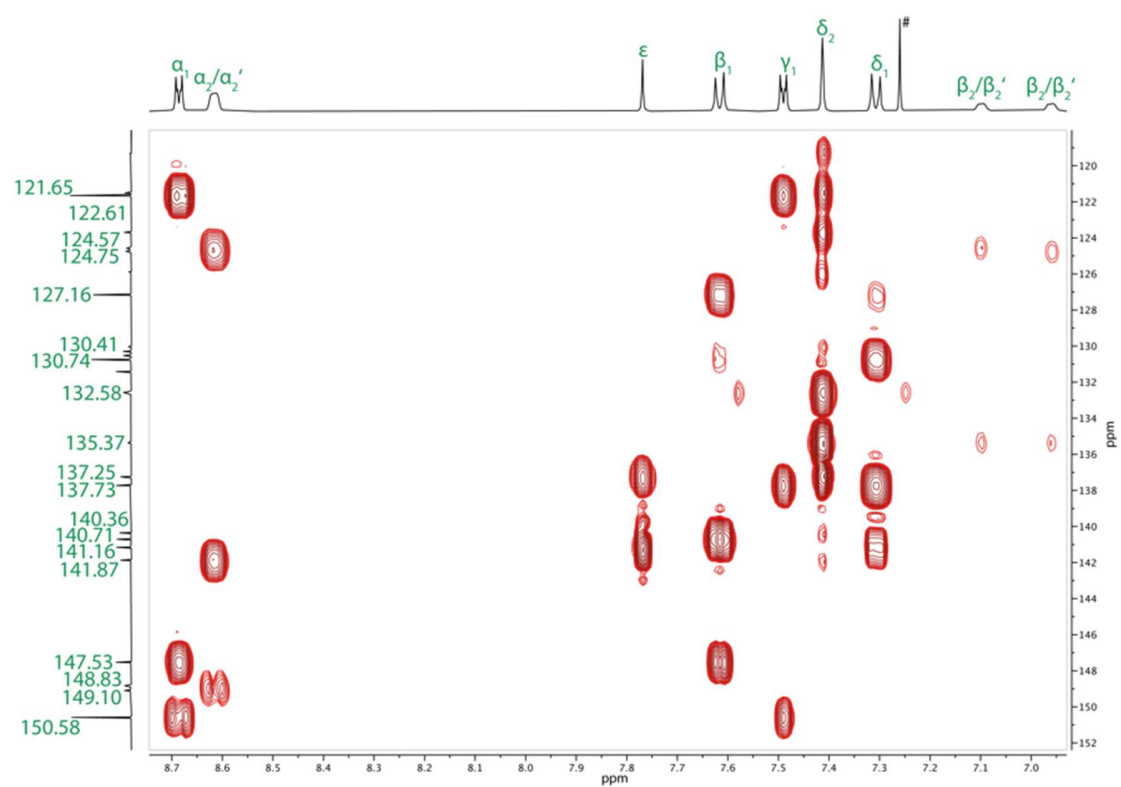
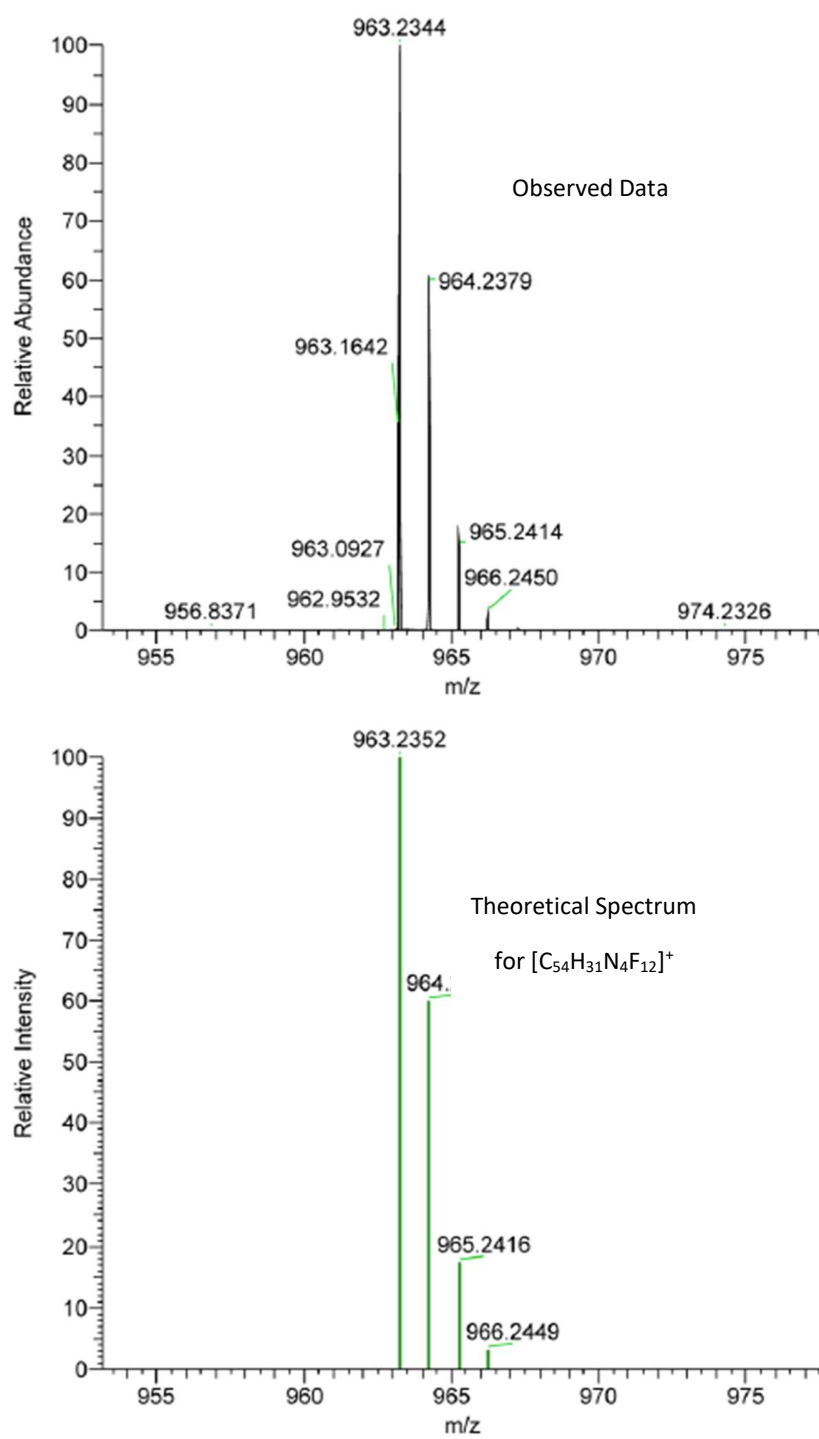


Figure S135.  $^1\text{H}$ - $^{13}\text{C}$  HSQC spectrum of  $\text{T4}_{2,3\text{F}}$  (500 MHz,  $\text{CDCl}_3$ , 298 K).





**Figure S136.**  $^1\text{H}$ - $^{13}\text{C}$  HMBC spectrum of **T4<sub>2,3F</sub>** (500 MHz,  $\text{CDCl}_3$ , 298 K).



**Figure S137.** Experimental HR-ESI spectrum of **T**<sub>4,3F</sub> (top) and simulated HR-ESI spectrum of [**T**<sub>4,3F</sub>+H]<sup>+</sup> [ $C_{54}H_{31}N_4F_{12}$ ]<sup>+</sup> (bottom).

## 16. NMR Spectra of Oxidation States

**c-P8[b<sub>6</sub>f<sub>2</sub>]•(T4)<sub>2</sub>:**

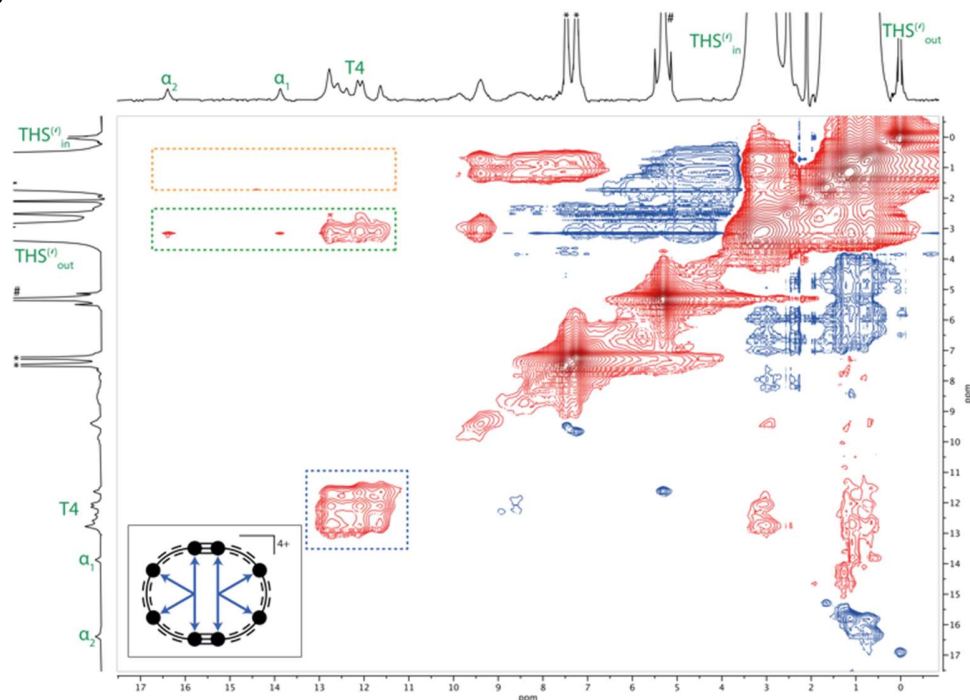


**Figure S138.** <sup>1</sup>H-<sup>1</sup>H NOESY spectrum of **c-P8[b<sub>6</sub>f<sub>2</sub>]•(T4)<sub>2</sub><sup>4+</sup>** (500 MHz, CD<sub>2</sub>Cl<sub>2</sub>, 223 K). Key correlations are highlighted with dashed boxes: NOE signals within the template region (blue); selective correlation between the template resonances and THS<sup>(II)</sup><sub>in</sub> (green); absence of a correlation between the template and THS<sup>(II)</sup><sub>out</sub> (orange). Peaks assigned with # and \* arise from CH<sub>2</sub>Cl<sub>2</sub> and neutral thianthrene, respectively.

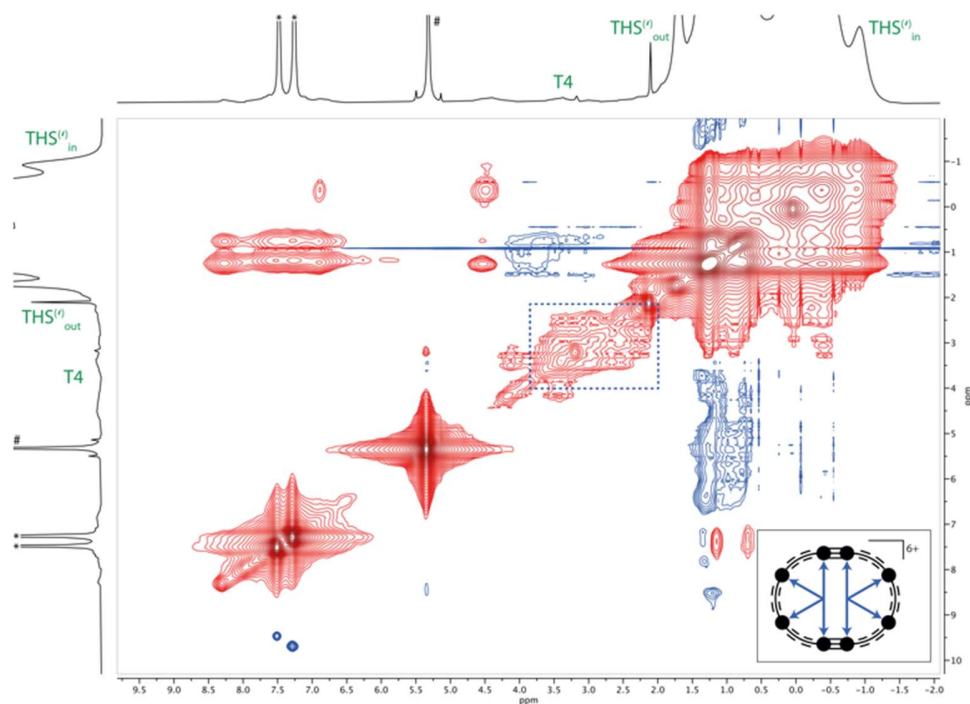


**Figure S139.** <sup>1</sup>H-<sup>1</sup>H NOESY spectrum of **c-P8[b<sub>6</sub>f<sub>2</sub>]•(T4)<sub>2</sub><sup>6+</sup>** (500 MHz, CD<sub>2</sub>Cl<sub>2</sub>, 223 K). Correlations within the template region are highlighted with a dashed box (blue). Peaks assigned with # and \* arise from CH<sub>2</sub>Cl<sub>2</sub> and neutral thianthrene, respectively.

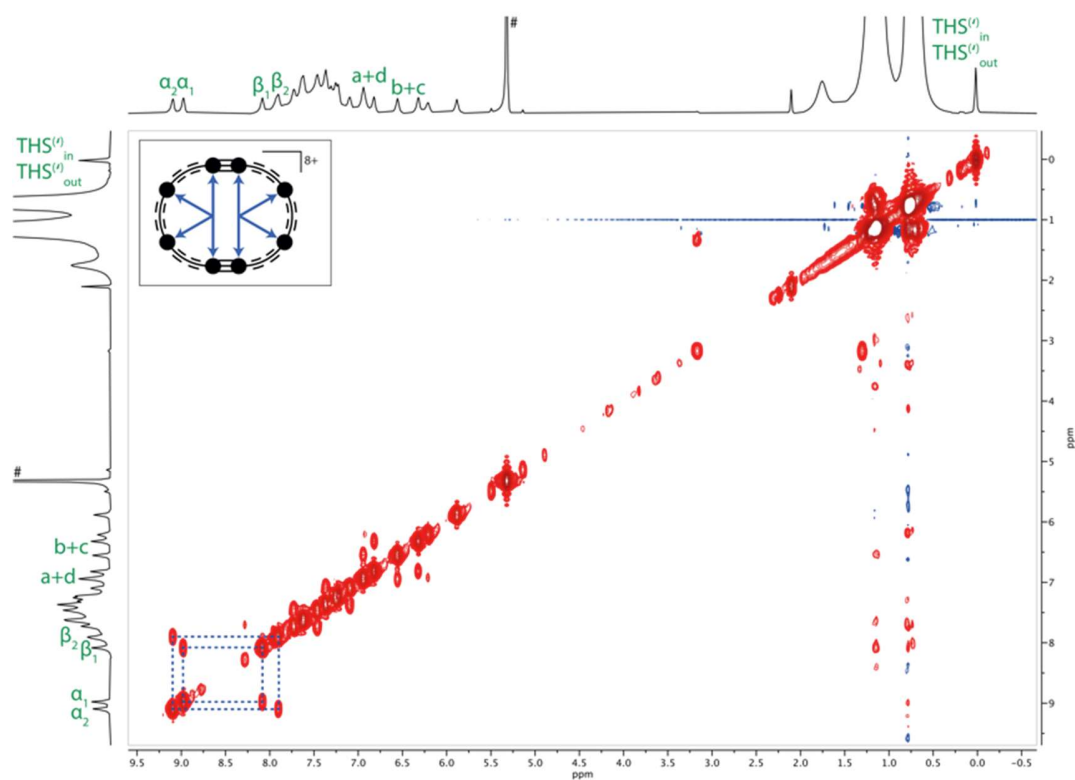


**Figure S140.**  $^1\text{H}$ - $^1\text{H}$  COSY spectrum of  $c\text{-P8}[\text{b}_6\text{f}_2]\bullet(\text{T4})_2^{8+}$  (500 MHz,  $\text{CD}_2\text{Cl}_2$ , 223 K). Correlations between  $\alpha$  and  $\beta$  resonances are highlighted in blue. Peaks assigned with # arise from  $\text{CHDCl}_2$ .

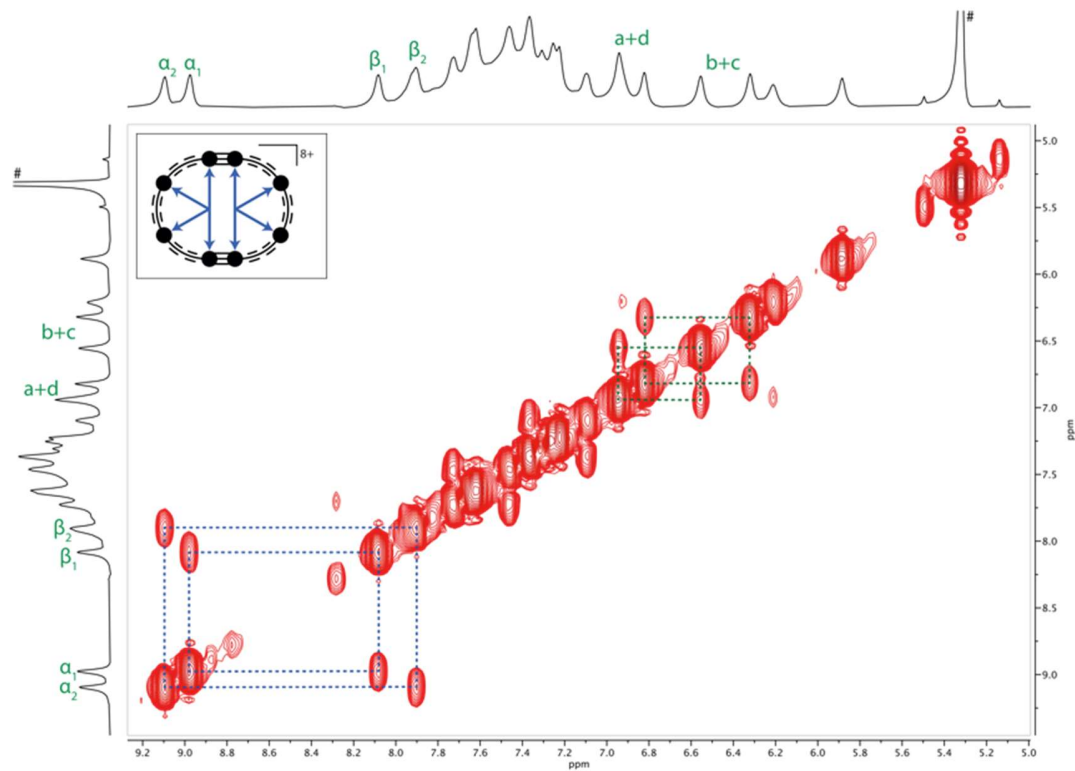


**Figure S141.** Enlarged region of the COSY spectrum of  $c\text{-P8}[\text{b}_6\text{f}_2]\bullet(\text{T4})_2^{8+}$  (500 MHz,  $\text{CD}_2\text{Cl}_2$ , 223 K). Correlations between  $\alpha$  and  $\beta$  resonances are highlighted in blue; those between  $\beta$  porphyrin resonances in green. Peaks assigned with # arise from  $\text{CHDCl}_2$ .

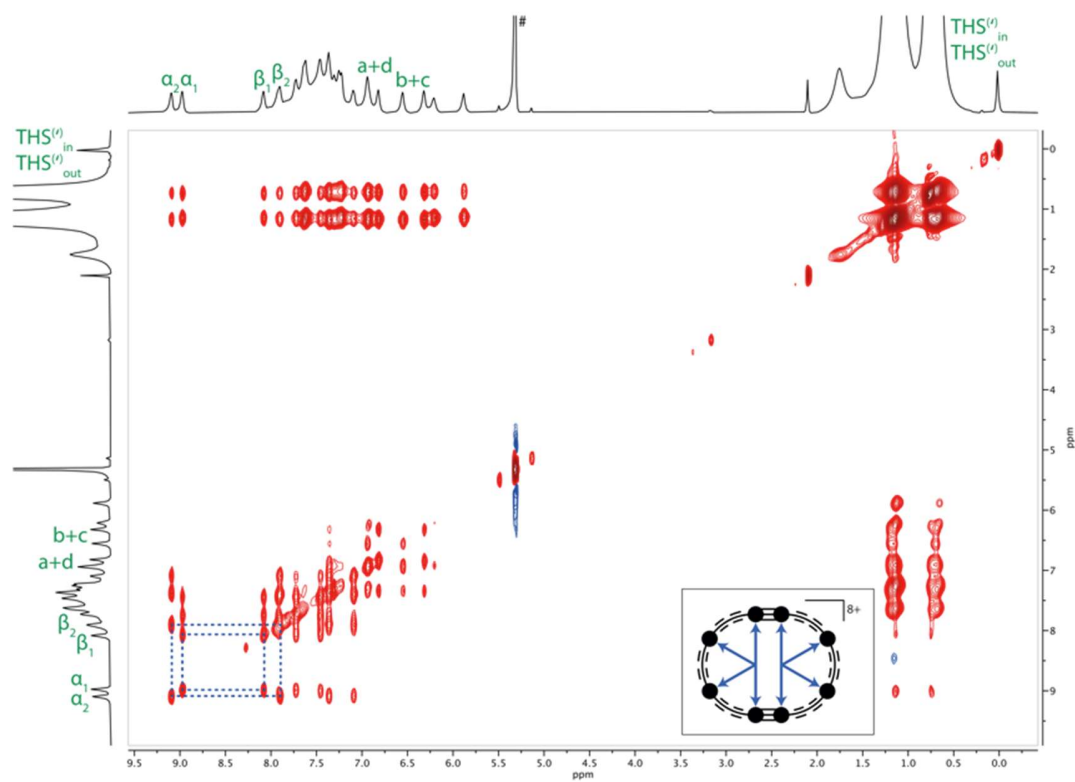


**Figure S142.**  $^1\text{H}$ - $^1\text{H}$  NOESY spectrum of  $c\text{-P8}[\text{b}_6\text{f}_2]\bullet(\text{T4})_2^{8+}$  (500 MHz,  $\text{CD}_2\text{Cl}_2$ , 223 K). Correlations between  $\alpha$  and  $\beta$  resonances are highlighted in blue. Peaks assigned with # arise from  $\text{CHDCl}_2$ .

**c-P8[b<sub>6</sub>f<sub>2</sub>]•(T4<sub>1,4F</sub>)<sub>2</sub>:**

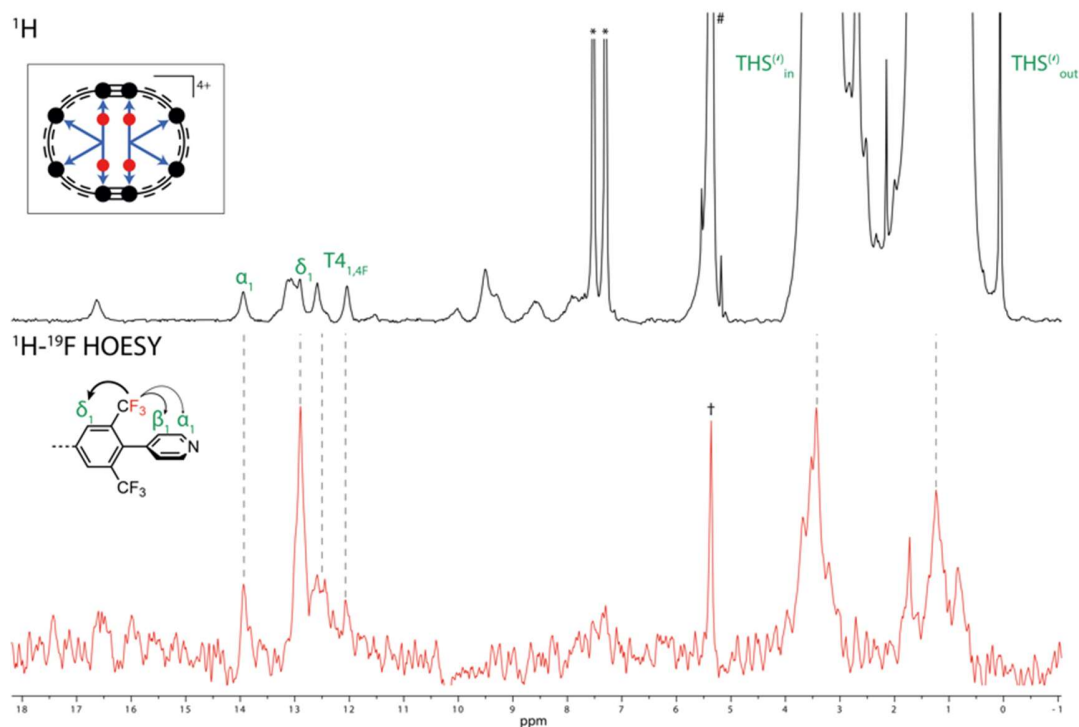


**Figure S143.** Combined <sup>1</sup>H (top) and 1D <sup>1</sup>H-<sup>19</sup>F HOESY (bottom, red) spectra of **c-P8[b<sub>6</sub>f<sub>2</sub>]•(T4<sub>1,4F</sub>)<sub>2</sub><sup>4+</sup>** (500 MHz, CD<sub>2</sub>Cl<sub>2</sub>, 223 K). Peaks assigned with # and \* arise from CHDCl<sub>2</sub> and neutral thianthrene, respectively. † indicates artefacts in the 1D <sup>1</sup>H-<sup>19</sup>F HOESY spectrum.

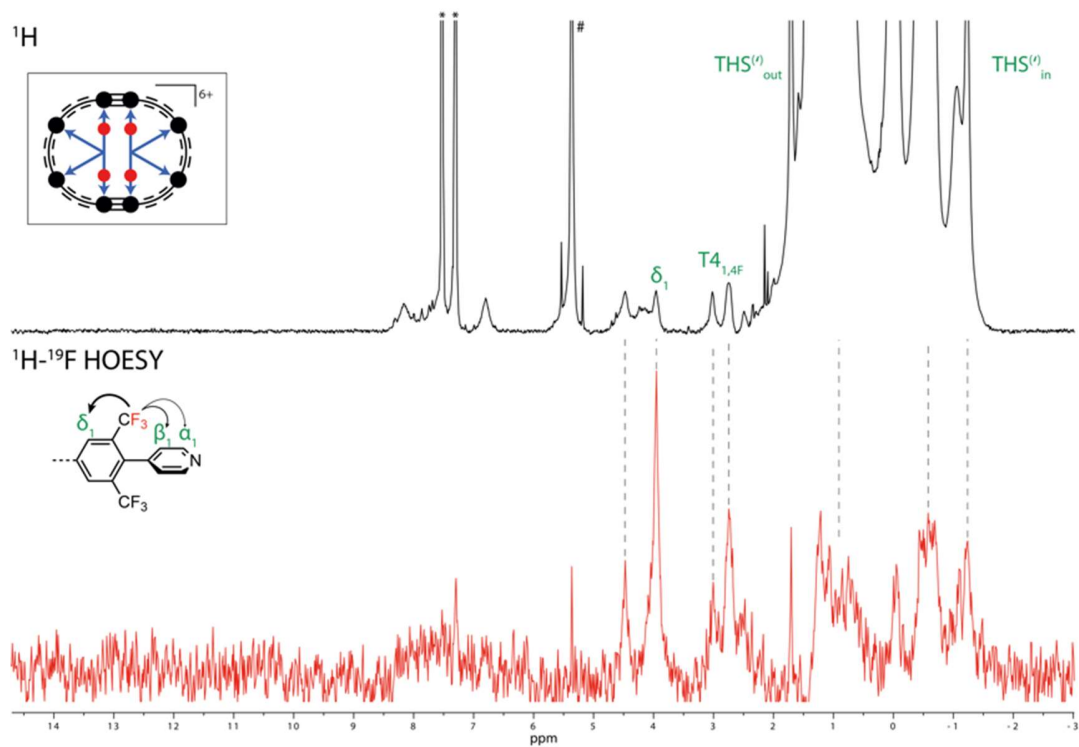


**Figure S144.** Combined <sup>1</sup>H (top) and 1D <sup>1</sup>H-<sup>19</sup>F HOESY (bottom, red) spectra of **c-P8[b<sub>6</sub>f<sub>2</sub>]•(T4<sub>1,4F</sub>)<sub>2</sub><sup>6+</sup>** (500 MHz, CD<sub>2</sub>Cl<sub>2</sub>, 223 K). Peaks assigned with # and \* arise from CHDCl<sub>2</sub> and neutral thianthrene, respectively.

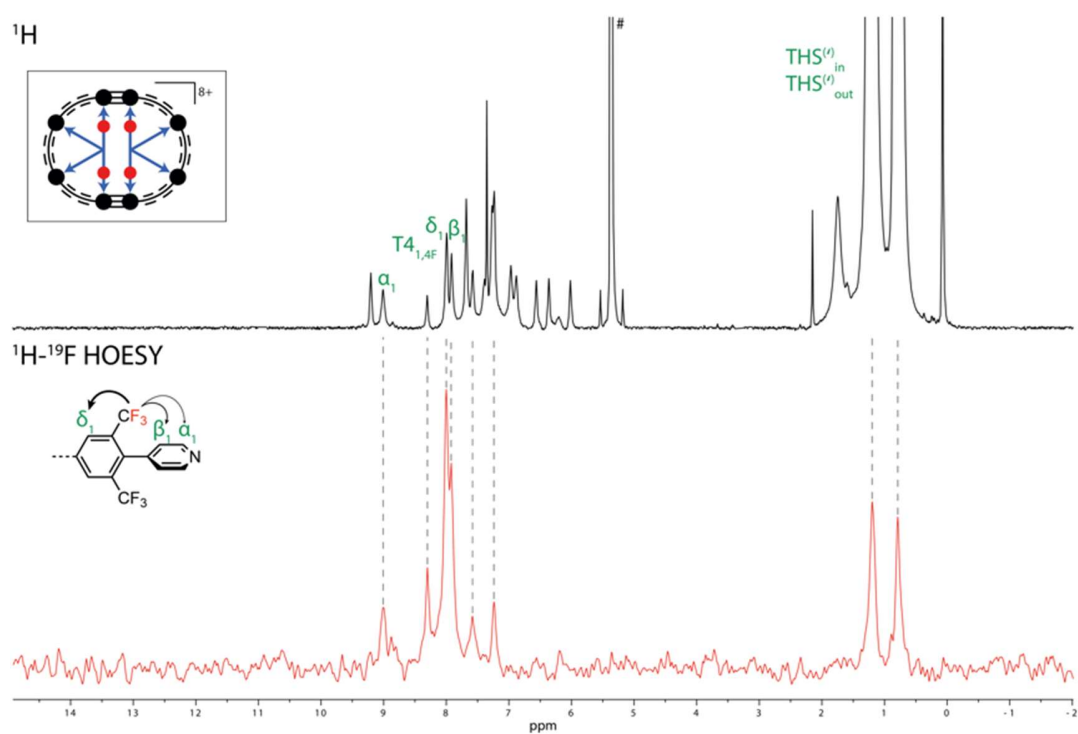


**Figure S145.** Combined  $^1\text{H}$  (top) and 1D  $^1\text{H}$ - $^{19}\text{F}$  HOESY (bottom, red) spectra of  $c\text{-P8}[\text{b}_6\text{f}_2] \bullet (\text{T4}_{1,4\text{F}})_2^{8+}$  (500 MHz,  $\text{CD}_2\text{Cl}_2$ , 223 K). Peak assigned with # arises from  $\text{CHDCl}_2$ .

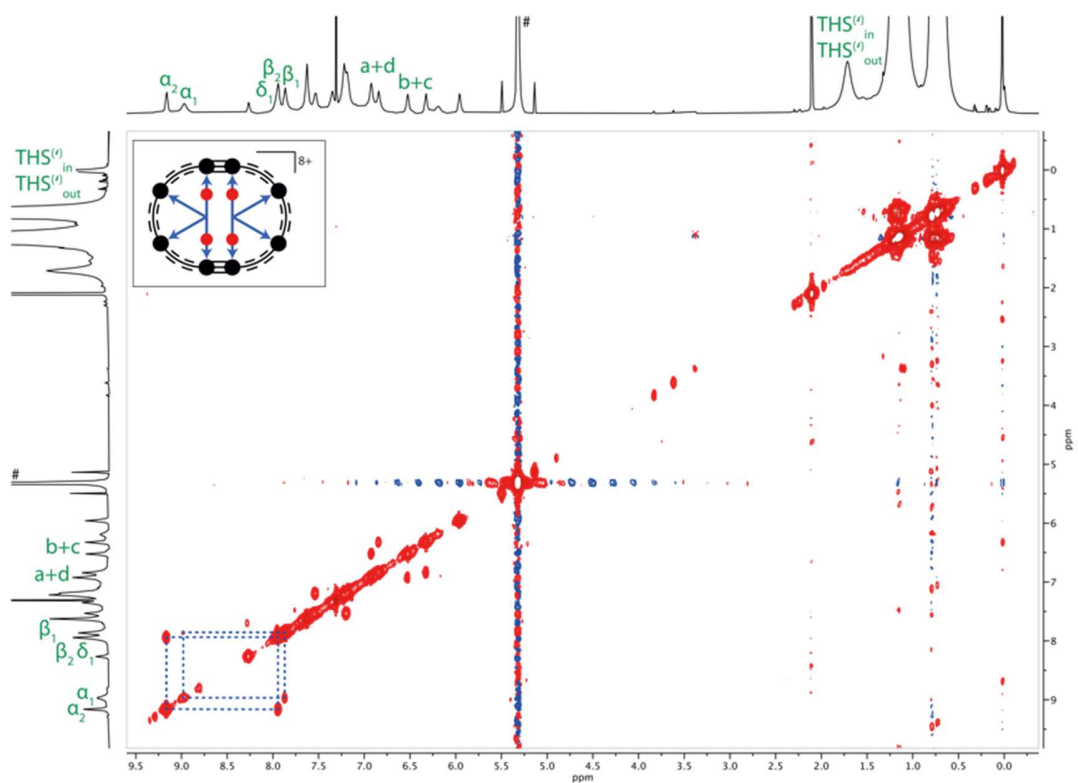


**Figure S146.**  $^1\text{H}$ - $^1\text{H}$  COSY spectrum of  $c\text{-P8}[\text{b}_6\text{f}_2] \bullet (\text{T4}_{1,4\text{F}})_2^{8+}$  (500 MHz,  $\text{CD}_2\text{Cl}_2$ , 223 K). Correlations between  $\alpha$  and  $\beta$  resonances are highlighted in blue. Peaks assigned with # arise from  $\text{CHDCl}_2$ .



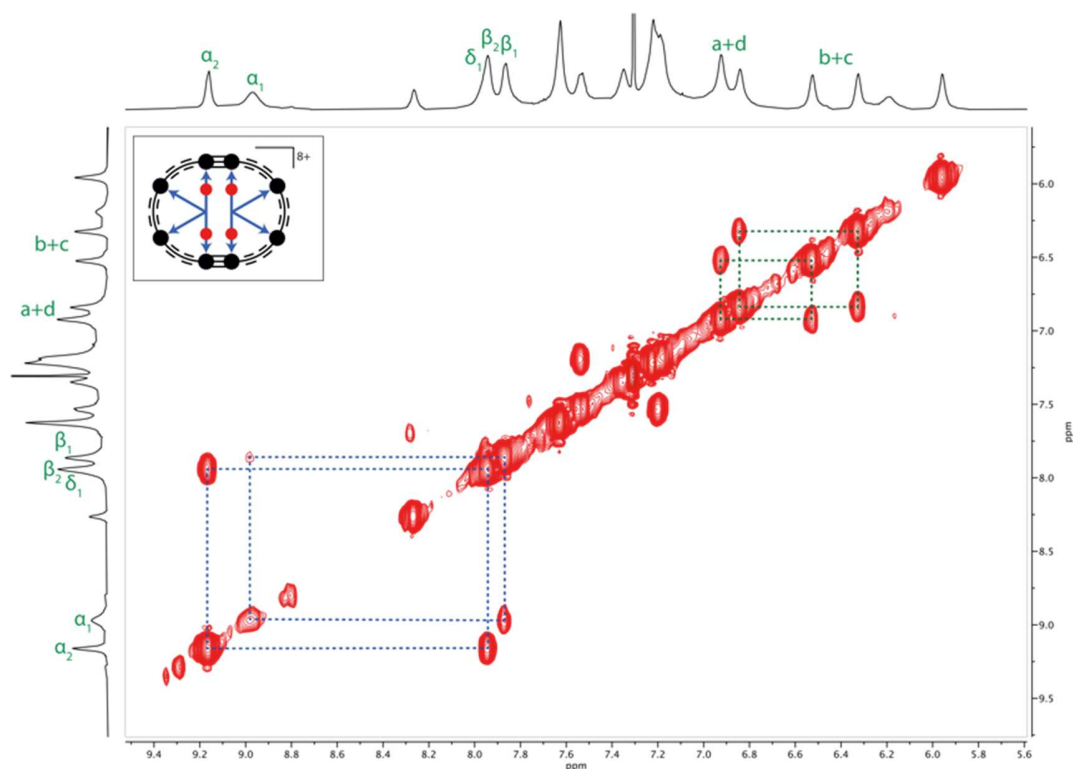


**Figure S147.** Enlarged region of the COSY spectrum of *c*-P8[b<sub>6</sub>f<sub>2</sub>]•(T<sub>4</sub><sub>1,4</sub>F)<sub>2</sub><sup>8+</sup> (500 MHz, CD<sub>2</sub>Cl<sub>2</sub>, 223 K). Correlations between  $\alpha$  and  $\beta$  resonances are highlighted in blue; those between *beta* porphyrin resonances in green.

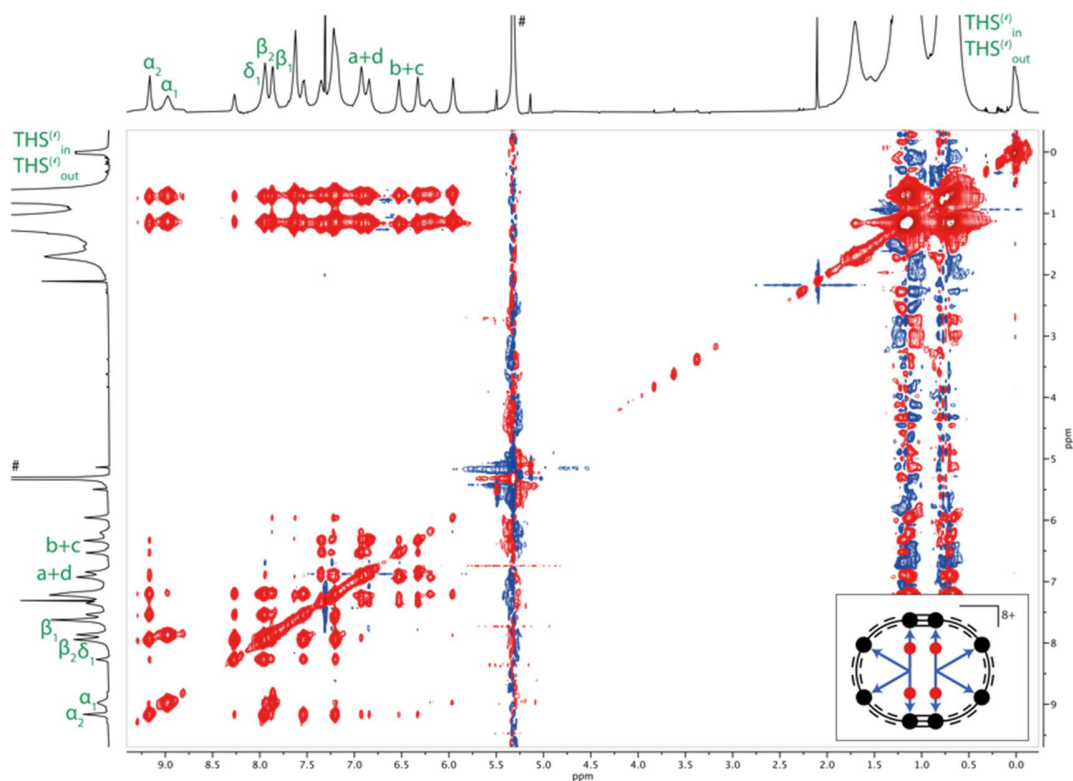


**Figure S148.** <sup>1</sup>H-<sup>1</sup>H NOESY spectrum of *c*-P8[b<sub>6</sub>f<sub>2</sub>]•(T<sub>4</sub><sub>1,4</sub>F)<sub>2</sub><sup>8+</sup> (500 MHz, CD<sub>2</sub>Cl<sub>2</sub>, 223 K). Peaks assigned with # arise from CHDCl<sub>2</sub>.



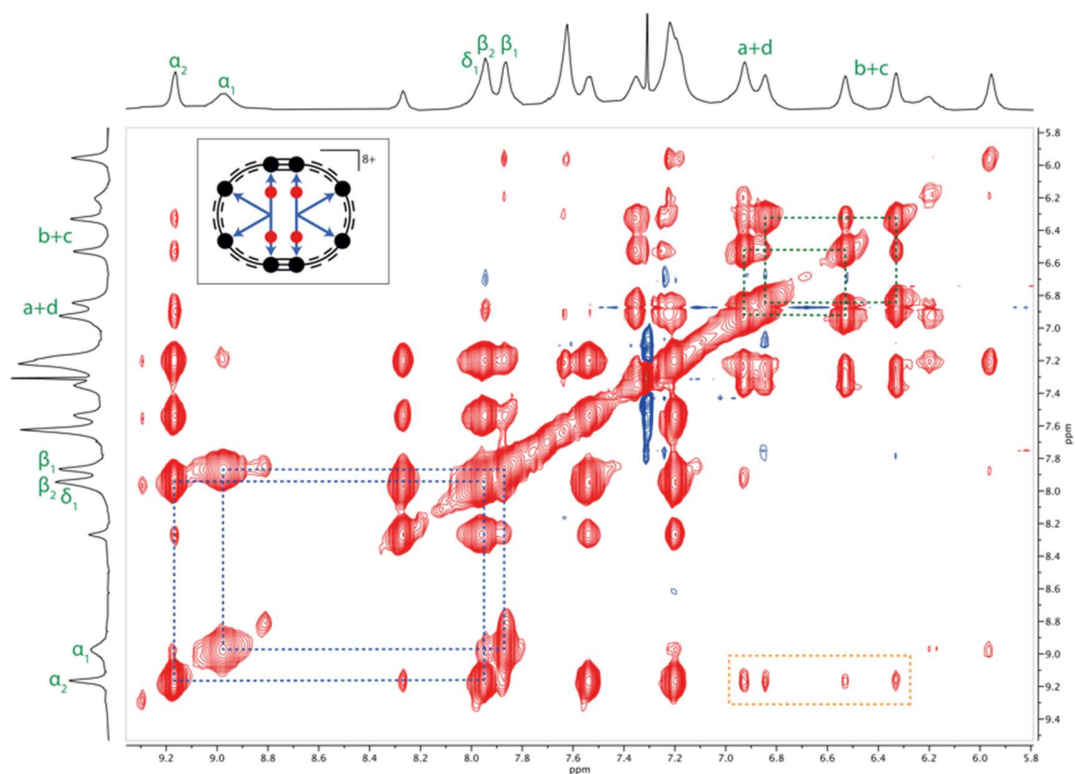


**Figure S149.** Enlarged region of the NOESY spectrum of **c-P8[b<sub>6</sub>f<sub>2</sub>]•(T<sub>41,4F</sub>)<sub>2</sub><sup>8+</sup>** (500 MHz, CD<sub>2</sub>Cl<sub>2</sub>, 223 K). Correlations between α and β resonances are highlighted in blue; those between *beta* porphyrin resonances in green. Selective correlations between α<sub>2</sub> and *beta* porphyrin resonances are highlighted with a dashed box (orange).

**c-P8[b<sub>6</sub>f<sub>2</sub>]•(T4<sub>2,3F</sub>)<sub>2</sub>:**

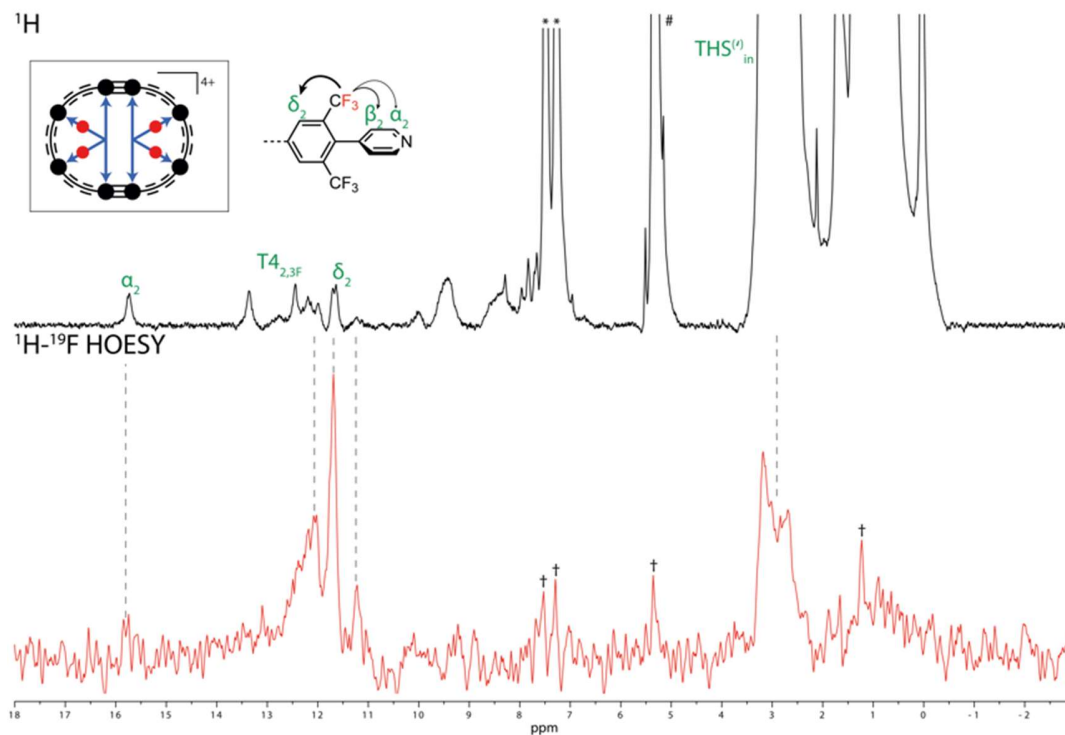


**Figure S150.** Combined <sup>1</sup>H (top) and 1D <sup>1</sup>H-<sup>19</sup>F HOESY (bottom, red) spectra of **c-P8[b<sub>6</sub>f<sub>2</sub>]•(T4<sub>2,3F</sub>)<sub>2</sub><sup>4+</sup>** (500 MHz, CD<sub>2</sub>Cl<sub>2</sub>, 223 K). Peaks assigned with # and \* arise from CHDCl<sub>2</sub> and neutral thianthrene, respectively. † indicates artefacts in the 1D <sup>1</sup>H-<sup>19</sup>F HOESY spectrum.

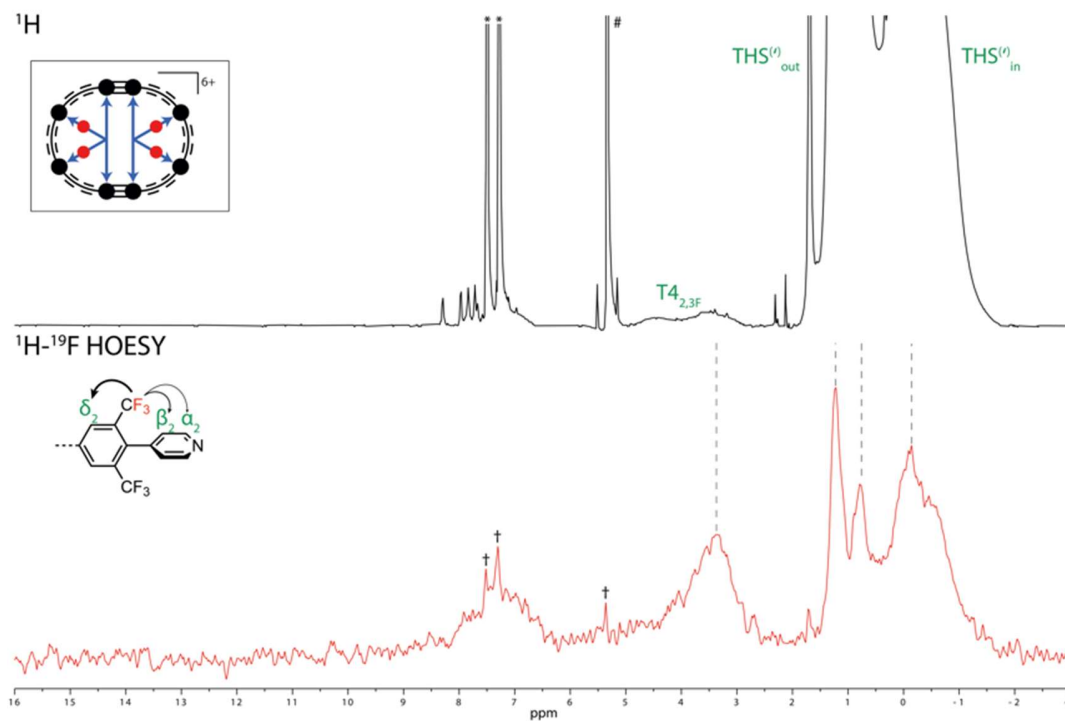


**Figure S151.** Combined <sup>1</sup>H (top) and 1D <sup>1</sup>H-<sup>19</sup>F HOESY (bottom, red) spectra of **c-P8[b<sub>6</sub>f<sub>2</sub>]•(T4<sub>2,3F</sub>)<sub>2</sub><sup>6+</sup>** (500 MHz, CD<sub>2</sub>Cl<sub>2</sub>, 223 K). Peaks assigned with # and \* arise from CHDCl<sub>2</sub> and neutral thianthrene, respectively. † indicates artefacts in the 1D <sup>1</sup>H-<sup>19</sup>F HOESY spectrum.

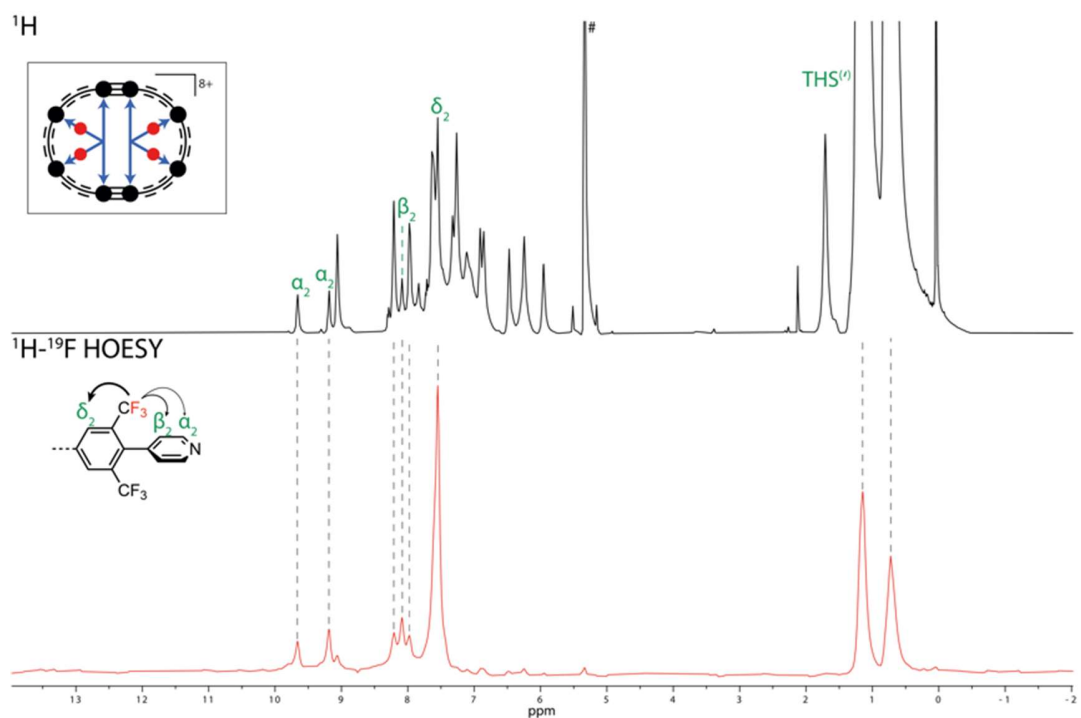


**Figure S152.** Combined  $^1\text{H}$  (top) and 1D  $^1\text{H}$ - $^{19}\text{F}$  HOESY (bottom, red) spectra of  $c\text{-P8}[\text{b}_6\text{f}_2]\bullet(\text{T4}_{2,3\text{F}})_2^{8+}$  (500 MHz,  $\text{CD}_2\text{Cl}_2$ , 223 K). Peak assigned with # arises from  $\text{CHDCl}_2$ .

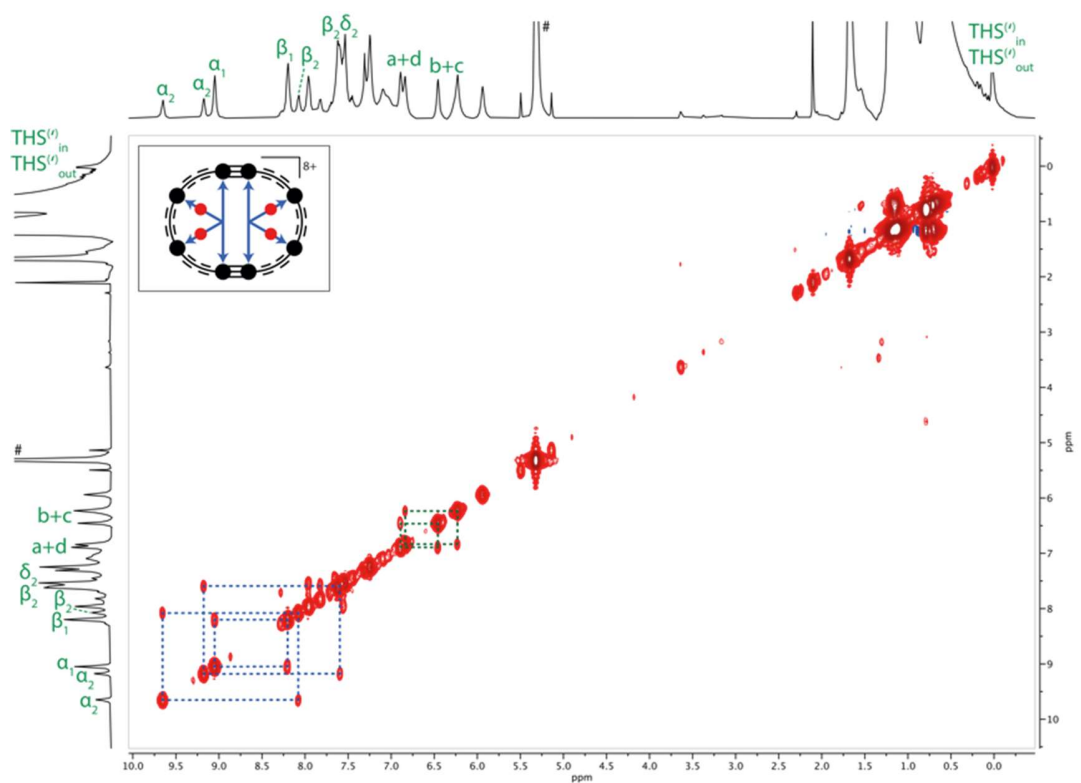


**Figure S153.**  $^1\text{H}$ - $^1\text{H}$  COSY spectrum of  $c\text{-P8}[\text{b}_6\text{f}_2]\bullet(\text{T4}_{2,3\text{F}})_2^{8+}$  (500 MHz,  $\text{CD}_2\text{Cl}_2$ , 223 K). Correlations between  $\alpha$  and  $\beta$  resonances are highlighted in blue; those between  $\beta$  porphyrin resonances in green. Peaks assigned with # arise from  $\text{CHDCl}_2$ .

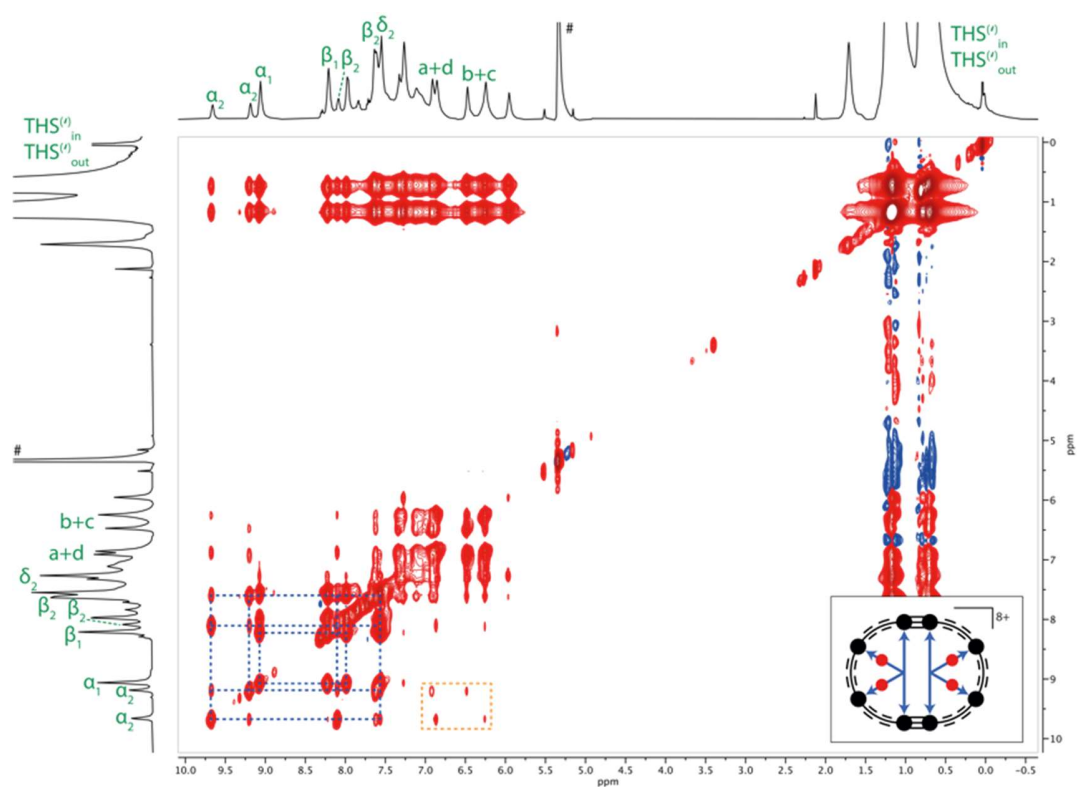


**Figure S154.** <sup>1</sup>H-<sup>1</sup>H NOESY spectrum of *c*-P8[b<sub>6</sub>f<sub>2</sub>]•(T<sub>42,3F</sub>)<sub>2</sub><sup>8+</sup> (500 MHz, CD<sub>2</sub>Cl<sub>2</sub>, 223 K). Correlations between α and β resonances are highlighted in blue. Selective correlations between α<sub>2</sub> and β porphyrin resonances are highlighted with a dashed box (orange). Peaks assigned with # arise from CHDCl<sub>2</sub>.

## 17. DOSY Analysis of the Self-assembly Complexes

We investigated the size difference between the self-assembly complexes of **Si-*I*-P4[b<sub>2</sub>f<sub>1</sub>]-Si** and **Si-*I*-P4[b<sub>3</sub>]-Si** with **T4** by <sup>1</sup>H DOSY NMR spectroscopy. The complexes were formed by the incremental addition of a solution of **T4** in CDCl<sub>3</sub> to a solution of **Si-*I*-P4[b<sub>2</sub>f<sub>1</sub>]-Si** or **Si-*I*-P4[b<sub>3</sub>]-Si** in CDCl<sub>3</sub>. The endpoint of the full complex formation was determined by the complete disappearance of the proton resonances of the unbound porphyrin tetramer and a broadening of the bound template resonances, which indicates a fast exchange between unbound and complexed **T4** (Figures S155 and S158). <sup>1</sup>H DOSY spectroscopy of the self-assembly product shows the clean formation of a single complex for **Si-*I*-P4[b<sub>2</sub>f<sub>1</sub>]-Si** and **T4** and **Si-*I*-P4[b<sub>3</sub>]-Si** and **T4** (Figures S156 and S159). Fitting of the diffusion decay curves to the Stejskal-Tanner equation<sup>31</sup> gives a mean diffusion coefficient of  $1.86 \pm 0.09 \times 10^{-10} \text{ m}^2 \text{ s}^{-1}$  and  $2.14 \pm 0.11 \times 10^{-10} \text{ m}^2 \text{ s}^{-1}$  for the self-assembly complexes of **Si-*I*-P4[b<sub>2</sub>f<sub>1</sub>]-Si** and **T4** and **Si-*I*-P4[b<sub>3</sub>]-Si** and **T4**, respectively (Figures S157 and S160). The significant difference in the diffusion coefficients suggest an about 15% larger hydrodynamic radius for the self-assembly complex of **Si-*I*-P4[b<sub>2</sub>f<sub>1</sub>]-Si** and **T4** compared to the self-assembly complex of **Si-*I*-P4[b<sub>3</sub>]-Si** and **T4** under the assumption of a spherical shape of the complexes in the Stokes-Einstein relationship.<sup>32</sup> <sup>1</sup>H DOSY analysis of **c-P8[b<sub>8</sub>](T4)<sub>2</sub>** and **c-P8[b<sub>6</sub>f<sub>2</sub>](T4)<sub>2</sub>** gives a mean diffusion coefficient of  $1.72 \pm 0.02 \times 10^{-10} \text{ m}^2 \text{ s}^{-1}$  and  $1.55 \pm 0.21 \times 10^{-10} \text{ m}^2 \text{ s}^{-1}$ , respectively (Figures S161–166), which was used as reference for the magnitude of the diffusion coefficient expected for a 2:2 complex. These findings suggest the predominant formation of the 2:2 complex (**Si-*I*-P4[b<sub>2</sub>f<sub>1</sub>]-Si**)<sub>2</sub>•(**T4**)<sub>2</sub> in the self-assembly of **Si-*I*-P4[b<sub>2</sub>f<sub>1</sub>]-Si** and **T4**, and the formation of the 1:1 complex (**Si-*I*-P4[b<sub>3</sub>]-Si**)•(**T4**) in the assembly of **Si-*I*-P4[b<sub>3</sub>]-Si** and **T4**.<sup>33,34</sup>

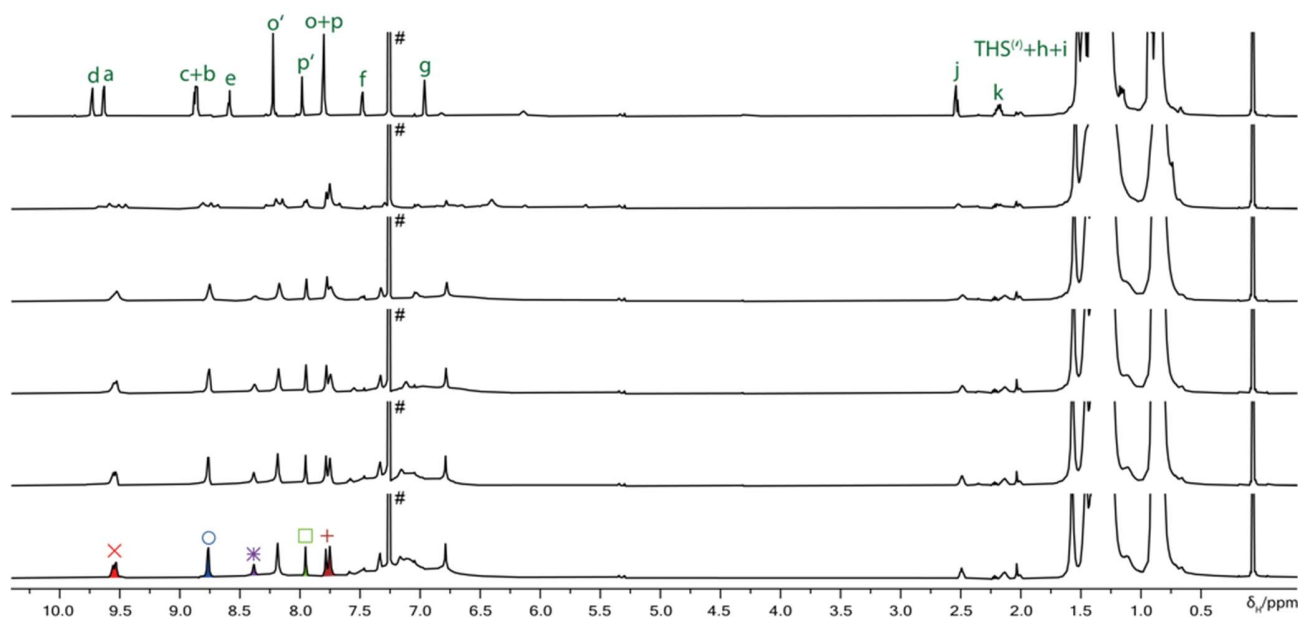


**Figure S155.** <sup>1</sup>H NMR spectra of the formation titration of (**Si-*I*-P4[b<sub>2</sub>f<sub>1</sub>]-Si**)<sub>2</sub>•(**T4**)<sub>2</sub> (500 MHz, CDCl<sub>3</sub>, 298 K). The top spectrum corresponds to unbound tetramer **Si-*I*-P4[b<sub>2</sub>f<sub>1</sub>]-Si**, and the bottom spectrum to the fully formed complex. Peaks assigned with # arise from CHCl<sub>3</sub>. The highlighted resonances in the bottom spectrum indicate the signals used in the fitting of the diffusion decay curves of the <sup>1</sup>H DOSY spectrum of (**Si-*I*-P4[b<sub>2</sub>f<sub>1</sub>]-Si**)<sub>2</sub>•(**T4**)<sub>2</sub>.

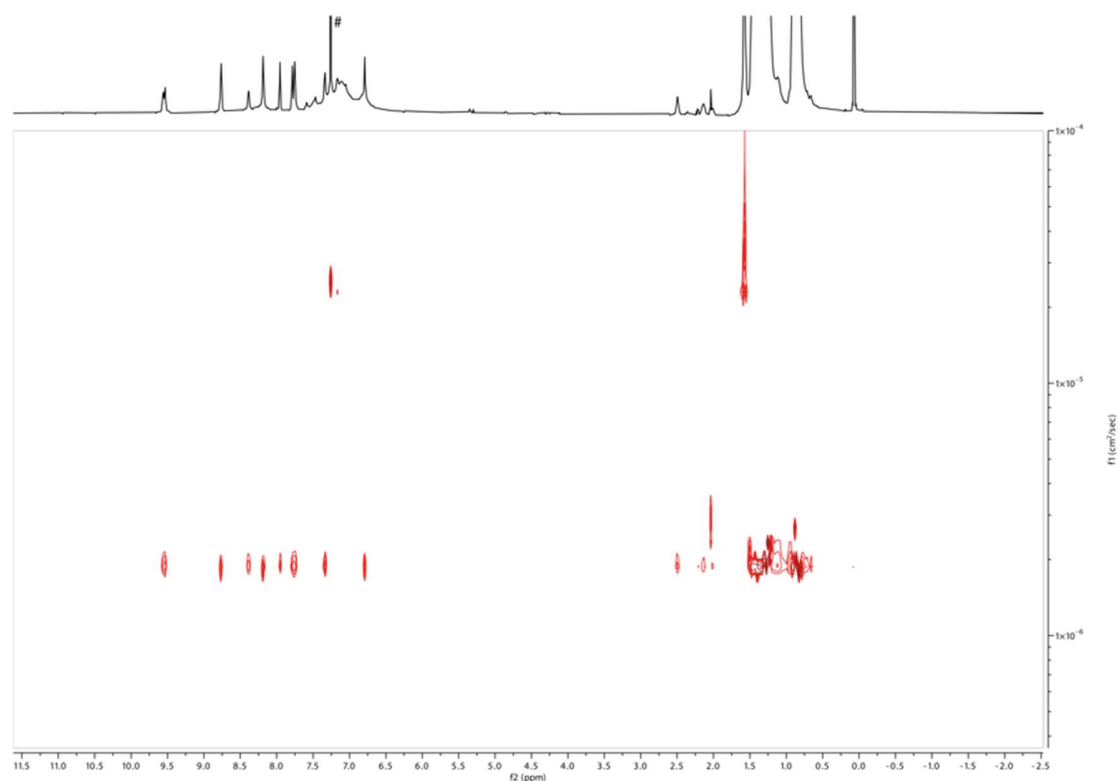


Figure S156.  $^1\text{H}$  DOSY plot of complex  $(\text{Si-/P4}[\text{b}_2\text{f}_1]\text{-Si})_2\bullet(\text{T4})_2$  (500 MHz,  $\text{CDCl}_3$ , 298 K). Peak assigned with # arises from  $\text{CHCl}_3$ .

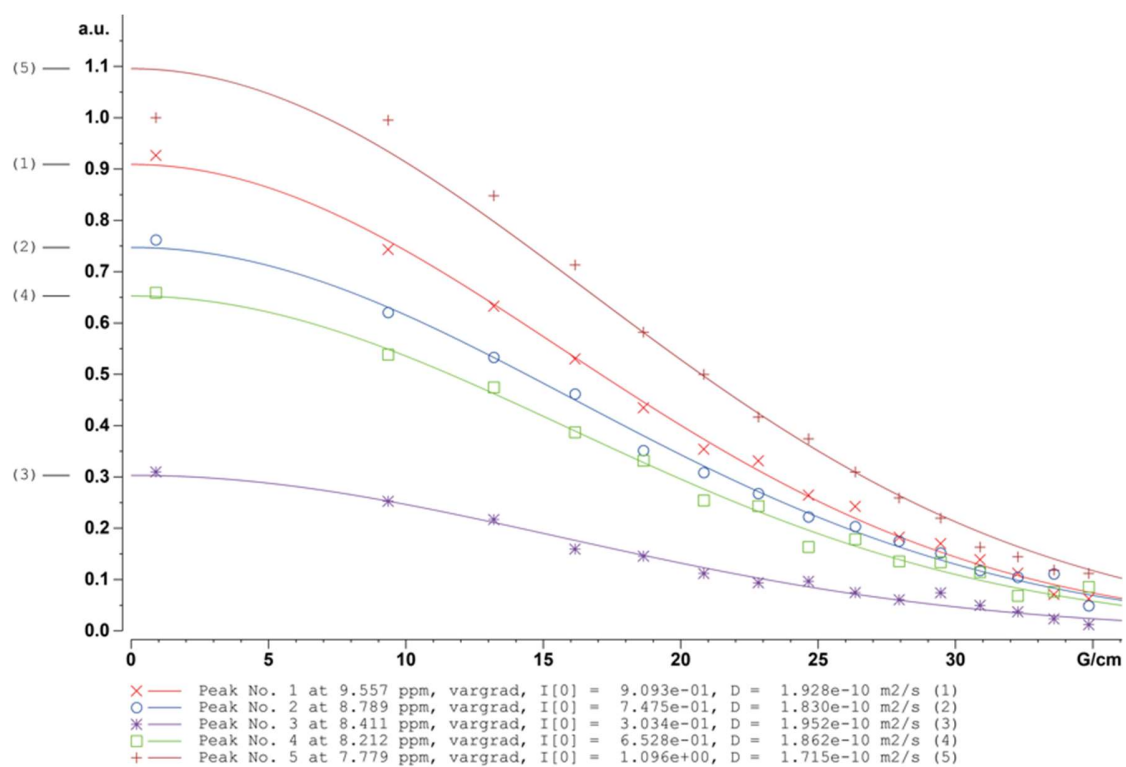
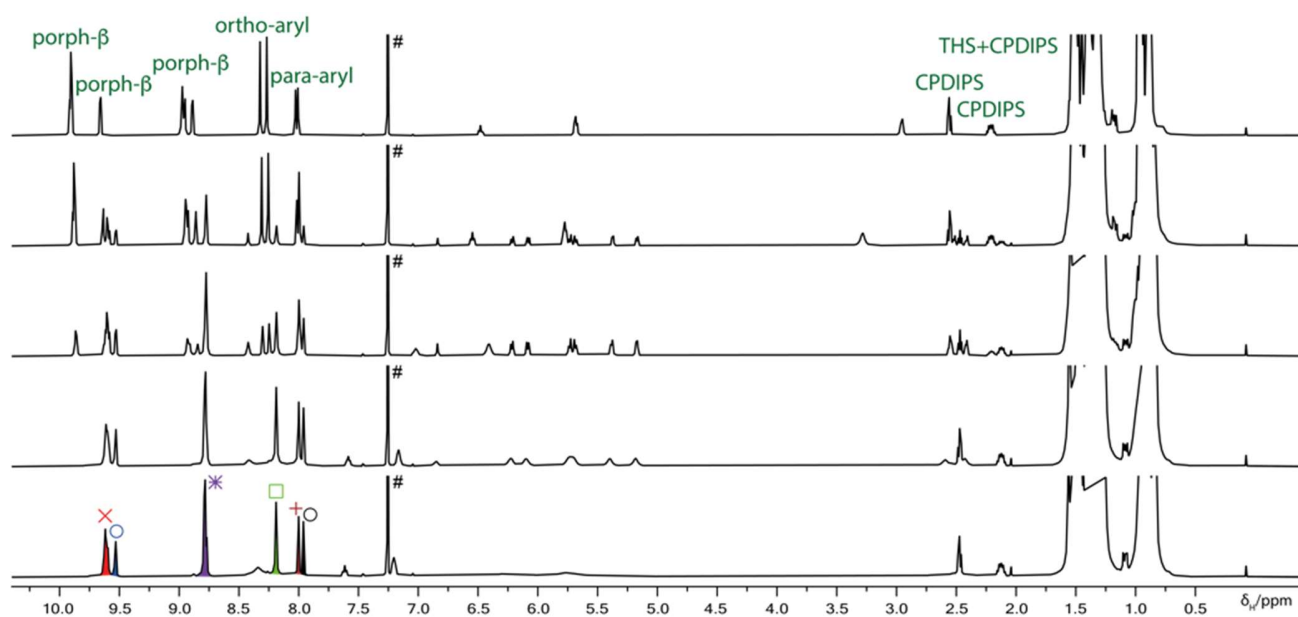
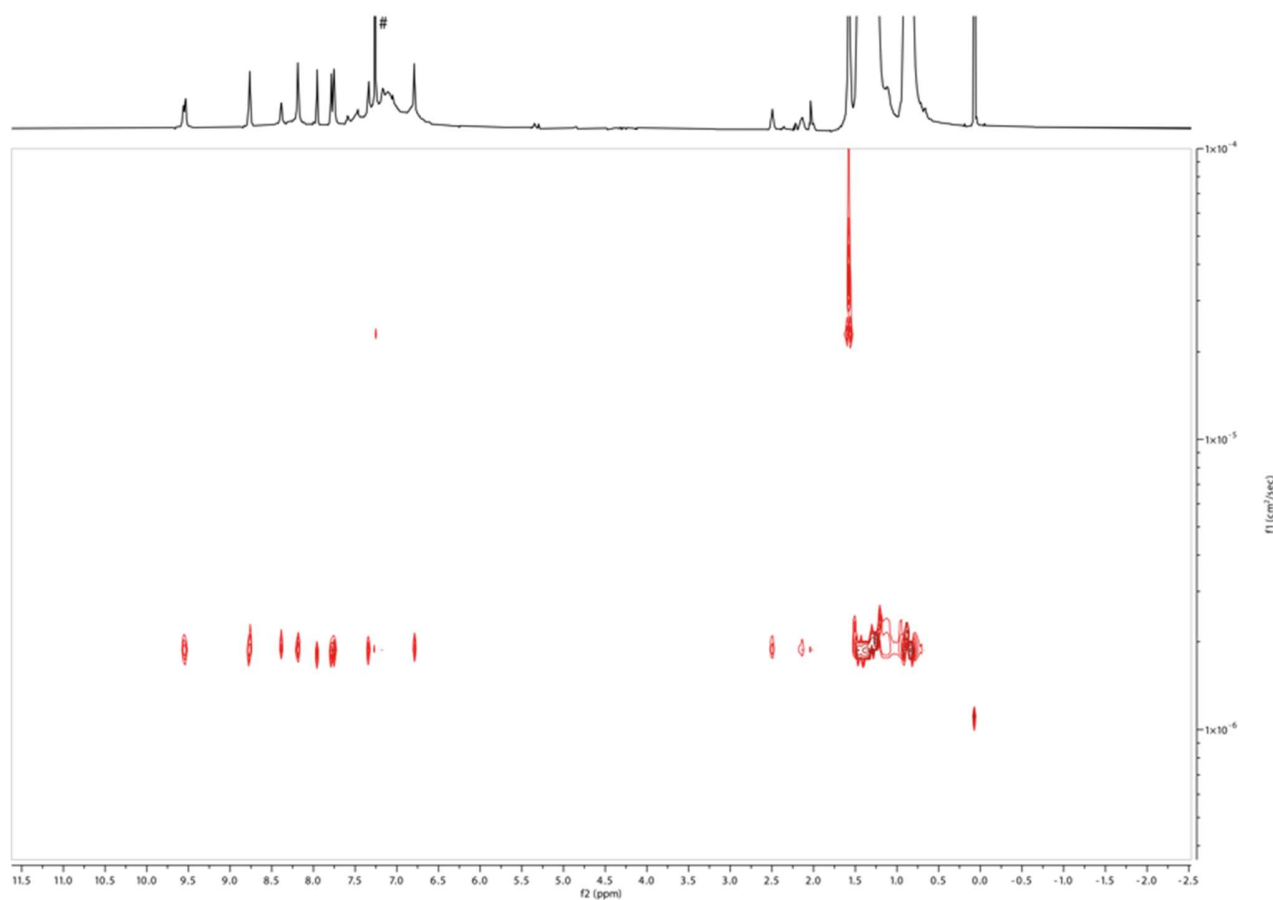


Figure S157. Fitted diffusion decay curves and resulting diffusion coefficients of  $(\text{Si-/P4}[\text{b}_2\text{f}_1]\text{-Si})_2\bullet(\text{T4})_2$  (500 MHz,  $\text{CDCl}_3$ , 298 K) with  $\Delta = 100$  ms,  $\delta = 2$  ms, and  $g = 0.90\text{--}36.06$   $\text{G cm}^{-1}$ . Averaging of the individual diffusion coefficients gives a mean diffusion coefficient of  $1.86 \pm 0.09 \times 10^{-10} \text{ m}^2 \text{ s}^{-1}$ .



**Figure S158.**  $^1\text{H}$  NMR spectra of the formation titration of  $(\text{Si-/P4}[\text{b}_3]\text{-Si})\bullet(\text{T4})$  (500 MHz,  $\text{CDCl}_3$ , 298 K). The top spectrum corresponds to unbound tetramer  $\text{Si-/P4}[\text{b}_3]\text{-Si}$ , and the bottom spectrum to the fully formed complex. Peaks assigned with # arise from  $\text{CHCl}_3$ . The highlighted resonances in the bottom spectrum indicate the signals used in the fitting of the diffusion decay curves of the  $^1\text{H}$  DOSY spectrum of  $(\text{Si-/P4}[\text{b}_3]\text{-Si})\bullet(\text{T4})$ .



**Figure S159.**  $^1\text{H}$  DOSY plot of complex  $(\text{Si-/P4}[\text{b}_3]\text{-Si})\bullet(\text{T4})$  (500 MHz,  $\text{CDCl}_3$ , 298 K). Peak assigned with # arises from  $\text{CHCl}_3$ .



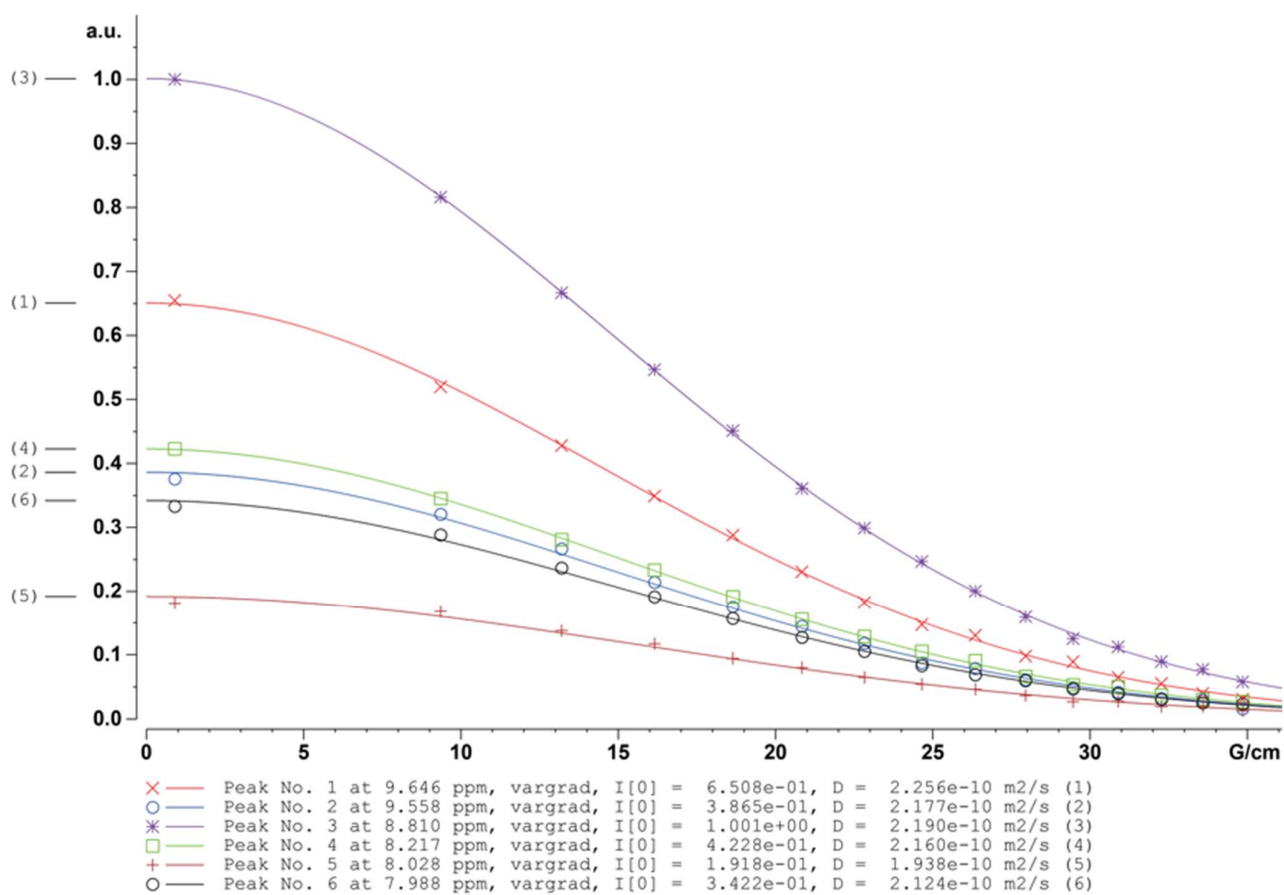


**Figure S160.** Fitted diffusion decay curves and resulting diffusion coefficients of **(Si-/P4[b<sub>3</sub>]-Si)•(T4)** (500 MHz, CDCl<sub>3</sub>, 298 K) with  $\Delta = 100$  ms,  $\delta = 2$  ms, and  $g = 0.90\text{--}36.06$  G cm<sup>-1</sup>. Averaging of the individual diffusion coefficients gives a mean diffusion coefficient of  $2.14 \pm 0.11 \times 10^{-10}$  m<sup>2</sup> s<sup>-1</sup>.

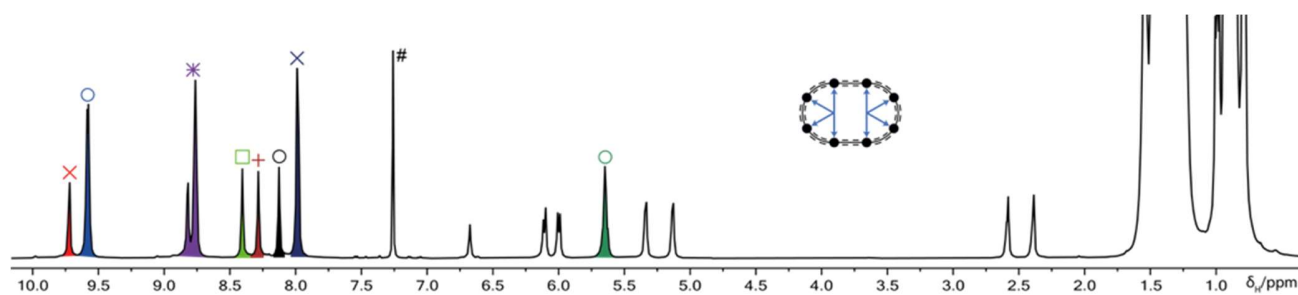


**Figure S161.** <sup>1</sup>H NMR spectrum of **c-P8[b<sub>8</sub>]•(T4)<sub>2</sub>** (500 MHz, CDCl<sub>3</sub>, 298 K). Peak assigned with # arises from CHCl<sub>3</sub>. The highlighted resonances indicate the signals used in the fitting of the diffusion decay curves of the <sup>1</sup>H DOSY spectrum.

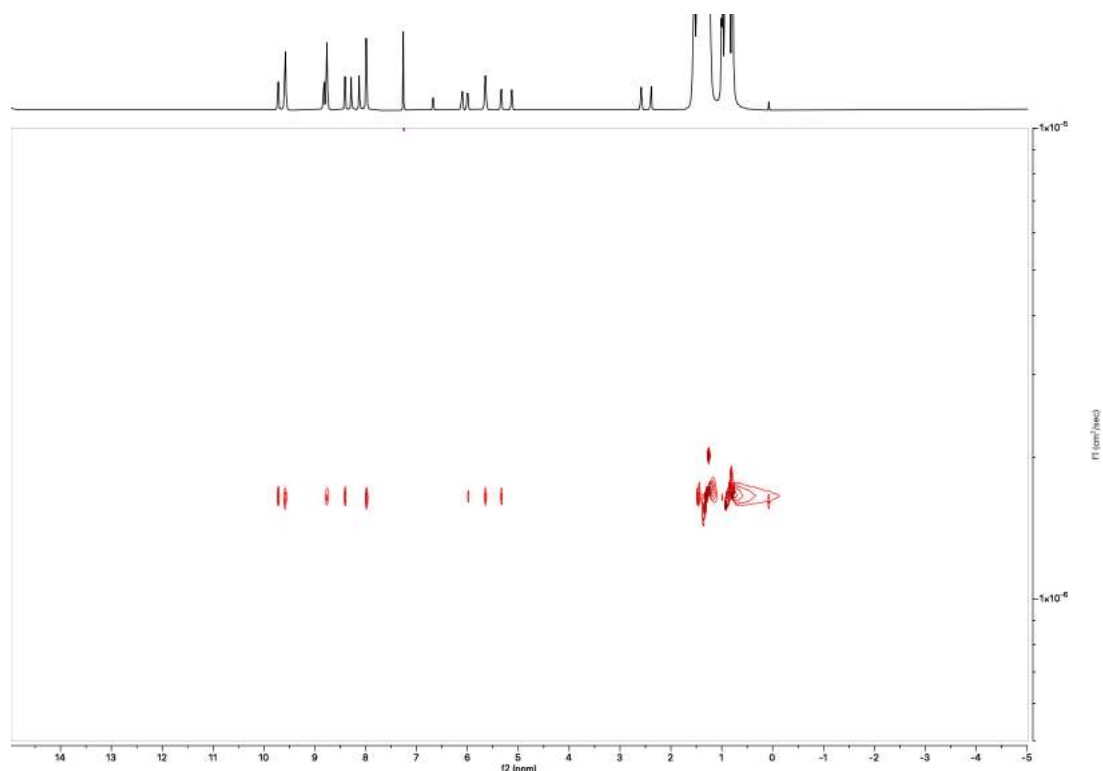


**Figure S162.**  $^1\text{H}$  DOSY plot of complex **c-P8[b<sub>8</sub>]•(T<sub>4</sub>)<sub>2</sub>** (500 MHz,  $\text{CDCl}_3$ , 298 K). Peak assigned with # arises from  $\text{CHCl}_3$ .

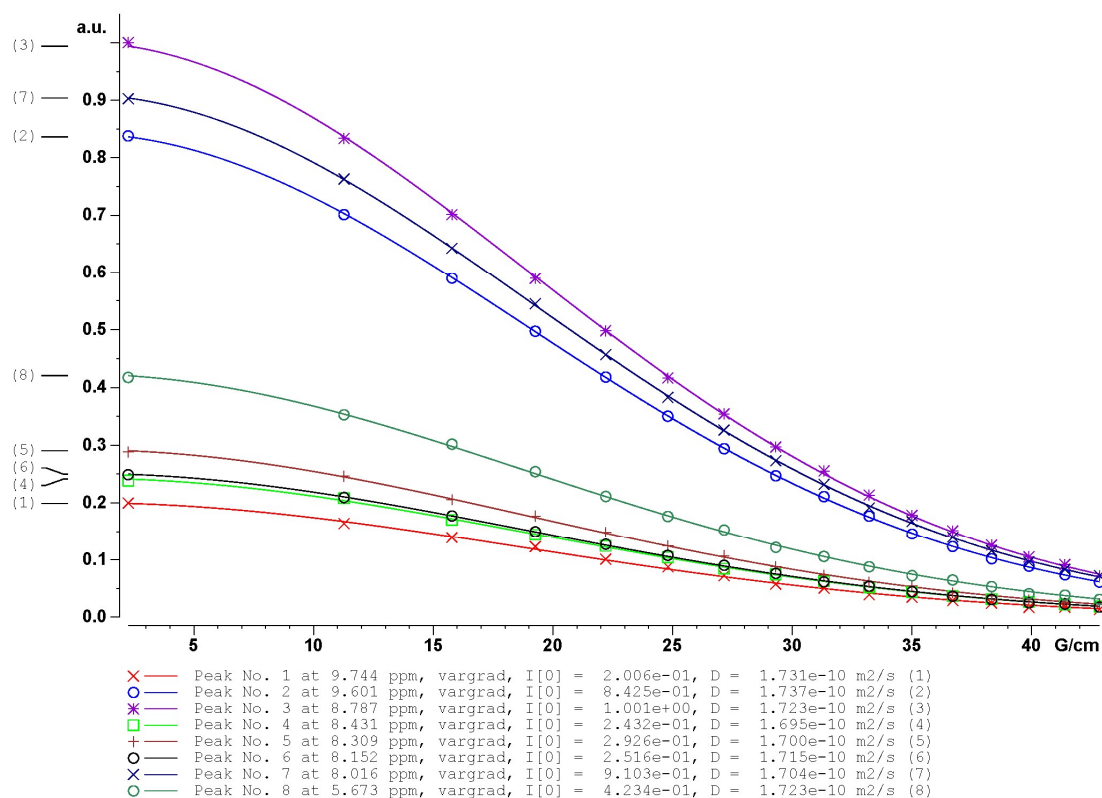


**Figure S163.** Fitted diffusion decay curves and resulting diffusion coefficients of **c-P8[b<sub>8</sub>]•(T<sub>4</sub>)<sub>2</sub>** (500 MHz,  $\text{CDCl}_3$ , 298 K) with  $\Delta = 100$  ms,  $\delta = 1.75$  ms, and  $g = 2.25\text{--}42.9$  G  $\text{cm}^{-1}$ . Averaging of the individual diffusion coefficients gives a mean diffusion coefficient of  $1.72 \pm 0.02 \times 10^{-10} \text{ m}^2 \text{ s}^{-1}$ .

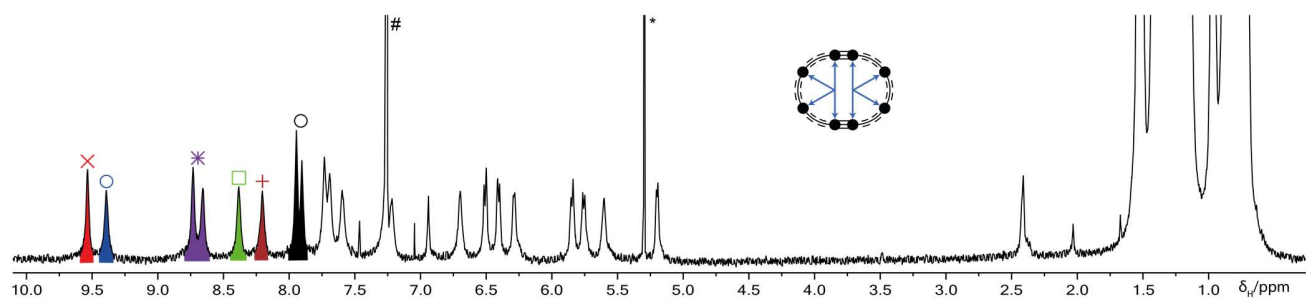


**Figure S164.**  $^1\text{H}$  NMR spectrum of **c-P8[b<sub>6</sub>f<sub>2</sub>]•(T<sub>4</sub>)<sub>2</sub>** (500 MHz,  $\text{CDCl}_3$ , 298 K). Peaks assigned with # and \* arise from  $\text{CHCl}_3$  and  $\text{CH}_2\text{Cl}_2$ , respectively. The highlighted resonances indicate the signals used in the fitting of the diffusion decay curves of the  $^1\text{H}$  DOSY spectrum.

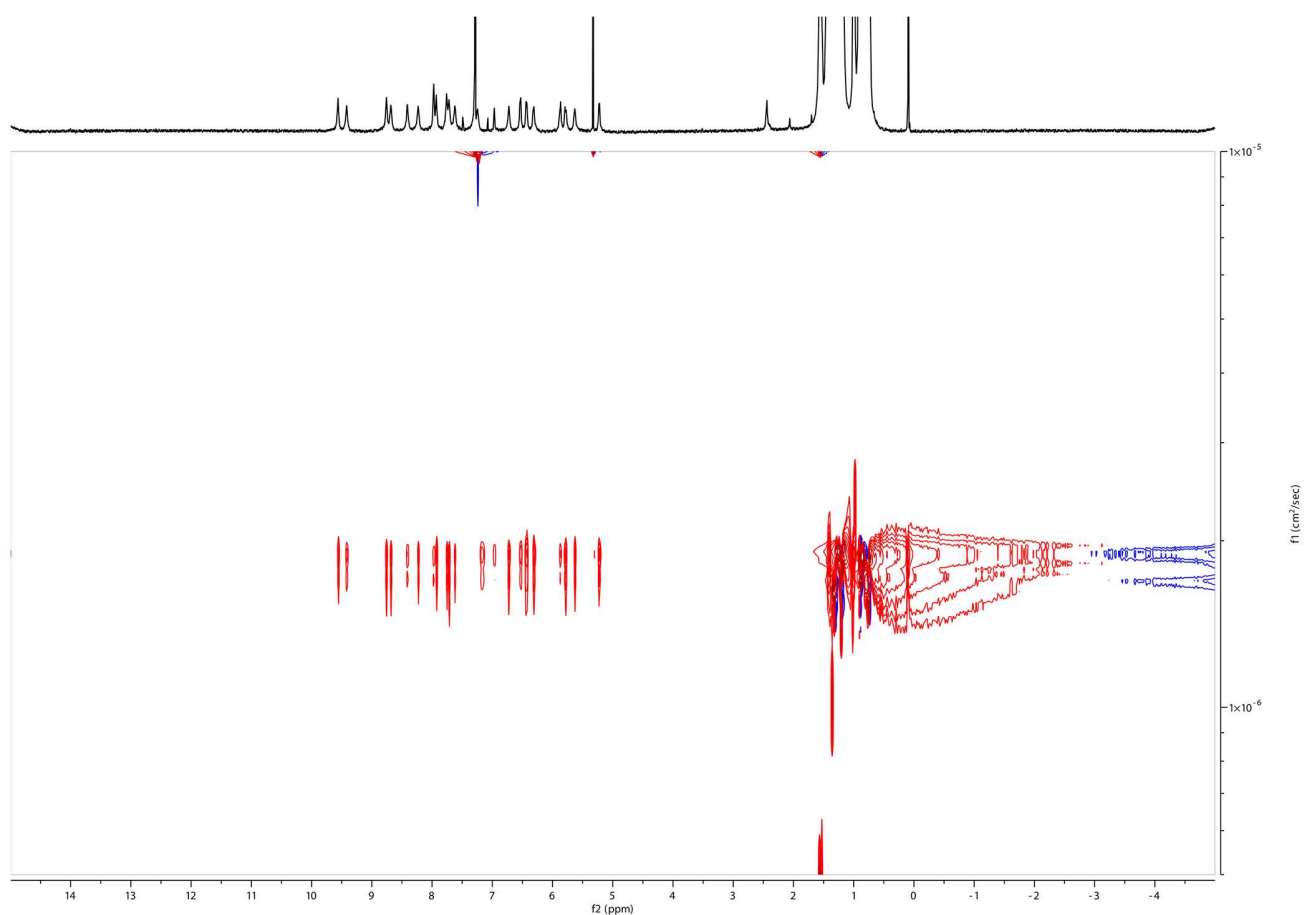


**Figure S165.**  $^1\text{H}$  DOSY plot of complex **c-P8[b<sub>6</sub>f<sub>2</sub>]•(T<sub>4</sub>)<sub>2</sub>** (500 MHz,  $\text{CDCl}_3$ , 298 K).

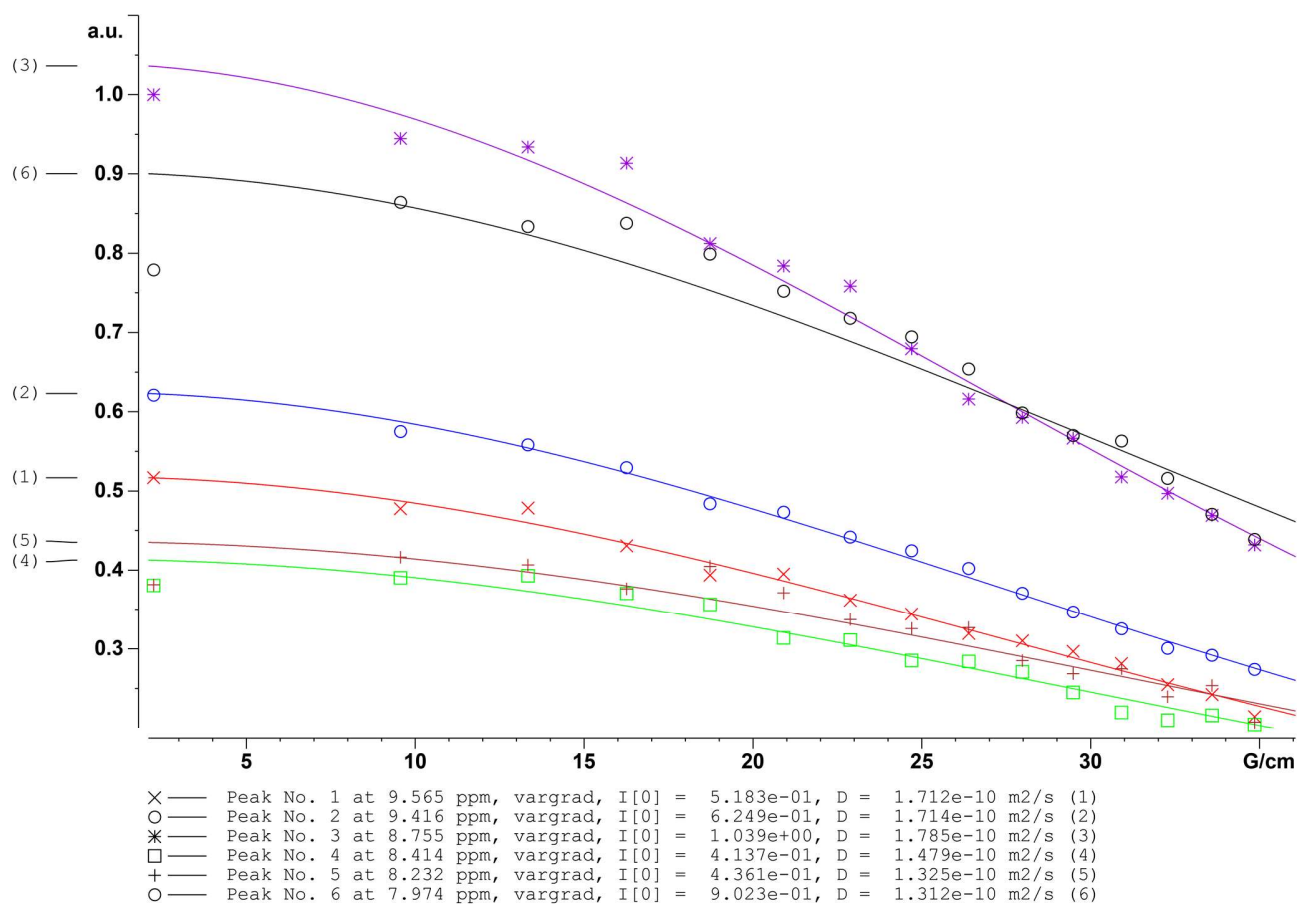


**Figure S166.** Fitted diffusion decay curves and resulting diffusion coefficients of **c-P8[b<sub>6</sub>f<sub>2</sub>]•(T4)<sub>2</sub>** (500 MHz, CDCl<sub>3</sub>, 298 K) with  $\Delta = 100$  ms,  $\delta = 1.20$  ms, and  $g = 2.25\text{--}36.1$  G cm<sup>-1</sup>. Averaging of the individual diffusion coefficients gives a mean diffusion coefficient of  $1.55 \pm 0.21 \times 10^{-10}$  m<sup>2</sup> s<sup>-1</sup>.

## 18. References

- (1) Keller, R.; Wyckoff, H. Copper(I) Chloride. *Inorg. Synth.* **1946**, 2, 1–4.
- (2) Bols, P. S.; Anderson, H. L. Shadow Mask Templates for Site-Selective Metal Exchange in Magnesium Porphyrin Nanorings. *Angew. Chem. Int. Ed.* **2018**, 57, 7874–7877.
- (3) Peeks, M. D.; Claridge, T. D. W.; Anderson, H. L. Aromatic and Antiaromatic Ring Currents in a Molecular Nanoring. *Nature* **2017**, 541, 200–203.
- (4) Rickhaus, M.; Jirasek, M.; Tejerina, L.; Gotfredsen, H.; Peeks, M. D.; Haver, R.; Jiang, H.-W.; Claridge, T. D. W.; Anderson, H. L. Global Aromaticity at the Nanoscale. *Nat. Chem.* **2020**, 12, 236–241.
- (5) Grozema, F. C.; Houarner-Rassin, C.; Prins, P.; Siebbeles, L. D. A.; Anderson, H. L. Supramolecular Control of Charge Transport in Molecular Wires. *J. Am. Chem. Soc.* **2007**, 129, 13370–13371.
- (6) Parkinson, P.; Knappe, C. E. I.; Kamonsutthipajit, N.; Sirithip, K.; Matichak, J. D.; Anderson, H. L.; Herz, L. M. Ultrafast Energy Transfer in Biomimetic Multistrand Nanorings. *J. Am. Chem. Soc.* **2014**, 136, 8217–8220.
- (7) Richert, S.; Limburg, B.; Anderson, H. L.; Timmel, C. R. On the Influence of the Bridge on Triplet State Delocalization in Linear Porphyrin Oligomers. *J. Am. Chem. Soc.* **2017**, 139, 12003–12008.
- (8) Holmes, D.; Lee, S.; Lotz, S.; Nguyen, S.; Schaller, G.; Schmidt-Radde, R.; Vollhardt, K. ( $\eta^6$ -[7]Heliphenyl)tricarbonylchromium via an Optimized Preparation of [7]Heliphenyl. *Synthesis* **2015**, 47, 2038–2054.
- (9) Li, G.; Yoon, K.-Y.; Zhong, X.; Zhu, X.; Dong, G. Efficient Bottom-Up Preparation of Graphene Nanoribbons by Mild Suzuki-Miyaura Polymerization of Simple Triaryl Monomers. *Chem. Eur. J.* **2016**, 22, 9116–9120.
- (10) Mallinger, A.; Crumpler, S.; Pichowicz, M.; Waalboer, D.; Stubbs, M.; Adeniji-Popoola, O.; Wood, B.; Smith, E.; Thai, C.; Henley, A. T.; Georgi, K.; Court, W.; Hobbs, S.; Box, G.; Ortiz-Ruiz, M.-J.; Valenti, M.; Brandon, A. D. H.; TePoele, R.; Leuthner, B.; Workman, P.; Aherne, W.; Poeschke, O.; Dale, T.; Wienke, D.; Esdar, C.; Rohdich, F.; Raynaud, F.; Clarke, P. A.; Eccles, S. A.; Stieber, F.; Schiemann, K.; Blagg, J. Discovery of Potent, Orally Bioavailable, Small-Molecule Inhibitors of WNT Signaling from a Cell-Based Pathway Screen. *J. Med. Chem.* **2015**, 58, 1717–1735.
- (11) Coey, J. M. D. Magnetostatics. *Magnetism and Magnetic Materials*, Cambridge University Press: Cambridge, 2010; pp 24–41.
- (12) Marques, H. M.; Cukrowski, I. Molecular Mechanics Modelling of Porphyrins. Using Artificial Neural Networks to Develop Metal Parameters for Four-Coordinate Metalloporphyrins. *Phys. Chem. Chem. Phys.* **2002**, 4, 5878–5887.
- (13) Marques, H. M.; Cukrowski, I. Molecular Mechanics Parameters for the Modelling of Four-Coordinate Zn(II) Porphyrins. *Phys. Chem. Chem. Phys.* **2003**, 5, 5499–5506.
- (14) Goldstein, E.; Ma, B.; Lii, J.-H.; Allinger, N. L. Molecular Mechanics Calculations (MM3) on Nitriles and Alkynes. *J. Phys. Org. Chem.* **1996**, 9, 191–202.
- (15) Jarowski, P. D.; Diederich, F.; Houk, K. N. Structures and Stabilities of Diacetylene-Expanded Polyhedranes by Quantum Mechanics and Molecular Mechanics. *J. Org. Chem.* **2005**, 70, 1671–1678.
- (16) Stewart, J. J. P. Optimization of Parameters for Semiempirical Methods VI: More Modifications to the NDDO Approximations and Re-optimization of Parameters. *J. Mol. Model.* **2013**, 19, 1–32.
- (17) Frisch, M. J.; Trucks, G. W.; Schlegel, H. B.; Scuseria, G. E.; Robb, M. A.; Cheeseman, J. R.; Scalmani, G.; Barone, V.; Petersson, G. A.; Nakatsuji, H.; Li, X.; Caricato, M.; Marenich, A. V.; Bloino, J.; Janesko, B. G.; Gomperts, R.; Mennucci, B.; Hratchian, H. P.; Ortiz, J. V.; Izmaylov, A. F.; Sonnenberg, J. L.; Williams-Young, D.; Ding, F.; Lipparini, F.; Egidi, F.; Rega, N.; Zheng, G.; Liang, W.; Hada, M.; Ehara, M.; Toyota, K.; Fukuda, R.; Hasegawa, J.; Ishida, M.; Nakajima, T.; Honda, Y.; Kitao, O.; Nakai, H.; Vreven, T.; Throssell, K.; Montgomery Jr., J. A.; Peralta, J. E.; Ogliaro, F.; Bearpark, M. J.; Heyd, J. J.; Brothers, E. N.; Kudin, K. N.; Staroverov, V. N.; Keith, T. A.; Kobayashi, R.; Normand, J.; Raghavachari, K.; Rendell, A. P.; Burant, J. C.; Iyengar, S. S.; Tomasi, J.; Cossi, M.; Millam, J. M.; Klene, M.; Adamo, C.; Cammi, R.; Ochterski, J. W.; Martin, R. L.; Morokuma, K.; Farkas, O.; Foresman, J. B.; Fox, D. J. *Gaussian 16, Revision A.03*. Gaussian Inc.: Wallingford CT 2016.
- (18) Ditchfield, R.; Hehre, W. J.; Pople, J. A. Self-Consistent Molecular-Orbital Methods. IX. An Extended Gaussian-Type Basis for Molecular-Orbital Studies of Organic Molecules. *J. Chem. Phys.* **1971**, 54, 724–728.

- (19) Hehre, W. J.; Ditchfield, R.; Pople, J. A. Self-Consistent Molecular Orbital Methods. XII. Further Extensions of Gaussian-Type Basis Sets for Use in Molecular Orbital Studies of Organic Molecules. *J. Chem. Phys.* **1972**, *56*, 2257–2261.
- (20) Hariharan, P. C.; Pople, J. A. The Influence of Polarization Functions on Molecular Orbital Hydrogenation Energies. *Theor. Chim. Acta* **1973**, *28*, 213–222.
- (21) Rassolov, V. A.; Pople, J. A.; Ratner, M. A.; Windus, T. L. 6-31G\* Basis Set for Atoms K through Zn. *J. Chem. Phys.* **1998**, *109*, 1223–1229.
- (22) Henderson, T. M.; Izmaylov, A. F.; Scalmani, G.; Scuseria, G. E. Can Short-Range Hybrids Describe Long-Range-Dependent Properties? *J. Chem. Phys.* **2009**, *131*, 044108.
- (23) Vydrov, O. A.; Scuseria, G. E. Assessment of a Long Range Corrected Hybrid Functional. *J. Chem. Phys.* **2006**, *125*, 234109.
- (24) Vydrov, O. A.; Heyd, J.; Krukau, A.; Scuseria, G. E. Importance of Short-Range versus Long-Range Hartree-Fock Exchange for the Performance of Hybrid Density Functionals. *J. Chem. Phys.* **2006**, *125*, 074106.
- (25) Vydrov, O. A.; Scuseria, G. E.; Perdew, J. P. Tests of Functionals for Systems with Fractional Electron Number. *J. Chem. Phys.* **2007**, *126*, 154109.
- (26) Chen, Z.; Wannere, C. S.; Corminboeuf, C.; Puchta, R.; Schleyer, P. v. R. Nucleus-Independent Chemical Shifts (NICS) as an Aromaticity Criterion. *Chem. Rev.* **2005**, *105*, 3842–3888.
- (27) Frisch, M. J.; Trucks, G. W.; Schlegel, H. B.; Scuseria, G. E.; Robb, M. A.; Cheeseman, J. R.; Scalmani, G.; Barone, V.; Mennucci, B.; Petersson, G. A.; Nakatsuji, H.; Caricato, M.; Li, X.; Hratchian, H. P.; Izmaylov, A. F.; Bloino, J.; Zheng, G.; Sonnenberg, J. L.; Hada, M.; Ehara, M.; Toyota, K.; Fukuda, R.; Hasegawa, J.; Ishida, M.; Nakajima, T.; Honda, Y.; Kitao, O.; Nakai, H.; Vreven, T.; Montgomery Jr., J. A.; Peralta, J. E.; Ogliaro, F.; Bearpark, M.; Heyd, J. J.; Brothers, E.; Kudin, K. N.; Staroverov, V. N.; Keith, T.; Kobayashi, R.; Normand, J.; Raghavachari, K.; Rendell, A.; Burant, J. C.; Iyengar, S. S.; Tomasi, J.; Cossi, M.; Rega, N.; Millam, J. M.; Klene, M.; Knox, J. E.; Cross, J. B.; Bakken, V.; Adamo, C.; Jaramillo, J.; Gomperts, R.; Stratmann, R. E.; Yazyev, O.; Austin, A. J.; Cammi, R.; Pomelli, C.; Ochterski, J. W.; Martin, R. L.; Morokuma, K.; Zakrzewski, V. G.; Voth, G. A.; Salvador, P.; Dannenberg, J. J.; Dapprich, S.; Daniels, A. D.; Farkas, Ö.; Foresman, J. B.; Ortiz, J. V.; Cioslowski, J.; Fox, D. J. *Gaussian 09 Revision D.01*. Gaussian Inc. Wallingford CT, 2013.
- (28) Geuenich, D.; Hess, K.; Koehler, F.; Herges, R. Anisotropy of the Induced Current Density (ACID), a General Method to Quantify and Visualize Electronic Delocalization. *Chem. Rev.* **2005**, *105*, 3758–3772.
- (29) Furche, F.; Ahlrichs, R. Adiabatic Time-Dependent Density Functional Methods for Excited State Properties. *J. Chem. Phys.* **2002**, *117*, 7433–7447.
- (30) Martin, R. L. Natural Transition Orbitals. *J. Chem. Phys.* **2003**, *118*, 4775–4777.
- (31) Stejskal, E. O.; Tanner, J. E. Spin Diffusion Measurements: Spin Echoes in the Presence of a Time-Dependent Field Gradient. *J. Chem. Phys.* **1965**, *42*, 288–292.
- (32) Einstein, A. Über die von der molekularkinetischen Theorie der Wärme geforderte Bewegung von in ruhenden Flüssigkeiten suspendierten Teilchen. *Ann. Phys.* **1905**, *322*, 549–560.
- (33) Hutin, M.; Sprafke, J. K.; Odell, B.; Anderson, H. L.; Claridge, T. D. W. A Discrete Three-Layer Stack Aggregate of a Linear Porphyrin Tetramer: Solution-Phase Structure Elucidation by NMR and X-ray Scattering. *J. Am. Chem. Soc.* **2013**, *135*, 12798–12807.
- (34) Neufeld, R.; Stalke, D. Accurate molecular weight determination of small molecules via DOSY-NMR by using external calibration curves with normalized diffusion coefficients. *Chem. Sci.* **2015**, *6*, 3354–3364.